

The Role of *jnk1* During Zebrafish Development

Paul William Chrystal

Submitted for the degree of
Doctor of Philosophy

**Institute of Genetic Medicine
Faculty of Medical Sciences
Newcastle University**

March 2015

Abstract

The c-Jun N-terminal Kinases 1-3 (*JNK1-3*) are mitogen activated protein kinases (MAPK) involved in the non-canonical Wnt / planar cell polarity (PCP) signalling pathway. In mouse models and human patients, mutations in the PCP pathway have been associated with congenital heart malformation; however investigating the function of *Jnk* using null mice has been difficult because of genetic redundancy and embryonic death that occurs in *Jnk1/Jnk2* compound mutants. Both human and mouse *JNK1* orthologs have four known transcripts which differ in sequence at two locations. Although evidence has been published to show that these transcripts have differential downstream binding affinities, no transcript-specific functions have been suggested.

Zebrafish possess two *jnk1* paralogs on chromosomes 12 (*jnk1b*) and 13 (*jnk1a*) that arose from the teleost genome duplication event. The aim of this thesis was to identify the *jnk1* transcripts that arose from the zebrafish *jnk1* genes and compare them to what is seen in human *JNK1*. Furthermore I aimed to knock-down zebrafish *jnk1* translation during development using morpholino oligonucleotides (MOs) and assess the phenotypes caused. Considering the involvement of PCP in cardiac development, I hypothesised that *jnk1* would be required for cardiac morphogenesis, and that some subfunctionalization would exist between zebrafish *jnk1a* and *jnk1b* paralogs which would explain the retention of both duplicated genes.

I was able to clone four different transcripts from each of the *jnk1* paralogs, and these transcripts closely resembled mouse and human orthologs. Semi-quantitative RT-PCR demonstrated that these transcripts had differential expression levels during development and in adult tissues. When knocked down, *jnk1a* and *jnk1b* morphants were viable (to 72hpf) but displayed multiple developmental defects that were paralog-specific. The *jnk1a* morphants displayed retinal layer underdevelopment, structural immaturity of the heart and uncoupling of the jog-loop cardiac morphogenetic movements. In contrast the *jnk1b* morphants displayed a high frequency of reversed cardiac situs with a milder overall heart phenotype, in addition to curled body axis formation and failure to form the somitic horizontal myoseptum. Dual knockdown resulted in a combination of paralog-specific defects, as well as developmental delay and a failure for the heart tube to loop. These results demonstrated that the human and zebrafish *JNK1* genes are highly conserved

and suggested that following genome duplication the zebrafish *jnk1* paralogs have undergone subfunctionalization. The *jnk1a* gene appears to have organ specific roles and in particular is required for heart growth whereas the *jnk1b* gene appears to be important for somatic left-right signalling and therefore heart looping and jogging.

This work expands on what is known about the two *jnk1* paralogs and strengthens their validity as a model of human *JNK1*. Establishment of a zebrafish knockdown model provides a powerful tool for the investigation of *jnk1* in an organism that has many advantages for developmental biology research. The demonstration that several organs require *jnk1* during development will allow for future work to investigate the exact role of this gene during organogenesis, and the involvement in left-right axis patterning strengthens the evidence that *JNK* acts in the PCP pathway.

Table of Contents

Abstract.....	I
Table of Contents.....	III
List of Figures	IX
List of Tables	XI
1.1 LEFT-RIGHT PATTERNING	2
1.1.1 EARLY SYMMETRY BREAKING.....	4
1.1.2 LEFT-RIGHT SYMMETRY IN THE LATERAL PLATE MESODERM.....	5
1.1.2.1 <i>The Node</i>	6
1.1.2.2 <i>Molecular Patterning of the Lateral Plate Mesoderm</i>	8
1.1.3 THE ROLE OF THE MIDLINE BARRIER	11
1.1.4 ORGAN RESPONSE TO LEFT-RIGHT PATTERNING.....	11
1.2 THE PLANAR CELL POLARITY PATHWAY	12
1.2.1 THE MOLECULAR GENETICS OF THE PCP PATHWAY	12
1.2.1.1 <i>Planar Cell Polarity in Drosophila</i>	13
1.2.1.2 <i>The Vertebrate PCP Pathway</i>	15
1.2.2 PCP SIGNALLING IS CRUCIAL FOR NORMAL DEVELOPMENT	17
1.2.2.1 <i>PCP Involvement in Ciliated Tissue</i>	17
1.2.2.2 <i>Convergent Extension and Neural Tube Closure</i>	17
1.2.2.3 <i>Participation of PCP in Heart Organogenesis</i>	18
1.3 THE MAP KINASE CASCADES	20
1.4 C-JUN N-TERMINAL KINASE 1	23
1.4.1 THE MAMMALIAN <i>JNK</i> GENES	23
1.4.2 THE ZEBRAFISH GENES APPEAR TO CORRELATE WITH HUMAN JNK1.....	24
1.4.3 THE ROLE OF THE <i>JNK</i> GENES DURING DEVELOPMENT	25
1.5 ZEBRAFISH AS A MODEL ORGANISM OF DEVELOPMENT	29
1.5.1 ADVANTAGES OF ZEBRAFISH AS A MODEL ORGANISM	29
1.5.2 LIMITATIONS OF ZEBRAFISH AS A MODEL ORGANISM	30
1.5.3 NORMAL ZEBRAFISH DEVELOPMENT	31
1.5.3.1 <i>The Zygote to Blastula Stage</i>	31
1.5.3.2 <i>Gastrulation and Convergent Extension</i>	33
1.5.3.3 <i>Segmentation Stage</i>	34
1.5.3.4 <i>Heart Development</i>	37
1.5.3.5 <i>Somite Development</i>	39

1.5.3.6 Eye Development.....	40
1.5.1 THE CURRENT <i>JNK1</i> GENETIC MODEL.....	41
1.5.1.1 The Nomenclature Usage of Zebrafish <i>jnk1</i>	41
1.5.2 THE CURRENT <i>JNK1</i> GENETIC MODEL IN ZEBRAFISH.....	43
1.5.2.1 Gene Structure and Splice-Variants.....	43
1.5.3 THE EXPRESSION PATTERN OF <i>JNK1</i>	50
1.5.3.1 Expression of Homologous <i>jnk1</i> Genes.....	50
1.5.3.2 <i>jnk1</i> Expression in the Zebrafish	50
1.5.4 THE FUNCTIONAL DOMAINS OF THE <i>JNK1</i> PROTEIN.....	52
1.6 SUMMARY	53
1.6.1 AIM OF THE THESIS.....	54
2.1 BIOINFORMATICS.....	56
2.1.1 DATABASES USED.....	56
2.1.2 GENE STRUCTURE FIGURES	57
2.1.3 DNA / PROTEIN ALIGNMENT	57
2.1.4 FUNCTIONAL DOMAIN IDENTIFICATION.....	58
2.1.5 PROTEIN SECONDARY STRUCTURE	58
2.1.6 PROTEIN TERTIARY STRUCTURE.....	58
2.1.7 TISSUE-SPECIFIC EXPRESSION ANALYSIS OF <i>JNK1</i> IN ZEBRAFISH, MOUSE AND HUMAN.....	59
2.1.8 <i>IN SILICO</i> PRIMER CHARACTERISTICS AND SPECIFICITY	60
2.2 MOLECULAR BIOLOGY TECHNIQUES	61
2.2.1 COMMONLY USED MOLECULAR BIOLOGY REAGENTS	61
2.2.2 LIST OF DNA PRIMERS	62
2.2.3 STANDARD TISSUE HOMOGENISATION PROCEDURE	62
2.2.4 STANDARD RNA EXTRACTION METHOD	63
2.2.5 QUANTIFICATION OF RNA/DNA	63
2.2.6 cDNA GENERATION (RANDOM HEXAMERS)	64
2.2.7 GEL EXTRACTION AND PCR PRODUCT CLEAN-UP.....	64
2.2.8 FULL-LENGTH <i>JNK1</i> VARIANT SUB-CLONING	65
2.2.8.1 Full-Length Transcript Primer Design	65
2.2.8.2 cDNA Generation (Oligo dT Primers).....	67
2.2.8.3 Full-length Transcript PCR.....	68
2.2.8.4 A-tailing of PCR Products.....	69
2.2.8.5 T-Clone Ligation.....	69
2.2.8.6 Bacterial Transformation	71
2.2.8.7 Colony PCR	71

2.2.8.8 Isolation of Plasmid DNA.....	72
2.2.9 GEL ELECTROPHORESIS.....	73
2.2.10 SEQUENCING.....	73
2.2.11 SPLICE-VARIANT SPECIFIC <i>JNK1</i> RT-PCRS.....	73
2.2.11.1 Forward Primer Design.....	74
2.2.11.2 Reverse Primer Design.....	75
2.2.11.3 Temperature Gradient RT-PCR.....	77
2.2.11.4 Testing RT-PCR Specificity (Plasmids).....	77
2.2.12 DEVELOPMENTAL AND TISSUE-SPECIFIC RT- PCR.....	78
2.2.13 PAN-JNK WESTERN BLOTTING.....	80
2.2.14 MYC-TAGGED WESTERN BLOTT.....	82
2.2.15 <i>IN SITU</i> HYBRIDISATION.....	83
2.2.16 DENSITOMETRY.....	85
2.2.17 STATISTICS.....	85
2.3 ZEBRAFISH HUSBANDRY, MORPHANT GENERATION AND SECTIONING	86
2.3.1 COMMONLY USED ZEBRAFISH TECHNIQUE REAGENTS.....	86
2.3.2 ZEBRAFISH LINES USED.....	86
2.3.3 BREEDING STRATEGY AND ZYGOTE COLLECTION.....	87
2.3.4 EMBRYO CULTURE CONDITIONS.....	87
2.3.5 MORPHOLINO PROTOCOLS.....	87
2.3.5.1 Morpholino Preparation.....	88
2.3.5.2 Microinjection.....	88
2.3.6 PRONASE DECHORIONATION.....	89
2.3.7 ANAESTHETISATION OF EMBRYOS AND MICROSCOPY.....	89
2.3.8 SCHEDULE 1 METHODS AND DISSECTION OF ADULT TISSUES.....	89
2.3.9 PARAFORMALDEHYDE FIXATION OF ZEBRAFISH EMBRYOS.....	90
2.3.10 RESIN SECTIONING.....	90
2.3.11 JOG / LOOP SCORING.....	91
2.3.12 UNCOUPLING SCORING.....	92
3.1 INTRODUCTION.....	94
3.1.1 AIMS OF THE CHAPTER.....	95
3.2 RESULTS	96
3.2.1 PROPOSED NEW MODEL OF ZF JNK1 SPLICE VARIANTS.....	96
3.2.1.1 Primer Design.....	96
3.2.1.2 Sub-Cloning of Full-Length <i>jnk1</i> Transcripts.....	97
3.2.2 THE IDENTIFICATION OF TWO UNPREDICTED JNK1A TRANSCRIPTS.....	97

3.2.3 THE IDENTIFICATION OF EXON 7 <i>JNK1B</i> AND TWO UNPREDICTED TRANSCRIPTS	97
3.2.4 OVERVIEW OF THE UPDATED MODEL OF ZEBRAFISH <i>JNK1</i> SPLICE-VARIANTS.....	98
3.2.5 CONSERVATION AND DIVERGENCE OF THE TWO ZEBRAFISH <i>JNK1</i> PARFORMS	101
3.2.5.1 <i>Sequence Identity is Strongly Conserved between ZF Jnk1 Protein Sequences in the Region of the Protein Kinase Domain</i>	101
3.2.5.2 <i>Sequence Divergence in the Middle Exon</i>	102
3.2.5.3 <i>Sequence Conservation at the 3' Alternative Splicing Acceptor</i>	103
3.2.6 SEQUENCE CONSERVATION OF ZEBRAFISH <i>JNK1</i> AND ITS ORTHOLOGS.....	104
3.2.7 DIFFERENTIAL EXPRESSION PATTERNS OF THE <i>JNK1</i> SPLICE-VARIANTS DURING DEVELOPMENT.....	106
3.2.7.1 <i>Optimisation of RT-PCR Melting Temperature</i>	107
3.2.7.2 <i>Testing Primer Specificity</i>	109
3.2.7.3 <i>Expression Patterns of jnk1 Splice-Variants during Development</i>	111
3.2.8 DIFFERENTIAL EXPRESSION PATTERNS OF THE <i>JNK1</i> SPLICE VARIANTS IN ADULT TISSUES	115
3.2.8.1 <i>Exon 7 Containing Variants are Predominantly Restricted to the Brain</i>	115
3.2.8.2 <i>Exon 8 Containing Variants are Expressed Fairly Ubiquitously</i>	116
3.2.9 COMPARISON OF <i>JNK1</i> EXPRESSION IN ZEBRAFISH, HUMAN AND MOUSE ADULT TISSUE	116
3.3 DISCUSSION	119
3.3.1 IDENTIFICATION OF NOVEL SPLICE-VARIANTS.....	120
3.3.1.1 <i>The ZF jnk1 Paralogs are Highly Similar to One Another and their Orthologs</i>	120
3.3.2 BIOINFORMATICAL ANALYSIS	122
3.3.2.1 <i>The jnk1 Paralogs Differ Most in Sequence Outside of the Protein Kinase Domain</i>	122
3.3.2.2 <i>Strong Conservation to Homologous Sequences Suggest Function is Preserved</i>	124
3.3.3 <i>JNK1</i> EXPRESSION ANALYSIS	124
3.3.3.1 <i>Differential Expression of Exon 8 Containing Splice-Variants Switch May Coincide with Proliferation Changes</i>	125
3.3.3.2 <i>Differential Expression of Exon 7 Containing Splice Variants Coincides with Brain Development</i>	126
3.3.3.3 <i>RT-PCR is Limited by being a Semi-Quantitative Measure of Gene Expression</i>	126
3.3.3.4 <i>Evidence of Tissue-Specific Gene Expression Pattern Conservation between Zebrafish, Mouse and Human</i>	128
3.3.3.5 <i>Concluding Remarks</i>	129
4.1 INTRODUCTION.....	131
4.1.1 THE ROLE OF <i>JNK1</i> DURING DEVELOPMENT.....	131
4.1.2 MORPHOLINO OLIGONUCLEOTIDES.....	132
4.1.2.1 <i>Morpholino Oligonucleotides Represent an Efficient and Specific Anti-Sense Reagent to Knock Down Gene Products</i>	132
4.1.2.2 <i>Limitations of Morpholino Oligonucleotides</i>	133
4.1.2.3 <i>Suitable Controls and Validation of MO Experiments</i>	135

4.1.2.4 Design of the <i>jnk1</i> Morpholinos	138
4.1.3 AIMS OF THE CHAPTER	140
4.1.4 RESULTS.....	141
4.1.4.1 3.2.1 Effect of the <i>jnk1</i> MOs on Survival	141
4.1.4.2 Survival of the <i>jnk1</i> Morphants between 7-24hpf.....	141
4.1.5 DEVELOPMENTAL DELAY.....	144
4.1.6 GROSS PHENOTYPE BY LIGHT MICROSCOPY	146
4.1.6.1 Characterisation of the <i>jnk1a</i> Morphant Gross Phenotype	146
4.1.6.2 Characterisation of the <i>jnk1b</i> Morphant Gross Phenotype	147
4.1.6.3 Morpholino Toxicity at a 6ng <i>jnk1a</i> Dose.....	151
4.1.6.4 Compound <i>jnk1a;jnk1b</i> Morphants Display Severe Phenotypic Changes	152
4.1.6.5 Deciding Upon Optimal <i>jnk1</i> Morpholino Doses	160
4.1.6.6 Frequency of Gross Phenotype Developmental Defects.....	161
4.1.7 HISTOLOGY OF THE <i>JNK1</i> MORPHANTS	162
4.1.7.1 Somitic Defects.....	163
4.1.7.2 Eye Defects	167
4.1.7.3 Heart Defects.....	170
4.1.8 PROOF OF KNOCKDOWN.....	173
4.1.8.1 Knockdown Analysis by Western Blot	173
4.1.8.2 Myc-Tagged Western Blot Analysis.....	175
4.2 DISCUSSION	179
4.2.1 MORPHOLINOS CAN SUCCESSFULLY BE USED TO STUDY <i>JNK1</i> DURING DEVELOPMENT	179
4.2.1.1 The <i>jnk1</i> Morpholinos Successfully Knock Down their Targets.....	179
4.2.1.2 The <i>jnk1</i> Morpholinos Cross-React.....	182
4.2.1.3 High Doses of <i>jnk1</i> Morpholino are Tolerated Without Causing Toxicity.....	183
4.2.2 THE <i>JNK1A</i> AND <i>JNK1B</i> GENES PLAY A ROLE IN DEVELOPMENT	183
4.2.2.1 <i>jnk1a</i> is Vital for Development of the Heart, Brain and Tail.....	183
4.2.2.2 <i>jnk1b</i> is Vital for Development of the Tail and Heart	185
4.2.2.3 The Zebrafish <i>jnk1</i> Morphant Results in Context of PCP	186
4.2.2.4 Similarities of the <i>jnk1</i> Retinal Phenotype to Ciliopathy-Associated Gene Knockdowns.....	188
4.2.2.5 Concluding Remarks.....	189
5.1 INTRODUCTION.....	192
5.1.1 BREAKING SYMMETRY OF THE VISCERAL ORGANS	192
5.1.1.1 Jogging and Looping Movements of the Heart	192
5.1.1.2 Uncoupling of Heart Movement.....	195
5.1.2 AIMS OF THE CHAPTER	196

5.2 RESULTS	197
5.2.1 LEFT-RIGHT PATTERNING DEFECTS OF THE JNK1 MORPHANT HEART	197
5.2.1.1 Zebrafish <i>jnk1</i> Knockdown Causes L-R Heart Defects in a Dose Dependent Manner	197
5.2.1.2 Uncoupling of the Jog-Loop Heart Progression	202
5.2.1.3 The Hearts of Compound <i>jnk1a</i> ; <i>jnk1b</i> Morphants Display an Inability to Loop	204
5.2.2 PATTERNING DEFECTS OF THE GUT	208
5.2.2.1 Normal Liver Laterality is Disrupted in <i>jnk1</i> Morphants	208
5.3 DISCUSSION	212
5.3.1 THE LEFT-RIGHT PATTERNING DEFECTS OF THE <i>JNK1A</i> MORPHANT MAY BE DUE TO MIDLINE BARRIER DEFECTS.....	213
5.3.2 THE <i>JNK1B</i> GENE HAS A GREATER ROLE IN L-R PATTERNING OF THE VISCERAL ORGANS.....	214
5.3.3 COMPOUND <i>JNK1A</i> ; <i>JNK1B</i> KNOCKDOWN EFFECTS THE ABILITY OF THE HEART TO LOOP	215
5.3.4 EVIDENCE FOR LEFT-RIGHT PATTERNING AND CILIOGENESIS DEFECTS IN <i>JNK1</i> MORPHANTS	216
5.3.5 CONCLUDING REMARKS	218
6.1 SUMMARY	220
6.2 DISCUSSION	221
6.2.1 SUMMARY OF FINDINGS	221
6.2.2 VALIDITY OF STUDYING <i>JNK1</i> FUNCTION IN THE ZEBRAFISH.....	222
6.2.2.1 Sequence Conservation to Human <i>JNK1</i>	222
6.2.2.2 Off-target Effects of Morpholinos	224
6.2.2.3 Similarity and Conflicts with other <i>jnk1</i> Research	225
6.2.3 EVIDENCE OF <i>JNK1</i> ACTION THROUGH THE PCP PATHWAY	228
6.2.4 EVIDENCE OF A ROLE IN LEFT-RIGHT PATTERNING AND CILIOGENESIS	229
6.3 FUTURE WORK	231
6.4 CONCLUDING REMARKS.....	234
7.1.1 ABBREVIATIONS	249

List of Figures

FIGURE 1 THE BODY PLAN OF ALL BILATERIA DISPLAY ASYMMETRY OF THE INTERNAL ORGANS.	3
FIGURE 2 LEFTWARD NODAL FLOW IS CRITICAL OF EMBRYONIC LEFT-RIGHT PATTERNING.	7
FIGURE 3 LEFT-RIGHT PATTERNING OF THE LATERAL PLATE MESODERM REQUIRES SEVERAL KEY TGF β -RELATED CYTOKINES.	10
FIGURE 4 SCHEMATIC REPRESENTATION OF THE PCP PATHWAY PROTEINS IN (A) DROSOPHILA AND (B) VERTEBRATES.	15
FIGURE 5 SCHEMATIC REPRESENTATION OF THE MAPK CELL SIGNALING PATHWAY.	21
FIGURE 6 THE SPLICE-VARIANTS OF HUMAN JNK.	24
FIGURE 7 ZEBRAFISH DEVELOPMENTAL SERIES.	36
FIGURE 8 ZEBRAFISH DEVELOPMENTAL TIMELINE.....	39
FIGURE 9 SIMILARITIES IN THE CHROMOSOMAL REGIONS SURROUNDING THE FOUR JNK1 GENES SUGGESTS THAT JNK1A AND JNK1B MAY HAVE ARISEN FROM A DUPLICATION EVENT.	42
FIGURE 10 SCHEMATIC REPRESENTATION OF THE ZEBRAFISH JNK1A AND JNK1B GENE STRUCTURE	44
FIGURE 11 JNK1B EXON 7 IS HOMOLOGOUS TO JNK1A EXON 8.	46
FIGURE 12 PREDICTED MODEL OF ZEBRAFISH JNK1 TRANSCRIPTION.....	49
FIGURE 13 SCHEMATIC REPRESENTATION OF THE HUMAN JNK1 FUNCTIONAL PROTEIN DOMAINS.	52
FIGURE 14 EXPLANATION OF THE FULL-LENGTH JNK1 PRIMERS.	67
FIGURE 15 PLASMID MAP OF THE FINAL JNK1 TRANSCRIPT-CONTAINING CLONING VECTOR.	70
FIGURE 16 DESIGN OF SPLICE-VARIANT SPECIFIC PRIMERS.	76
FIGURE 17 A NEW MODEL OF THE EXPERIMENTALLY PROVEN SPLICE-VARIANTS OF ZEBRAFISH JNK1.....	100
FIGURE 18 SEQUENCE ALIGNMENTS BETWEEN THE ZEBRAFISH JNK1 PARALOGS DNA AND PROTEIN SEQUENCES.	102
FIGURE 19 SEQUENCE ALIGNMENTS AT THE REGION OF THE SPLICING EVENTS.	103
FIGURE 20 SEQUENCE ALIGNMENT OF THE ZEBRAFISH JNK1 PROTEINS TO THEIR ORTHOLOGS.	106
FIGURE 21 DESIGN OF SPLICE-VARIANT SPECIFIC PRIMERS.	106
FIGURE 22 MELTING TEMPERATURE OPTIMISATION OF SPLICE-VARIANT SPECIFIC PRIMERS.....	108
FIGURE 23 THE SPLICE-VARIANT PRIMERS ARE SPECIFIC TO ONLY A SINGLE TRANSCRIPT.	110
FIGURE 24 EXPRESSION PATTERNS OF THE JNK1 SPLICE-VARIANTS DURING DEVELOPMENT.	114
FIGURE 25 RT-PCR EXPRESSION OF JNK1 SPLICE-VARIANTS IN ADULT TISSUES.	116
FIGURE 26 STRUCTURAL 3-D MODEL OF THE JNK1 PROTEIN SHOWS THE LOCATION OF THE MIDDLE EXON WITHIN THE STRUCTURE.	123
FIGURE 27 MORPHOLINO OLIGONUCLEOTIDES WERE DESIGNED TO BIND TO THE JNK1A AND JNK1B GENES.....	139
FIGURE 28 PERCENTAGE SURVIVAL OF JNK1A AND JNK1B MORPHANTS.	142
FIGURE 29 PERCENTAGE SURVIVAL OF COMPOUND JNK1A; JNK1B MORPHANTS.	143
FIGURE 30 HIGH COMPOUND JNK1A;JNK1B MORPHOLINO DOSES CAUSE DEVELOPMENTAL DELAY. STAGING OF JNK1 MORPHANTS BY SOMITES COUNTING AT 22HPF.	145
FIGURE 31 GROSS MORPHOLOGY OF JNK1 MORPHANTS AT 28HPF.	149
FIGURE 32 GROSS MORPHOLOGY OF JNK1 MORPHANTS AT 48HPF.	150

FIGURE 33 THE MORPHOLINO TOXICITY OF 6NG JNK1A CAN BE RESCUED BY 4NG P53 MO.	151
FIGURE 34 LOW COMPOUND JNK1A; JNK1B MORPHOLINOS DOSES CAUSED DEVELOPMENTAL DEFECTS AT 28HPF.	154
FIGURE 35 THE COMPOUND JNK1A; JNK1B MORPHANTS DISPLAY SIGNIFICANT BODY DEFECTS AND OEDEMA AT 48HPF.	156
FIGURE 36 AT 4NG JNK1A; 4NG JNK1B DOSE THE MORPHANTS DISPLAY SEVERE DEVELOPMENTAL DEFECTS.	158
FIGURE 37 AT 48HPF 4NG 1A; 4NG 1B MORPHANTS DISPLAYED SEVERE TAIL DEFECTS, OEDEMA AND BRAIN DEFECTS.	159
FIGURE 38 JNK1A AND JNK1B MORPHANTS DISPLAY DIFFERENT DEFECTS IN SOMITE FORMATION.	164
FIGURE 39 SOMITE SIZE WAS AFFECTED BY THE KNOCKDOWN OF JNK1A AND JNK1B.	166
FIGURE 40 HISTOLOGY OF THE EYE IN JNK1A AND JNK1B MORPHANTS.	168
FIGURE 41 RETINAL LAMINATION SIZES WERE AFFECTED BY JNK1A KNOCKDOWN.	169
FIGURE 42 HEART HISTOLOGY OF SINGLE MORPHANTS AT 48HPF.	171
FIGURE 43 HEART HISTOLOGY OF SINGLE MORPHANTS AT 72HPF.	172
FIGURE 44 PAN-JNK WESTERN BLOT REVEALED PARTIAL KNOCKDOWN OF JNK PROTEIN.	174
FIGURE 45 THE JNK1 MORPHOLINOS KNOCKDOWN BOTH PARALOGS OF JNK1.	178
FIGURE 46 SCHEMATIC REPRESENTATION OF JOGGING AND LOOPING MOVEMENTS OF THE ZEBRAFISH HEART TUBE.	194
FIGURE 47 HEART LATERALITY DEFECTS ARE OBSERVABLE IN CONTROLS AND MORPHANTS AT 48HPF.	198
FIGURE 48 JNK1 KNOCKDOWN RESULTS IN AN INCREASED PREVALENCE OF HEART O-LOOP AND L-LOOP FORMATION IN A DOSE DEPENDENT MANNER.	200
FIGURE 49 JNK1 KNOCKDOWN RESULTS IN SIGNIFICANT LOSS OF NORMAL HEART LATERALITY.	201
FIGURE 50 THE 4NG JNK1A MORPHANTS DISPLAYED HEART FORMATION DELAY AND UNCOUPLING OF JOG / LOOP MOVEMENTS.	203
FIGURE 51 COMPOUND JNK1A; JNK1B MORPHANTS DISPLAY HIGH LEVELS OF HEART LATERALITY DEFECTS AND A PREFERENCE FOR O-LOOP AT THE HIGH DOSE.	205
FIGURE 52 NORMAL HEART LOOPING LATERALITY IS GREATLY DISRUPTED BY KNOCKDOWN OF BOTH JNK1 PARALOGS.	206
FIGURE 53 COMPOUND JNK1A; JNK1B KNOCKDOWN RESULTS IN HEART MOVEMENT UNCOUPLING IN A DOSE-DEPENDENT MANNER.	207
FIGURE 54 JNK1 MORPHANTS MAY DISPLAY LATERALITY DEFECTS OF THE DEVELOPING LIVER.	209
FIGURE 55 JNK1 MORPHANTS DISPLAY HETEROTAXY OF THE VISCERAL ORGANS.	211
FIGURE 56 THE ZEBRAFISH JNK1 SPLICE-VARIANTS ARE HOMOLOGOUS TO HUMAN JNK1.	222
FIGURE 57 THE BINDING SITES OF THE FULL-LENGTH JNK1 PRIMERS.	238
FIGURE 58 ALIGNMENT OF THE FOUR JNK1A VARIANTS IDENTIFIED IN THIS STUDY.	241
FIGURE 59 ALIGNMENT OF THE FOUR JNK1B VARIANTS IDENTIFIED IN THIS STUDY.	244
FIGURE 60 DNA ALIGNMENT OF ALL THIRTEEN EXONS OF JNK1A AND JNK1B.	246
FIGURE 61 PROTEIN ALIGNMENT OF ALL THIRTEEN EXONS OF JNK1A AND JNK1B.	246
FIGURE 62 THE BINDING SITES OF THE JNK1 MORPHOLINOS.	247
FIGURE 63 THE BINDING SITES OF OUR TRANSLATION BLOCKING AND THE SEO ET AL. SPLICE-VARIANT MORPHOLINOS.	248

List of Tables

TABLE 1 NAMING CONVENTIONS FOR THE JNK FAMILY HOMOLOGUES.	43
TABLE 2 SOURCES OF GENE AND PROTEIN SEQUENCING DATA PLUS ACCESSION NUMBERS.	56
TABLE 3 LIST OF GENE EXPRESSION STUDIES USED TO DETERMINE TISSUE-SPECIFIC EXPRESSION OF THE MOUSE JNK1 AND HUMAN JNK1 GENES.	59
TABLE 4 LIST OF PRIMER SEQUENCES.....	62
TABLE 5 SEQUENCES AND CHARACTERISTICS OF THE SPLICE-VARIANT SPECIFIC JNK1 PRIMERS.	74
TABLE 6 MORPHOLINO SEQUENCES.....	87
TABLE 7 PROPOSED NEW NAMING CONVENTION OF THE CORE JNK1 SPLICE-VARIANTS.	99
TABLE 8 PERCENTAGE IDENTITY OF THE ZF JNK1 PARALOGS AND THEIR ORTHOLOGS.	104
TABLE 9 IMPORTANCE OF THE TIMEPOINTS CHOSEN FOR RT-PCR.....	112
TABLE 10 RELATIVE TISSUE-SPECIFIC EXPRESSION LEVELS OF ZEBRAFISH JNK1A AND JNK1B, MOUSE JNK1 AND HUMAN JNK1 GENES.	117
TABLE 11 LIST OF JNK1 MORPHOLINO DOSES TRIALLED	142
TABLE 12 THE FREQUENCY OF GROSS PHENOTYPIC DEFECTS AT THE CHOSEN OPTIMAL DOSES.....	162
TABLE 13 DIFFERENT DOSES OF MYC-TAGGED JNK1 RNA AND MORPHOLINO USED TO DEMONSTRATE MORPHOLINO SPECIFICITY.	177

CHAPTER 1 - INTRODUCTION

The c-Jun N-terminal Kinase (JNK) family genes have been shown to function in both the mitogen activated protein kinase (MAPK) and planar cell polarity (PCP) signalling pathways. Through these two pathways the JNK proteins mediate the appropriate tissue-specific responses to both intracellular and extracellular stimuli, and have been implicated with many different cellular processes and disease progressions. However, the understanding of JNK signalling has been hampered by the quantity and diversity of upstream signals, moderating co-factors, and downstream targets which have been identified. A further complexity to understanding the role of each *JNK* gene individually is the existence of genetic redundancy that has been shown between the different mouse *Jnk* genes - loss of a single *Jnk* isoform does not cause any overt physical phenotypic changes (Kuan et al., 1999). The aim of this thesis was therefore to characterise the two zebrafish *jnk1* genes (*jnk1a* and *jnk1b*), compare them to the human gene, and examine their expression pattern during development and between different tissues. Furthermore a *jnk1* morpholino oligonucleotide method was developed, and phenotypic analysis was performed in order to explore the functions of the two *jnk1* genes during zebrafish embryogenesis. It is hoped that this research will expand upon what is currently known about the *jnk1* genes and offer an amenable system for the study of *jnk1* function during development.

1.1 LEFT-RIGHT PATTERNING

Externally the human body appears symmetrical across the left-right axis, however internally many of the organs are located on one side, or are left-right asymmetrical (Figure 1A). This asymmetry is most apparent amongst the visceral organs where the heart, stomach, spleen and pancreas are predominantly left sided, whereas the liver and gall bladder are right sided. Furthermore the left side of the heart is far thicker whereas the lungs possess two right and three left-sided lobes. The normal asymmetrical arrangement of the body is known as situs solitus, and is a feature common to all of the bilateria (organisms with one axis of symmetry), which include all major phyla of animals except for the sponges and *Hydra* (Blum et al., 2014).

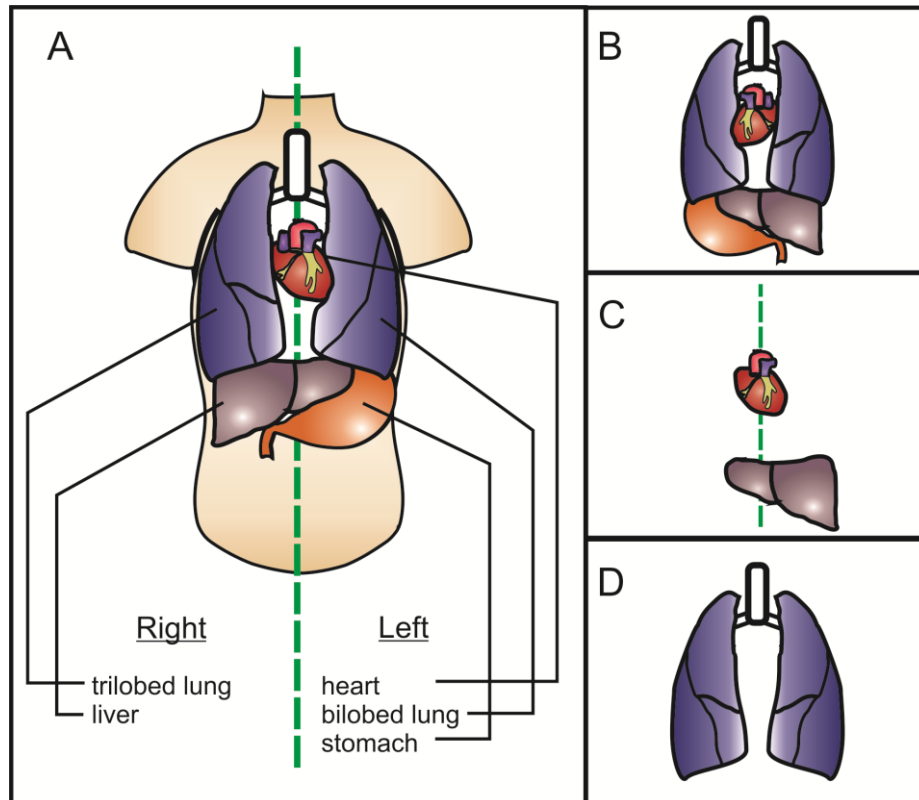


Figure 1 *The body plan of all bilateria display asymmetry of the internal organs.*

A) Internally the human visceral organs display asymmetrical shape or placement with respect to the anterior-posterior axis. The normal arrangement of organs is known as *situs solitus*. B) Complete reversal of normal situs is *situs inversus totalis*. C) *Heterotaxy* is when there exists a discordance of organ situs (e.g. normal heart and reversed liver situs). D) *Isomerism* of an organ is where both sides are symmetrical (mirrored) and display either left-sided or right-sided isomerism (e.g. bilateral trilobed lungs).

The mechanisms by which *situs solitus* is established have been well studied between several species, and many key pathways are found to be universally used. When left-right patterning is disrupted the result is a heterogeneous spectrum of disorders ranging from complete reversal or “mirror image” of organ situs (*situs inversus totalis*) (Figure 1B), discordance between the situs of different organs (*heterotaxy*) (Figure 1C) or isomerism of organs (Figure 1D) such as right atrial isomerism, bilateral trilobed lungs, or polysplenia (Lin et al., 2000, Kaulitz et al., 2004, Hashmi et al., 1998, Yokoyama et al., 1993, Bartram et al., 2005). The incidence of abnormal situs in humans is estimated at about 1:10,000 (Lin et al., 2000) and is thought to account for 1-3% of congenital heart defects (Bartram et al., 2008, Sutherland and Ware, 2009).

Congenital heart defects (CHDs), represent one of the most common human congenital disorders, having an incidence of between 6 and 19 per 1000 live births (Hoffman and Kaplan, 2002). These defects include conditions as diverse as hypoplastic left heart, double outlet right ventricle, atrial or ventricular septal defects, bicuspid aortic valve and patent ductus arteriosus. A link between organ situs and heart defects has long been described (Ferencz, 1964, Icardo and Sanchez de Vega, 1991, Merklin and Varano, 1963), however more recently it has been suggested that a vast number of complex CHDs may arise from subtle laterality defects that result in improper formation of the developing organ (Ramsdell, 2005, Francis et al., 2012). Due to the prevalence and severity of defects caused by defects of organ situs, it is important to understand the genetic pathways involved in proper left-right patterning.

1.1.1 Early Symmetry Breaking

The origin of embryonic asymmetry has long been contested, and still remains unclear (for review see (Vandenberg and Levin, 2010)). Despite much of the left-right patterning research being focused upon the function of motile cilia during post-gastrula stages of development (see section 1.1.2) the first break in symmetry has been shown to occur much earlier in several species. Since the issue was first contemplated it has been suggested that the left-right axis is patterned by default once the other two body axes (anterior-posterior, dorsal-ventral axes) are established (Brown and Wolpert, 1990). Indeed pre-gastrula stage left-right asymmetries have been shown to exist in *Xenopus*, chick and zebrafish (Adams et al., 2006, Aw et al., 2010, Fukumoto et al., 2005, Levin et al., 2002, Morokuma et al., 2008, Vandenberg et al., 2013) although the mechanisms by which this asymmetry is established are not well understood.

In *Xenopus* and chicken it has been shown that during the first few cell cleavages there is a left-sided depolarisation of the embryo mediated by several ATP-dependent ion channels. Inhibition of these ion channels (H^+/K^+ -ATPase, H^+ -V-ATPase, KCNQ1 and KCNE1 K^+ channels) results in disruption of normal organ situs independent of the other embryonic axes (Adams et al., 2006, Levin et al., 2002, Morokuma et al., 2008). It has also been shown that inhibition of H^+/K^+ -ATPases in zebrafish between 0-10 hours post fertilisation can

randomise organ situs via retinoic acid signalling (Kawakami et al., 2005) Although most of the channels found to play a role in early left-right symmetry breaking are asymmetrically distributed in the blastomere, possibly under the control of Rab GTPases (Vandenberg et al., 2013, Aw et al., 2010), K⁺-ATPase channels are symmetrically distributed but also lead to situs defects when inhibited.

Early symmetry breaking has also been described in the chick where depolarisation is observable at primitive streak stages and this is also dependent upon ion channel function (Levin et al., 2002). This bioelectrical gradient controls the distribution of maternally inherited serotonin in both chick and *Xenopus* long before organ asymmetry is observed. Inhibition of serotonin during development, particularly in the right ventral blastomere of *Xenopus* causes heterotaxia of the visceral organs later during development (Fukumoto et al., 2005).

Despite the recent accumulation of evidence there still remains no evidence in mouse that there exists left-right asymmetry in the embryo earlier than appearance of the node, therefore the idea of early embryonic asymmetry is still widely viewed as a species-specific phenomenon.

1.1.2 Left-Right Symmetry in the Lateral Plate Mesoderm

Although few papers have examined the earliest breaks of left-right patterning during development, there is a wealth of evidence generated concerning left-right asymmetry breaking during somitic stages of development. The majority of this work has been performed in mouse and therefore so will much of the literature discussed here. Where evidence from other animal models is available it will be stated. One of the most important discoveries in understanding the somitic transmission of left-right signals through the embryo was defining the function of the node.

1.1.2.1 *The Node*

The node is a transient vesicle present during somitogenesis of the mouse (Sulik et al., 1994), frog (Schweickert et al., 2007) and zebrafish (Essner et al., 2005b), although in the latter it is known as Kupffer's vesicle. The vesicle is filled with extraembryonic fluid and small cilia project from the cells on the ventral surface into the node (Nonaka et al., 1998, Okada et al., 1999). Motile cilia within this population rotate in a clockwise manner to generate a right-to-left fluid flow known as the nodal flow (Figure 2A+B). This nodal flow has been studied thoroughly in mouse and zebrafish and is critical for correct laterality of both the visceral organs and certain structures of the brain (Essner et al., 2005b); disturbance of normal cilia length (Nonaka et al., 1998, Lopes et al., 2010), cilia motility (Essner et al., 2005b, Kramer-Zucker et al., 2005), or fluid flow directly (Nonaka et al., 2002) may disturb normal organ situs (Figure 2C). The mechanism by which fluid flow translates to organ situs is contested, however shortly after node formation several key genes in left-right determination establish an asymmetric expression pattern through the left lateral plate mesoderm (Long et al., 2003b). There are two alternative (non-mutually exclusive) hypotheses about how nodal flow translates to asymmetric gene expression.

The first theory of symmetry breaking in the node states that the TGF β -related protein NODAL is itself physically shuttled to the embryonic left by nodal flow, or that nodal vesicular particles (containing Sonic Hedgehog and Retinoic acid) are shuttled which upregulate NODAL expression (Figure 2D) (Nonaka et al., 1998, Tanaka et al., 2005). As a secreted cytokine, a small imbalance of Nodal may be caused on the left side by nodal function which will be amplified since nodal is capable of increasing its own expression (Saijoh et al., 2000).

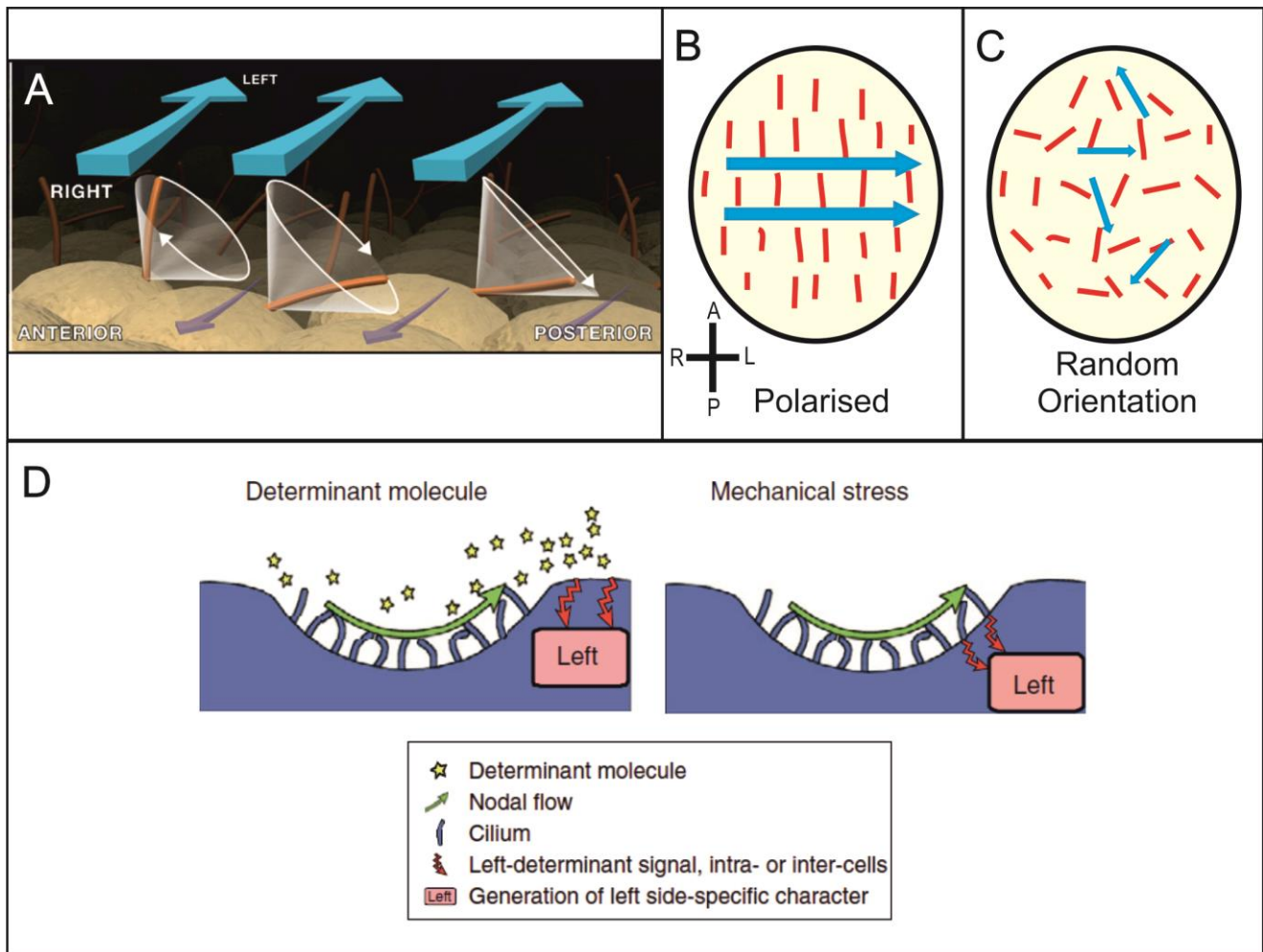


Figure 2 Leftward nodal flow is critical of embryonic left-right patterning.

A) The node contains posterior-facing motile cilia that beat and produce a net leftward fluid flow (taken from (Hirokawa et al., 2006)). B) Net leftward flow (blue) is dependent upon polarised cilia positioning (red). C) Disruption of cilia orientation creates turbulent nodal flow without net leftward movement. D) Two theories exist to explain the role of nodal fluid flow. The determinant model suggests that some molecular determinant is shuttled to the left side of the embryo by nodal flow, establishing a gene expression asymmetry. The mechanical model suggests that physical fluid flow is sensed by mechanosensory cilia at the edge of the node which influences downstream left-determination (taken from (Shiratori and Hamada, 2006)).

The opposing theory postulates that there exist sensory cilia within the node that react to the mechanical forces of nodal flow, and increase intracellular calcium on the left side (Figure 2D) (Tabin and Vogan, 2003). It has been shown comprehensively in mouse that there are two distinct populations of cilia within the node, a central motile population which require the left-right dynein (Lrd) to generate nodal flow, and a peripheral immotile population (McGrath et al., 2003). Both cilia populations contain the calcium channel protein polycystin-2 which is also found on the mechanosensory renal cilia that increase

intracellular calcium in this environment in response to flow (Nauli et al., 2003). Furthermore left-sided asymmetrical calcium signalling has been reported in the node of mouse (McGrath et al., 2003) and zebrafish (Francescatto et al., 2010), and mutations of polycystin-2 cause loss of nodal signalling resulting in heterotaxy (Pennekamp et al., 2002, Bisgrove et al., 2005, Obara et al., 2006). Both theories therefore have supportive experimental evidence and neither has definitively been shown to be the dominant mechanism of symmetry breaking in the LPM. However, as stated above these two mechanisms are not mutually exclusive and could cooperate in order to establish left sidedness in the embryo. Regardless of the mechanism by which left-right patterning is established within the lateral plate mesoderm, the eventual readout is left-sided *Nodal* expression.

Further evidence for the importance of the node in left-right patterning has come from a subset of genetic conditions that affect cilia formation or function. Primary ciliary dyskinesia is an autosomal recessive disorder that is characterised by immotile primary cilia of the respiratory tract and sperm cells (Afzelius, 1976). Over 30 genes have been identified in this disorder, which encode components of the primary cilia or genes involved in the assembly of cilia (Leigh, 2015). Approximately half of the patients that present with primary ciliary dyskinesia also display organ laterality defects that are thought to be caused by incorrect function of nodal cilia.

1.1.2.2 Molecular Patterning of the Lateral Plate Mesoderm

Although earlier breaks of left-right patterning have been described, the node is responsible for transmitting left-right asymmetry through the lateral plate mesoderm by establishing asymmetrical gene expression. NODAL is one of the most critical determinants of “leftness” for patterning of the left-right axis in mouse (Collignon et al., 1996), frog (Lowe et al., 1996), chick, and zebrafish (Ahmad et al., 2004). Nodal is initially expressed symmetrically in perinodal cells around the node before it becomes restricted to the left LPM (Figure 3) (Collignon et al., 1996). Once an imbalance is present on the left, *Nodal* may upregulate its own expression via binding to a *Nodal*-responsive transcriptional enhancer (Saijoh et al., 2000, Yashiro et al., 2000) which allows for very rapid amplification of *Nodal* on the left. In order to self regulate, *Nodal* upregulates the expression of two of its antagonists, the TGFβ-

related cytokines *Lefty1* and *Lefty 2*. These proteins, in zebrafish at least, diffuse more quickly than *nodal* (Muller et al., 2012) and antagonise *Nodal* action by competing for receptor binding (Varlet et al., 1997, Cheng et al., 2004, Meno et al., 1999). Although the expression of *Lefty2* somewhat overlaps that of *Nodal* (Long et al., 2003b), *Lefty1* expression is restricted to the midline and is postulated to play a role in the chemical midline barrier (Figure 3). Both NODAL and LEFTY function has been shown to be critical for normal organ situs in mouse (Lowe et al., 1996, Meno et al., 1999, Meno et al., 1998), zebrafish (Ahmad et al., 2004, Long et al., 2003a, Long et al., 2003b, Meno et al., 1999), and *Xenopus* (Osada et al., 2000, Cheng et al., 2000, Toyozumi et al., 2005).

Numerous other genes are also critical for left-right patterning of the embryo including embryonic growth/differentiation factor 1 (GDF1). In mouse, *Gdf1* is bilaterally expressed around the node at the same time as *Nodal*, and knockout *Gdf1* mice fail to establish left-sided nodal expression (Rankin et al., 2000, Wall et al., 2000). *Gdf1* may be considered a cofactor of *Nodal* since the two form heterodimers which greatly increases the activity and range of *Nodal* (Shiratori and Hamada, 2014, Tanaka et al., 2007). Although *Gdf1* appears to perform a role in left-right determination in human (Karkera et al., 2007), to date no zebrafish ortholog has been reported.

Right-sided antagonism is also critical for normal organ situs around the time when NODAL is expressed. *Cerl2* (*Dand5*) pre-empt Nodal expression, and is predominantly right-sided around the node (Figure 3). *Cerl2* antagonises *Nodal* function and null mouse mutants present with bilateral or right sided *Nodal* expression (Marques et al., 2004). The zebrafish homolog *charon* is initially bilateral, but switches to right-sided by the 8-10 somite stage (Lopes et al., 2010). *Charon* binds directly to southpaw (zebrafish nodal) and disruption of this gene results in organ situs defects (Hashimoto et al., 2004). The interplay of both agonists and antagonists of vertebrate NODAL are thought to set up a gradient so that expression of NODAL becomes restricted to the left lateral plate mesoderm (Matsui and Bessho, 2012, Shiratori and Hamada, 2014).

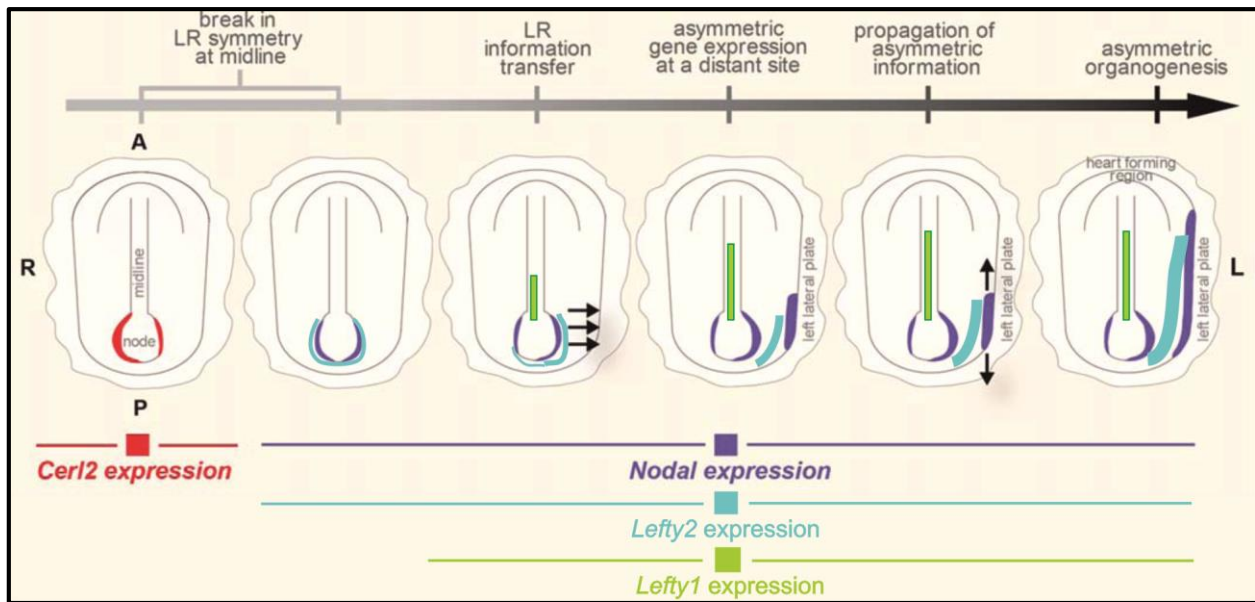


Figure 3 Left-right patterning of the lateral plate mesoderm requires several key $TGF\beta$ -related cytokines.

Schematic representation of the expression patterns displayed by mouse *Nodal*, *Cerl2*, *Lefty1* and *Lefty2* during L-R patterning. *Cerl2* is expressed predominantly on the left of the node, before expression of *Nodal*, and antagonises it. *Nodal* is initially bilaterally expressed at the node but becomes predominantly left-sided over a few hours. *Lefty2* is a *Nodal* antagonist whose expression is upregulated by *Nodal*. Much of the expression pattern of *Lefty2* overlaps *Nodal*. *Lefty1* forms part of the molecular midline barrier and is predominantly expressed in the notochord and floor plate. Figure modified from (Saijoh et al., 2014).

Despite being a left-determinant, the temporal expression of *Nodal* is fairly short, between 2 to 10 somites in the mouse (Lowe et al., 1996), but at its peak includes the entirety of the left lateral plate mesoderm. However *Nodal* activity, in combination with *Cited2*, upregulates the expression of *Pitx2*, a bicoid-type homeobox gene, in the left lateral plate mesoderm (Bamforth et al., 2004). *Pitx2* expression can be detected as late as E10.5 in mouse (Yoshioka et al., 1998) and is thought to be responsible for transmission of leftness to the organs such as the lungs and heart. Indeed *Pitx2* is expressed in the left side of the cardiac crescent (heart progenitor population) as well as the left side of the developing organ itself (Campione et al., 2001). Aberrant expression of *Pitx2* results in organs situs defects to the heart, lungs, and gut (Kitamura et al., 1999, Lu et al., 1999, Campione et al., 1999).

1.1.3 The Role of the Midline Barrier

Although *NODAL* diffuses through the lateral plate mesoderm, it is restricted to the left side of the embryo by the function of the midline barrier. The midline barrier is proposed to have both a physical and molecular component which separates the embryo left and right and prevents *NODAL* propagation. The physical midline barrier is thought to be composed of midline structures such as the notochord and floor plate. In *Xenopus*, surgical removal of the notochord and adjacent tissue resulted in a randomisation of cardiac loop direction (Danos and Yost, 1996). Furthermore, zebrafish mutants such as no tail (*Brachyury*) and floating head (*Xnot*) which are known to have defects in these midline structures (Schulte-Merker et al., 1994, Halpern et al., 1993) also display visceral organ laterality defects (Danos and Yost, 1996). The molecular barrier is composed of the *NODAL* inhibitor *LEFTY1* in mouse (Meno et al., 1998), zebrafish (Meno et al., 1999, Bisgrove et al., 1999) and *Xenopus* (Cheng et al., 2000), which is restricted to the notochord, floor plate, and adjacent left axial mesoderm. This antagonist prevents diffusion of *NODAL* across the midline and loss results in bilateral *NODAL* expression (Meno et al., 1998). Although *LEFTY1* represents a critical component of the midline barrier, its expression does not span the whole of the embryonic midline, and cannot act in anterior regions such as the brain where *NODAL* signalling is known to act (Long et al., 2003a, Long et al., 2003b). Instead other midline barrier genes have been hypothesised to be expressed in regions where *LEFTY1* is not, and recently two of these antagonists were discovered in zebrafish. *lefty2* and an unidentified BMP member were shown to be expressed in the midline and extend the barrier anteriorly and posteriorly (Lenhart et al., 2011); whether these genes truly act as midline barriers remains to be seen.

1.1.4 Organ Response to Left-Right Patterning

With the loss of *NODAL* and *LEFTY* expression before development of the visceral organs, it is thought that the *NODAL* target *PITX2* confers leftness during organogenesis (Campione et al., 2001, Logan et al., 1998). This role of *PITX2* has been shown conclusively in the heart where *PITX2* is required for looping and formation of the left atrium (Franco et al., 2014). In *Xenopus*, heart laterality can be disturbed by right-sided injection of *pitx2*, and similar situs disturbance is observed in the chicken with *pitx2* knockdown (Campione et al., 1999, Linask

et al., 2002). However, a loss of *Pitx2* in the mouse does not result in looping defects suggesting that some genetic redundancy may exist in this model (Lin et al., 1999, Kitamura et al., 1999). Instead *Pitx2* deficient mice display body wall closure defects and more interestingly right atrial and right pulmonary isomerism, suggestive that *Pitx2* signals leftness in the atrium at least (Kitamura et al., 1999). *Pitx2* does show expression within the cardiac progenitors, and in the left side of the primitive heart tube consistent with this theory. Furthermore, overexpression of *Pitx2* has been shown to upregulate *Islet1* and *Mef2c* which are early lineage markers of cardiomyocyte fate (Lozano-Velasco et al., 2011).

1.2 THE PLANAR CELL POLARITY PATHWAY

In addition to the apical / basal polarity, many tissues also display a polarity within the plane of a tissue (Karner et al., 2006b). This tissue or planar cell polarity (PCP) is critical for correct tissue development and function and has been linked to cytoskeletal rearrangement, cell migration, oriented cell division, cell fate specification and cilia formation (Winter et al., 2001, Kilian et al., 2003, Saburi et al., 2008, Yang et al., 2002, Kim et al., 2010). In vertebrates the PCP pathway has been shown to respond to the Frizzled ligands Wnt5a and Wnt11 without action of β -catenin, and is therefore also known as the non-canonical wnt pathway. Critically, the PCP pathway has also been comprehensively linked to left-right patterning of the lateral plate mesoderm during vertebrate development.

1.2.1 The Molecular Genetics of the PCP Pathway

The PCP pathway controls cell polarity within a tissue by establishing a proximal-distal asymmetry within the cell in response to global cues (Karner et al., 2006a). The ultimate readout of PCP signalling is the rearrangement of the actin cytoskeleton. The exact mechanism by which PCP signalling rearranges the cytoskeleton has not been fully elucidated, however, the most complete theory suggests that there are three layers of signalling which progress linearly to lead to cytoskeletal changes: the upstream “global” cues, the core PCP members and the downstream, tissue specific effectors (for review see (Simons and Mlodzik, 2008)). Although the PCP pathway has been shown to be well

conserved between species, much of the research has been conducted in *Drosophila* so this will be discussed first.

1.2.1.1 Planar Cell Polarity in *Drosophila*

The most upstream level of polarity determination in *Drosophila* involves the atypical cadherins *daschous* (*ds*) and *fat* (*ft*) (Yang et al., 2002). These proteins are able to form heterodimers at the cell surface in one of two orientations between cells at cell-cell boundaries (Matakatsu and Blair, 2004). The Golgi transmembrane protein *four-jointed* (*fj*) acts upon these *ds-ft* heterodimers and phosphorylates both proteins. The result of this modification is to bias the assembly of the dimers in one orientation over the other because the ability of *ft* to bind *ds* increases while the ability of *ds* to bind *ft* is weakened (Figure 4A) (Axelrod, 2009, Zeidler et al., 1999, Brittle et al., 2010, Simon et al., 2010, Strutt et al., 2004). This mechanism is thought to pattern a global tissue orientation because *Drosophila* displays opposing transcriptional gradients of *fj* and *ds* in polarised tissues (Yang et al., 2002). Once heterodimer orientation is established it has been hypothesised that these proteins may stabilise the asymmetric localisation of the core PCP proteins. When members of the upstream module are mutated the result is retention of cellular core protein polarity, but a loss of global polarity across the tissue as a whole (Yang et al., 2002, Zeidler et al., 1999).

The core PCP proteins in *Drosophila* are *frizzled* (*fz*), *dishevelled* (*dsh*), *flamingo* / *starry night* (*fmi* / *stan*), *strabismus* / *van gogh* (*stbm* / *vang*), *prickle* (*pk*) and *diego* (*dgo*), and each of these have been shown to have at least one mammalian ortholog (Simons and Mlodzik, 2008). These core PCP proteins co-localise asymmetrically at adherens junctions to the proximal or distal poles of the cell. The G-protein coupled receptor protein *frizzled* localises to the distal cell membrane and putatively forms a complex with the ankyrin repeat protein *diego* and cytoplasmic *dishevelled* (Theisen et al., 1994). At the proximal pole the four-pass transmembrane protein *strabismus* complexes with cytoplasmic *prickle* (Figure 4A). The final core PCP protein is the protocadherin-like protein *starry night* which localises to both proximal and distal poles (Gao and Chen, 2010). Once formed, these asymmetrical complexes are able to transmit polarity to neighbouring cells in a cell non-autonomous manner (Vinson and Adler, 1987, Taylor et al., 1998, Gubb and Garciabellido, 1982). This interaction with surrounding cells is thought to occur between the transmembrane proteins

strabismus, frizzled and flamingo (Strutt and Strutt, 2009, Wu and Mlodzik, 2008) and interactions between these transmembrane proteins ensures polarity of neighbouring cells coincide.

The downstream module of PCP signalling is composed of tissue-specific effectors that modify cellular morphology to ensure proper function (Karner et al., 2006a). This downstream module is the least well understood aspect of the PCP pathway but the genes involved are responsible for regulating the morphological changes appropriate to the tissue. In *Drosophila* it has been shown that the small GTPases Rac and Rho are downstream of the core proteins, and may be involved in mediating the tissue specific response to PCP signalling (Fanto et al., 2000, Strutt et al., 1997). Despite the classical hypothesis that each layer of the PCP pathway is affected by the layer above in the cascade, it has been shown that the upstream module may bypass the core proteins in certain tissues (Casal et al., 2006). In these situations the loss of core PCP proteins can be mitigated by overexpression of *ft* or *ds*, and polarisation of the tissue is rescued.

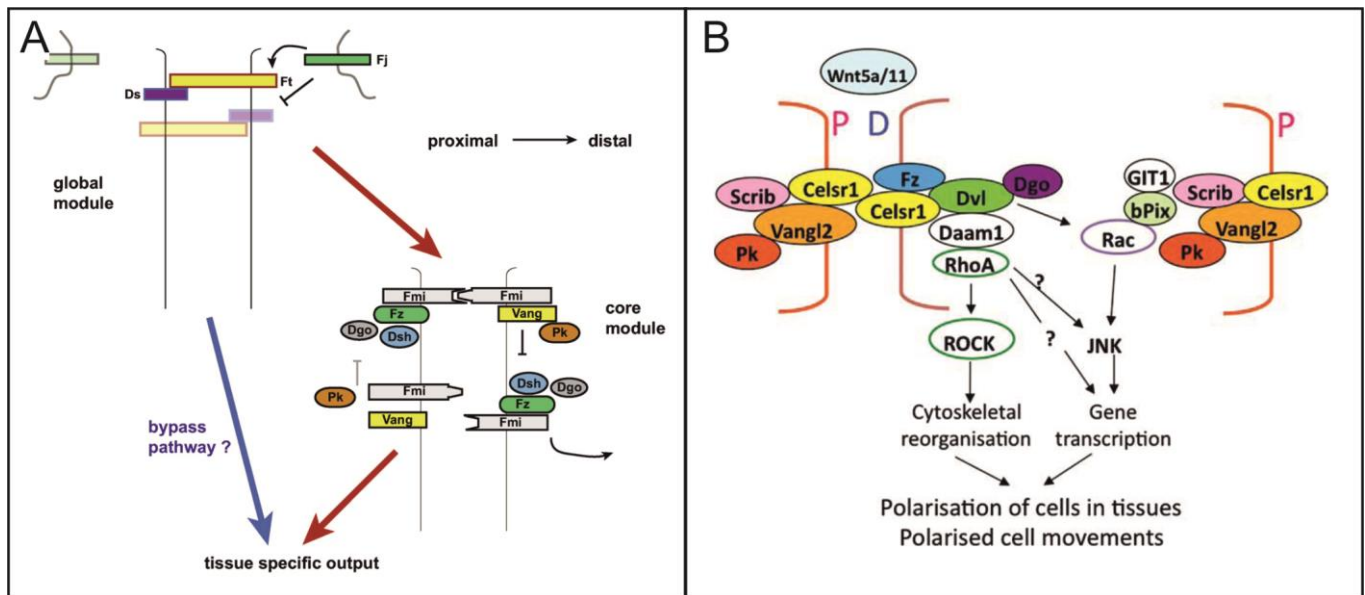


Figure 4 Schematic representation of the PCP pathway proteins in (A) *Drosophila* and (B) vertebrates.

A) The PCP pathway is composed of three discrete modules. The upstream module establishes global polarity via heterodimer formation of Ft and Ds. The interaction of Fj ensures that correct orientation of the dimer is achieved. Global cues mediate the asymmetrical localisation of the core proteins to the proximal and distal sides of the cell. This core module acts in a cell non-autonomous manner to ensure uniform polarity throughout the tissue. The core module then acts through tissue specific effectors to ensure an appropriate tissue response. In addition the global module may be able to bypass the core module and moderate tissue specific effectors directly. Taken from (Axelrod, 2009) B) In vertebrates the core proteins have also been shown to localise asymmetrically between the proximal and distal membrane however this is thought to occur in response to activation by the non-canonical WNT proteins Wnt5a and Wnt11. The core module then activates the small GTPases RhoA and Rac which themselves activate the kinases ROCK and JNK. Appropriate tissue responses are achieved through the phosphorylation of downstream targets, leading to changes in cell morphology. Taken from (Henderson and Chaudhry, 2011)

1.2.1.2 The Vertebrate PCP Pathway

Although many of the *Drosophila* PCP components are shared there are additional levels of complexity found within vertebrates. Firstly, the degree to which the Ft/Ds/Fj pathway patterns global polarity cues appears to be less pronounced in vertebrates than it is in flies. Although knockdown of mouse *Fat1*, *Fat4*, or *Dchs1* cause PCP-related phenotypes such as defects in the renal glomeruli, cystic kidney disease, shortening of the inner ear cilia and wider neural tube, the polarity disruption is modest (Ciani et al., 2003, Saburi et al., 2008, Mao et al., 2011). A more potent global cue for vertebrate polarity comes from the wingless (WNT) family glycoproteins, WNT5a and WNT11. In zebrafish and *Xenopus* the wnt5a and

wnt11 proteins have been shown to increase jnk activity through binding to frizzled, however critically there is no effect on β -catenin levels (which demonstrates that it is not acting through the canonical wnt pathway) (Kilian et al., 2003, Yamanaka et al., 2002, Garriock et al., 2005). Loss of these non-canonical wnts results in pronounced shortening of the anterior-posterior body axis (Heisenberg et al., 2000, Yamanaka et al., 2002, Kilian et al., 2003) via the disruption of convergent extension cell movements during gastrulation. Convergent extension (CE) movements involve the intercalation of cells in order to extend the anterior-posterior axis and have been shown to be regulated by the PCP pathway (Tada and Smith, 2000, Djiane et al., 2000, Gong et al., 2004). In mouse it has been shown that Wnt5a binds to Frizzled but does not act through the canonical Wnt pathway (Oishi et al., 2003). A loss of Wnt5a function leads to loss of tissue polarisation in the inner ear, convergent extension-like defects and incomplete neural tube closure defects (Qian et al., 2007), all phenotypes linked with PCP. Despite evidence in vertebrates, no convincing evidence of a wnt (wingless) contribution is seen in *Drosophila* PCP.

The core PCP module is particularly well conserved in vertebrates and asymmetric localisation to the cell membrane is observed. At the proximal side the complex of Celsr (mouse fmi), Prickle, and Vangl2 (mouse strb) is formed while at the distal side the Celsr, Frizzled, Dishevelled and Deigo complex forms (Figure 4B). The core proteins activate the downstream GTPases Rho and Rac, which themselves activate the protein kinases c-Jun N-terminal Kinase and Rho Kinase (Habas et al., 2003, Djiane et al., 2000, Goto and Keller, 2002, Curtin et al., 2003, Montcouquiol et al., 2003). The tissue-specific effects of the PCP pathway are thought to be orchestrated by these two kinases via cytoskeletal reorganisation and gene transcription.

1.2.2 PCP Signalling is Crucial for Normal Development

1.2.2.1 PCP Involvement in Ciliated Tissue

One of the most well studied examples of PCP can be seen in the epidermal tissue of the *Drosophila melanogaster* wing where each cell of the monolayer projects a single trichome (small hair). These hairs project in a distal direction, parallel to their neighbours, and disruption to tissue polarity results in randomised positioning of the trichomes (Gubb and Garciabellido, 1982).

Similar tissues in vertebrate species have also been described including the apparatus for transduction of sound – the organ of Corti – and the node (section 1.1.2.1). In the mammalian inner ear, stereocilia project from the apical cell surface and form v-shaped arrays with a single kinocilia at the apex (Kimura et al., 1964). It is critical to the function of these stereocilia that they point in the same direction as disruption of this uniformity results in defective hearing. The uniform polarisation of these cilia is under the control of the PCP pathway and several mutants of the PCP pathway such as *Vangl2*, *Celsr1*, *Frizzled*, and *Dsh* have randomisation of stereocilia orientation (Curtin et al., 2003, Wang et al., 2006b, Davies et al., 2005, Montcouquiol et al., 2003, Yu et al., 2010). The cells of the node are also ciliated and these cilia are vital for creating the nodal flow that propagates left-right patterning through the lateral plate mesoderm. Loss of several zebrafish PCP members have been shown to cause either a failure for Kupffer's Vesicle (node) to form, improper cilia formation, or misaligned polarity of the cilia (for review see (Matsui and Bessho, 2012)). Loss of core PCP genes such as *vangl2*, *pickle* and *frizzled*, as well as the downstream kinase *rock2b* cause defects of Kupffer's Vesicle and associated left-right patterning defects (Oishi et al., 2006, Wang et al., 2011, Oteiza et al., 2010, Borovina et al., 2010).

1.2.2.2 Convergent Extension and Neural Tube Closure

The role of PCP signalling is much more diverse than simply the correct alignment of hairs within the body, and disruption of PCP members has been shown to affect many developmental processes including cell migration, polarised cell division and convergent extension movements. Convergent extension movements during development have been thoroughly studied in the zebrafish and *Xenopus* models thanks to their external

development (for review see (Tada and Heisenberg, 2012)). During early and mid-gastrula stages, the mesendoermal cells undergo collective migration as a sheet, as well as intercalation of the cells which results in extension of the anterior-posterior axis and narrowing of the medio-lateral axis. This process requires considerable cellular cohesion and polarisation of the cells in the direction of movement which has been shown to require PCP signalling (Carreira-Barbosa et al., 2009, Choi and Han, 2002).

In the zebrafish a loss of the non-canonical *wnts*, *pk*, *vangl2*, and *jnk2* have been shown to cause convergent extension defects resulting in short and fat embryos (Heisenberg et al., 2000, Seo et al., 2010, Kilian et al., 2003, Veeman et al., 2003, Jessen et al., 2002, Carreira-Barbosa et al., 2009). In *Xenopus* convergent extension defects are also observed in PCP mutants and are often associated with neural fold closure defects (Goto and Keller, 2002, Wallingford and Harland, 2002), a process which involves elevation of the neural fold, migration of the epithelial and mesenchymal cell sheets and fusion at the embryonic midline (Sadler, 1998). The failure to close the neural tube due to PCP pathway disruption is conserved in the mouse (including in *Jnk1*^{-/-} *Jnk2*^{-/-} mice), and also human *VANGL2* mutations have been described with presentation of neural tube defects (Curtin et al., 2003, Wang et al., 2006b, Lei et al., 2010, Hamblet et al., 2002, Kuan et al., 1999). Although neurulation does not occur in *Drosophila*, a similar process of dorsal closure does occur. Dorsal closure also requires convergence of two cell sheets at the midline which fuse, in a process which resembles that of neural tube closure. In *Drosophila*, PCP mutants such as of the frizzled and basket (*jnk*) orthologs display a failure of dorsal closure and it has been suggested that the mechanisms by which these two processes occur are shared between species (RiesgoEscovar et al., 1996).

1.2.2.3 Participation of PCP in Heart Organogenesis

Planar cell polarity signalling has been shown to be critical during development of several vertebrate organs (for reviews see (Karner et al., 2006a, Wu et al., 2011, Papakrivopoulou et al., 2014), however, one of the most well-studied examples is the heart. During early development of the heart, two cardiac progenitor fields are located in the left and right lateral plate mesoderm, and fuse together at the embryonic midline. In zebrafish, loss of function of the PCP member *diversin* (diego ortholog) and *dishevelled* result in failure of the

cardiac progenitors to migrate and a cardia bifida phenotype (Moeller et al., 2006, Matsui et al., 2005). Although less prevalent (~10%) cardia bifida defects are also observed in a *wnt11-R* knockdown *Xenopus* model (Garriock et al., 2005). These results highlight the importance of PCP in cell migration during formation of the early heart.

As discussed in section 1.1 the left-right patterning of the lateral plate mesoderm is responsible for symmetry breaking of the developing visceral organs. The PCP pathway is instrumental in normal development of the embryonic node, ensuring that *NODAL* expression is restricted to the embryonic left. Loss of several different PCP members have been shown to cause aberrant left-right patterning, such as in the zebrafish where a loss of PCP kinase *rock2b* results in between 30-40% of embryos displaying incorrect organ situs. In *Xenopus* also, a loss of *wnt11b* results in ~50% of embryos with absent *pitx2* expression – a key determinant in heart asymmetry (see section 1.1.4). In the mouse *Inversin* (core PCP cofactor) null there is presentation of cardiac situs defects, although in this model system there is a propensity for situs inversus totalus (mirror image) of the visceral organs (Yokoyama et al., 1993). Other mouse mutants such as the loss-of-function *Vangl2* and *Dvl2* mutants present with heart defects including double outlet right ventricle (Henderson et al., 2001, Hamblet et al., 2002) – a defect which may result from subtle left-right patterning defects (Ramsdell, 2005). However, in these models it is also notable that they possess severe outflow tract and ventricular septal defects which may indicate defects in cell migration to the developing heart (in addition or instead of a L-R defect). The link between PCP and left-right patterning is convincing, however there are many PCP mutants which do not have organ situs defects which still need to be explained. To date no link between loss of *JNK* and left-right patterning defects have been published in vertebrates.

1.3 THE MAP KINASE CASCADES

The mitogen-activated protein kinases (MAP kinases, MAPKs) are a superfamily of serine / threonine (ser/thr) protein kinases that are well conserved in eukaryotes (Krens et al., 2006a, Widmann et al., 1999). These MAPKs act through distinct signalling cascades in order to mediate the cellular response to diverse intracellular and extracellular signals including cytokines, mitogens, hormones, growth factors, UV radiation, heat shock and endoplasmic reticular stress. The ultimate outcome of MAPK activation also spans a vast diversity of cellular processes such as proliferation, differentiation, apoptosis, cytoskeletal rearrangement and migration (Goetze et al., 1999, MagiGalluzzi et al., 1997, Gururajan et al., 2005, Derijard et al., 1994, Park et al., 2005, Jono et al., 2003, Nguyen and Shiozaki, 1999, Crean et al., 2002, Yosimichi et al., 2001, Xu et al., 2008). The functional scope and diversity of the MAPK cascades has implicated them in both embryonic development and disease progression, although elucidating the exact role of each MAPK component has proven complex.

In mammals the MAPKs may be split into four families: extracellular signal-related kinase 1/2 (ERK1/2), p38, c-Jun N-terminal kinase (JNK) and ERK5. Broadly speaking the ERK1/2 cascade has roles in regulating cell proliferation and differentiation, whereas JNK and p38 mediate apoptosis in response to cellular stress, and ERK5 has roles in both proliferation and stress responses. However, some functional overlap exists between these MAPK cascades, for example JNK activation may promote proliferation of hepatocytes and the ERK1/2 cascade has been shown to regulate apoptosis in response to cellular stress (Bacus et al., 2001, Schwabe et al., 2003). Clearly the MAPK cascades do not function in isolation but cooperate as a complete system, perhaps to ensure that the signalling is robust. Indeed, genetic redundancy is observed within the MAPK system as mouse models are able to compensate for loss of *Jnk1*, *Jnk2*, *Erk1*, *p38 β* , *p38 γ* or *p38 δ* with only very mild or no discernible phenotype observed (Kuan et al., 1999, Pages et al., 1999, Beardmore et al., 2005, Sabio et al., 2005). Conversely compound *Jnk1*^{+/-} *Jnk2*^{-/-} are embryonic lethal.

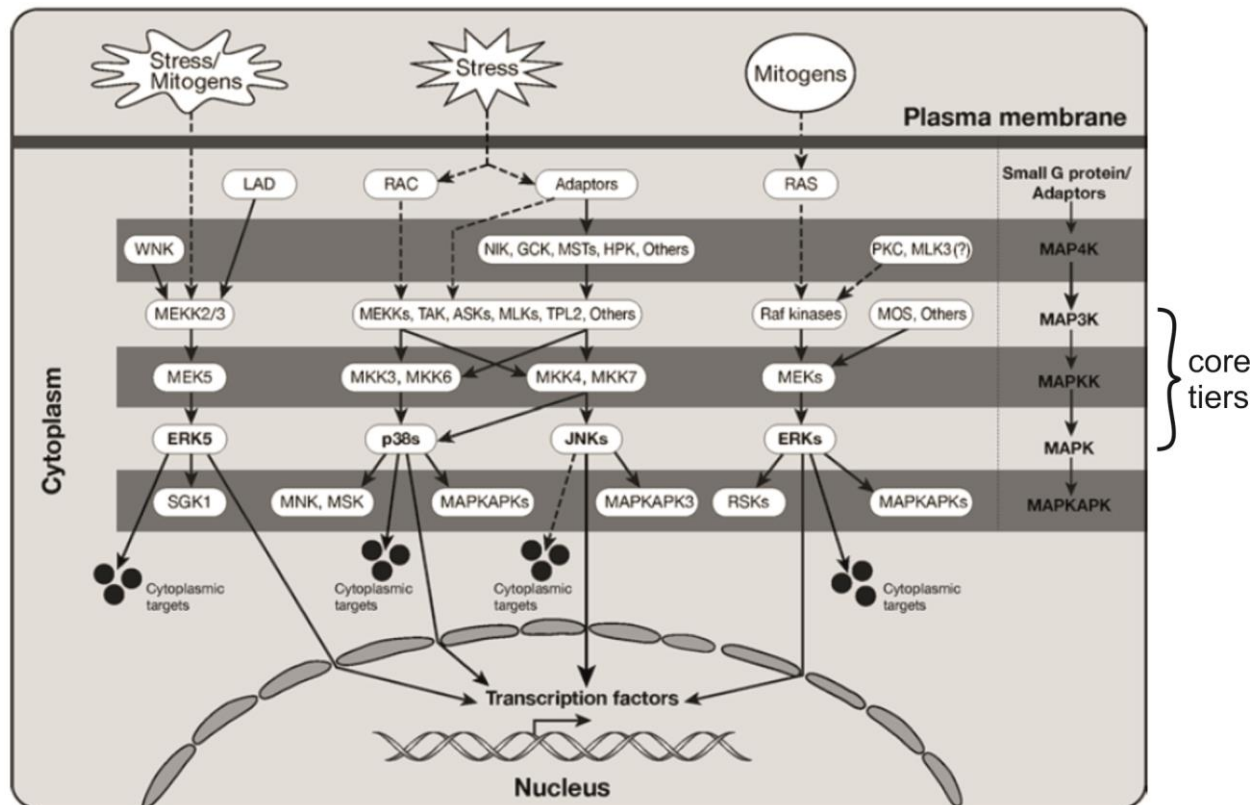


Figure 5 Schematic representation of the MAPK cell signaling pathway.

The mammalian MAPK pathway is split between four cascades: ERK5, p38, JNK, ERK1/2. The core tiers are composed of a MAP3K which phosphorylates a MAPKK (MEK), which phosphorylates the MAPK of each cascade. Cellular responses may be evoked directly by activation of cytoplasmic or nuclear targets, or through another tier of kinases – the MAPKAPKs. In some situations the core MAPK pathway may respond to cellular stress or morphogens directly, or via small G proteins and protein adaptors, which transmit the signal through MAP4Ks. The MAPK pathway has been linked to numerous cellular processes including proliferation, apoptosis and differentiation. Figure modified from (Keshet and Seger, 2010).

The MAPK cascades are generally considered to consist of five protein tiers although only the three core tiers are indispensable in every scenario (Figure 5) (Keshet and Seger, 2010). The core MAPK cascades are structured so that the MAPK protein lies downstream of, and may be phosphorylated by, a MAPKK (MEK/MKK), which is itself phosphorylated by a MAPKKK (MAP3K). At each level of the cascade two sites (either serine or tyrosine and threonine) must be phosphorylated within the activation domain in order to activate the enzyme. The MEK and MAP3K proteins usually favour one cascade, for example JNK is activated by MKK4 and MKK7 (Fleming et al., 2000) which are themselves activated by MAP3Ks such as TAK and ASK. However, crosstalk between cascades has been shown

between MKK4/7 (predominantly JNK MKKs) and p38 MAPK (Dashti et al., 2001, Derijard et al., 1995) and several MAP3Ks activate both p38 and JNK cascades (Keshet and Seger, 2010). Upstream of the core cascade there are a further subset of kinases (MAP4K) which are activated by small GTPases or adapter proteins under the control of cellular stress or mitogens (Figure 5). Downstream of the core cascade there are a further subtype of kinases known as the MAP kinase-activated protein kinases (MAPKAPKs). In total there are about 70 genes which code for members of the MAPK system, and with the inclusion of each splice-variant that these genes encode for that brings the value to almost 200 pathway components (Keshet and Seger, 2010).

Once activated the MAPK proteins may act within the cytosol, or translocate to the nucleus and phosphorylate downstream targets. ERK1/2 has at least 160 substrates whereas 52 substrates have been described for JNK and similarly high numbers are expected for the other MAPKs (Bogoyevitch and Kobe, 2006a, Keshet and Seger, 2010). Considering the high number of substrates that lie downstream of the MAPK pathway ensuring that the correct cellular response is achieved requires tight regulation. Several methods of regulation have been proposed which including protein phosphatases, subcellular localisation, differential function of each splice-variant and interactions with other signalling pathways (Keshet and Seger, 2010, Raman et al., 2007, Karlsson et al., 2006). The reality is probably a contribution from each of these levels of regulation in order to invoke the correct response for each circumstance.

The MAPK cascades have also been implicated in disease progression, and although a full review of pathogenicity of this pathway is beyond the scope of this thesis it is interesting to note the link between the MAPKs and cell cycle progression. JNK and p38 control cell cycle progression through mediation of cyclin-dependent kinase and p53 (Ambrosino and Nebreda, 2001, Thornton and Rincon, 2009, Das et al., 2007, Fuchs et al., 1998) and both have been implicated in human cancers such as hepatocellular carcinoma and lung cancer (Wagner and Nebreda, 2009, Taylor et al., 2013, Huynh et al., 2003). Furthermore JNK activity has been shown to initiate apoptosis of cardiomyocytes during ischemic heart disease, and may be a therapeutic target for diseases such as atherosclerosis and cardiac infarction (Wei et al., 2011, He et al., 1999).

1.4 C-JUN N-TERMINAL KINASE 1

The JNK genes are components of both the MAPK and PCP pathways although their role in PCP signaling is poorly understood. Originally identified as an oncogene when stimulated by ultraviolet (UV) exposure (Hibi et al., 1993), *JNK* phosphorylates many downstream targets including *c-Jun* (a component of the activator protein 1 complex), *p53* and *C-Myc* (critical for cell apoptosis and proliferation respectively) and *paxillin* (microtubule-associated protein 2 that helps regulate cell architecture) (Bjorkblom et al., 2005, Huang et al., 2003a, Bogoyevitch and Kobe, 2006b, Pulverer et al., 1991).

1.4.1 The Mammalian *JNK* Genes

The mammalian *JNK* family consists of three different genes: *JNK1*, *JNK2* and *JNK3*, and between them they produce at least ten different transcripts which arise from differential exon splicing (Figure 6). The splice-variants differ by their length at the 3' end (producing 46kDa or 54kDa proteins) and the inclusion of one of two different exons that contribute to the kinase domain. It has been shown that these different splice-variants have different affinities to downstream transcription factors (Gupta et al., 1996). Each JNK member contains a protein kinase domain which allows for phosphorylation of downstream targets, as well as both an adenosine triphosphate (ATP) binding site, and threonine/tyrosine (TPY) phosphorylation domain which is responsible for activating the molecule (Uniprot: P45983).

The three different *JNK* genes have also been shown to have different expression patterns in mouse, with *Jnk1* and *Jnk2* being ubiquitously expressed whilst *Jnk3* is primarily restricted to the central nervous system (CNS) (Kuan et al., 1999). There is also evidence to suggest that the three genes may have genetic redundancy as single *Jnk1* or *Jnk2* knockout mice are viable, as are compound *Jnk1* + *Jnk3* and *Jnk2* + *Jnk3* nulls. However, compound *Jnk1* + *Jnk2* null mice die before E12.5 displaying reduced forebrain apoptosis and hindbrain exencephaly, representing a failure to close the neural tube. These data demonstrates that the JNK proteins are critical for early development but are capable of compensating for the loss of one isoform.

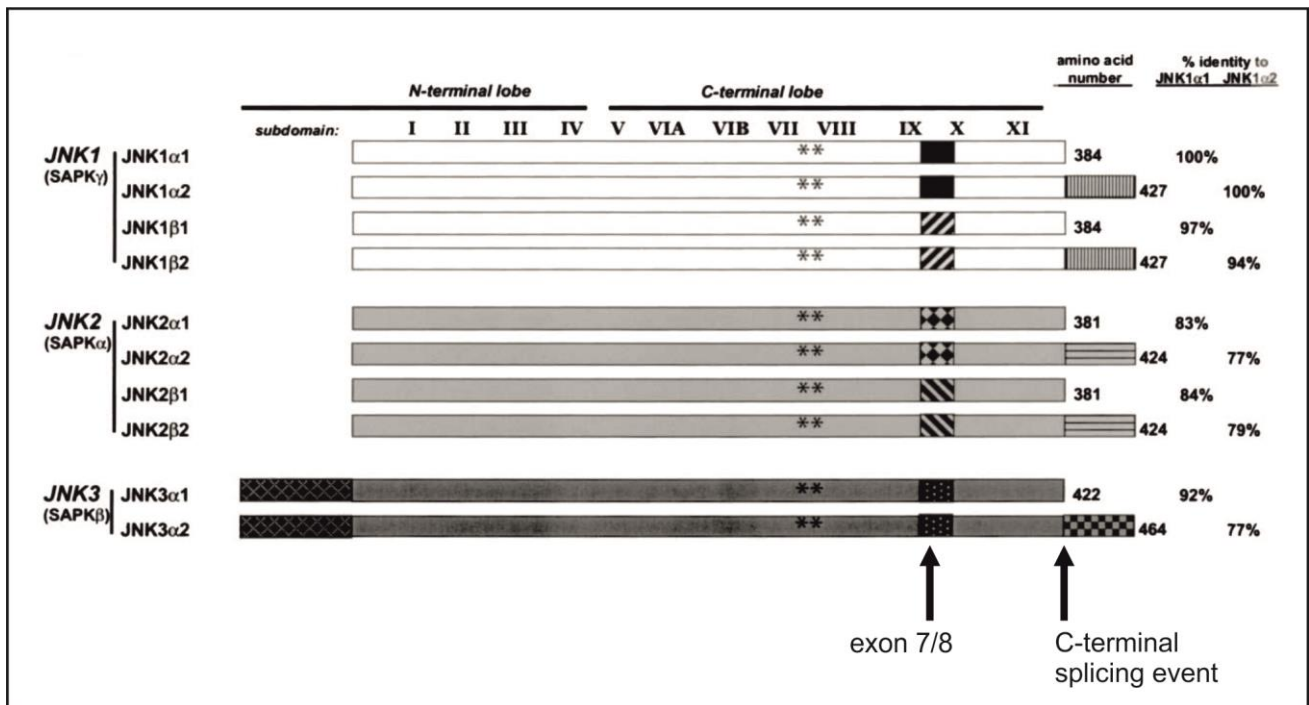


Figure 6 The splice-variants of human JNK.

Schematic representation of the three human JNK genes and their ten different transcripts: 4 JNK1, 4 JNK2, and 2 JNK3 splice-variants. Each gene has 11 subdomains that contribute to the N-terminal or C-terminal lobe of the tertiary structure. The general structure of each variant is well conserved between genes and they differ in the inclusion of either exon 7 or exon 8 and in a C-terminal splicing event which determines overall length. The asterisks donate the location of the Tyr/Thr phosphorylation sites that regulate JNK activity. Values on the far right show the amino acid sequence identity of each gene compared to either JNK1α1 or JNK1α2. Modified from (Barr and Bogoyevitch, 2001).

1.4.2 The Zebrafish Genes Appear to Correlate with Human JNK1

As has been discussed above, the MAPK genes have been shown to be well conserved between species, including the *JNK1* gene (Krens et al., 2006a, Widmann et al., 1999). As is expected, the similarities are greater in species that diverged most recently, and zebrafish show very good consistency with human *JNK1*. Human *JNK1* is found on chromosome 10 and codes for at least four different splice-variants (Gupta et al., 1996). These four variants differ in two locations, in the middle of the gene where one of two exons is included in the variant, and at the 3' end where alternative splice-acceptor site usage creates a short (1152bp) or a long (1281bp) variant. Interestingly it has been found that in mouse the middle exon usage alters the binding affinity of the variants to the downstream

transcription factors Atf2, Elk-1 and Jun (Gupta et al., 1996). The four transcripts code for proteins that are either 46kDa or 54kDa in weight. Despite experimental evidence for only four *JNK1* transcripts, the ENSEMBL Genebuild pipeline has predicted sixteen possible splice-variants that may arise from the human *JNK1* gene (www.ensembl.org ENSG00000107643).

Zebrafish possess two orthologs of human *JNK1* which are thought to have arisen from the teleost genome duplication event. Evidence for this duplication has been shown via assessment of the genes surrounding *jnk1a* and *jnk1b*, and analysis shows four genes surrounding the *jnk1* genes have also been duplicated (see Figure 9, modified from Unpublished data, Tania Papoutsis PhD Thesis). These putative paralogs (duplicate genes that have arisen from a species-specific genome duplication event) are known as *jnk1a* and *jnk1b* and are found on chromosome 13 and 12 respectively. ENSEMBL annotations predict that *jnk1a* possesses five splice-variants whereas *jnk1b* possesses four variants. Despite this duplication of the *jnk1* genes there appears to be a lot of similarity between the zebrafish and human homologs. Two of the zebrafish *jnk1a* homologs are 1284bps in length and code for proteins of 54kDa in size. Furthermore these two variants differ only by the alternate use of a middle exon, identical to what is observed in the human $\alpha 2$ and $\beta 2$ (see Figure 6). The zebrafish *jnk1b* paralog also produces two variants which show similarity to what is seen in human *JNK1*. Two of the *jnk1b* paralogs are predicted to be 1152bp and 1284bp in length and code for proteins that are 46kDa and 54kDa in size respectively (www.ensembl.com ENSDARG00000031888 and ENSDARG00000009870). These data suggest that the two zebrafish genes each possess one-half of the splice-variants known to exist in human *JNK1*, and may therefore have shared the function of the *JNK1* gene between these two paralogs.

1.4.3 The Role of the *JNK* Genes during Development

The single *Drosophila* homologue of JNK is known as *basket* (Bsk) and loss-of-function mutations within *basket* have been shown to cause dorsal closure defects during development (RiesgoEscovar et al., 1996). Incomplete dorsal closure causes mis-localisation of the internal organs as a secondary defect, however the role of Bsk in organ development can be examined via altering the function of *puckered* - a Bsk phosphatase. *Puckered* loss of function and *puckered* overexpression were found to cause left-right laterality defects in the

developing gut. The *Drosophila* anterior-midgut breaks symmetry at stage 15 by leftward tilting before rotating anterioposteriorly at stage 16. Over a third of *puckered* loss-of-function mutants displayed anterior-midgut laterality inversion, which is rescued by Bsk dominant-negative overexpression. Furthermore overexpression of *puckered* under the *hs-GAL4* promoter also results in anterior-midgut laterality defects, suggesting that a regimented dose of Bsk is required for correct organ laterality (Taniguchi et al., 2007).

In vertebrates, *JNK* has been shown to be vital for convergent extension (CE) movement, a process known to require PCP signalling. *Wnt5a* is a non-canonical Wnt that activates PCP signalling and increases the activity of *JNK* in vivo (Kilian et al., 2003). The inhibition of *Xenopus wnt5a* causes convergent extension defects in xenopus by acting through the MKK7/JNK pathway (Yamanaka et al., 2002). The *JNK* gene responsible for CE moderation has been further narrowed down in zebrafish by the use of morpholino oligonucleotides (MO). It was shown that knockdown of *jnk2* results in CE defects during development whereas this defect is not seen in *jnk1* knockdown (Seo et al., 2010). Interestingly in *Xenopus* it has been shown that *jnk1* overexpression is capable of rescuing CE defects caused by dominant negative (XENLA) *rhoA* overexpression (Kim and Han, 2005). However, this result does not necessarily contradict the zebrafish data as a *jnk2* rescue was not attempted, nor did they examine whether inhibition of *jnk1* by itself could cause convergent extension defects. This leaves open the possibility that overexpression of one form may compensate for the loss-of-function of another isoform via genetic redundancy.

The role of the *jnk* proteins during development have also been investigated in the zebrafish by the use of the pan-jnk inhibitor SP600125 (Bennett et al., 2001). Incubation of developing embryos in 5µM SP600125 between 0-30hpf caused oedema, failure of the swim bladder to inflate, reduced body length and bent tail and trunk defects. Furthermore, embryos were shown to have disorganisation of brain structure, underdeveloped retinal layers, multiple or ectopic lens development, and underdeveloped jaw formation (Valesio et al., 2013). Dosing of the embryos between 18-24hpf or 22-28hpf caused milder defects, although oedema and failure of the swim bladder to inflate was still observed. Later work confirmed the occurrence of oedema, body length reduction and underdifferentiated retinal layers when SP600125 was used at 1.4µM between 0-72hpf (Xiao et al., 2013). In addition this report showed that this treatment also resulted in undifferentiation of the gonadal cells in *jnk*

inhibited embryos, and cranial bone deficiencies when embryos were dosed with 0.8 μ M after 72hpf; at the 1.4 μ M dose there was almost 100% mortality. Interestingly the Xiao et al. (2013) paper also attempted to knockdown *jnk1* specifically with an siRNA approach, however, at this 300ng dose there was approximately 90% mortality observed before 24hpf. Those embryos which survived longer than 24hpf were shown to harbour yolk abnormalities, developmental delay and curling of the body axis, although the validity of these data is questionable considering the percentage death that was observed. Those phenotypes that have been described may be due to a general failure of development, and stress-linked signalling rather than directly due to *jnk1* knockdown.

As described previously the compound knockout of *Jnk1* and *Jnk2* in mice is lethal due to the failure to close the neural tube. Loss of a single *Jnk* gene was initially reported to have no phenotypic effect as mice were viable and phenotypically normal, suggesting that genetic redundancy may exist between the genes (Kuan et al., 1999). However, further investigation revealed that single *Jnk* knockouts do display differences to controls, although these defects are relatively mild compared to what is described in other model organisms. One of the major roles for *Jnk* signalling that has been discovered in the mouse is in the immune response. *Jnk1* and *Jnk2* null mice have been shown to be immunodeficient (Constant et al., 2000) and these *Jnk* isoforms are critical for T-cell maturation (for review see (Huang et al., 2009)). Furthermore single *Jnk* 1, 2 and 3 null mice show different explorative behaviour when presented with behavioural tests (Reinecke et al., 2013) suggestive of roles for JNK in the CNS. *Jnk3*, whose expression is primarily restricted to the brain, has been shown to have a role in controlling processes in neuronal tissue such as axonal branching (Yang et al., 2012) and retinal cell death (Fernandes et al., 2012). However, *Jnk1* and *Jnk2* have also been shown to have roles in the CNS, highlighting the fact that *Jnk3* does not exclusively control processes in the brain (Kuan et al., 1999).

Despite the severe mouse defect observed in compound *Jnk1* and *Jnk2* knockouts, no convergent extension or heart defects were described. Interestingly, knockout of c-Jun (one of JNKs major downstream effectors) is lethal due to the heart defect persistent truncus arteriosus. Furthermore, conditional knockout of Jun restricted to the second heart field lineage causes a plethora of CHDs (Zhang et al., 2013) including some which have been hypothesised as being caused by situs ambiguous i.e. septal defect, double outlet right

ventricle, and aortic arch defect. It is therefore unclear why compound *Jnk1* and *Jnk2* knockouts would not display heart defects, especially considering the laterality defect observed in *Drosophila*. It is possible that other *Jun* activators may be more important in regulating heart development, or that they are able to compensate when JNK signalling is quashed. Taken together these results suggest that the JNK genes do indeed have a role in normal development, although there appears to be little consistency between the results of different model organisms. I believe that this inconsistency comes from the relative lack of experimental evidence that has been acquired on the role of JNK in development, and indeed a lot more work is required to fully elucidate the exact roles of these genes.

1.5 ZEBRAFISH AS A MODEL ORGANISM OF DEVELOPMENT

1.5.1 Advantages of Zebrafish as a Model Organism

Zebrafish were established as a model organism in the 1970s by George Streisinger at the University of Oregon (Nüsslein-Volhard and Dahm, 2002). His first publication in 1981 detailed how to create homozygous, diploid clones (Streisinger et al., 1981). Since then the zebrafish has become an established model organism for genetics, development, pharmacology and toxicology research (Chen and Ekker, 2004, Glickman and Yelon, 2002, Hill et al., 2005, Lieschke, 2001, Morris and Fadool, 2005, Parng et al., 2002, Vogel and Weinstein, 2000). Zebrafish possess many advantages which make them favourable for the study of vertebrate development; they are small, robust and have high fecundity which allows for a single breeding pair to spawn several hundred eggs every week. Although the generation turnover of four months is not significantly quicker than other vertebrate models, the less complex organs of the embryo have developed before 5 days post fertilisation (Kimmel et al., 1995).

Zebrafish embryos are able to survive quite significant insult during development allowing for genetic and pharmacological modification that would not be possible in the mouse. For example, lack of a functional cardiac system is survivable up until 5 days post fertilisation due to diffusion of oxygen from the media (Pelster and Burggren, 1996). Furthermore developing embryos require only basic media and temperatures of between 25-33°C, making them amenable to high throughput techniques (Nüsslein-Volhard and Dahm, 2002, Kimmel et al., 1995). The external fertilisation, relatively large embryo size and transparency of embryos up until 24hpf all allow for very high resolution microscopy of live samples. Pigment production can be prevented beyond this stage by the addition of 1-phenyl 2-thiourea (PTU) into the media ensuring transparency for the duration of the treatment (Karlsson et al., 2001). As a result many live imaging techniques are permissive when using zebrafish that can track real-time changes during development or under treatment conditions (Ko et al., 2011, McLean and Fetcho, 2008, Miura and Yelon, 2011).

One of the greatest benefits for zebrafish biologists is that the whole genome has been mapped to a high standard, annotated and is maintained by the European Molecular Biology Laboratory (EMBL). The zebrafish genome (completed in 2009) contains >26,000 genes

found on 25 chromosome pairs (www.ensembl.org) (Flicek et al., 2014). In addition to the genetic sequence, the ENSEMBL project also provides intron/exon annotation, single nucleotide polymorphism data and prediction of alternative splice-variants. Furthermore several reverse genetic approaches have superseded the N-ethyl-N-nitrosourea mutagenesis techniques of the past, allowing for directed manipulation of target genes. Morpholino oligonucleotides (MOs) are a popular antisense technology that enable up to 85% of target mRNA to be knocked down. Injected before the 8-cell stage, MOs do not require large time-scales to generate stable, germline mutants, and provide high specificity to the gene of interest (Summerton and Weller, 1997b). Recently the clustered regularly interspaces short palindromic repeats (CRISPR) / Cas system has been introduced which is an RNA directed genome-editing system capable of causing double stranded breaks which may result in insertion-deletion mutations following nonhomologous end joining repair (Cong et al., 2013, Mali et al., 2013). The efficiency of this system to generate heritable mutations is being reported as being between 86-100% making it a powerful tool for the generation of mutant lines (Hwang et al., 2013a, Hruscha et al., 2013, Sung et al., 2014). These genetic techniques are therefore allowing for greater ability to study gene function in the zebrafish.

1.5.2 Limitations of Zebrafish as a Model Organism

One of the greatest strengths of the zebrafish model is the wealth of genomic information that is freely available from EMBL. However, zebrafish, being a teleost, underwent a genome duplication event following their divergence from mammals. The result is that many orthologs of human and mouse genes possess two copies in zebrafish (Taylor et al., 2001), known as paralogs. Where both copies have persisted, this abrogates the evolutionary pressure to conserve function of both copies and therefore there is potential for these paralogs to have partial or novel function not observed within other organisms (Force et al., 1999). Due to the higher probability of deleterious over gain of function mutations, it is believed that where both copies have persisted, there could be some subfunctionalization meaning that both copies are required to fulfil the complete function of the ancestral gene (Taylor and Raes, 2004). *Jnk1* is one gene that has maintained both duplicated copies and therefore care is necessary when extrapolating results back to human.

When using zebrafish as a model of human development there are obviously significant anatomical and physiological differences which do not permit the zebrafish to model humans in every circumstance. Although typically a lot of the core processes are conserved between distant species, certain aspects cannot be modelled. For example, the zebrafish neural tube forms via secondary neurulation (formation of a solid neural rod which later forms a central lumen) compared to by primary neurulation in mammals. Furthermore, the zebrafish heart has only two chambers, and lack separate systemic and respiratory systems. As such it is not possible to study septation of the chambers or outflow tract in this model. Despite these differences a great amount of developmental processes are conserved between zebrafish and mammals and they certainly have an important role in understanding the complexity of development.

1.5.3 Normal Zebrafish Development

1.5.3.1 The Zygote to Blastula Stage

Zebrafish oocytes are externally fertilised and thus normal development has been well characterised in the literature (Kimmel et al., 1995). When fertilised, the zygote is made up of a large vegetal portion (yolk), and smaller animal portion (first cell) (Figure 7A). The yolk persists to provide nutrition for the developing embryo until feeding begins at around 120hpf. Before the first cleavage the cytoplasm of the first cell increases in size. Due to the transparency of the zygote it is possible to see the cytoskeletal bridges projecting from the cell into the vegetal layer. These cytoplasmic bridges shuttle maternal proteins and mRNA into the cell and provide a means of delivery for morpholino oligonucleotides (MOs) (Shestopalov and Chen, 2010). The first cell cleavage occurs after approximately 40 minutes following fertilisation and each subsequent cleavage-stage division takes 15 minutes. These early cleavages happen synchronously, but are incomplete up to the 8-cell stage, as the cells do not become fully separated from one another and share cytoplasm (Figure 7B). This ensures that any administered MO will enter every cell of the embryo if injected up to the eight-cell stage (Nasevicius and Ekker, 2000).

Each subsequent cleavage is complete, fully separating each cell from its neighbour, although all cells remain in contact with the surface of the yolk until the 32-cell cycle. The

blastula stage of the zebrafish embryo is considered to be between the 128-cell stage until the start of gastrulation ($2\frac{1}{4}$ - $5\frac{1}{4}$ hpf at 28.5°C). During the early blastula stage cell divisions stop occurring synchronously and cells enter a mid-blastula transition where the G₁ and G₂ stages are introduced to the cell cycle, at the 10th cell cleavage in zebrafish. Also at the 10th division maternal-to-zygotic transition occurs when zygotic mRNA is first transcribed (Aanes et al., 2011), and the yolk syncytial layer (YSL) develops (Figure 8), a feature unique to the teleosts. The marginal cells which lie immediately adjacent to the yolk release their cytoplasm and nuclei into the adjacent yolk to form a ring of about 20 nuclei. The YSL cells continue to divide for 3 cycles and at later stages are critical for directing cell movements. The YSL cells give rise to the dorsal forerunner cells during gastrulation, and these cells later form Kupffer's vesicle (the node).

Epiboly in the zebrafish begins at around $4\frac{2}{3}$ hpf, and is the process whereby the animal hemisphere thins and expands to form an epidermal layer that will eventually surround the yolk completely. During epiboly the embryo's deep cells spread out radially, and intercalate with more superficial cells to produce a blastoderm of roughly even thickness; at the same time the yolk domes upwards underneath the advancing cells. Two populations of yolk syncytial layer cells arise during epiboly: the first remains between the yolk and animal hemispheres and is termed the internal YSL (I-YSL). Meanwhile the second population advances ahead of the spreading blastoderm and is termed the external YSL (E-YSL) / dorsal forerunner cells (DFCs) (Oteiza et al., 2008). The migration of the deep cells towards the vegetal hemisphere is dependent upon the E-YSL cells, and separation of these two cell types results in failure of the blastoderm to migrate.

1.5.3.2 Gastrulation and Convergent Extension

Gastrulation commences with the involution of the blastoderm which occurs at around 50% epiboly in zebrafish (5 $\frac{1}{3}$ hpf at 28.5°C) (Figure 7D). Gastrulation occurs despite the absence of a blastopore (as in the case of amphibians) and instead occurs around the entire margin of the advancing blastoderm, leading to a thick ring known as the germ ring. This involution produces two different cell layers known as the epiblast (superficially) and the hypoblast (internally). The cells that remain in the epiblast once gastrulation is complete become the definitive ectoderm, whereas the hypoblastic cells contribute to mesodermal and endodermal lineages. During the initiation of involution epiboly pauses, but resumes about 1 $\frac{1}{2}$ hours after the start of gastrulation. Gastrulation is typically considered as complete once 100% epiboly is reached, however, gastrulation-like cell movements are reported to continue after this time (Kimmel et al., 1995).

Shortly after involution commences there is a dorsal convergence of cells from all regions of the blastoderm. Cellular convergence occurs within both tissue layers and results in the formation of a thickened structure known as the shield (Figure 7E). The shield is critical for patterning the dorsal axis of the embryo and is equivalent to the organiser in *Xenopus*. Convergence and extension also occurs anteriorly from the shield along the dorsal midline, marking the embryonic axis. This convergent extension (CE) in combination with orientated cell division extends the embryonic axis under the control of the planar cell polarity (PCP) pathway (Gong et al., 2004). By the midpoint of gastrulation the dorsal epiblast thickens along the dorsal midline and gives rise to the chordamesoderm, a precursor of the notochord. This thickening at the anterior pole of the embryo reveals the future position of the head. At around 80% epiboly the DFCs converge into an “oval-cluster” near the vegetal pole as a precursor to Kupffer’s vesicle formation (Oteiza et al., 2008). In the posterior of the embryo a clear separation can be detected between the axial hypoblast and the flanking paraxial hypoblast. The paraxial hypoblast forms much of the somites during segmentation which will form the vertebrae and skeletal muscle of the trunk. At 100% epiboly a swelling appears at the posterior of the embryonic axis, signifying the region of the tail bud. Also at this time the dorsal forerunner cells begin to become organised and a lumen appears in the primitive Kupffer’s vesicle (Figure 8) (Oteiza et al., 2008). The distance between head and

tail bud, as well as the tail buds lifting away from the yolk can be used to stage the embryo during the next developmental stage (Figure 7F).

1.5.3.3 Segmentation Stage

When gastrulation is complete the yolk sac is totally enveloped by blastoderm and the embryo has a clear animal axis which wraps around it. Soon afterwards the somites begin to “bud” in bilateral pairs from the preaxial mesoderm in an anterior to posterior direction at a rate of two per hour (three per hour for the first six somites) (Figure 7G). During this segmentation the somites are initially separated by the formation of somitic furrows and then the surrounding tissue becomes epithelialized. Convergent extension cell migration and proliferation causes the embryonic axis to elongate, and the head and tail of the embryo grow closer to one another. Lumen growth of Kupffer’s vesicle in the tail bud increases by around 12-fold between the 1 and 4 somite stage, and ciliogenesis occurs (Oteiza et al., 2008). At around the 4 somite stage the neural keel forms, in an anterior to posterior direction via secondary neurulation, and cavitation later forms the lumen of the mature neural tube. The optic primordia can also be seen budding from the presumptive brain shortly after this stage. By the eight somite stage the early pronephros is apparent which forms the renal system. Constriction of the yolk adjacent to the developing tail causes a “kidney-bean” appearance of the yolk sac. This yolk constriction later goes on to form the yolk extension which is a cylindrical projection of the main yolk sac that runs parallel to the trunk (Kimmel et al., 1995).

Over the next few hours of development the brain rudiment forms ten swellings known as neuromeres. The anterior three neuromeres produce the diencephalon, telencephalon and mesencephalon of the brain while the remaining seven become rhombomeres. Also around this time the olfactory and otic placodes form from thickened ectoderm at the level of the neural keel which will give rise to the olfactory and auditory organs. In the trunk the older somites have begun to take on a chevron shaped appearance. At 19hpf (20 somite stage) the trunk of the embryo finally begins to straighten out away from the central yolk sac, however the head does not straighten out until much later in development. Most of the somites are chevron shaped and the first contractions appear as the muscle is innervated. The otic placode hollows out into the otic vesicle and two otoliths (sensory components of

gravity and movement) form within each vesicle. The brain ventricles also begin to inflate, independent of the circulatory system. The last timepoint at which the somites might reliably be used to stage the embryos is at 22hpf (26 somite stage) (Figure 7H) as the last somites form more slowly and vary between 30-34 pairs (Kimmel et al., 1995). At this stage the heart precursors have migrated and fused on the midline and begin to form the linear heart tube (Glickman and Yelon, 2002). The first heartbeat can be seen by around 24hpf (Figure 7I).

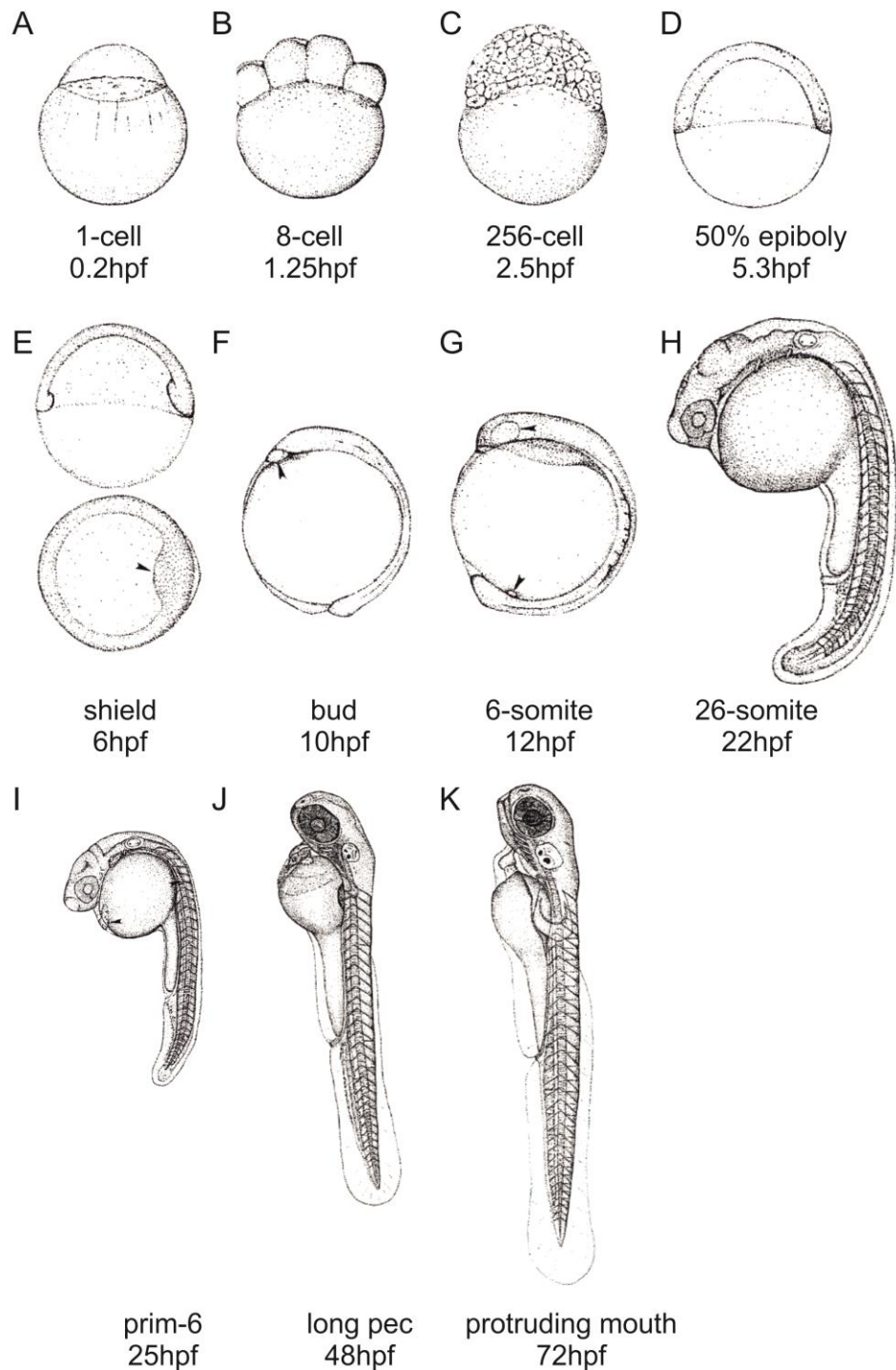


Figure 7 Zebrafish developmental series.

Schematic representation of normal zebrafish development at 28.5°C at (A) 1-cell stage, (B) 8-cell stage the latest timepoint when cytoplasm is shared between all cells, (C) 256-cell stage, (D) 50% Epiboly half way through gastrulation, (E) Shield stage – the shield (arrowhead) is homologous to the amphibian organiser, (F) tail-bud stage elongation of the anterior-posterior axis and formation of the hatching gland rudiment (arrowhead), (G) 6-somite stage displaying the eye primordium and kupffer's vesicle (anterior and posterior arrowheads respectively), (H) 26-somite stage the latest that somite number can accurately measure developmental stage, (I) 25hpf the heart (arrowhead) can be seen beating on the midline, (J) 48hpf heart looking complete and embryo is now pigmented, (K) 72hpf jaw developed and embryos begin to hatch from chorion (Adapted from (Kimmel et al., 1995)).

1.5.3.4 Heart Development

The developmental processes that lead to zebrafish heart formation are fairly well conserved with those of mammals, but the zebrafish heart represents a more simplified structure with only two contractile chambers. The cardiac progenitor cells differentiate from the anterior lateral plate mesoderm and form two bilateral cardiac primordia either side of the midline by 16hpf (Yelon et al., 1999). The first heart field cells express the transcription factor *tbx2-5* whereas the putative second heart field express *mef2cb* and latent TGF- β binding protein 3 (Lazic and Scott, 2011, Zhou et al., 2011, Chen and Fishman, 1996). An initial phase of migration brings cardiomyocytes to the embryonic midline where they fuse in a posterior to anterior manner to form the cardiac cone at around 19hpf (Yelon et al., 1999). Elongation of the cone establishes the linear heart tube which is composed of a single layer of cardiomyocytes surrounding a single layer of endocardium on the embryonic midline (Peal et al., 2011). These early phase cardiomyocytes (Figure 8) contribute to the future ventricle and inner curvature of the atrium (de Pater et al., 2009). Between 19 and 26hpf there is addition of cardiomyocytes to the venous end of the heart tube contributing to the outer curvature of the atrium from the presumptive second heart field. Later second phase cardiomyocyte migration also adds to the venous pole between 34-48hpf (de Pater et al., 2009).

Almost as soon as the linear heart tube forms the heartbeat can be seen as a peristaltic contraction in a caudal to rostral wave (Yelon et al., 1999). Between 24 and 28hpf this heart tube breaks symmetry from the embryonic midline and the caudal heart rotates over to the left side of the embryo in a process known as heart jogging (Figure 8) (Chin et al., 2000). This process is generally thought of as specific to the teleosts, however a leftward caudal heart tube movement has been reported in the mouse heart prior to looping which may be homologous (Biben and Harvey, 1997). Zebrafish cardiac jogging establishes the heart in its mature position with the majority on the left side of the body and precedes looping. Looping of the zebrafish heart involves bending of the linear heart tube at the atrioventricular canal, moving the ventricle to a more posterior position with respect to the atrium (Chin et al., 2000). Consistent with the mammalian system, looping of the heart tube acts to orientate the chambers relatively to one another in the conformation of the adult organ. By the time that heart looping has occurred (~36hpf) the heart contraction has

changed to a sequential atrial / ventricular beat (Glickman and Yelon, 2002) enabling easy identification of the two chambers.

Although the heart beat and circulation of blood occurs early in zebrafish heart development, the formation of the valve does not occur until after heart looping. The earliest events in zebrafish valve formation are cell morphology changes in the endocardium and myocardium between 36-40hpf (Beis et al., 2005, Chi et al., 2008). These cell changes coincide with increasing concentration of cardiac jelly at the atrioventricular canal, causing a constriction between the two chambers, and forming the presumptive endocardial cushions (Peal et al., 2011, Walsh and Stainier, 2001). Cardiac jelly is an extracellular matrix which resides between endocardial and myocardial cell layers and contains collagen, proteoglycans and hyaluronic acid (Little and Rongish, 1995). By 55hpf the primitive valve has begun to form and consists of about 20 endothelial cells which continue to develop until 28 days post fertilisation (Peal et al., 2011, Beis et al., 2005).

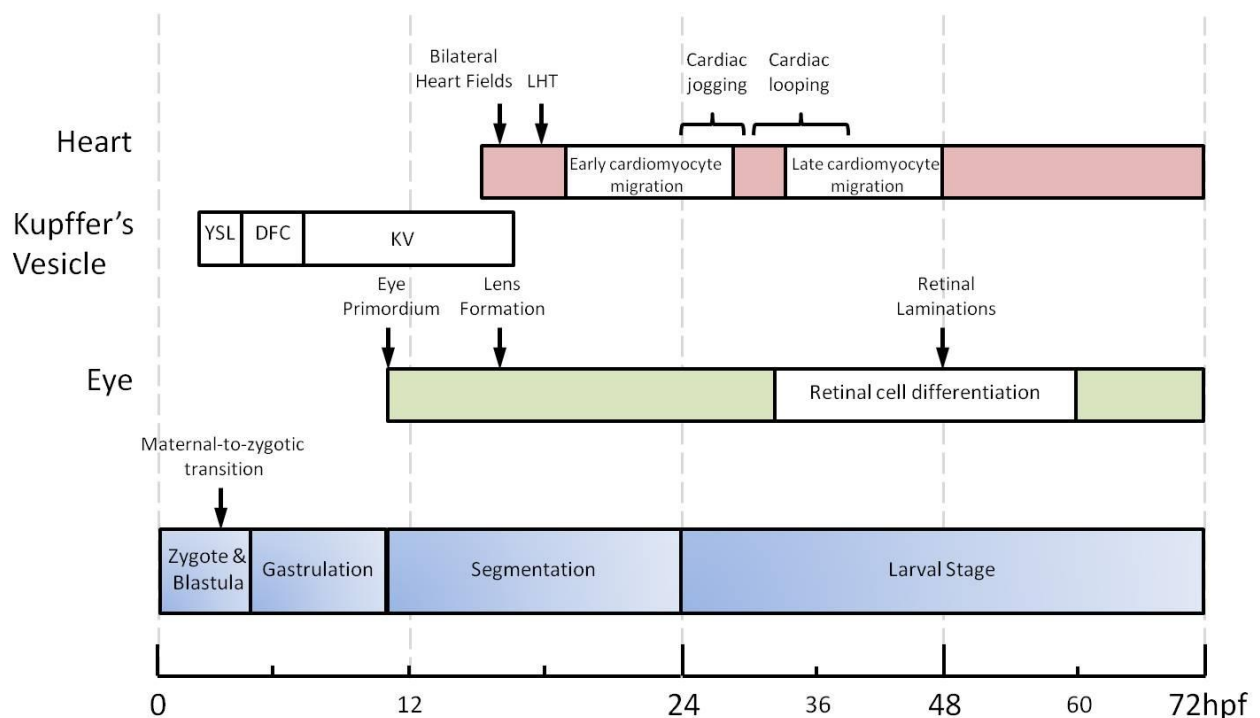


Figure 8 Zebrafish Developmental Timeline

Schematic depicting major developmental events during zebrafish development between 0 and 72hpf. Zebrafish development has been grouped into stages by (Kimmel et al., 1995) dependent upon major developmental events (blue boxes), and at 28.5°C these events show strict temporal regulation. Above is represented major developmental events in development of the heart, Kupffer's Vesicle and the Eye, that are important in this thesis, as well as the time at which they occur. LHT=linear heart tube. YSL=yolk syncytical layer differentiation and migration. DFC=dorsal forrunner cell (node progenitors) migration. KV=Kupffer's Vesicle formation and duration.

1.5.3.5 Somite Development

During development, all vertebrate species display a stage where segmentation occurs through the trunk along the anterior-posterior (AP) axis. This segmentation occurs within the preaxial mesoderm to form discrete bilateral pairs of somites (Stickney et al., 2000). Somites form adjacent to the axial mesoderm (tissue which contributes to the notochord and neural tube) and is reliant upon signalling from this tissue for correct somite formation. In zebrafish the segmentation period occurs between ~10 and 24hpf (Figure 8) with somites “budding” sequentially in an anterior to posterior manner at a rate of approximately 2 somites per hour (Kimmel, 1995). Epithelialisation at the borders of the somites results in

segmentation by the somitic furrows, a process which is strictly regulated by a molecular oscillator known as the segmentation clock (for review see (Holley and Takeda, 2002, Pourquie, 2003)).

The embryonic somite is composed of three compartments – dermatome, myotome, and sclerotome that give rise to the dermis, skeletal muscle and axial skeleton respectively (Rida et al., 2004). The myotome of the anamniotes such as the zebrafish is much larger than that of the higher vertebrates, due primarily to the increased support afforded by the surrounding water (Scaal and Wiegrefe, 2006). This myotome goes on to form slow muscle fibres (SMFs) which develop exclusively at the superficial surface of the somite and the fast muscle fibres (FMFs) which develop in the remainder of the myotome (Chong et al., 2009). Slow muscle fibres differentiate from an axial mesoderm lineage adjacent to the notochord and are patterned by sonic hedgehog signalling (Barresi et al., 2000, Blagden et al., 1997). These SMFs then migrate to the outer edge of the somite until they surround the FMFs. A thin layer of these SMFs runs through the somite in the coronal plane, separating the somites into dorsal and ventral hemispheres. This population of cells composed of pioneer slow muscle cells is known as the horizontal myoseptum and contributes to the chevron shape of the somites; in the absence of SMFs the somites take on a u-shaped appearance (van Eeden et al., 1996). Interestingly, the number of slow-muscle cells is dependent upon convergent extension movements that bring the putative SMF cells into contact with the notochord. Failure of CE results in fewer cells being driven down the SMF fate, and cause reduced numbers of these cell types and can result in failure to establish the horizontal myoseptum (van Eeden et al., 1996, Yin and Solnica-Krezel, 2007).

1.5.3.6 Eye Development

The bilateral optic vesicles develop from the forebrain around 12hpf and invaginate to form the optic cup between 16hpf and 22hpf (Kimmel et al., 1995, Fadool and Dowling, 2008, Li et al., 2000). The inner layers continue to proliferate to form the 1 glial and 6 neural cell types that make up the retina. The cornea and lens develop from the overlying ectoderm at around 16-18hpf (Zhao et al., 2006) and lens detachment is achieved by apoptosis of the surrounding cells. The first differentiation of retinal cells (ganglion cells) occurs at around 32hpf and these form part of the inner most layer of the eye. The last cells to differentiate

(bipolar cells) do so after 60hpf (Figure 8), and the first responses to visual cues occurs after almost three days (Easter and Nicola, 1996). Pigmentation of the retinal pigmented epithelium can be detected by light microscopy by 42hpf and the different retinal laminations are achieved by 48hpf (Kimmel et al., 1995, Fadool and Dowling, 2008) As in mammals the retinal lamina are composed of three nuclear layers – the photoreceptor, outer nuclear and ganglion layer – that contain the retinal cells, with the two intermediate layers – inner and outer plexiform layers – containing the cellular processes.

1.5.1 The Current *jnk1* Genetic Model

1.5.1.1 The Nomenclature Usage of Zebrafish *jnk1*

The scientific literature has gone through several different naming iterations for the *JNK* family genes since they were first identified (Hibi et al., 1993). In human the contemporary naming convention for the three different genes is *MAPK8 (JNK1)*, *MAPK9 (JNK2)* and *MAPK10 (JNK3)*. However, for this body of work I will refer to the genes as *JNK1*, *JNK2*, and *JNK3* to ensure that there is a clear distinction between the *JNK* genes and the wider mitogen-activated protein kinase (*MAPK*) family to which they belong. Zebrafish possess four orthologous *JNK* genes: *jnk2*, *jnk3* and two *jnk1* genes. The two orthologs of human *JNK1* are thought to have arisen from the teleost genome duplication event (Taylor et al., 2001). If these two genes have indeed resulted from a duplication event then the standard naming convention would be *jnk1a* and *jnk1b* (www.zfin.org). Evidence to support the two zebrafish *jnk1* genes being paralogs (duplicate genes that have arisen from a species-specific genome duplication event) was found by a previous student in our lab (Unpublished data – Papoutsis, 2011 PhD Thesis). This data shows that four genes that flank the *jnk1a* gene are duplicated in the same flanking position around the *jnk1b* gene (Figure 9). Comparatively *jnk2* contains only one, and *jnk3* contains two duplicated genes in the surrounding region of the chromosome.

In this thesis standard naming conventions for human and mouse nomenclature is observed, including the use of italics and capitals for gene symbols and protein products i.e. (HUMAN) *JNK1* and JNK1, (MOUSE) *Jnk1* and JNK1. Zebrafish standard nomenclature is an all lower case and italicised gene symbol with the protein name having a single capital without italics

i.e. *jnk1* and Jnk1. Where other species are mentioned the gene name is prefixed by the common species abbreviation in parentheses (<http://www.uniprot.org/docs/speclist>). The only exception to this is for *Drosophila melanogaster* which has a single JNK ortholog known by its locus name “basket” (*bsk*)

(http://flybase.org/static_pages/docs/nomenclature/nomenclature3.html#11.1).

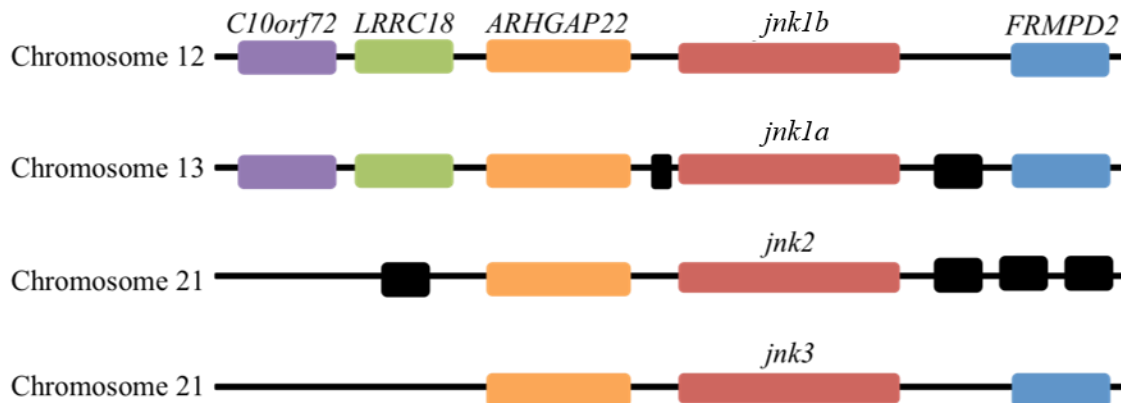


Figure 9 Similarities in the Chromosomal Regions Surrounding the Four *jnk1* Genes Suggests that *jnk1a* and *jnk1b* may have Arisen from a Duplication Event.

Modified from Papoutsis, 2011 PhD Thesis. Examination of the flanking regions of the four zebrafish *jnk1* genes reveals that several genes are duplicated between the different chromosomes. Four of the genes flanking *jnk1a* possess duplicates that flank *jnk1b*, whereas there are only one and two duplicated genes that flank the *jnk2* and *jnk3* genes respectively. This high similarity between the surrounding regions of *jnk1a* and *jnk1b* suggest that they are more closely related to one another than to the other *jnk* genes, and is consistent with two genes that have arisen through a genome duplication event. Genes are represented as coloured boxes where there also exists a duplicate gene on another chromosome. Black boxes are genes that are not duplicated.

Species	Gene Symbol	AKA	Protein Symbol
Human	<i>JNK1</i>	<i>SAPK1 / MAP8</i>	JNK1
Mouse	<i>Jnk1</i>	<i>Sapk1 / Mapk8</i>	JNK1
Zebrafish	<i>jnk1a</i>	<i>mapk8a</i>	Jnk1
Zebrafish	<i>jnk1b</i>	<i>mapk8b</i>	Jnk1
Xenopus Laevis	(XENLA) <i>jnk1</i>		(XENLA) Jnk1
Chicken	(CHICK) <i>jnk1</i>		(CHICK) Jnk1
Drosophila	<i>bsk</i>		Bsk

Table 1 Naming conventions for the JNK family homologues.

Human, mouse and zebrafish standard naming conventions are conserved when referring to gene names and protein products. Where other species are referenced they are prefixed by their common species abbreviation in parenthesis, as described on (<http://www.uniprot.org/docs/speclist>). The single *Drosophila* JNK is referred to by its locus name “basket”.

1.5.2.1 Gene Structure and Splice-Variants

The Zebrafish Genome Project includes two putative orthologs of human *JNK1* in the current build (Zv9 release 77), which is accessible via the ENSEMBL website (http://www.ensembl.org/Danio_rerio/Info/Index). The database provides comprehensive data on these two protein coding genes: *jnk1a* (ENSDARG000000031888) and *jnk1b* (ENSDARG000000009870), including the complete gene sequence, exon and intron annotation and a prediction of different splice-variants that arise. These data provided a strong foundation of knowledge that helped in the design of experimental reagents such as primers in later experiments. These gene annotations were automated by the ENSEMBL genebuild pipeline – a collection of different gene annotation pipelines. The genebuild pipeline aligns species-specific protein sequences to the compiled genome sequence where possible, or uses a closely related species where proteomic sequence is sparse. From these alignments the software is able to identify genic regions and predict intron-exon boundaries. In addition, cDNA and expressed sequence tag (EST) sequences are aligned to the genomic sequence and is able to strengthen evidence of gene structure, as well as identify 5' and 3' untranslated regions in some instances (www.ENSEMBL.org).

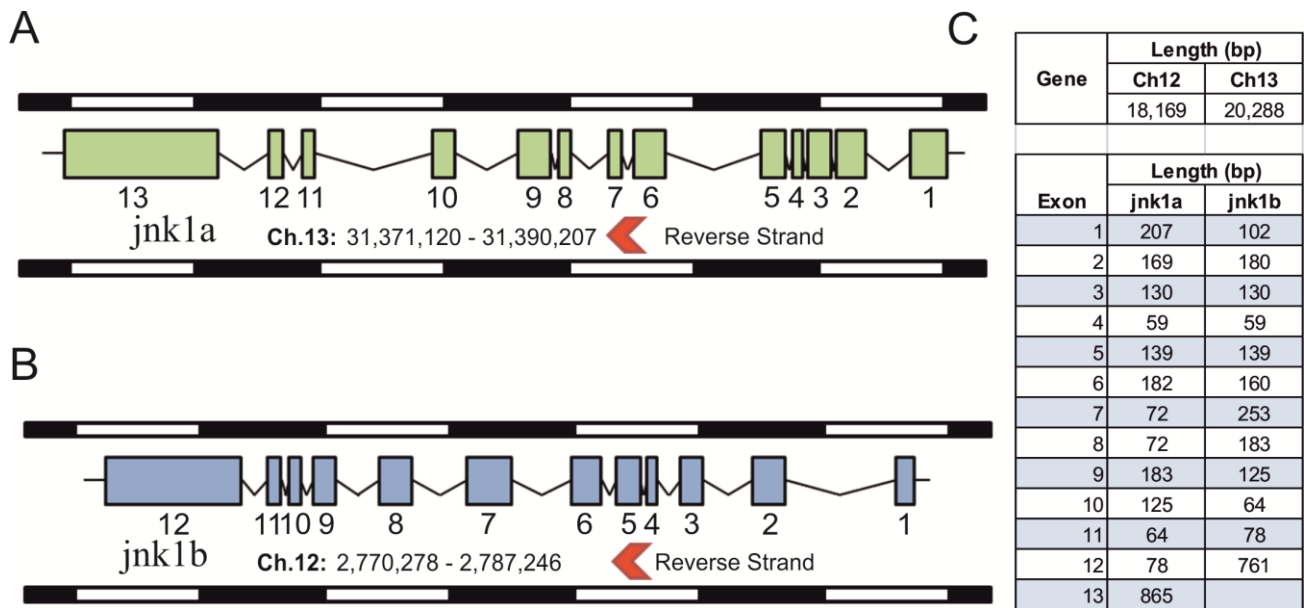



Figure 10 Schematic representation of the zebrafish *jnk1a* and *jnk1b* gene structure

A) *jnk1a* is found on the reverse strand of chromosome 13 and consists of thirteen exons B) *jnk1b* is found on the reverse strand of chromosome 12 and consists of 12 exons. The size of the exons are representative of nucleotide number. C) Table displaying the total nucleotide length of each gene (introns and exons) and the length of each exon individually. Figure based upon gene information taken from the ENSEMBL website.

The gene *jnk1a* is 20,288 basepairs (bp) long and found on the antisense strand of zebrafish chromosome 13 (Figure 10A). In total the gene possesses thirteen exons, of which twelve are predicted to contribute to the coding sequence (CDS), whereas exon 1 provides upstream untranslated region (UTR) only. Exon 7 and exon 8 of this gene are of identical length (72bp) (Figure 10C) and are predicted to be used alternatively to produce different mRNA transcripts (Figure 12A cf. “-001” and “-002”). This integration of alternative exons into the middle of the sequence is common to human *JNK1*, where the exon switch has been shown to alter transcription factor binding (Gupta et al., 1996). However, this has not been investigated in zebrafish. The final exon of zebrafish *jnk1a* is 865bps in length although most of this sequence is predicted to contribute to the 3' UTR with only 146bp contributing to the protein coding sequence (Figure 12).

The gene *jnk1b* is 18,169bp in length and is found on the antisense strand of chromosome 12 (Figure 10B). *jnk1b* consists of twelve exons, of which eleven contribute to the CDS, with exon 1 contributing only 5' UTR, and a majority of the final exon providing 3' UTR (Figure 12B). Since *jnk1b* possesses only 12 exons, it appears that one exon has been lost since the divergence from a common ancestor with humans: human *JNK1* and zebrafish *jnk1a* have 13 exons but *jnk1b* has retained only 12. When a sequence alignment is run against *jnk1a* and *jnk1b* we see that the exon which has been lost is exon 7 - one of the two “middle exons” which are alternatively spliced into the transcripts of *jnk1a*. The exonic sequence which has been retained in the *jnk1b* gene shows greater sequence identity to *jnk1a* exon 8 suggesting that the exon which has been lost is homologous to *jnk1a* exon 7 (Figure 11). This absence also explains why *jnk1b* is not predicted to have splice-variants which differ in the alternative splicing in the middle of the gene. Despite being homologous to exon 8, *jnk1b* exon 7 is much longer (253bp) than the 72bp of the *jnk1a* exon (Figure 10C); although interesting only 72bps of this long exon contribute to the CDS of two of the predicted splice-variants (Figure 12B). The other two variants are predicted to use a greater proportion of this longer middle exon which is a feature that is not observed in humans, and may therefore be unique to zebrafish.

A



```

jnk1b Exon7      1 TTGATGTCTGGTCTATTGGCTGCATCATGGCTGAAATGGTCAGAGGTAGTGTCTTGTTC
jnk1a_Exon8      1 TGGATGTGTGGTCTGTCGGCTGTATCATGGCTGAAATGGTCAGAGGTAGTGTATTATTTC
jnk1a_Exon7      1 TGGACATTGGTCTGTGGCTGCATTTGGCAGAAATGGTCCGTCACAAAATCCCTTTTC

jnk1b_Exon7      61 CTGGCACAGACCGTATCCTTACCTGGTTGTCTTTACTGTCCCATTTTAAGTGTGTCTGT
jnk1a_Exon8      61 CCGGTTTCAGATC-----
jnk1a_Exon7      61 CTGGGAGGGACT-----

jnk1b Exon7      121 TTGTTTGTGTTTGTGTTTGTGTTTATTTTACCTTAATATGTGTTGCCATTGATGCCTGAGA
jnk1a_Exon8      -----
jnk1a_Exon7      -----

jnk1b_Exon7      181 CCAAATGAAACAAAGGTAGTTTTGTTTTTAATATGATGAAAAAAAAAAAAAAAAAGTCCTT
jnk1a_Exon8      -----
jnk1a_Exon7      -----

jnk1b Exon7      241 GTTTTACTTTGGA
jnk1a_Exon8      -----
jnk1a_Exon7      -----

```

B

	% Sequence ID		
	jnk1b Exon7	jnk1a Exon7	jnk1a Exon8
jnk1b Exon7	-	79.17	84.72

Figure 11 jnk1b Exon 7 is Homologous to jnk1a Exon 8.

A) An alignment of the ENSEMBL provided exonic sequence for jnk1b exon 7 against jnk1a exons 7 and 8. The alignment shows that exon 7 of jnk1b shares greater sequence identity with exon 8 of jnk1a, particularly in the region between basepairs 26 and 54 (|--|). B) This greater sequence identity can be quantified by examining the percentage sequence identity. These data also reveal that jnk1b exon 7 is more similar to jnk1a exon 8 than exon 7.

A comparison of exon length between the two zebrafish paralogs revealed that seven of the exons are of identical length, suggesting that these exons may be homologous to one another (Figure 10C). This conservation of length of so many exons is also complimentary with the idea that these two genes resulted due to a duplication event. Furthermore, as discussed above, although the middle exon of *jnk1b* is 253bp long compared to the 72bp of *jnk1a*, this long exon only contributes 72bp to the CDS of several exons and may therefore be homologous to exon 8 of *jnk1a*.

The different splice-variants of *jnk1a* and *jnk1b* that appear on the ENSEMBL website have been automatically generated by the predictive ENSEMBL pipeline. The *jnk1a* gene is predicted to give rise to five different splice-variants that differ in exon usage and length (Figure 12A); three of these variants are greater than 1,500bp in length whereas two are smaller than 800bp. The three longest variants of *jnk1a* have the greatest amount of evidence supporting their existence. One of these splice-variants, *jnk1a*-001, has been shown to exist experimentally (Seo et al., 2010), and is listed on NCBI (NM_001110389). Additionally, *jnk1a*-201 is identical in the sequence of the CDS to variant *jnk1a*-001; the only differences between these two variants exists in the 5' UTR region where the -001 variant possesses more sequence upstream of the transcriptional start site (Figure 12A). If both of these variants do exist then they would code for identical proteins, but could be subject to different post-transcriptional regulation as has been shown to occur for certain genes involved in embryonic development or those that are receptive to levels of iron (Klausner et al., 1993, van der Velden and Thomas, 1999). The third long splice-variant predicted to arise from the *jnk1a* gene is variant -002. This variant has a long 5' UTR the same as variant -001 but also has a very long 3' UTR. Within the CDS the only difference that exists between *jnk1a*-002 and the other two long variants is the alternative splicing of exon 7 into the transcript, replacing exon 8 (Figure 12A). As has been discussed earlier, this process of alternatively splicing a middle exon into the transcript has been described in human *JNK1* where it also involves two exons that are 72bp long (Gupta et al., 1996). This similarity between what is observed in humans and what is predicted to occur in zebrafish therefore provides some circumstantial evidence to support the existence of both -001 and -002 transcripts; however sequencing of different zebrafish transcripts is required for confirmation.

Although evidence can be found for the existence of the long *jnk1a* splice-variants, no published research supports the existence of the two predicted short variants. Variant *jnk1a*-004 is the shortest variant predicted at only 421bp and represents an incomplete transcript (Figure 12). ENSEMBL lists variant -004 as “CDS 3’ incomplete” because it has arisen from an incomplete clone during the genome sequencing, and is subsequently missing sequence at the 3’ end. The real transcript may therefore be much longer than what is shown here. Variant *jnk1a*-003 is 746bp in length but is not predicted to be protein coding (Figure 12). This transcript is also predicted to retain some exonic sequence (N.B. not shown in Figure 4).

The gene *jnk1b* is predicted to give rise to four different splice variants which differ in length from each other. *jnk1b*-001 is 2,059bp long, including a large 3’ UTR region, and is translated into a 384 amino acid protein (Figure 12B). This splice-variant has been shown to exist experimentally (Krens et al., 2006b) and is listed on NCBI (NM_131721), as well as having a human ortholog. *jnk1b*-002 is a shorter DNA sequence of 1,287bp but is not predicted to have any 5’ or 3’ UTR and is translated into a 428 amino acid protein. The longer open reading frame (ORF) of variant -002 results from a “skipping” of 5bp at the start of the final exon (Figure 12B arrow) but no experimental evidence for this zebrafish transcript have yet been published. However, there has been a human ortholog described (N.B. ortholog is 427 amino acids in length) which shows the same skipping of 5bp at the start of the final exon. This splicing event represents the presence of an alternative splice-acceptor site within the final exon which allows for a short and long variant to be transcribed (Gupta et al., 1996). There is therefore circumstantial evidence to suggest that this variant does exist in zebrafish.

Both of the remaining predicted variants (*jnk1b*-003 and -201) start identically to variant *jnk1a*-001 but use a larger amount of exon 7. As described earlier, exon 7 of *jnk1b* is 253bp long – much longer than the 72bp of exon 7 and 8 in *jnk1a*. Variants *jnk1b*-003 and -201 are predicted to transcribe larger regions of this exon before reaching a STOP codon within this exon. Interestingly the -201 variant is also predicted to skip 4bp within the middle of exon 7 (Figure 12B arrow) in a splicing event reminiscent of what is seen in variant -002. However, no published evidence of these variants or known orthologs exist.

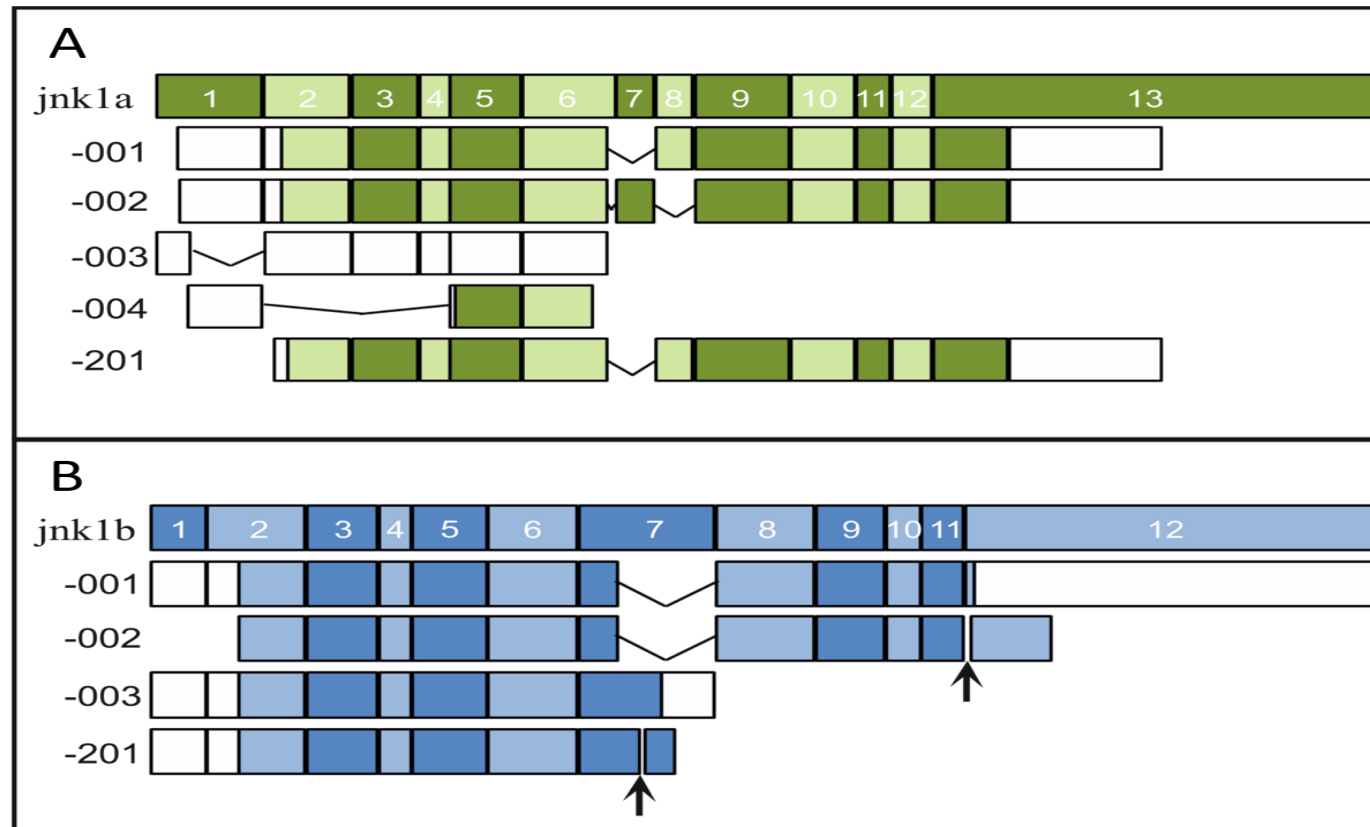


Figure 12 Predicted Model of Zebrafish jnk1 Transcription.

Schematic representation of the ENSEMBL predicted jnk1 transcripts where length is representative of basepair length. The exons of each gene are numbered and alternate exons are represented in light and dark shades. Where regions of UTR are predicted these are coloured in white. A) Top line is a model of the jnk1a gene exonic sequence displaying all thirteen exons. Below shows the five different splice-variants predicted to arise, each is accompanied by their numerical code designated on the ENSEMBL site. B) The top line shows a model of the jnk1b gene exonic sequence with all twelve exons. Below the four predicted splice-variants are shown with ENSEMBL designated codes. The arrows (→) depict where bases are skipped in the two 3' splicing events. Both result in a frame-shift and longer open reading frame. All information for this schematic has been taken from ENSEMBL Zv9 release 77 (jnk1a [ENSDARG00000031888], jnk1b [ENSDARG00000009870]).

1.5.3 The Expression Pattern of *jnk1*

The expression pattern of a gene shows when the gene is being actively expressed in the cell, and can be informative about function. Unfortunately, there is little known about the expression pattern of zebrafish *jnk1*, and even less about differences in expression between splice-variants. To gain some insight into zebrafish expression I therefore examined the limited literature as well as what was known about orthologs of *jnk1*.

1.5.3.1 Expression of Homologous *jnk1* Genes

Very few papers deal with the topic of *JNK1* expression, however those that exist broadly agree that the gene is ubiquitously expressed during development: mouse (Kuan et al., 1999), *Xenopus* (Yamanaka et al., 2002), and in adult tissue: human (Derijard et al., 1994). A majority of the focus of *JNK1* expression has been centred on the brain in mouse (Sabapathy et al., 1999) and the skeletal muscle of *Xenopus* during somitogenesis (Yamanaka et al., 2002) however there is no consistency between species of a single organ or developmental process that is most reliant on *jnk1* function.

1.5.3.2 *jnk1* Expression in the Zebrafish

In Krens et al. (2006) it was shown by wholemount in situ hybridisation that zebrafish pan-*jnk1b* expression (all splice-variants) is primarily restricted to the brain and gut at 24 and 48hpf (Krens et al., 2006b). This result was unexpected because it differs from what is observed in mouse and frog where expression was shown to be ubiquitous during development. The Krens et al. paper also utilised reverse transcription PCR (RT-PCR) to measure mRNA abundance during development, and showed that pan-*jnk1b* has weak maternal inheritance but is expressed strongly thereafter up to about 18hpf (Krens et al., 2006b). Expression of *jnk1b* later in development falls to low levels, although by adulthood the abundance is once again high (adult tissue type not stated). Since different tissue types were not examined during the developmental time series it is not clear whether these RT-PCR results support the in situ findings, although it does suggest that this gene may be important during early development. Within our own lab in situ hybridisation analysis of pan-*jnk1b* (using a newly generated riboprobe) showed ubiquitous expression within the

embryo at 24hpf but a more restricted pattern by 36hpf- anteriorly in the embryo, and with very clear staining in the heart, gut and head (Unpublished data – Papoutsis, 2011 PhD Thesis). These results do not match exactly what was shown by Krens et al. or what has been shown to occur in other species. These data highlight some uncertainty in the expression of *jnk1b* during zebrafish development.

More recently an in-depth examination of *jnk1b* expression patterns was conducted by Xiao et al. (2013) where both immunoblotting and RT-PCR were utilised in order to determine *jnk1b* expression over development and in adult zebrafish tissues (Xiao et al., 2013). This paper showed that expression of *jnk1b* mRNA is very variable during the course of development, particularly between 5 ¼ hours post fertilisation (hpf) and 10hpf where expression drops about three-fold, and also between 11 ⅔ hpf – 16hpf where there is an ~six-fold increase. Conversely the western blots appeared to show that protein levels of Jnk1 (the antibody bound to both the Jnk1a and Jnk1b proteins) start low due to maternal inheritance, but increase steadily during early development and reach a moderate and stable level by brain differentiation stages (<24hpf). These protein levels (although they represent the combined abundance of protein from both genes) did not replicate the variability of the mRNA levels. This discrepancy between results may be caused by the methodology of the two experiments, since the western blot measured protein from both paralogs of *jnk1*, whereas the RT-PCR measured only the contribution of *jnk1b*. However it does seem unlikely that the protein contribution of *jnk1a* would be able to compensate for the sharp rises and falls that were shown in the *jnk1b* transcript level, and therefore retain a steady protein band on the blot. I believe that this discrepancy therefore highlights the importance of considering the role of both *jnk1* paralogs within my own analyses. The Xiao paper also examined the expression of pan-Jnk1 within different adult tissues by western blot. The results suggest that expression is high in heart, muscle, liver and ovary with low levels in kidney and negligible levels in the testis (Xiao et al., 2013). Interestingly the blots resolved only one band for Jnk1 protein despite multiple different sized products being predicted by the ENSEMBL pipeline. Since the authors do not state what antibody was used, it is difficult to know why this may be the case, but it could be binding to only certain splice-variants, and not to others.

The published work on the expression pattern of the zebrafish *jnk1* paralogs is incomplete and contradictory. I have aimed to address this problem in this Thesis and improve the knowledge of expression of *jnk1* in the zebrafish.

1.5.4 The Functional Domains of the jnk1 Protein

Although no information specifically about zebrafish Jnk1 protein functional domains exist, there is far more research on the human and murine forms of the protein. Analysis of the human and mouse JNK1 proteins on UniProt (<http://www.uniprot.org> HUMAN - P45983, MOUSE - Q91Y86) reveals that there are several functional domains within the amino acid sequence. The main functional domain is a protein kinase domain that spans over 250 amino acid residues and is shared amongst all of the *JNK* genes. Within this protein kinase domain is an ATP binding domain that exists at position 55 and is necessary to phosphorylate downstream targets. The second important motif is the threonine / tyrosine (Thr/Tyr) phosphorylation site at position 183-185. This phosphorylation site is the main regulator of JNK1 activity and when both of these residues are phosphorylated the protein becomes active. Interestingly the middle exons (exons 7 and 8), which are used alternately for different splice-variants in both human and mouse *JNK1*, is present within the protein kinase domain, suggesting that it could have a role in regulating the activity of this MAP kinase.

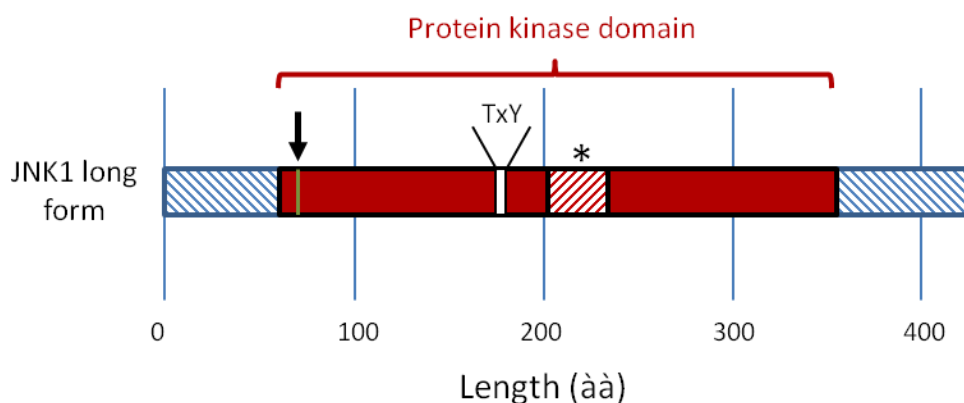


Figure 13 Schematic Representation of the Human JNK1 Functional Protein Domains.

JNK1 contains a large protein kinase domain (solid red) which spans exons 2-10. Within this domain is the ATP binding domain (arrow) and a Thr/Tyr phosphorylation motif (white). The middle exon of *JNK1* contributes to the protein kinase domain (*), and lies close to the phosphorylation domain. Figure based upon human *JNK1* structure from UniProt site (P45983).

Overall, the amount of information that is known about the structure and function of the zebrafish *jnk1* genes and their products is limited. In order to gain some insight into these genes it was therefore necessary to utilise what is known about orthologous genes and use this as a basis of what might occur in the zebrafish. Indeed there are some similarities shown between human *JNK1* and the two zebrafish paralogs i.e. *jnk1a* variants show alternative middle exon splicing, and different length *jnk1b* variants arise from an in-frame 3' splicing event. However, a far better knowledge of the zebrafish *jnk1* genes was required in order to develop a targeted morpholino. The first priority of this project was therefore to expand upon what is known about zebrafish *jnk1* and its transcripts.

1.6 SUMMARY

In this thesis the zebrafish *jnk1* genes were investigated and the role of each of these genes was examined during development through the use of morpholino oligonucleotides. This introduction has introduced the topics that are important in understanding the project, including what is currently known about the role of the *JNK* genes and the developmental processes which the PCP and MAPK signalling pathways are thought to contribute to. Firstly the concept of left-right organ asymmetry and the mechanisms of symmetry breaking were introduced in the context of humans and model organisms. Second the PCP pathway was discussed and the link that has been shown between this signalling pathway and left-right signalling in the lateral plate mesoderm. Then the MAPK pathway was considered and the developmental processes which are known to be controlled through this signalling cascade. Following this the *JNK1* gene was discussed in greater detail, highlighting what we know about the splice-variants created from this gene in man and zebrafish, and what role this gene is thought to have during normal embryogenesis. Finally the zebrafish was discussed as a model organism for developmental research, highlighting the advantages and limitations of using this model, and detailing normal embryogenesis for this species.

1.6.1 Aim of the Thesis

The aim of this thesis was to expand upon what was known about the zebrafish *jnk1* genes (*jnk1a* and *jnk1b*) particularly examining the different splice-variants that arise from the two genes. The automated annotation of the ENSEMBL pipeline predicted that the two genes each possess two splice-variants which are putatively orthologs of variants shown to arise in human *JNK1*, and confirmation that these variants have been shared between the two genes which arise from a duplication may suggest a sharing of gene function (subfunctionalization). Once the splice-variants of the *jnk1* genes had been identified I aimed to characterise the different expression of these transcripts as a way to identify if they had functional roles in different tissue-types or at different times during development.

The second major aim of this thesis was to develop a *jnk1* morphant knockdown in the zebrafish in order to determine which developmental processes and which organs required the *jnk1* genes for normal development. Once doses suitable for experimentation were determined I aimed to look at specific organ development, with a particular emphasis on the heart, to determine what changes were affected in embryos with knockdown of the *jnk1* genes. It was also hypothesised that the *jnk1* genes may act through the PCP pathway to control left-right patterning in the embryo, as has been shown for *rock2b* (Wang et al., 2011), and therefore organ situs was also examined.

- Investigate the existence of different transcripts that arise from the *jnk1a* and *jnk1b* genes and determine their expression pattern between different tissue and over development.
- Develop a *jnk1a* and *jnk1b* morpholino knockdown and characterise the gross phenotypic consequences of loss of these genes.
- Determine whether situs defects arise in the visceral organs of *jnk1* morphants.

CHAPTER 2 - MATERIALS AND METHODS

2.1 BIOINFORMATICS

2.1.1 Databases Used

Predicted as well as experimentally validated gene and protein sequences were obtained from freely-accessible online databases. The majority of the zebrafish genomic data was obtained from the automatically annotated ENSEMBL Zv9 assembly release 70 (www.ensembl.org). This source provided gene sequences for *jnk1a* and *jnk1b*, intron and exon structure, and predicted splice variants for both genes. Where possible these splice-variants were validated with experimentally generated CDS data uploaded to the NCBI nucleotide database (<http://www.ncbi.nlm.nih.gov/nucleotide>). This resource contains a few uploaded zebrafish *jnk1* sequences that have been characterised in journal publications. All of the protein sequences used were taken from the UniProt protein sequence database (<http://www.uniprot.org>), apart from three exceptions. Protein alignments of the zebrafish *jnk1* sequences were generated from translating the sequencing data obtained within this project. Finally the 3D rendering of human JNK1, and the contributing sequence, was obtained from the RCSB Protein Data Bank (<http://www.rcsb.org/pdb/home/home.do>). A list of all the sequences used and their accession numbers is listed below in Table 2.

Gene / Protein Name	Species	DNA / Protein	Source	Accession Number
<i>jnk1a</i>	<i>D. rerio</i>	DNA	ENSEMBL	ENSDARG00000031888
<i>jnk1a</i>	<i>D. rerio</i>	DNA	NCBI	NM_001110389
<i>jnk1b</i>	<i>D. rerio</i>	DNA	ENSEMBL	ENSDARG00000009870
<i>jnk1b</i>	<i>D. rerio</i>	DNA	NCBI	NM_131721
jnk1	<i>C. elegans</i>	protein	UniProt	Q8WQG9
jnk1	<i>D. melanogaster</i>	protein	UniProt	P92208
jnk1	<i>X. laevis</i>	protein	UniProt	Q8QHK8
jnk1	Chicken	protein	UniProt	E1C1H4
Jnk1	Mouse	protein	UniProt	Q91Y86
JNK1	Human	protein	UniProt	P45983
JNK1	Human	protein	PDB	2XRW_A

Table 2 Sources of gene and protein sequencing data plus accession numbers.

2.1.2 Gene Structure Figures

The sequencing data and genomic annotation of zebrafish *jnk1* were downloaded from the ENSEMBL database in order to create schematic representation of the genes and their transcripts. The intron-exon structure of each gene was generated in powerpoint by producing boxes that were of sizes relative to the length of the exonic sequence. These representations of the exons were then distributed at a distance apart that was an estimation of intronic distance, but was not to scale. Lines were used to represent the intronic sequence. The transcript variant figure was also designed in powerpoint. The intronic sequences were excluded and only exonic sequence was represented (without spaces). The transcript sequences were then downloaded from the ENSEMBL database and aligned in order to determine which exon, and how much, each transcript used. The exon usage of each transcript was then represented graphically by boxes of a size relative to sequence length. Lines were used to denote where parts or whole exons were skipped in the transcript.

2.1.3 DNA / Protein Alignment

DNA and Protein alignments were performed using ClustalW2 (<http://www.ebi.ac.uk/Tools/msa/clustalw2>) and Clustal Omega (<http://www.ebi.ac.uk/Tools/msa/clustalo>) websites. These programs also generate a score for sequence identity which was used to compare similarity between species. The alignment .text files were inputted into BoxShade (http://www.ch.embnet.org/software/BOX_form.html) in order to achieve the shaded figures included in this thesis. Where appropriate annotations were made to the shaded files to indicate exon number, functional protein domains etc.

To graphically represent the sequence identity between *jnk1a* and *jnk1b* at the nucleotide and protein level the sequences were aligned in Clustal Omega and inputted into JalView 2.8.1 (Waterhouse et al., 2009). The shading of the alignment was changed to “percentage identity” and the individual nucleotide/amino acid letters were hidden. For nucleotide alignment the standard blue colour was used, but this was changed to red for the protein alignment. An image file was generated from the alignment and transformed in Adobe

Photoshop® to compress the alignment of several hundred bases / amino acids so that it would fit onto an A4 page. In the final alignment the coloured regions are sequences with conserved sequence identity and gaps are regions that do not have the same sequence.

2.1.4 Functional Domain Identification

The functional domain annotation of human JNK is accessible from UniProt (P45983). Alignment of human and zebrafish *JNK1* genes revealed that sequence identity was high, and the kinase domain, ATP binding domain, Thr/Tyr phosphorylation sites were all conserved between the two species (Figure). Running the two zebrafish genes through protein domain prediction software InterProScan (<http://www.ebi.ac.uk/Tools/pfa/iprscan5/>) confirmed that these domains were conserved but did not identify any other functional domains.

2.1.5 Protein Secondary Structure

Secondary structure of the *jnk1* genes was predicted and compared by use of the JalView 2.8.1 tool JNet Secondary Structure Prediction (Waterhouse et al., 2009). This tool predicted areas of helix and sheet in the sequence and produced a graphical representation. The graphical representation of secondary structure was used in Figure 19 to estimate how well secondary structure is conserved between *jnk1a* exon 7 and 8 and *jnk1b* exon 7 and 8.

2.1.6 Protein Tertiary Structure

The X-ray crystallographic tertiary structure of human *JNK1* (2XRW_A) was downloaded from the Protein Database (<http://www.rcsb.org/pdb/home/home.do>) and opened in the freeware program Cn3D 4.3.1 for identification of which 3D structures the “middle exons” contributed to and for generation of 3D image files (downloaded from <http://www.ncbi.nlm.nih.gov/Structure/CN3D/cn3d.shtml>).

2.1.7 Tissue-Specific Expression Analysis of *JNK1* in Zebrafish, Mouse and Human

Gene expression data for human and mouse *JNK1* genes were obtained from the EBI Expression Atlas (<https://www.ebi.ac.uk/gxa>) by searching for *MAPK8* and *Mapk8* respectively. In total six adult human and six adult mouse studies were returned and analysed for this study (Table 3). The studies where expression was measured in less than five different tissues were excluded from the analysis to reduce outlying results from skewing the analysis; this meant that two mouse studies were excluded at this point. Expression results from each tissue were then taken and upper and lower quartile values were calculated over all measurements. Any tissues where expression was less than the lower quartile (Q1) was considered low gene expression and any value higher than the upper quartile (Q3) was considered high gene expression. Use of quartiles was used for this test to again prevent skew of the data since it does not assume normal distribution of the dataset.

Mouse Studies Used	Human Studies Used
Tissues - 49 FANTOM5 project - adult	Tissues - 68 FANTOM5 project - adult
Tissues - 9 in 3 strains - CD1 mus strain *	Tissues - 53 GTEx
Tissues - 9 in 3 strains - DBA/2J *	Tissues - 32 Uhlen's Lab
Tissues - 6	Tissues - Illumina Body Map
Tissues - Mammalian Kaessmann	Tissues - Mammalian Kaessmann
Tissues - Vertebrates	Proteomics - Tissues - Human Proteome Map - adult

Table 3 List of Gene Expression Studies used to Determine Tissue-Specific Expression of the mouse *Jnk1* and Human *JNK1* Genes.

*To determine the tissue-specific expression of mouse *Jnk1* and human *JNK1* genes all expression studies from the EBI Expression Atlas (<https://www.ebi.ac.uk/gxa>) to include these genes in adult tissue were analysed – twelve studies in total. An “*” identifies a study that was later discounted from analysis due to expression abundance being stated for too few tissues which would have introduced errors of data skew into the analysis.*

Once all six human and four mouse studies were analysed and low, medium or high expression was determined in each tissue of each experiment, the results were refined to include only tissues that had been analysed in the zebrafish RT-PCR: heart, skeletal muscle, testis, liver and brain. A consensus expression amount was then reached for each of the five tissues for human and for mouse. This consensus was made by comparing the value in each experiment; where $\geq 75\%$ of values were the same (e.g. low) then this value was used as

consensus (i.e. low). Where <75% of values were the same then the different values were listed (e.g. low/med). This method was therefore able to provide a qualitative estimate of gene expression in different tissues that could be compared to the qualitative densitometry results generated by RT-PCR of zebrafish tissue.

2.1.8 *In silico* Primer Characteristics and Specificity

Primers were generated manually using sequence alignments to identify regions of poor conservation between the four zebrafish *jnk1* genes. Several candidate primers were generated and the characteristics (melting temperature, GC content, dimerisation and secondary structure probability) were predicted by use of the primer design tool from Sigma-Aldrich® (<http://www.sigmaaldrich.com/united-kingdom.html>). Once suitable primers were chosen they were run through the Primer-BLAST software (<http://www.ncbi.nlm.nih.gov/tools/primer-blast/>) to determine whether they were predicted to amplify any unintended targets. Although it was predicted that the primers may amplify unintended targets between 30-380bp long, no other bands were detected in RT-PCRs except the ~500bp *jnk1* amplicons.

2.2 MOLECULAR BIOLOGY TECHNIQUES

2.2.1 Commonly Used Molecular Biology Reagents

Tris-acetate-EDTA (TAE) Buffer:

0.04M Tris-Acetate

0.001M EDTA

Tris buffered saline (TBS) / TBS-Tween (TBS-T):

50mM Tris-Hcl

150mM NaCl

Adjust pH to 7.5 with 1M HCl

Top up to 1L with ddH₂O

Add 0.1% Tween 20 for TBS-T

Phosphate buffered saline (PBS):

Made by dissolving 10 PBS tablets (Oxoid) into 1L ddH₂O

137mM NaCl

2.7mM KCl

10mM Na₂HPO₄

1.8mM KH₂PO₄

Diethylpyrocarbonate (DEPC) Water (DEPC-H₂O):

1ml DEPC (Sigma-Aldrich®) in 1L ddH₂O,

Leave at room temp in fume hood overnight,

Autoclave before use.

4% Paraformaldehyde (PFA):

40g PFA in 800ml PBS,

Dissolve at 60°C and add 1ml 1M NaOH,

Top-up to 1L with PBS and aliquot.

2.2.2 List of DNA Primers

Several primers were used in this study, and are listed below. All primers were obtained from Sigma-Aldrich®.

Gene / Binding Site	Forward Primer Sequence	Reverse Primer Sequence
Full-length <i>jnk1a</i>	AGAGAGGGATCCATGAACAAA AATAAGCGAGAG	TAGTAGCTCGAGTCATCTGCAGCAG CTCAG
Full-length <i>jnk1b</i>	AGAGAGGGATCCATGAACAGG AATAAGCGCGAG	AGAGAGTCTAGATCATCTGCAGCAG TGCAGCGC
pGEM-T Easy T7 site / SP6 site	TAATACGACTCACTATAGGG	CTATAGTGTACCTAAATAGCTTGGC
<i>jnk1a</i> exon 7	TTTGGCAGAAATGGTCCGTC	(short / long reverse primer)
<i>jnk1a</i> exon 8	GAGGTAGTGTATTATTTCCGGG TTC	(short / long reverse primer)
<i>jnk1a</i> short	(Exon 7 / 8 forward primer)	CTGCTGCACCTGTGCTAGG
<i>jnk1a</i> long	(Exon 7 / 8 forward primer)	TTGATCACTGCTGCACCTAGG
<i>jnk1b</i> exon 7	TAACGTGGATATTTGGGCTGTT	(short / long reverse primer)
<i>jnk1b</i> exon 8	GCTAACGTTGATGTCTGGTCTA TTG	(short / long reverse primer)
<i>jnk1b</i> short	(Exon 7 / 8 forward primer)	TGCTGCACCTGTGCTAGC
<i>jnk1b</i> long	(Exon 7 / 8 forward primer)	GCTCACTGCTGCACCTAGC
<i>elfa1</i>	CTTCTCAGGCTGACTGTGC	CCGCTAGCATTACCCTCC

Table 4 List of Primer Sequences

2.2.3 Standard Tissue Homogenisation Procedure

Tissue homogenisation for RNA extraction and western blotting was performed by passing the material through a gradient of needles with increasing gauges. Depending upon the biological material required, RNA or protein, the tissue was added to half the total volume of TRIzol® or laemmli buffer respectively on ice in a fume hood. Homogenisation was achieved by sucking the tissue up and down through a 19G needle and 1ml syringe for 30 seconds. This process was repeated using the same syringe with a 21G and 23G needle. The remaining TRIzol® or laemmli buffer was added (up to a final volume of 1ml TRIzol® or 400µl laemmli) and the tissue was homogenised for a further 1 minute using a 23G needle.

Homogenised tissue was used immediately for downstream methods to minimise degradation of the reagent.

2.2.4 Standard RNA Extraction Method

Total RNA extraction was performed using TRIzol® reagent (Ambion) in 1.5ml eppendorf tubes in accordance with the manufacturer's instruction. Briefly, the tissue of 40 embryos was homogenised in 1ml of TRIzol (see 2.2.1) and incubated at room temperature for 5 minutes. To the TRIzol® 0.2ml chloroform was added, the tube was vortexed and then incubated for a further 3 minutes. Phase separation was achieved at 12,000 x g for 15 minutes at 4°C, and the aqueous phase was removed by pipette. In a fresh eppendorf the aqueous phase was added to 0.5ml isopropanol and incubated on ice for 30 minutes, before RNA precipitation was achieved by centrifuging a second time. The supernatant was removed to leave the RNA pellet, and one wash in 75% ethanol was performed followed by centrifugation at 7,500 x g for 5 minutes to collect the pellet. The wash was removed and the pellet was air dried for 5 minutes. The RNA pellet was resuspended in 50µl of DEPC-H₂O and quantification was performed by NanoDrop™ spectrophotometry (see 2.2.5).

RNA clean-up was performed by addition of 110µl lithium chloride / EDTA solution, and incubation at -80°C for 48 hours. The RNA was then precipitated by centrifugation at 12,000 x g for 20 minutes at 4°C before the pellet was washed in 1ml 75% ethanol by inversion of the tube. The pellet was collected as before and air dried for 5 minutes before RNA was quantified by NanoDrop™ spectrophotometry.

2.2.5 Quantification of RNA/DNA

RNA and DNA yields were quantified by the NanoDrop™ 8000 spectrophotometer. Values of absorbance at 260nm were used to quantify the RNA/DNA abundance per sample, and 260/280 and 260/230 values were used as an indicator for contamination with co-purified agents.

2.2.6 cDNA Generation (Random Hexamers)

For the purpose of RT-PCR analysis, cDNA was generated with random hexamer primers using the High-Capacity cDNA Reverse Transcription kit (Applied Biosciences). Briefly the RNA was diluted down to 0.2µg/µl in a 10µl volume and stored on ice until used. The kit reagents were thawed and a master mix was made for as many reactions that were required as follows:

Reagent	Volume per Reaction
10x Buffer	2.0
25x dNTPs	0.8
10x Random Hexamer Primers	2.0
Multiscribe Transcriptase	1.0
dH ₂ O	4.2
Total Volume	10.0

Once vortexed, the master mix was aliquoted out to 0.2ml PCR tubes and all 10µl of dilute RNA were added to each reaction. The cDNA reactions were performed in a thermocycler under the conditions in following conditions:

Time (min)	Temperature (°C)
10	25
120	37
5	85
Pause	4

2.2.7 Gel Extraction and PCR Product Clean-up

PCR products were cleaned-up with or without gel electrophoresis and gel extraction by use of the Wizard® SV Gel and PCR Clean-Up System (Promega). Where gel extraction was required the DNA was visualised in the agarose gel by the UV transilluminator, and bands were excised with a clean scalpel blade. The gel was then weighed and dissolved in an equal amount (volume:weight) of Membrane Binding Solution at 65°C with frequent vortexing. PCR products that did not require gel extraction were added to an equal volume of Membrane Binding Buffer, and then the two methods were identical.

The melted gel or PCR product was added to an SV Minicolumn and allowed to bind at 1 minute at room temperature, before centrifuging at 16,000 x g for 1 minute. Flowthrough was discarded and 700µl of Wash Solution was added before centrifuging for 1 minute. This step was repeated but 500µl of wash buffer was used this second time, and the tube was centrifuged for 5 minutes. The SV minicolumn was transferred to a 1.5ml eppendorf tube and 50µl of DEPC-H₂O was added directly to the membrane. The column was incubated at room temperature for 1 minute before the DNA was collected in the eppendorf by centrifuging for 1 minute.

2.2.8 Full-length *jnk1* Variant Sub-Cloning

The sub-cloning of full-length *jnk1* transcripts was performed to both gain accurate sequences of the *jnk1* genes in the AB zebrafish strain, and to prove the existence of different splice-variants. The variants with the most published evidence for their existence were targeted for cloning through the use of primers designed to bind at the beginning and end of the sequence. The two *jnk1a* variants targeted were *jnk1a*-001 and -002, whereas the two *jnk1b* variants were *jnk1b*-001 and -002 (See Figure 12). In both instances only a single primer pair was required to pull out both transcripts.

2.2.8.1 Full-Length Transcript Primer Design

In order to pull out the targeted full-length transcripts of *jnk1a* and *jnk1b* only two primer pairs were required. In the case of *jnk1a* where both variants are of equal size (but differ in the middle) it is obvious that primers at both ends will be capable of pulling out both variants. The targeted variants only differ in their use of either exon 7 or exon 8 in the middle of the sequence, therefore both variants will be amplified by the primers. However, in the case of *jnk1b* where two different sized products are predicted it is not so obvious why only one primer set is necessary. The two targeted *jnk1b* variants (-001 and -002) have the same start site, however the STOP codon of variant -001 is 132bp further upstream. The reverse *jnk1b* primer was therefore designed to bind at the STOP codon of the longest variant (-002), allowing for this whole sequence to be amplified. In the case of the shorter variant (-001) the primer was predicted to bind within the 3' UTR sequence (See **Figure**

14, Appendix Figure 57) allowing for the whole CDS plus some 3'UTR to be amplified. The result of the PCR is therefore that the full CDS of both variants is successfully amplified, but a small amount of 3' UTR is also amplified in the *jnk1b*-001 variant.

In order to design the full-length primers there were several challenges that had to be considered. Firstly the primers were designed against sequence obtained from the Tübingen zebrafish strain. This ENSEMBL sequence was the only available sequence that detailed alternative splice-variants so there was no other alternative to using this sequence. However I was aware, that the primers may not have been 100% complimentary to their target within the AB strain. Secondly, the desire to obtain full-length sequences that could be transcribed to mRNA and injected into the embryo without further modifications meant that primer sites were restricted to the start and end of the coding sequence; these regions are fairly well conserved between the two paralogs so there was a risk that primers may amplify both paralogs. The sequence identity between the primers and their unintended target is between 81-89% (**Figure 14**). However, since clonal colonies were created, and each insert was fully sequenced, some cross-reactivity of the primers could be tolerated.

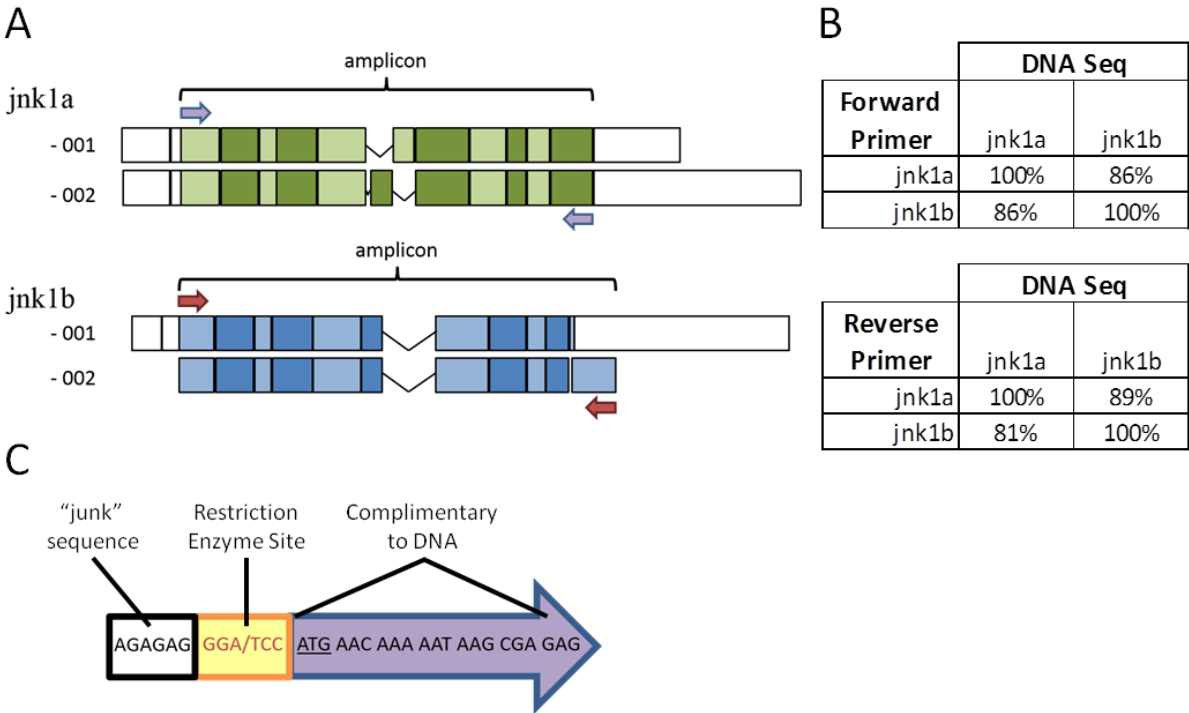


Figure 14 Explanation of the Full-Length jnk1 Primers.

A) Schematic representation of the four jnk1 transcripts that were targeted by this sub-cloning method as well as where the primers were designed to bind (arrows). The predicted amplicons are the full length sequence, plus a small amount of 3' UTR in the case of jnk1b-001. B) Table of the percentage complementarity of the primers to their target gene, as well as to the unintended paralog. The primers share between 81-89% sequence identity to the unintended paralog. C) Schematic of the various features designed within the forward primer of jnk1a. Each primer contains all three of these features.

2.2.8.2 cDNA Generation (Oligo dT Primers)

Template cDNA for the full-length transcript PCR was obtained from 40 AB zebrafish at 72hpf. This tissue was homogenised and RNA was extracted via standard methodologies. Full-length cDNA transcripts were generated via the use of oligo dT primers in a reverse transcription reaction using the SuperScript™ III kit (Life Technologies). Briefly, the reagents were thawed and into a 0.2ml PCR tube was added 1µl 10mM dNTPs, 1µl dT primers, 5µg total RNA, and DEPC-H₂O to top up to 12µl total volume. These reagents were mixed and incubated at 65°C for 5 minutes, before being chilled on ice for 2 minutes. A master mix containing 4µl 1st strand buffer, 4µl 0.1M DTT and 1µl DEPC-H₂O per reaction was made and 6µl of this solution was added to each RT reaction. The PCR tubes were then incubated at

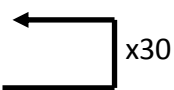
42°C for 2 minutes before 1µl SuperScript III reverse transcriptase was added, and the reactions were allowed to progress at 42°C for 1 hour. The reaction was finally terminated at 70°C for 15 minutes and the PCR products were purified by the Wizard SV Gel and PCR Clean-Up System (2.2.7).

2.2.8.3 Full-length Transcript PCR

Full-length *jnk1* splice-variants were amplified by reverse-transcription PCR prior to sub-cloning using the primers discussed in section 2.2.8.1. Reactions were performed using Phusion (NEB®) high-fidelity polymerase such that each reaction was set-up as below:

Reagent	Final Concentration
5x Phusion Buffer	1x
dNTPs	0.2mM of each dNTP
Forward Primer	0.5mM
Reverse Primer	0.5mM
cDNA	50ng
Phusion polymerase	1 unit
DEPC-H ₂ O	Top up to 20µl

Time (second)	Temp (°C)
30	98
10	98
20	72
40	72
120	72
Pause	4



Following the PCR reaction the product was purified via PCP Clean-Up System column (2.2.7).

2.2.8.4 A-tailing of PCR Products

Poly-A tails were added to full-length transcripts in order to perform T-cloning into pGEM-T Easy (Promega) vector. The products generated by PCRs using full-length primers were cleaned-up via SV Wizard columns (section 2.2.7) to remove the 3' exonuclease activity of the high-fidelity polymerase. To this cleaned-up DNA (dissolved in 50µl) was added 5.5µl of 5x GoTaq® buffer, dATP to a final concentration of 0.2M, and 1µl of GoTaq® DNA polymerase (Promega®). The reaction was run at 72°C for 10 minutes and then a further SV Wizard clean-up set was performed.

2.2.8.5 T-Clone Ligation

Ligation of the full-length transcripts into pGEM-T Easy (Promega) was performed at 4°C overnight as per the manufacturer's guidelines. Briefly, the reagents were thawed and vortexed before the experimental, one positive and one negative control reaction was set up in 0.2ml PCR tubes as below:

Reagent	Experimental	Positive Control	Negative Control
Rapid Ligation Buffer	5µl	5µl	5µl
pGEM-T Easy® Plasmid	1µl	1µl	1µl
PCR Product	3µl	-	-
Control Insert	-	2µl	-
T4 DNA Ligase	1µl	1µl	1µl
DEPC-H ₂ O	-	1µl	3µl

Reactions were incubated at 4°C overnight before bacterial transformations. For difficult ligations it was necessary to titre the quantities of plasmid and insert such that three reactions were performed per PCR reaction- 3:1, 1:1 and 1:3 vector to insert. A plasmid map for the resulting cloning products is shown in Figure 15.

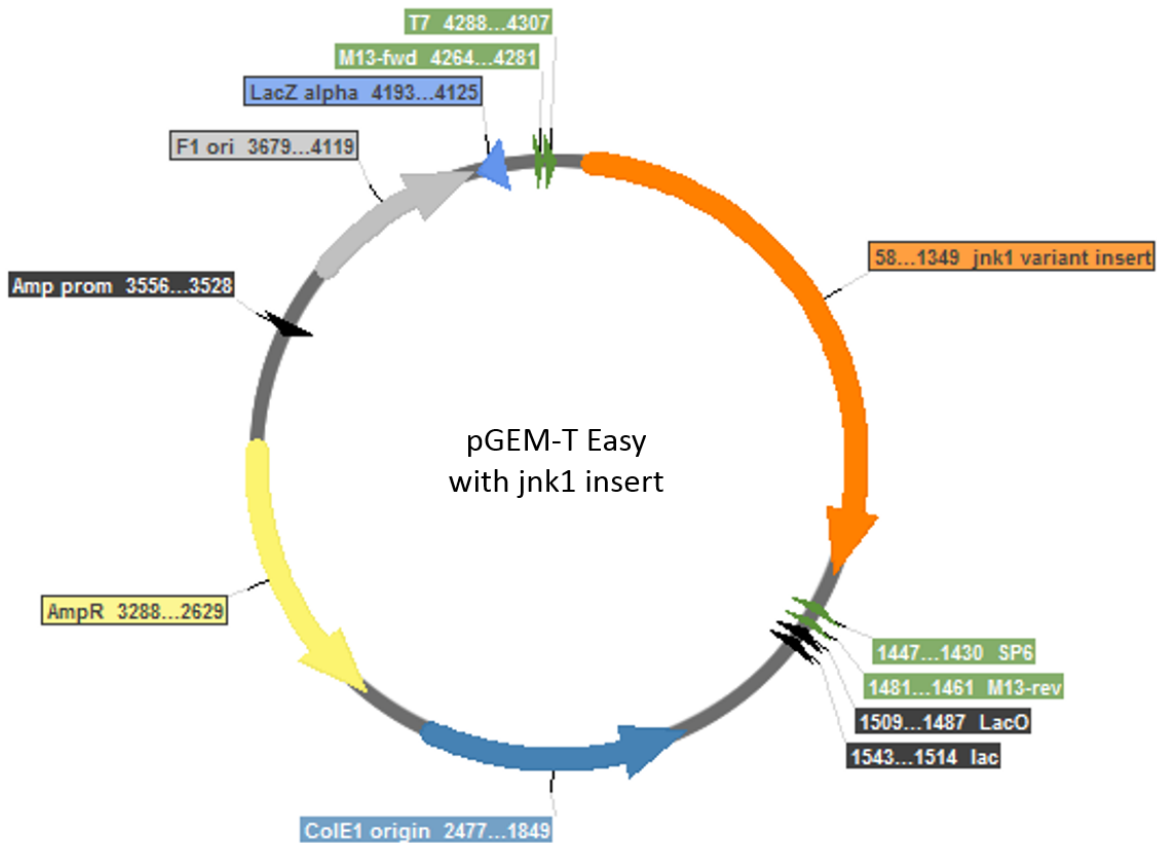


Figure 15 Plasmid map of the final *jnk1* transcript-containing cloning vector.

Schematic representation of the pGEM-T Easy (Promega®) cloning vector following the ligation of a zebrafish *jnk1* splice-variant. Schematic shows the physical location and basepair start and end of the *jnk1* variant insert, SP6 promoter, T7 promoter, M13 forward primer site, M13 reverse primer site, F1 origin of replication, ampicillin resistance gene (AmpR), ampicillin promoter, colicin E1 origin of replication, LacZ alpha gene, and LacZ origin of replication site. Plasmid map created with SerialCloner 2.6.1 freeware (<http://serialbasics.free.fr>).

2.2.8.6 Bacterial Transformation

To amplify transcripts and for production of clonal colonies DH5 α cells (Invitrogen™) were transformed with the plasmid vectors. Subcloning efficiency, competent DH5 α cells were thawed on ice and 5 μ l of the ligation was added to 25 μ l of cells. Following a 30 minute incubation on ice, the cells were heat-shocked at 42°C for 30 seconds and then returned to ice. The cells were topped up to 1ml with pre-warmed LB broth and incubated at 37°C for one hour while being shaken. From these starter colonies 100 μ l was plated onto LB-agar plates with 100 μ g/ml ampicillin at dilutions of 0.1x, 1x and 10x starter culture. Plates were grown for 12-16 hours at 37°C.

LB Medium:

10g bacto tryptone,
2.5g bacto yeast extract
5g NaCl
500ml ddH₂O

LB Agar:

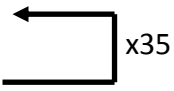
10g bacto tryptone,
2.5g bacto yeast extract,
5g NaCl,
7.5g bacto agar,
500ml ddH₂O
Agar and medium autoclaved before use.

2.2.8.7 Colony PCR

Colony PCRs were performed in order to determine whether inserts of an appropriate size had been ligated into the plasmid vectors. A p200 tip was used to pick single colonies from an agar/ampicillin plate and then transfer it to both a stab-plate, and 0.2ml PCR tube. Each PCR tube corresponded to a single colony on the stab-plate which was then incubated at 37°C until colonies were visible. Standard Taq polymerase reactions were set up as in section 2.2.11.4 and primers against the SP6 and T7 sites (Table 4) in the pGEM-T Easy (promega) multiple cloning site were used. The amplification time and number of cycles

used were high to ensure amplification of the ~1.2Kb amplicon that was expected with full-length *jnk1* transcripts:

Time (second)	Temp (°C)
120	95
30	95
30	64
90	72
300	72
Pause	4



The PCR product was run through a 1% agarose gel to determine whether the insert was the correct size. A sample of these colonies were then selected for isolation and sequencing.

2.2.8.8 Isolation of Plasmid DNA

Selected colonies were picked with a p200 pipette tip and grown in LB/ampicillin liquid culture for 12-16 hours at 37°C under shaking at 225rpm. Plasmid DNA was isolated from bacterial cells by use of the QIAprep® Miniprep kit (QIAGEN) as per the manufacturer's instruction. Briefly, the liquid colonies were centrifuged at 6,000 x g for 15 minutes at 4°C to pellet the cells and the supernatant was decanted. The pellet was resuspended in 0.25ml P1 buffer and transferred to a 1.5ml eppendorf tube. To the tube was added 0.25ml P2 buffer and the tubes were inverted to mix before the reaction was terminated by addition of 0.35ml N3 and mixed thoroughly.

The lysis solution was centrifuged at 18,000 x g for 10 minutes and then the supernatant was decanted into a QIAprep spin column and centrifuged for 1 minute. The flowthrough was discarded and 0.5ml PB buffer was added before centrifuging for a further minute. The flowthrough was discarded and the column was washed with 0.75ml PE buffer before centrifuging for 1 minute. The remaining buffer was removed with another 1 minute of centrifugation before the column was transferred to a fresh 1.5ml eppendorf tube, 50µl of DEPC-H₂O was added and the column was centrifuged for 1 minute to collect the DNA. Plasmid DNA abundance was qualified via NanoDrop Spectrophotometry (see 2.2.5).

2.2.9 Gel Electrophoresis

Agarose gel electrophoresis was performed in order to resolve and visualise different sized DNA bands during the project. In general 2% (weight/volume) agarose gels were used, however for full-length transcripts a 1% agarose gel was preferred. The necessary amount of agarose was dissolved in TAE solution and heated in a microwave until all the agarose had dissolved. After some cooling one drop of ethidium bromide (Sigma-Aldrich[®]) was added, and the agarose was poured into the mould and allowed to solidify before use. Gel electrophoresis was performed with the gel submerged in TAE for 25 minutes under a constant 125V or until the bands of interest had been successfully resolved.

2.2.10 Sequencing

Purified plasmids were sent for forward and reverse Sanger sequencing to GATC Biotech (<https://www.gatc-biotech.com/en/index.html>). SP6 and T7 primers within the plasmid multiple cloning site were used for this purpose.

2.2.11 Splice-Variant Specific *jnk1* RT-PCRs

Following the identification of eight different *jnk1* splice-variants arising from two genes it was decided to investigate the differential expression of these variants. Considering the large regions of conservation between variants of the same gene, and lesser but still considerable conservation of sequence between variants of different genes, the design, optimisation and validation of this experiment was complex. Despite this, primers were designed that do successfully target only a single splice-variant and were shown to be specific.

2.2.11.1 Forward Primer Design

In order to design four forward primers capable of binding to only one of the four middle exons specifically I began by performing a sequence alignment of these exons (Figure 16B). Sequence alignment showed that there are very few regions completely unique to each exon (Figure 16B white). Where there was divergence between exon 7 and 8 of one paralog, the change was often mirrored in the other paralog. Similarly, where differences were seen between exon 7 of *jnk1a* and *jnk1b*, these changes were often mirrored in exon 8 of the same paralog (Figure 16B grey). The conservation of the four sequences made it difficult to find primer targets that were sufficiently unique as to be specific to each splice variant. The forward primers that were finally chosen had the highest number of mismatches between both the variants arising from the same paralog, but using the opposite exon, and those variants arising from the opposite paralog, but using the same exon (Table 5). Where multiple possible sites existed with the same number of mismatches, those primers that had the lowest amount of secondary structure and which were not predicted to dimerise were chosen preferentially. All but one of the primers contained 5 or more mismatches to the unintended targets and none were predicted with strong secondary structure.

Name	Sequence	# Mismatches in Sequence of		# Bases	Tm (oc)	Secondary Structure	Dimers
		Same Paraform, Opposite Exon	Opposite Paraform, Same Exon				
<i>jnk1a_ex7</i>	TTTGGCAGAAATGGTCCGTC	5	4	20	67.1	None	No
<i>jnk1a_ex8</i>	GAGGTAGTGTATTATTTCCGGGTTC	13	5	25	63.8	None	No
<i>jnk1b_ex7</i>	TAACGTGGATATTGGGCTGTTG	5	5	23	66.4	V. Weak	No
<i>jnk1b_ex8</i>	GCTAACGTTGATGCTGGTCTATTG	5	6	25	65.5	None	No
<i>jnk1a_short</i>	CTGCTGCACCTGTGCTAGG	6	1	19	64.9	Strong	No
<i>jnk1a_long</i>	TTGATCACTGCTGCACCTAGG	6	1	21	65.3	Weak	No
<i>jnk1b_short</i>	TGCTGCACCTGTGCTAGC	6	2	19	64.0	Weak	No
<i>jnk1b_long</i>	CTGCTCACTGCTGCACCTAGC	5	3	21	67.6	Weak	No

Table 5 Sequences and Characteristics of the Splice-Variant Specific *jnk1* Primers.

The splice-variant primers were designed to be unique to one splice variant only with as high a number as possible mismatches with the other transcripts. Other factors were also considered including the number of base pairs which directly affects the melting temperature of the primers (Tm). Primers with low levels of secondary structure as well as those that were not predicted to dimerise were chosen preferentially when multiple choices were available.

2.2.11.2 Reverse Primer Design

The splice-variant specific reverse primers were designed to target the two different 3' splice acceptor sites of the *jnk1* paralogs. The two splice-acceptors lie just 5bp apart from one another so the ~20bp primers were able to completely overlap this site. I designed the reverse primers to take advantage of the fact that successful amplification by the transcription complex is most susceptible to mismatches at the 3' end of the primer (Kwok et al., 1990). By designing the 3' end overlapping the splice-acceptor sites there are at least 5bp different between the short form and long form (Table 5). However, as was shown in Figure 19 the region around the two splice acceptor sites is conserved between *jnk1a* and *jnk1b*; the only differences in sequencing occurring upstream or downstream of this region. Therefore there were very few mismatches (between one and three) between each primer and the corresponding splice-variant of the opposite paralog (Table 5). The reverse primers are therefore unlikely to be paralog specific; however they will be specific to either the short or long variant. It is therefore necessary that the forward primers are paralog specific to ensure that, as a pair, the primers are capable of amplifying only one splice-variant each.

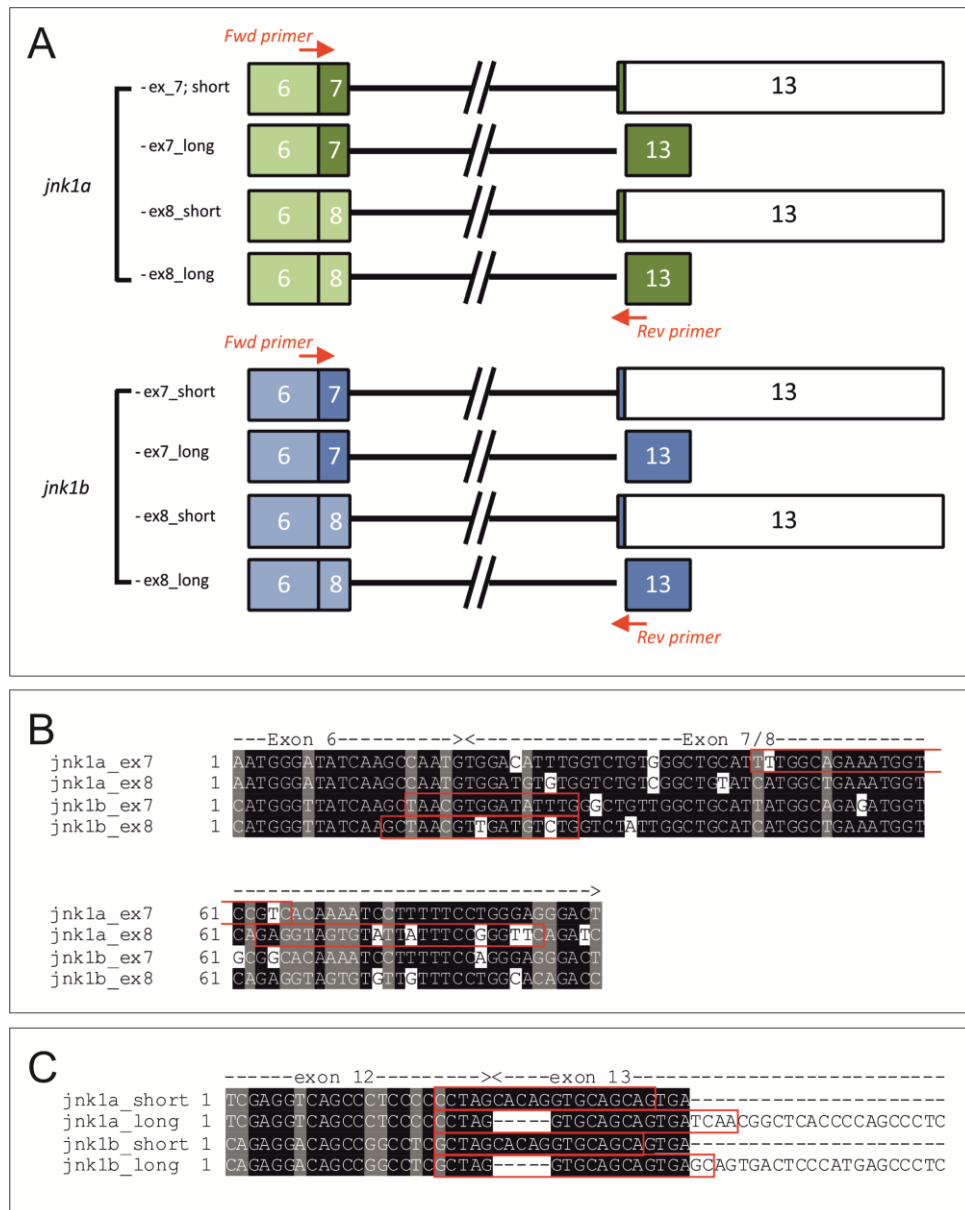


Figure 16 Design of Splice-Variant Specific Primers.

A) Schematic representation of where the splice-variant specific primers have been designed to bind. Coloured boxes represent the exons where binding takes place and the white boxes representing the 3' UTR. The remaining exons are not shown. The forward primers were designed to bind within exon 7 or overlapping the exon 6 / exon 7 boundary. The reverse primers were designed within exon 13 overlapping the two alternative splice acceptor sites. In the long form this is represented by a gap at the start of exon 13. B) Sequence alignments of the middle exons from *jnk1a* and *jnk1b* showing where the primers bind. Nucleotides conserved between all four exons are highlighted black and mismatches are white. Regions where half the variants have one nucleotide and half the variants have another nucleotide are shaded grey. Primer binding site shown by the red boxes. C) Sequence alignment of exon 12 and exon 13 of *jnk1a* and *jnk1b* showing sequence conservation. The primer binding sites are shown by red boxes.

2.2.11.3 Temperature Gradient RT-PCR

In order to determine the highest annealing temperature that remained unrestrictive for amplification of the splice-variant specific RT-PCRs, the reaction was gauged over a temperature gradient. A total of eight master mixes were made up (as in section 2.2.11.4) for each *jnk1* splice-variant including in the mix the primer pairs. The template cDNA used was an equal mixture of cDNA from each of the nine developmental stages that were analysed in this project. One positive control for the *jnk1a* and one for the *jnk1b* variants was included which was the same master mix but with a plasmid DNA template containing the *jnk1* variant. Distilled water was used to replace the cDNA content for a negative control. The PCRs were conducted under the same temperature and time conditions as the colony PCRs (section 2.2.8.7) except that for the annealing temperature step, the thermocycler plate was set up over a temperature gradient. Each PCR reaction within a set had an annealing temperature 2°C higher than the last between 62°C and 70°C. Following gel electrophoresis the bands were examined to determine the optimal temperature to use for future PCRs that would be specific but still allowed amplification. The optimal temperature values are listed in section 2.2.11.4.

2.2.11.4 Testing RT-PCR Specificity (Plasmids)

The specificity of the splice-specific *jnk1* primers were trialled against plasmid DNA to ensure that the primers could amplify only one splice-variant of *jnk1*. The plasmid DNA was clonal and contained only a single *jnk1* variant, therefore only one primer pair should amplify from each template DNA. To test this theory master eight mixes of 4.5 reactions each were made up containing all the reagents listed in section 2.2.12 except for the DNA. Each of the eight mixes contained a primer set targeted to one of the eight different *jnk1* variants. Each of the *jnk1* master mixes were aliquotted into a 0.2ml PCR plate and a 1µl of plasmid DNA was added to each reaction to make the final volume up to 20µl. The table below represents the template and primer pair grid that was constructed in the PCR plate, only reactions where template and primers match was there expected to be any amplification:

		Primer Pair Used			
		jnk1a_7;short	jnk1a_7;long	jnk1a_8;short	jnk1a_8;long
Template DNA	jnk1a_7;short	match	-	-	-
	jnk1a_7;long	-	match	-	-
	jnk1a_8;short	-	-	match	-
	jnk1a_8;long	-	-	-	match
		Primer Pair Used			
		jnk1b_7;short	jnk1b_7;long	jnk1b_8;short	jnk1b_8;long
Template DNA	jnk1b_7;short	match	-	-	-
	jnk1b_7;long	-	match	-	-
	jnk1b_8;short	-	-	match	-
	jnk1b_8;long	-	-	-	match

The PCRs were run under standard temperatures (see section 2.2.11) and PCR conditions (see section 2.2.12) and gel electrophoresis was performed to determine whether amplification had been successful.

2.2.12 Developmental and Tissue-Specific RT- PCR


Developmental and tissue-specific RT-PCRs were both conducted under optimised conditions using Taq polymerase and the relevant splice-variant specific primers (Table 4). The template cDNA was generated from animals 4 months of age via sacrifice and dissection of the required tissues (section 2.3.8). RNA extraction and cDNA generation was then performed by standard methodology.

The tissue-specific RT-PCRs were conducted by producing a standard master mix where each reactions contained:

Reagent	Final Concentration
GoTaq® Flexi Buffer	1x
MgCl ₂	1.5mM
dNTPs (10mM)	0.2mM each dNTP
Forward Primer (10mM)	0.5µM
Reverse Primer (10mM)	0.5µM
cDNA	50ng
Hot-Start GoTaq® Polymerase	1.25 units
DEPC-H ₂ O	Top up to 20µl

The RT-PCRs were run in a thermocycler under standard conditions, although the number of cycles was dependent upon the splice-variant:

Time (second)	Temp (°C)
120	95
30	95
30	X
30	72
300	72
Pause	4



Splice- Variant	Annealing Temperature (X) °C	Number of RT-PCR Cycles (Y)
<i>jnk1a_7</i> ;short	64	35
<i>jnk1a_7</i> ;long	64	31
<i>jnk1a_8</i> ;short	64	33
<i>jnk1a_8</i> ;long	64	31
<i>jnk1b_7</i> ;short	67	35
<i>jnk1b_7</i> ;long	67	35
<i>jnk1b_8</i> ;short	67	35
<i>jnk1b_8</i> ;long	67	35
<i>elfa1</i>	62	21

2.2.13 Pan-*jnk* Western Blotting

Western blot analysis on morphant tissue was conducted using a polyclonal pan-JNK antibody (Cell Signalling: #9252) and gapdh loading control (abcam®: ab9485). The protocol used was based upon the detailed protocol published by Abcam® (<http://www.abcam.com/index.html?pageconfig=resource&rid=11375>). The tissue was collected from 100 embryos at 48hpf for three conditions: uninjected controls, 4ng *jnk1a* and 4ng *jnk1b* morpholino. Embryos were batch dechorionated (section 2.3.4) and deyolked to reduce background binding as in Link et al. (Link et al., 2006). Briefly the embryos were washed three times in ice-cold deyolking buffer and transferred to a fresh 1.5ml ependorff tube. A cOmplete Mini protease inhibitor (Roche) was dissolved into 5ml of deyolking buffer, and then 1ml of this solution was added to each tube. The embryos were passed up and down a p200 pipette tip thirty times to disrupt the yolk sac followed by 5 minutes of shaking at 1100rpm to emulsify the yolk. The tubes were centrifuged at 4°C for 30 seconds at 1,900rpm to pellet the embryos and the supernatant was discarded.

Following deyolking, 200µl of laemmli buffer (half the total volume) was added to each tube and the tissue was homogenised through a needle gradient of 19G, 21G and 23G (section 2.2.3) before 200µl more laemmli buffer was added. The samples were boiled for 5 minutes at 95°C and 20µl of each was loaded into a 10% Mini-PROTEIN® gel (Bio-Rad) along with 10µl PageRuler Plus Prestained protein ladder (Thermo Fisher Scientific). Electrophoresis was performed at 80V for 20 minutes and 125V for 1.5 hours before Semi-dry transfer to a PVDF membrane was achieved by using the Tran-Blot® SD system (Bio-Rad) at 15V for 45 minutes.

Following successful transfer the membrane was cut in two with a clean scalpel at the 40kDa band. The membrane with low (≤ 40 kDa) molecular weight proteins was used for a loading control and blocked in 5% milk / TBS-T, whereas the high molecular weight membrane was blocked in 5% BSA / TBS-T for 2 hours in a falcon tube while being rolled. The membranes were exposed to antibody (low weight with 1:20,000 anti-gapdh, high weight with 1:5,000 anti-jnk) overnight at 4°C while being rolled. The following day both membranes were washed thoroughly in TBS-T before horseradish peroxidase conjugated swine anti-rabbit secondary antibodies (Dako® P0399) were applied (low weight with 1:20,000, high weight with 1:5,000) and incubated at room temperature for 2 hours.

Once membranes were thoroughly washed with TBS-T 4x 10 minutes the SuperSignal Chemiluminescent solution (ThermoScientific) was applied and photographic film was used to detect luminescence. Film was developed using a film processor (Konica Minolta) scanned on a flatbed scanner, and densitometry was performed on each lane individually to determine relative protein abundance. The gapdh loading band was compared between samples to generate a normalisation value, and this was used to normalise the jnk protein bands. Components of all of the western blot specific solutions are listed below:

Deyolking Buffer:

55mM NaCl,
1.8mMKCl,
1.25mM NaHCO₃

Laemmli Buffer:

4% SDS,
10% 2-mercaptoethanol,
20% glycerol,
0.004% bromophenol blue,
0.125M Tris HCL
pH to 6.8

Running Buffer:

25mM Tris Base,
0.19M Glycine,
0.1% SDS,
Dissolved in 1 litre dH₂O

Transfer Buffer:

48mM Tris Base,
39mM Glycine,
20% Methanol
Dissolve in 0.8 litre dH₂O

2.2.14 Myc-tagged Western Blott

Sample generation for the myc-tagged mRNA western blots was carried out via microinjections (section 2.3.5.2) although there were multiple injections required per sample. Large clutches of embryos were selected immediately after being spawned and 120 embryos were taken and injected with *jnk1a* morpholino. These morphants were then split between three dishes and injected with either 400pg *jnk1a*-myc mRNA, 400pg *jnk1b*-myc mRNA, or no mRNA. This process was repeated with *jnk1b* morpholino and then the standard Gene-Tools® CMO resulting in a total of nine sample conditions. Morpholino microinjection was carried out by me whereas mRNA injection was performed by Dr. Simon Ramsbottom. The sharing of microinjections reduced the required time for the injections and meant that all nine conditions could be generated within the same clutch of eggs before the eight-cell stage. Embryos were then allowed to develop under normal conditions until 48hpf before tissue was processed by standard methods (see sections 2.2.3 and 2.2.13).

The anti-myc western blot was then carried out by Dr. Simon Ramsbottom. Briefly the nine samples were loaded into a 10% Mini-PROTEIN® gel (Bio-Rad) such that 1 protein abundance per well equated to 1 embryo per lane. The electrophoresis was performed for 20 min at 80V followed by 1.5 hours at 125V in running buffer solution. Semi-dry transfer of protein to PVDF membrane was achieved at 15V for 45 min with the Trans-Blot® SD system (Bio-Rad). The membrane was blocked in milk for one hour and then cut in two at 45kDa allowing for the top and bottom of the membrane to be probed separately. The top of the membrane was probed with anti-MYC (abcam®: ab1326) whereas the bottom of the membrane was probed with 1:20,000 anti-GAPDH antibody (abcam®: ab9485) overnight at 4°C. The following day the horseradish peroxidase conjugated swine anti-rabbit (Dako® P0399) secondary antibody was incubated with the membranes at room temperature for 2 hours. Following thorough washing steps the membrane was treated with SuperSignal Chemiluminescent solution (ThermoScientific) and exposed to photographic film. The resulting photographic images were scanned on a flatbed scanner to be included in this thesis.

2.2.15 *In Situ* Hybridisation

In situ probes were generated from plasmid templates of the zebrafish *myl7* (*cm1c2*) (Yelon et al., 1999) and *foxa3* (Odenthal and Nusslein-Volhard, 1998) genes by RNA polymerase using the DIG RNA Labeling Kit (Roche Diagnostics). RNA transcription of the templates was performed with labelling using digoxigenin-UTP by setting up of the reactions as below:

10µl 5x transcription buffer (Roche Diagnostics)
 2.5µl 10x dig NTP mix
 5µl 100mM Dithiothreitol
 2µl RNase inhibitor
 3µl T7 RNA polymerase
 0.5µg template DNA
 Top up to 50µl with DEPC-H₂O

The reaction was run at 37°C for 2 hours in a thermocycler and then 2µl of the reaction was run through a 1.5% agarose gel to check that the reaction had worked. The template DNA was destroyed by adding 1µl of DNase I to the reaction and incubating at 37°C before cleaning up with an ammonium acetate RNA precipitation. The probe was redissolved in DEPC-H₂O and the concentration was quantified by Nanodrop® spectrophotometry (2.2.5).

Wholemount *in situ* hybridisation was performed on embryos at 48hpf with *cm1c2* and *foxa3* RNA probes that are expressed in cardiomyocytes and pan-endodermal tissue respectively. Fixed embryos were equilibrated into phosphate buffered saline (PBS) with 0.1% tween 20 and then washed in PBS-T four times for 5 minutes each. The embryos were permeabilised with a 10 minute treatment in 10µg/ml proteinase K and the reaction was stopped by two quick PBT washes and then a 30 minute refixation step in 4% paraformaldehyde at room temperature. The embryos were thoroughly washed in PBS-T to remove all PFA 5 times for 5 minutes. Embryos were transferred to warm (65°C) hybridisation mix (HM) for 10 minutes before they were transferred to HM plus (HM+) which contained heparin and tDNA. After 2 hours at 65°C the HM+ was replaced with fresh HM+ containing the 2µl each of the RNA probes, and hybridisation was performed overnight.

The following day the embryos were washed twice for ten minutes in HM and then progressed through a gradient of 75%, 50%, 25%, 0% HM / 2x saline sodium citrate (SSC) buffer. Two longer washes of 30 minutes were then performed for 30 minutes in 0.2x SSC. The embryos were passed through into Tris buffered saline (TBS) with 0.1% tween 20 at

room temperature by 75%, 50%, 25%, 0% 0.2x SSC / TBS-T gradient before being blocked in 2% Roche block (Roche Diagnostics), 20% heat-treated lamb serum (Life Technologies®) at room temperature for 2 hours. The antibody incubation was performed overnight at 4°C using 1:5000 Anti-Digoxigenin-AP, Fab fragments (Roche Diagnostics) in blocking solution. The embryos were thoroughly washed in TBS-T over two days before they were developed. Development was performed using alkaline phosphatase buffer for 90 minutes at room temperature before washing thoroughly in PBS and then dehydration into 100% methanol.

Hybridisation Mix:

50% formamide
5x SSC
0.1% Tween 20
Adjust pH to 6.0 with citric acid
Dissolve in ddH₂O

Add 50µg/ml Heparin and 500µg/ml tRNA for HM+

20x SSC:

3M NaCl
0.3M Trisodium citrate
Adjust pH to 7.0 with 1M HCl
Dissolve in ddH₂O

Blocking Solution:

10% Roche® Blocking solution
20% heat-treated lamb serum
70% TBS-T

Alkaline phosphatase buffer:

100mM Tris-HCl
50mM MgCl₂
100mM NaCl
0.1% Tween 20
Dissolve in ddH₂O

2.2.16 Densitometry

Densitometry of DNA and protein bands was performed digitally on uploaded image files in the freeware program FIJI (<http://fiji.sc/Fiji>) by the methodology described here (<http://lukemiller.org/index.php/2010/11/analyzing-gels-and-western-blots-with-image-j/>). PCR gel images were saved as .tif files directly whereas western blot photographic films were scanned at 300 dpi resolution on a flatbed scanner (Epson) and saved as .tif. The files were opened with FIJI and boxes were drawn around each band individually. The “Gels” tools were used to plot the intensity of each band and then the area under the peaks was quantified with the “wand” tool. Once quantified the band intensities could be compared statistically.

2.2.17 Statistics

All statistics were performed in the SPSS (Statistics Package for the Social Sciences) suite (IBM) and appropriate tests were chosen by use of the flowchart in the statistical guidebook by Ennos (2006) (Ennos, 2006). Due to comparisons between multiple groups it was most commonly appropriate for the use of one-way ANOVA tests which compare the variance within groups with that between groups. Where significant differences were detected the 2-sided Dunnett post-hoc test was performed in order to determine which groups were significantly different. Significance was indicated on the graphs in this thesis by asterisks such that * is $p<0.05$, ** is $p<0.01$ and *** is $p<0.001$.

2.3 ZEBRAFISH HUSBANDRY, MORPHANT GENERATION AND SECTIONING

2.3.1 Commonly Used Zebrafish Technique Reagents

E3 Medium:

5.0 mM NaCl

0.17mM KCl

0.33mM CaCl

0.33mM MgSO

Dissolve in 1L ddH₂O and adjust to pH 7.0 with 1M NaOH

E3 / PTU Medium:

Add 0.2mM 1-phenyl-2-thiourea (PTU) to working E3.

“Blue Water”:

Add 2ml of 0.1% methylene blue to 1L aquarium tank water.

Tricaine pH 7.0 (1 litre):

4g Tricaine powder in 800ml ddH₂O

Adjust solution to pH 7 with 1M Tris-HCl

Top-up to 1L with ddH₂O

2.3.2 Zebrafish Lines Used

The husbandry of adult zebrafish was performed as described in Westerfield, 1995 and all procedures were performed under regulations of the Home Office (Westerfield, 1995). The AB wildtype line (Zebrafish International Resource Centre) was used for most experiments except where stated. The *Tg(myl7:EGFP)* line (Huang et al., 2003b) was used for fluorescent imaging of the heart. The *Tg(myl7:EGFP)* line has an enhanced green fluorescent protein sequence downstream of the cardiomyocyte-specific myosin light chain 7 promoter, and EGFP is expressed in the cell cytoplasm.

2.3.3 Breeding Strategy and Zygote Collection

Adult fish were put-out the day prior to use in breeding traps such that male and female were separated. The following morning the adults were put-together and eggs fell to the bottom of the trap through a grid. Fertilised eggs were collected at fifteen minute intervals and washed with blue water prior to use.

2.3.4 Embryo Culture Conditions

Embryos were grown in plastic petri dishes of E3 media at 28.5°C in a fan incubator. Numbers of failed embryos were counted at 8hpf and 24hpf and these were removed. Media was replaced at 24hpf with fresh E3 or E3 / PTU when abolition of pigment development was required.

2.3.5 Morpholino Protocols

Start-site (AUG) translation-blocking Morpholino oligonucleotides for the *jnk1a* and *jnk1b* genes were designed by Gene-Tools®. These morpholinos overlapped the AUG translation start site of *jnk1a* or *jnk1b* which are found within exon 2 of the respective genes (Appendices Figure 63).

Morpholino	Sequence
<i>jnk1a</i>	5' - CTCTCGCTTA TTTTGTTCA TGGTG - 3'
<i>jnk1b</i>	5' - CTTTCTCGCG CTTATTCCTG TTCAT - 3'

Table 6 Morpholino sequences

Upon arrival 2.5mg of each MO was dissolved in 300µl ddH₂O and this master solution was kept frozen at -20°C and defrosted when working solutions of MO were required.

2.3.5.1 Morpholino Preparation

Working solutions of MO were generated by thoroughly defrosting the master, and then heating to 60°C for 5 min before vigorous vortexing to ensure that the MO was well dissolved. A mix of master MO solution, ddH₂O and phenol red (0.5%) was then produced to create the working solution, with the quantities required depending upon the final dose of morpholino that was desired.

	1ng Dose	2ng Dose	3ng Dose	4ng Dose	6ng Dose	8ng Dose
MO Conc. (µg/µl)	0.5	1.0	1.5	2.0	3.0	4.0
Master MO Volume (µl)	1.2	2.4	3.6	4.8	7.2	9.6
0.5% Phenol Red (µl)	2.0	2.0	2.0	2.0	2.0	2.0
ddH ₂ O (µl)	16.8	15.6	14.9	13.2	10.8	8.4
Final Volume (µl)	20	20	20	20	20	20

Phenol red was used in the working solutions in order to visualise the morpholino drops during the microinjection process.

2.3.5.2 Microinjection

Morpholinos were injected by glass capillary microneedle into the yolk sac at no later than the 4-cell stage (Nasevicius and Ekker, 2000). Microneedles were pulled from 1.2mm capillaries using a needle puller (Sutter Instrument Co) under the following conditions: Heat=635, Pull=50, Velocity=80, Time=200. Morpholino was rear-loaded and the end of the needle was snapped with fine watchmakers forceps. A 1mm graticule was used to measure droplet size of the morpholino injected into oil. A 160µm (2nl) droplet was achieved by using a Femtojet[®] compressor (Eppendorf) with settings: 280 hPa injection pressure, 0.3 sec injection time and 17 hPa compensation pressure. The droplet size remained the same (2nl) regardless of morpholino dose, and instead the concentration of morpholino loaded was altered. Embryos were lined up against a slide and 2nl of morpholino was injected into each before embryos were placed in E3 in the incubator at 28.5°C. For compound *jnk1a* and *jnk1b* knockdown the morpholinos were injected as a mixture in the same needle to ensure equal dosing. Morpholino doses trialled:

2ng jnk1a	1ng jnk1b	1ng 1a; 1ng 1b
3ng jnk1a	2ng jnk1b	2ng 1a; 1ng 1b
4ng jnk1a	4ng jnk1b	1ng 1a; 2ng 1b
6ng jnk1a		2ng 1a; 2ng 1b
		4ng 1a; 4ng 1b

2.3.6 Pronase Dechoriation

Embryos were batch dechorionated in 2mg/ml pronase as in Westerfield et al. (Westerfield, 1993). Approximately 50 embryos were added to 5ml pronase and incubated at 28.5°C for 1 minute, before rinsing with 20ml E3 solution 3 times. Swirling of the petri-dish during washes helped to release the embryos from the chorions which could then be removed with a pipette.

2.3.7 Anaesthetisation of Embryos and Microscopy

Zebrafish embryos between 24-72hpf were anaesthetised in 0.2mg/ml Tricaine® for five minutes prior and during microscopy techniques. Embryos were allowed to recover for 5 minutes in fresh E3 media before being returned to their petri dish.

Embryos were imaged under anaesthesia using a dissection light microscope (Leica). The samples were orientated using fine watchmakers forceps on a layer of 1.5% agarose. For fluorescent images of the heart a fluorescent bulb was applied and samples were viewed under GFP filter.

2.3.8 Schedule 1 Methods and Dissection of Adult Tissues

For the purpose of dissection, adult fish were euthanized in 2mg/ml Tricaine® pH 7.0 for 10 minutes. The heart, brain, testes, liver, and skeletal muscle were dissected from 4 month male zebrafish as per (Gupta and Mullins, 2010). Tissue was added to 0.5ml TRIzol and homogenised as in section 2.2.3.

2.3.9 Paraformaldehyde Fixation of Zebrafish Embryos

All zebrafish embryos before 120hpf that were used for sectioning and in situ hybridisation were fixed in the same manner. Embryos were transferred to a sterile 20ml bijou tube and all E3 solution was removed. The embryos were then submerged in 2.5ml of chilled 4% paraformaldehyde / PBS and incubated overnight at 4°C. The following day the PFA was removed and embryos were equilibrated through a methanol (MeOH) gradient: 25% MeOH / ddH₂O, 50% MeOH/ddH₂O, 75% MeOH/ddH₂O and finally two replicates of 100% MeOH. Embryos were incubated in each solution for 5 minutes at room temperature, before it was replaced by the following solution. Once embryos were in 100% MeOH they were transferred to an Eppendorf tube in fresh MeOH and stored at -20°C until the tissue was used.

2.3.10 Resin Sectioning

Fixed and dehydrated embryos at the desired timepoints (48hpf and 72hpf) were washed 2x 30 min in 100% ethanol before being transferred to the Technovit 8100 base solution (Electron Microscopy Sciences®). Once equilibration of 10 minutes was complete the embryos were moved into Hardner 1 solution and allowed to equilibrate for 1 hour at 4°C. The chemical hardening resin was made with the mixture of Hardener 1 and Hardener 2 as by the manufacturer's guidelines and then plastic moulds were filled with this solution. Two zebrafish embryos were embedded into each resin block in different orientations (one for sagittal and one for coronal sections) by adding them to the plastic mould and orientating gently with a pipette tip. The resin was allowed to set briefly on the bench to prevent embryos rolling, and then transferred to the fridge surrounded in silica gel to set at 4°C for two days in a low humidity environment.

Sections were cut from the blocks using a glass knife and rotary microtome at 5µm thickness and transferred to positively charged glass slides (Leica Biosystems®) and allowed to dry for four hours at room temperature. Lee's Methylene Blue-Basic Fuchsin staining (http://www.ebsciences.com/staining/methyl_bl.htm) was performed in order to visualise the tissue. Slides were transferred to a rack and stained in batches of 20 at a time as below:

20 sec Methylene blue – basic fuchsin
 10 sec ddH₂O
 10 sec 95% ethanol
 10 sec ddH₂O

Following the staining of the tissue the slides were allowed to dry overnight in the fume hood and then mounted using Histomount (National Diagnostics). Images were captured on an Axioplan compound microscope (Zeiss) and colour balanced in Adobe Photoshop® CS3.

2.3.11 Jog / Loop Scoring

In order to assess the zebrafish heart laterality of *jnk1* morphants, heart position was assessed at two separate timepoints. Morphants were generated at various doses using wildtype strains and allowed to develop under normal conditions until 24hpf. At 24hpf the E3 media was switched to fresh media containing 0.2mM 1-phenyl 2-thiourea (PTU) which inhibits melanogenesis (Karlsson et al., 2001), ensuring that the transparency of embryos persisted. At 28hpf the embryos were anaesthetised in E3 media containing 0.2mg/ml Tricaine for five minutes before jogging direction was scored. Fine watchmaker forceps were used on the chorion to manipulate each embryo, enabling visualisation of the heart from a ventral orientation (through the yolk sac). Jogging status was scored as left, right or midline depending on movement of the heart. As proposed by Chin et al. the heart was judged to have jogged if the angle formed between the anterior-posterior embryonic axis and linear heart tube was 5° or greater; deviation from the midline of less than 5° was considered to have not jogged, and scored as a midline heart. In the case of 4ng *jnk1a* and compound 4ng *jnk1a*; 4ng *jnk1b* morphants the heart displayed developmental delay. In these cases the jogging status was instead determined at 32hpf. Once scoring was complete the morphants were separated into different dishes of E3 / PTU depending on their jogging status and returned to the incubator.

Looping of the heart was scored upon the same embryos that were examined for jogging. At 48hpf the embryos were reanaesthetised in Tricaine-containing media for five minutes and then examined under a dissection light microscope. Forceps were again used to orientate the embryos (which remained in the chorion at this age) so that visualisation of the heart

could be made through the yolk. Looping status was scored by determining the relative position of the ventricle compared to the atrium. A D-loop was scored when the ventricle had moved to the right side of the atrium, whereas an L-loop was scored when the ventricle was present on the left. Where the ventricle remained midline with regard to the atrium it was considered that looping had failed to occur and these morphants were scored as O-loops (see for Figure 46 schematic representation).

2.3.12 Uncoupling Scoring

The determination of whether morphants displayed uncoupling of heart tube movements was performed post-hoc on heart laterality data. Uncoupling was scored as being where the jogging status of the embryo was not predictive of the looping status i.e. where left jog did not result in D-loop, or where right jog did not result in L-loop. Since the looping status of those embryos that fail to jog cannot be predicted (Chin et al., 2000) as looping direction appears to be random, this group was discounted from the analysis.

CHAPTER 3 - BIOINFORMATIC AND GENE EXPRESSION ANALYSIS OF ZEBRAFISH JNK1

3.1 INTRODUCTION

Evidence has shown that zebrafish have two paralogs of the *JNK1* gene (*jnk1a* and *jnk1b*) which may have arisen during the teleost genome duplication event. However, to date there have been no publications examining the different transcripts that arise from these two genes nor comparisons to the mammalian *JNK1* genes which are more well studied. Automated predictions of *jnk1* splice-variants suggests that several of the variants observed in human may also be translated from the zebrafish genes (www.ENSEMBL.org), however each gene may be capable of transcribing only a subset of the full human splice-variant complement (See Figure 12). To determine whether the zebrafish is a comparable genetic model for human *JNK* function it is important to characterise the variants which are produced in zebrafish.

In addition, the expression pattern of the *jnk1* genes in zebrafish is limited to the gene or protein level, and these studies were produced when only a single zebrafish *jnk1* gene was identified (Krens et al., 2006b, Xiao et al., 2013). However, evidence in human cell lines has shown that the different splice-variants have different affinities to downstream effectors, and putatively different function (Gupta et al., 1996). If there are indeed functional differences between *jnk1* splice-variants then this may be reflected in the expression pattern of each variant. Examination of splice-specific expression over development and within different tissue types could therefore provide further evidence of functional differences in between the *jnk1* transcripts.

3.1.1 Aims of the Chapter

The aim of this chapter was to expand upon what is known about the zebrafish *jnk1* paralogs, their different splice variants, and their expression patterns. In order to do this there were several objectives:

1. Identify whether the predicted, core *jnk1* transcripts do exist in zebrafish, and obtain accurate sequences for them in the AB zebrafish strain.
2. Determine to what degree the splice-variants differ in sequence and identify any regions of high conservation or divergence in the sequence.
3. Compare the zebrafish *jnk1* sequences to their orthologs.
4. Determine whether it is possible to investigate the specific expression patterns of individual splice-variants.
5. Characterise the expression pattern of *jnk1a* and *jnk1b* over development and in adult tissues.

3.2 RESULTS

3.2.1 Proposed New Model of ZF *jnk1* Splice Variants

The current model of zebrafish *jnk1* splice-variants comes from the ENSEMBL predictive pipeline (<http://www.ensembl.org>) which has annotated the raw genomic sequence of the Tübingen line using published protein and cDNA/EST alignments. To achieve the aims of this project it is necessary to have accurate sequences of the *jnk1* paralogs from which reagents can be designed e.g. primers. However, use of the wildtype strain in our lab (AB) meant that differences in sequence were likely to be present between the genomes of our animals and the animals sequenced by the Zebrafish Genome Project. The first experiment conducted was therefore to obtain accurate, full-length sequences from the AB line from which primers and morpholinos could be designed. To this end primers were designed that were capable of pulling out the full-length splice variants of *jnk1a* and *jnk1b*.

3.2.1.1 Primer Design

Despite there being a total of nine predicted splice-variants shared between the *jnk1* paralogs (Figure 12), evidence for only four full-length variants has been published (Seo et al., 2010, Keightley et al., 2013, 2010) i.e. *jnk1a*-001 and -002, *jnk1b*-001 and -002. To maximise the chance of successfully pulling out *jnk1* splice-variants I therefore decided to target only those that had published full-length sequences to support their existence (**Figure 14**). Those variants targeted were *jnk1a*-001 and -002 and *jnk1b*-001 and -002.

Once the target variants had been identified, primers were designed that were capable of pulling out the full-length sequences (for more detail see section 2.2.8). Two primer pairs were designed, one per paralog, where the forward primers overlapped the ATG “START” codon, and the reverse primers overlapped the “STOP” codon of the longest variant (see appendices Figure 57). For both paralogs of *jnk1*, only a single primer pair was necessary to pull out both predicted splice-variants (See **Figure 14**).

3.2.1.2 Sub-Cloning of Full-Length *jnk1* Transcripts

Tissue from 40 whole AB strain embryos was collected at 72hpf, and RNA extraction was conducted via use of TRIzol® reagent via phase separation. cDNA was prepared from 2 µg of RNA using the Superscript III kit (Life Technologies) which synthesises full-length cDNA transcripts through the use of dT primers. Full-length cDNA transcripts were T-cloned into the pGEM-T Easy plasmid (Promega) via T4 ligase and transformed and cultured in DH5α competent cells for 16 hours at 37°C. Colony PCR using the same full-length primers confirmed the presence of ~1.2kb inserts in a majority of the colonies, and those positive for an insert were re-picked and grown up for 16 hours in liquid culture. Plasmid was retrieved through the use of a “Mini-Prep Kit” column (QIAgen) and then sent for forward and reverse Sanger sequencing (GATC Biotech).

3.2.2 The Identification of Two Unpredicted *jnk1a* Transcripts

The full-length sequencing data that was obtained from this experiment confirmed that the two full-length *jnk1a* variants targeted (-001 and -002) had been sub-cloned successfully. These two variants were 1284bp long, consisting of a single ORF, and integrated either exon 7 or exon 8 into the sequence (Figure 17 *jnk1a_7;long* and *8;long*). However, two additional and novel *jnk1a* variants were also present. These previously unpredicted variants integrated either exon 7 or exon 8 into the sequence, however, the ORF of these variants ended 129bp sooner into the sequence. The discrepancy in length between the long and short splice-variants arose from the presence of an alternative splice acceptor site in exon 13. The two splice-acceptor sites were separated by only 5bps but resulted in a frame-shift that introduced a STOP codon much sooner in the sequence (Appendix Figure 58).

3.2.3 The Identification of Exon 7 *jnk1b* and Two Unpredicted Transcripts

Analysis of the full-length *jnk1b* sequences revealed the successful sub-cloning of the two targeted splice-variants (-001 and -002). As predicted by the ENSEMBL pipeline the ORF of variant -001 was 132bp shorter than -002. This variation was caused by the use of an alternative splice-acceptor site, which resulted in the inclusion of an extra 5bp of the final exon, resulting in a frame shift (Appendix Figure 59). Both variants also contained a 72bp

region in the middle of the sequence which was predicted to arise from the exon homologous to exon 8 *jnk1a*. However, two additional variants were also discovered in the sequencing data which had not been previously characterised in zebrafish. These variants were similar to variants -001 and -002 in that the length of the reading frame was 1155bp or 1287bp respectively, however, the two novel variants differed in the sequence contributed by the middle exon. These novel variants contained a 72bp sequence in the middle of the sequence that shared only 67% sequence identity to the putative exon 8 (Figure 19C). I therefore theorised that this sequence arose from an unidentified exon of *jnk1b* which was integrated into the splice-variants in a mutually exclusive manner; this is the same scenario that is observed in *jnk1a*.

In order to determine whether the novel 72bp of sequence within the *jnk1b* splice variants arose from an annotative error by the ENSEMBL pipeline I aligned the sequence to the raw (unannotated) genomic DNA of *jnk1b* (www.ensembl.org). This 72bp sequence does indeed exist within the *jnk1b* gene data, in a region annotated as being intron 6-7. This novel exon is therefore likely to be the seventh exon of the *jnk1b* gene which has not been correctly annotated. Every exon following exon 7 must therefore increase in number by one. From this sequencing data I was able to construct a new model for the splice-variants of the zebrafish *jnk1* paralogs (Figure 17) where each paralog gives rise to four unique splice-variants that differ in both length and middle exon usage.

To ensure that the sequences obtained from this experiment were correct I repeated this cloning methodology and obtained the same results. This replicate was performed using different cDNA samples, a separate PCR reaction and all fresh reagents. Sequencing results came back identically proving that all of the sequencing data was correct, and no amplification errors had been introduced.

3.2.4 Overview of the Updated Model of Zebrafish *jnk1* Splice-Variants

Discovery of novel splice-variants from both *jnk1* paralogs has made it necessary to propose a new model of *jnk1* transcription. The proposed model consists of four unique splice-variants per paralog which differ in two regions: the middle exon, and length of the ORF (Figure 17). These transcripts represent the variants that I have gained experimental

evidence for, however, there may also exist 2-3 shorter transcripts per paralog which have been predicted by the ENSEMBL pipeline. I chose not to investigate these variants because there is no full-length sequence data to support their existence in the literature, some are not protein coding, or are produced from incomplete sequencing data. These variants may exist but are left out of my working model because they have not been experimentally verified.

In addition to the model I also proposed a different naming convention for the eight variants. The current nomenclature are complex and non-descriptive, so for the purpose of this thesis I have decided upon an alternative naming convention. As mentioned above, each *jnk1* splice-variant differs at only two locations: middle exon (use of either exon 7 or exon 8) and the 3' splice acceptor site (changing the length of the transcript). I have used these two features to name each variant (Table 7) e.g. *jnk1a_7;short* refers to the splice variant of *jnk1a* that contains exon 7 and uses the upstream splice-acceptor of exon 13, causing an earlier STOP codon. This table also contains the nomenclature which is used upon the ENSEMBL database for reference.

Paralog	Middle Exon Usage	OFR Length (bp)	Naming Convention	ENSEMBL Nomenclature
<i>jnk1a</i>	7	1155	<i>jnk1a_7;short</i>	unidentified
	7	1284	<i>jnk1a_7;long</i>	-002
	8	1155	<i>jnk1a_8;short</i>	unidentified
	8	1284	<i>jnk1a_8;long</i>	-001 / -201
<i>jnk1b</i>	7	1155	<i>jnk1b_7;short</i>	unidentified
	7	1287	<i>jnk1b_7;long</i>	unidentified
	8	1155	<i>jnk1b_8;short</i>	-001
	8	1287	<i>jnk1b_8;long</i>	-002

Table 7 Proposed New Naming Convention of the Core *jnk1* Splice-Variants. Due to the non-descriptive naming convention of the ENSEMBL pipeline I propose a naming convention of the *jnk1* splice-variants that reflects the structure of the transcript. This convention enables easy determination of which splicing events have occurred in each variant.

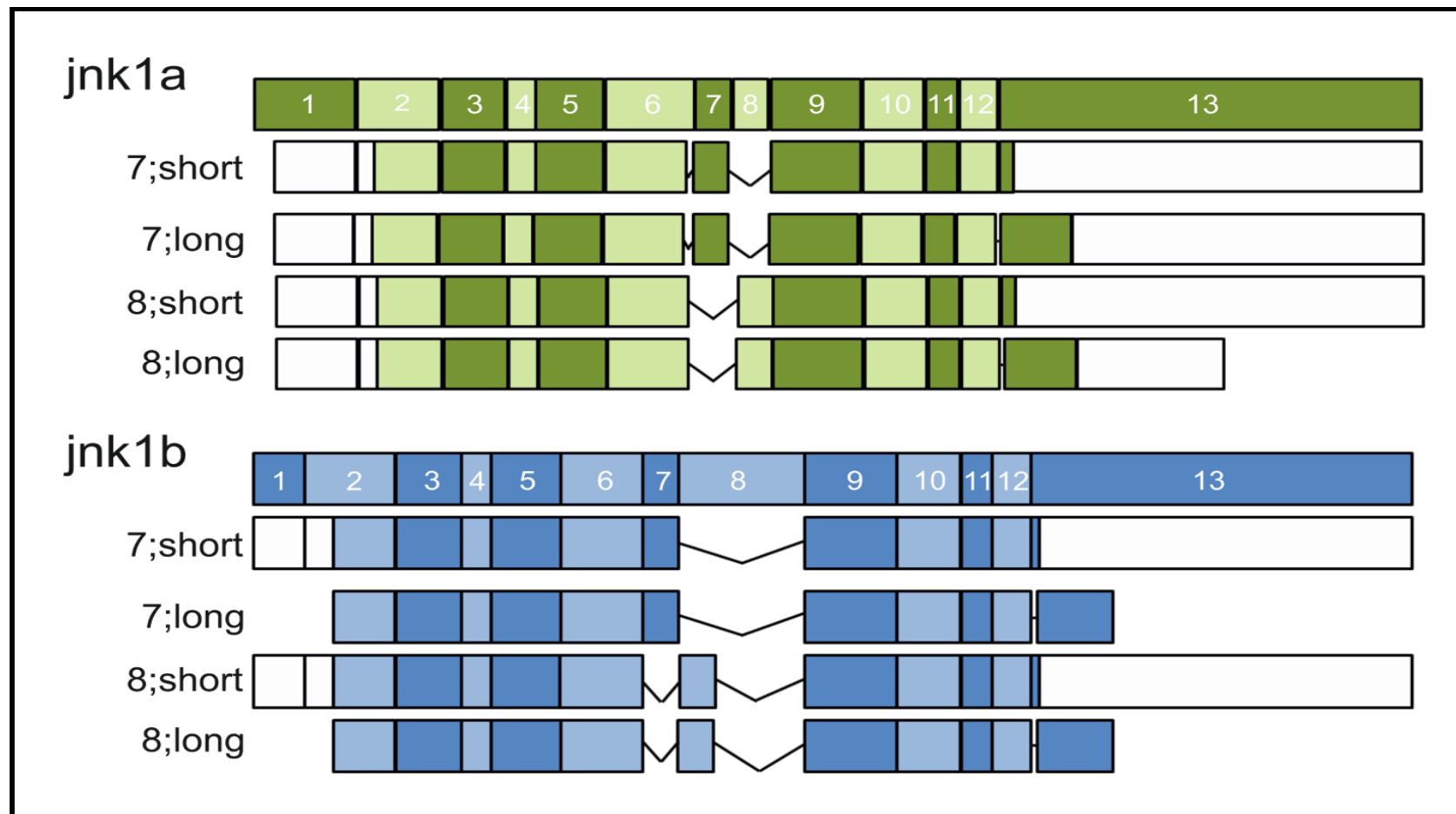


Figure 17 A New Model of the Experimentally Proven Splice-Variants of zebrafish jnk1.

Both jnk1 paralogs contain thirteen exons, of which twelve can contribute to the coding sequence. Above the exons are numbered and the transcripts are represented below. Length of each box represents how much of the exon contributes to the CDS of the splice variant. Alternative exons are shown in light and dark shades with UTR in white. Each paralog has four splice-variants that differ depending on which middle exon (7 or 8) they use and how much of exon 13 contributes to the CDS.

3.2.5 Conservation and Divergence of the two Zebrafish *jnk1* Parforms

Once full-length sequences of both paralogs were obtained I used in silico methods to determine how closely conserved the sequences were. The two *jnk1* paralogs are likely to have arisen from the teleost genome duplication event (Taylor et al., 2001), meaning that they arose from a common ancestral gene. Genetic drift will have introduced changes into the sequence, however regions critical to function may have experienced selective pressures ensuring that they are conserved. Most duplicated genes in the teleost genome have lost one of the redundant copies and where both copies do remain it is theorised that the paralogs may have different, although possibly overlapping, functions or be differentially expressed (Force et al., 1999, Howe et al., 2013). If this is the case within the *jnk1* paralogs then identifying where the differences in sequence occur could help to predict what functional changes have evolved.

3.2.5.1 *Sequence Identity is Strongly Conserved between ZF Jnk1 Protein Sequences in the Region of the Protein Kinase Domain*

At the level of the DNA there is a considerable amount of divergence in sequence between the two paralogs, with only 81.5% sequence identity conserved (Figure 18A, appendix Figure 60). Furthermore, the changes seem to be shared equally through the sequence without any long stretches with high conservation. From this result, all that can be concluded is that the two sequences have changed considerably since their divergence and that the changes are spread throughout the DNA sequence.

Examining these paralogs at the protein level is more informative since multiple codons code for the same amino acid. I therefore repeated the alignments but instead used translations from the DNA sequence. The result of this alignment shows that the two paralogs are indeed very highly conserved (91.6%), particularly within the protein kinase domain (Figure 18B+C) which contains the ATP binding domain and the TXY phosphorylation site (both conserved). Within the protein kinase domain there are on average 4.7 changes per 100 amino acids whereas outside this domain there are 16.5 changes per 100 amino acids. Such high conservation within the kinase domain suggests that kinase function is conserved between the two paralogs and that any functional changes that are present are due to motifs outside of the protein kinase domain. Unfortunately, predictive software was

unable to identify functional domains outside of the kinase domain so it is not possible to identify exactly what effect these changes have by *in silico* methods.

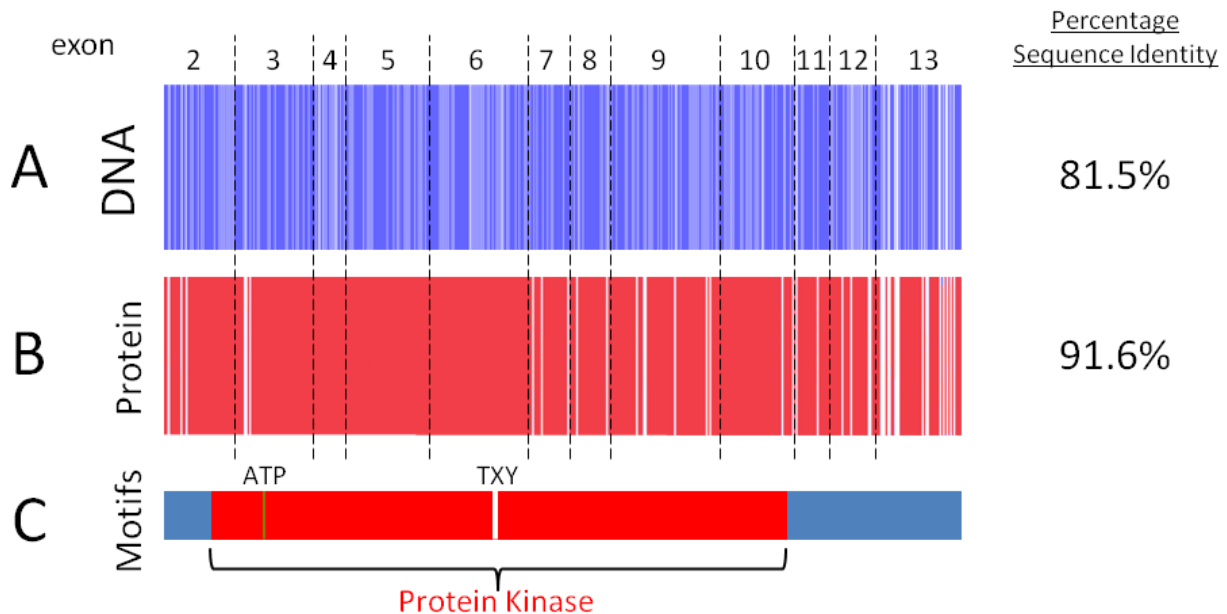


Figure 18 Sequence Alignments between the Zebrafish *jnk1* Paralogs DNA and Protein Sequences.

Schematic representation of sequence alignments between *jnk1a* and *jnk1b*, where white represents a mismatch. A) At the DNA level, many sequence changes are present between the two paralogs and sequence identity is 81.5%. B) At the protein level there is far more concordance between the sequences, with a percentage identity of 91.6%. C) The region with least conservation is at the 3' end of the sequences and lies outside of the protein kinase domain.

3.2.5.2 Sequence Divergence in the Middle Exon

Identification of the new splice-variants for both *jnk1* paralogs shows that the two paralogs are more similar to one another than has been predicted by the ENSEMBL pipeline. The two paralogs have the same number of exons, and each produces variants that differ by the middle exon usage, and by length. To confirm that the newly identified middle exon of *jnk1b* is indeed homologous to *jnk1a* exon 7 I ran sequence alignments between both middle exons of each paralog to determine which were most similar. Alignment supports the theory that the novel *jnk1b* exon is homologous to *jnk1a* exon 7 as they share far greater sequence identity (89%) to one another than to exon 8 (Figure 19A). The differences that do exist between the middle exons (resulting in amino acid changes) largely avoid the major region

of secondary structure – a helix (Figure 19B) – and instead fall within the random coil region. The low frequency of amino acid changes within the region of secondary structure suggests that this structure may be important for protein function, and that function between the transcripts may be well conserved.

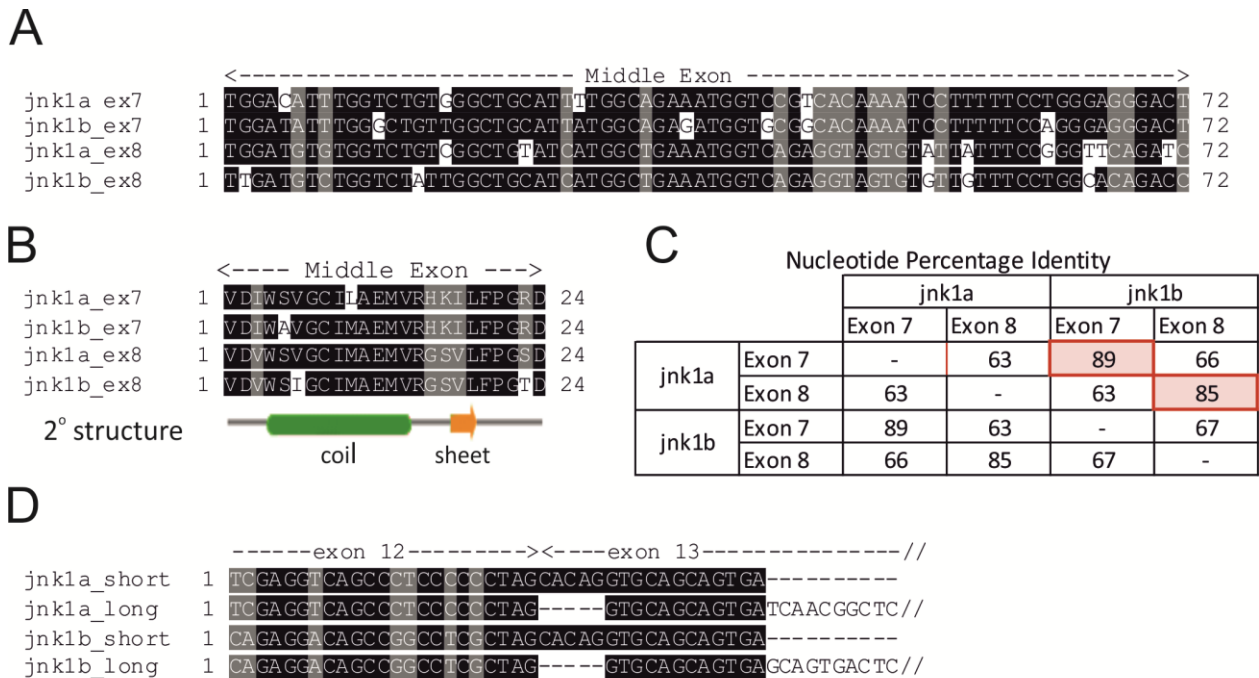


Figure 19 Sequence Alignments at the Region of the Splicing Events.

A) Nucleotide alignment of the middle exons of jnk1. B) Amino acid alignment of the middle exon with predicted secondary structure schematic below. Helix (green), beta-sheet (orange), random coil (black line). C) Table displaying the quantitative alignment results between the middle exons of both jnk1 paralogs. D) Nucleotide alignment of 3' splicing event. For all text-based alignments black is 100% identity (4/4), gray is identity between half the sequences (2/4) and white is residue lacking identity to the other sequences.

3.2.5.3 Sequence Conservation at the 3' Alternative Splicing Acceptor

The 3' splicing event results from the use of an alternative splice acceptor site in exon 13 of *jnk1*. The two alternative splice acceptor sites are 5bp apart (Figure 19D) but results in a frameshift which drastically changes the mRNA: use of the downstream acceptor increases the RNA length by 129bp (appendix Figure 58 and Figure 59). Alignment of the 3' splicing event shows that the sequence is identical in both paralogs of *jnk1* where the two splicing

acceptors reside (Figure 19D). The only differences in the sequence that do occur are several nucleotides upstream or downstream of the splicing sites in exon 12 of the paralogs.

3.2.6 Sequence Conservation of Zebrafish *jnk1* and its Orthologs

Due to the lack of experimental work performed on zebrafish *jnk1* when I started this project I searched the literature for homologous *jnk1* genes as a way to predict the function and expression of the paralogs. Now that I have full length sequences for both *jnk1* paralogs I am able to gauge whether this was a valid methodology in a post-hoc test for similarity in protein sequence. I therefore performed pair-wise sequence alignments on the protein sequences of the zebrafish *jnk1* genes and orthologous sequences that are published within Uniprot; the higher the sequence identity the more likely that function of the proteins will be conserved. Protein sequences were compared because this bypasses the issue of silent basepair changes that code for the same amino acid.

Whereas *Drosophila melanogaster* contains only a single *Jnk* homologue known as basket, vertebrates have three forms of the protein. Comparison of the two zebrafish Jnk1 proteins to their orthologs showed how well conserved the proteins are between very distant species – basket shares 76% identity with human JNK1 (Table 8). This conservation is even higher between the vertebrates and human JNK1; the two zebrafish paralogs share over 85% homology with human JNK1.

	Human	Mouse	Chicken	Xenopus L.	ZF jnk1a	ZF jnk1b	Drosophila	C. Elegans
Human	-	98.7	96.4	91.8	87.8	85.7	76.1	58.1
Mouse		-	97.7	92.5	87.0	86.7	76.1	64.6
Chicken			-	94.8	85.4	85.7	78.0	68.6
Xenopus L.				-	83.8	82.9	75.3	59.4
ZF jnk1a					-	91.8	73.9	57.6
ZF jnk1b						-	73.4	57.0
Drosophila							-	68.8
C. Elegans								-

Table 8 Percentage Identity of the ZF *Jnk1* Paralogs and their Orthologs.

Sequence alignment of orthologous Jnk1 proteins shows high conservation of the protein between species. The zebrafish versions are marked in red. These data show that there is greater than 85% of the sequence conserved between zebrafish and human JNK1.

CAEEL	1	MEERLSTSSYPSPHPGRSVEEDHNTLLASSSISSIIRGTRGHLNNFIESVGNWLPSSSG	NLRRLIGSGAQGIVCSA	DTVRNEQVAIKLSRPFQNVTHAKRAYRELK	LMSLVNHKNIIG
DROME	1	-----	NLRPIGSGAQGIVCAAYDTIT	QONVAIKLSRPFQNVTHAKRAYRE	FKLMKLVNHKNIIG
XENLA	1	-----	NLKPIGSGAQGIVCAADAVLERHVAIKLSRPFQNVTHAKRAYREL	VLMKCVNHKNIIG	
CHICK	1	-----	NLKPIGSGAQGIVCAAYDAILERNVAIKLSRPFQNVTHAKRAYREL	VLMKCVNHKNIIG	
HUMAN	1	-----	NLKPIGSGAQGIVCAAYDAILERNVAIKLSRPFQNVTHAKRAYREL	VLMKCVNHKNIIG	
MOUSE	1	-----	NLKPIGSGAQGIVCAAYDAILERNVAIKLSRPFQNVTHAKRAYREL	VLMKCVNHKNIIG	
jnk1a_BRARE	1	-----	NLRPIGSGAQGIVCSAYDNNLERNVAIKLSRPFQNVTHAKRAYREL	VLMKCVNHKNIIG	
jnk1b_BRARE	1	-----	NLRPIGSGAQGIVCSAYDHVLDLERNVAIKLSRPFQNVTHAKRAYREL	VLMKCVNHKNIIG	
ATP binding domain					
-----PROTEIN KINASE DOMAIN-----					
CAEEL	181	ILNCFTPOKKLDEFNDLYIVMELMDANLCQVIQMLDHERISYLLYQMLCGIRHLHSAGIIHRDLKPSNIVVSDCTLKILDFGLARTAI	IEAFMMTPYVVTRY	YRAPEVILGMGYKENVD	
DROME	86	LLNAFTPOKNLEEFQDVYIVMELMDANLCQVIQMLDHRMSYLLYQMLCGIKHLHSAGIIHRDLKPSNIVVKADCTLKILDFGLARTAGT	IFMMTPYVVTRY	YRAPEVILGMGYTENVD	
XENLA	88	LLNVFTPOKSLLEEFQDLYIVMELMDANLCQVIQMLDHERMSYLLYQMLCGIKHLHSAGIIHRDLKPSNIVVKS	SDCTLKILDFGLARTAGTSFMMTPYVVTRY	YRAPEVILGMGYKENVD	
CHICK	88	LLNVFTPOKSLLEEFQDVYIVMELMDANLCQVIQMLDHERMSYLLYQMLCGIKHLHSAGIIHRDLKPSNIVVKS	SDCTLKILDFGLARTAGTSFMMTPYVVTRY	YRAPEVILGMGYKENVD	
HUMAN	88	LLNVFTPOKSLLEEFQDVYIVMELMDANLCQVIQMLDHERMSYLLYQMLCGIKHLHSAGIIHRDLKPSNIVVKS	SDCTLKILDFGLARTAGTSFMMTPYVVTRY	YRAPEVILGMGYKENVD	
MOUSE	88	LLNVFTPOKSLLEEFQDVYIVMELMDANLCQVIQMLDHERMSYLLYQMLCGIKHLHSAGIIHRDLKPSNIVVKS	SDCTLKILDFGLARTAGTSFMMTPYVVTRY	YRAPEVILGMGYKENVD	
jnk1a_BRARE	88	LLNVFTPOKSLLEEFQDVYIVMELMDANLCQVIQMLDHERISYLLYQMLCGIKHLH	AAGIIHRDLKPSNIVVKS	SDCTLKILDFGLARTAGTGL	IMTPYVVTRY
jnk1b_BRARE	88	LLNVFTPOKSLLEEFQDVYIVMELMDANLCQVIQMLDHERISYLLYQMLCGIKHLH	AAGIIHRDLKPSNIVVKS	SDCTLKILDFGLARTAGTGL	IMTPYVVTRY

Thr/Tyr					
CAEEL	301	VWSIGCIEGELIRGRVLFPGGDHIDQWTRIIIEQLGTFDRSFLERLQPTVRNYVENRPRYQATPFEVLES	DNMFPM	TA	SSRLITCAQARDLLSKMLVIDPERRISVDLALRHPYINWVED
DROME	206	IWSVGCIMGEMIRGGVLFPGTDHIDQWNKIIIEQLGTFSSFSFMORLQPTVRNYVENRPRYTGYSFDELFPDGLFP	NDNNQNSRRKAS	DARNLLSKMLVIDPEQRISVDEALKHE	YINWYD
XENLA	208	IWSVGCIMGEMIKGGVLFPGTDHIDQWNKVIEQLGTPCTEFMKKLQPTVRTYVENRPRYAGYSFEKLFDPVLF	FPADSEHN	KLKASQARDLLSKMLVIDASKRISVD	ALQHPYINWYD
CHICK	208	IWSVGCIMGEMIKGGVLFPGTDHIDQWNKVIEQLGTPCPEFMMKKLQPTVRTYVENRPRYAGYSFEKLFDPVLF	FPADSEHN	KLKASQARDLLSKMLVIDASKRISVD	ALQHPYINWYD
HUMAN	208	IWSVGCIMGEMVCHKILFPGRDYIDQWNKVIEQLGTPCPEFMMKKLQPTVRTYVENRPRYAGYSFEKLFDPVLF	FPADSEHN	KLKASQARDLLSKMLVIDASKRISVD	ALQHPYINWYD
MOUSE	208	IWSVGCIMGEMVCHKILFPGRDYIDQWNKVIEQLGTPCPEFMMKKLQPTVRTYVENRPRYAGYSFEKLFDPVLF	FPADSEHN	KLKASQARDLLSKMLVIDASKRISVD	ALQHPYINWYD
jnk1a_BRARE	208	IWSVGCILAEVMVRHKLFPGRDYIDQWNKVIEQLGTPCTEFILKL	QSVRTYVENRPRYTGYSF	EKLFPDVLF	FPADSEHSKLKASQARDLLSKMLVIDASKRISVD
jnk1b_BRARE	208	IWAVGCILAEVMVRHKLFPGRDYIDQWNKVIEQLGTPSQEFMMKL	QSVRTYVENRPRYAGYSFEKLFDPVLF	FPADS	SHNKLKASQARDLLSKMLVIDASKRISVD
CAEEL	420	EIEVYAPPPLPYDHNDV-EQNVSWEHIFREITDYARTHDIYS	-----		
DROME	326	AEVVDAPAPEPYDHSVDEREHTVEQWKELIYEEVMDYEAHNTNNRTR	-----		
XENLA	327	PLEAEAPPPKIPDKQLDEREHTVEEWKELIYKEVLDWEERAKNGVIRGQPAPLGAAVTDG	SQAH	S	SSSGAASSMSTDPTASD
CHICK	327	PSEAEAPPPKIPDKQLDEREHTVEEWKELIYKEVMDLEERTKNGVIRGQPAPLQVQQ	-----		
HUMAN	327	PSEAEAPPPKIPDKQLDEREHTVEEWKELIYKEVMDLEERTKNGVIRGQPSPLGAAVINGS	QHP	SSSSVNDVSSMSTDPTASD	TSSLEAAAGPLGCCR
MOUSE	327	PSEAEAPPPKIPDKQLDEREHTVEEWKELIYKEVMDLEERTKNGVIRGQPSPLQVQQ	-----		
jnk1a_BRARE	327	PAEVEAPSPILITDKQLDEREHTVEEWKELIYKEVLDWEERAKNGVIRGQPSPLGAAVINGS	PQP	SSSSINDVSSMSTEPTASD	TSSLEASAGPLSCCR*
jnk1b_BRARE	327	PSEVEAPPPAITDKQLDEREHSVEEWKELIYKEVLDWEERTKNGVIRGQPASLGAAVSSD	SHEPS	TSSSSINDVSSMSTEPTASD	TSSQETSNGALHCCR*

Figure 20 Sequence Alignment of the Zebrafish Jnk1 Proteins to their Orthologs.

The Jnk1 protein sequences are well conserved between species, particularly within the protein kinase domain. The ATP binding domain (red) and Thr/Tyr phosphorylation sites (***) are conserved between all species. Conserved amino acids highlighted black, conservation of charge between $\geq 50\%$ sequences highlighted grey. jnk1a= translated sequence of jnk1a_7;long, jnk1b= translated sequence of jnk1b_7;long, all other sequences from UniProt: CAEEL (Q8WQG9), DROME (P92208), XENLA (Q8QHK8), CHICK (E1C1H4), HUMAN (P45983), MOUSE (Q91Y86).

3.2.7 Differential Expression Patterns of the *jnk1* Splice-Variants During Development

Having identified eight different splice-variants that are produced by the two zebrafish *jnk1* paralogs I wanted to determine if they showed different expression patterns during development. In order to achieve this it was necessary to design primers that were capable of distinguishing between the eight different variants. As the variants within the same paralog differ in only two locations (the middle exon and the 3' splicing acceptor) these sites were the only places where isoforms-specific primers could be targeted (Figure 16A).

Primer design for amplification of only one of the eight identified *jnk1* splice-variants was complex because of the strong sequence homology between multiple variants. However, by aligning these sequences it was possible to identify sites of greatest divergence, and the most robust primers possible were designed as described in the methods section (See section 2.2.11 page 73). These eight primer pairs were then rigorously validated to ensure that each was specific to only a single *jnk1* splice-variant.

3.2.7.1 Optimisation of RT-PCR Melting Temperature

In order to ensure high specificity of the splice-variant specific RT-PCRs I began by optimising the melting temperature of each primer pair PCR. The aim was to determine the highest melting temperature possible that still allowed primer annealing and yielded high amplicon abundance from cDNA. The PCR reactions were performed under the standard conditions (see section 2.2.12 page 78) except that a temperature gradient between 62-70°C was utilised over five reactions. The products were run out on a 2% agarose gel side-by side to determine when melting temperature became too restrictive to allow amplification. A positive control (1ng plasmid DNA at 62°C annealing) and negative (water replacing template DNA) control were also included.

The amplicon abundance when using *jnk1a* primers was reduced when a 66°C T_m was used compared to 64°C; by 68°C no product was seen in the wells (Figure 22A). In contrast there were still very strong bands visible at 66°C when using *jnk1b* primers (Figure 22B). Using these optimised conditions I decided to perform subsequent splice-variant specific RT-PCRs at 64°C when using *jnk1a* primers and 66°C when using *jnk1b* primers.

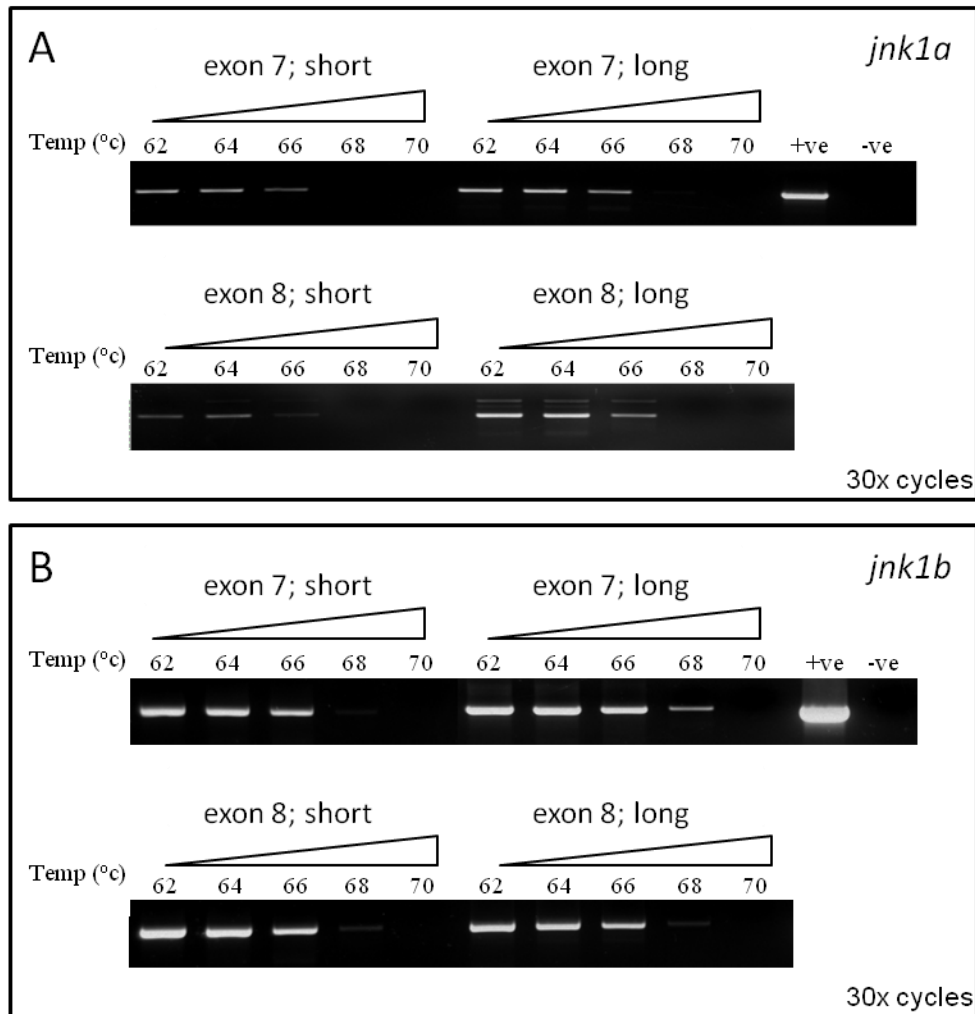


Figure 22 Melting Temperature Optimisation of Splice-Variant Specific Primers.

Temperature gradient RT-PCR on cDNA to determine how high melting temperature could be before becoming restrictive. A) *jnk1a* primers. Positive control is 1ng *jnk1a_7;long* in pGEM-T Easy at 62°C T_m. B) *jnk1b* primers. Positive control is 1ng *jnk1b_7;long* in pGEM-T Easy at 62°C T_m. All reactions performed for 30 cycles and 10µl loaded into 2% agarose gel.

3.2.7.2 Testing Primer Specificity

The design of eight primer combinations each capable of amplifying a single *jnk1* splice-variant was complex. Multiple sequence alignments showed that there were between four and six mismatches between the forward primers, and between one and six mismatches between the reverse primers and unintended targets (see Table 5). In order to confirm that the eight primer sets were each capable of picking out a single *jnk1* splice variant I performed multiple PCR reactions. A PCR master mix sufficient for 4.5 reactions was made containing one of the four *jnk1a* primer pairs and split between four different tubes before template cDNA was added to each tube separately. Template for the reaction was 1ng of one of the four full-length *jnk1a* variants sub-cloned into the pGEM-T Easy plasmid. The PCRs were then conducted under the optimised conditions and products were run side-by-side on an agarose gel. This method was then repeated for the *jnk1b* templates using the *jnk1b* primers. From this experiment I expected to see that when the primer combinations matched that of the template DNA there was amplification, however when primers did not match up, no amplification occurred. If amplification was seen when primers did not match the target DNA then this would have shown that the primers were not variant-specific. However, this experiment did prove primer specificity since PCR amplification was only achieved when the template DNA and the primer sets matched up (Figure 23). When other primer combinations were used, there was no amplification.

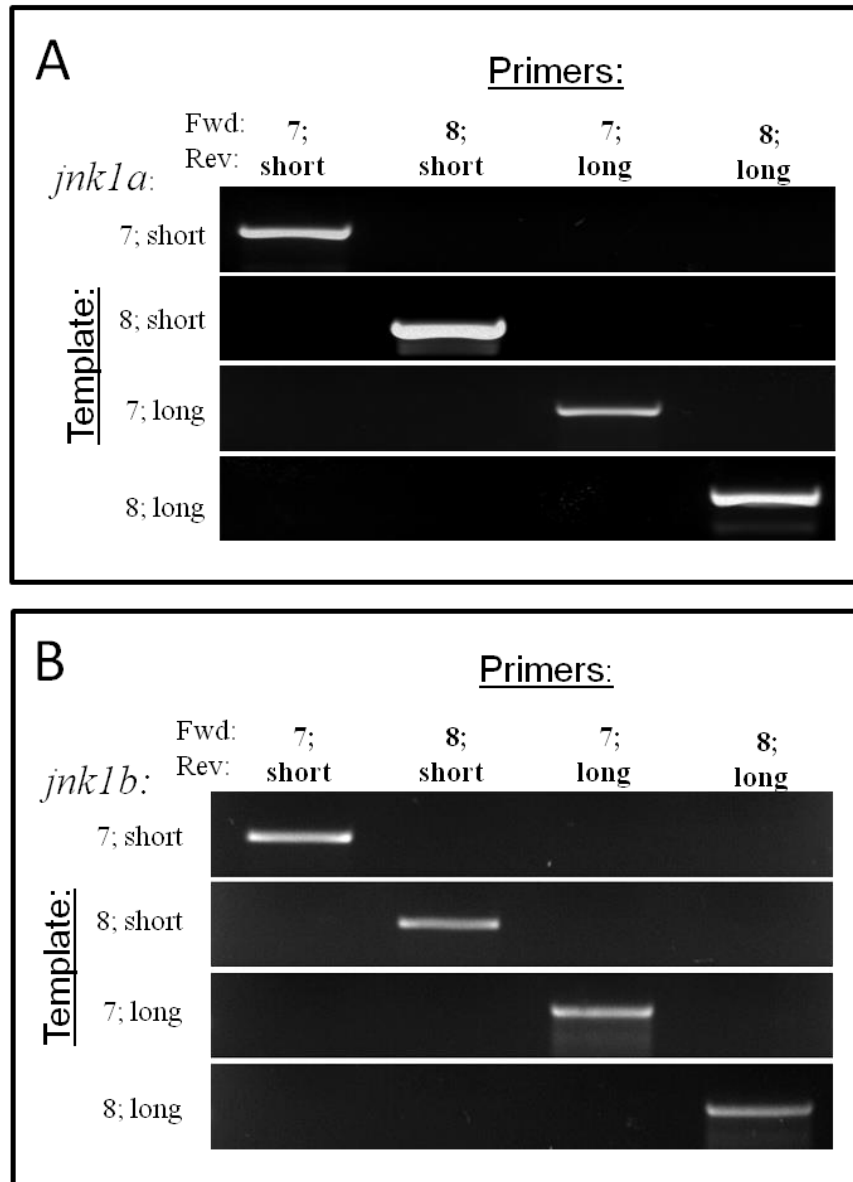


Figure 23 The Splice-Variant Primers are Specific to only a Single Transcript.

Parallel RT-PCR reactions of each *jnk1* splice-variant with different primer pairs of the same *jnk1* paralog. A) *jnk1a* variants with *jnk1a* primers. B) *jnk1b* variants with *jnk1b* primers. In both panels amplification is only seen when the primer set matches exactly the splice-variant. Each PCR is 1ng template in plasmid, 35x cycles, 20μl loaded per well and ran out on 2% agarose gel.

3.2.7.3 Expression Patterns of *jnk1* Splice-Variants during Development

Once the variant-specific *jnk1* primers had been shown to be specific and the PCR conditions had been optimised, they were used to determine what the expression pattern of different *jnk1* variants was during development. In total nine different developmental time-points were analysed which spanned both critical, early developmental processes, and late, broader time-points (Table 9).

For splice-variant specific PCRs a master mix sufficient for 47 reactions was made without primers or template DNA before being split between nine tubes. To each of the nine tubes was added cDNA from a different developmental timepoint (50ng / reaction) and then each of these tubes were split (18µl per PCR well) between a further 5 wells of a PCR plate (45 reactions total). The forward and reverse *jnk1a* primers and the housekeeping control primers (*elfa1*) were added to each tube individually such that the final plate contained 5 replicates of the developmental time series PCR each with a different *jnk1a* primer pair, or *elfa1* control primer pair. The housekeeping gene *elfa1* was chosen because it has been shown to have very stable expression levels during development and between different tissue types (McCurley and Callard, 2008). This experiment was repeated on cDNA generated from three different AB clutches and each band was scored for its intensity, before the experiment was repeated with *jnk1b* primers with an *elfa1* control. The average and SEM of the intensities were then plotted against hours post fertilisation.

Timepoint (hpf)	Importance
0	Maternal inheritance
4	Zygotic expression
5.25	Start of gastrulation
12	Kupffer's vesicle stage
19	Lateral plate mesoderm
24	Heart field fused / heartbeat
48	Heart movements completed
72	Mid-larval stage
120	Late-larval stage

Table 9 Importance of the Timepoints Chosen for RT-PCR

From the developmental series PCRs of *jnk1a* splice-variants it was clear that *jnk1a_7;short* was maternally inherited but that band intensity decreased over the next 12 hours until the transcript could not be picked up (Figure 24A). Expression of *jnk1a_7;short* does not return until around 24hpf and peaks at 72hpf. When the experiment was finished at 120hpf the expression still remained high. Similarly the variant *jnk1a_7;long* is maternally inherited but drops to zero by 12hpf (Figure 24A). Expression is present but very low at 24hpf but peaks at 72hpf as can be seen on the graph of band intensity (Figure 24B). The expression of *jnk1a_7;long* appears to drop off by 120hpf which is a situation also observed in the other exon 7 containing variant.

The expression pattern of the exon 8 containing *jnk1a* genes appears very distinct from those that contain exon 7. *jnk1a_8;short* has its highest abundance within the first 5 ½ hours of development, before settling to a low but consistent abundance during the other timepoints (Figure 24A). A very similar pattern is seen for *jnk1a_8;long* as maternal inheritance is very high and this high level drops over the next 5 ½ hours before becoming very low by 12hpf. After 12hpf the abundance remains low but constant until 5 days post fertilisation (Figure 24B).

The expression patterns of the *jnk1b* variants over development seem to closely resemble those of *jnk1a*. The variant *jnk1b_7;short* is inherited in small abundance but by 12hpf no transcript can be picked up (Figure 24C). Expression is once again seen by 48hpf and remains constant until 120hpf. The other exon 7 containing variant of *jnk1b* (*jnk1b_7;long*) is also weakly inherited and levels drop to zero by 12hpf. Similarly this expression is seen again at 48hpf and over the next two days remains fairly constant (Figure 24D). The exon 8 containing *jnk1b* variants have similar expression patterns to one another. *jnk1b_8;short* is highly maternally inherited but abundance drops over the next 12 hours and remains at low levels. Similarly the *jnk1b_8;long* transcript is high at early timepoints but by 12hpf is at a low, baseline level until 120hpf (Figure 24D).

These data seem to suggest segregation in the expression pattern of the *jnk1* splice-variants based upon middle-exon usage. The expression of the exon 7 containing *jnk1a* variants is low initially but high expression is seen during 48-120hpf. Interestingly this result is mirrored in the *jnk1b* variants that contain exon 7 only reach high expression during late development. The exon 8 containing variants of both paralogs contrast this pattern because they are most strong at early timepoints before falling to baseline levels by 12hpf. These results suggest that the variants are needed at different times in development.

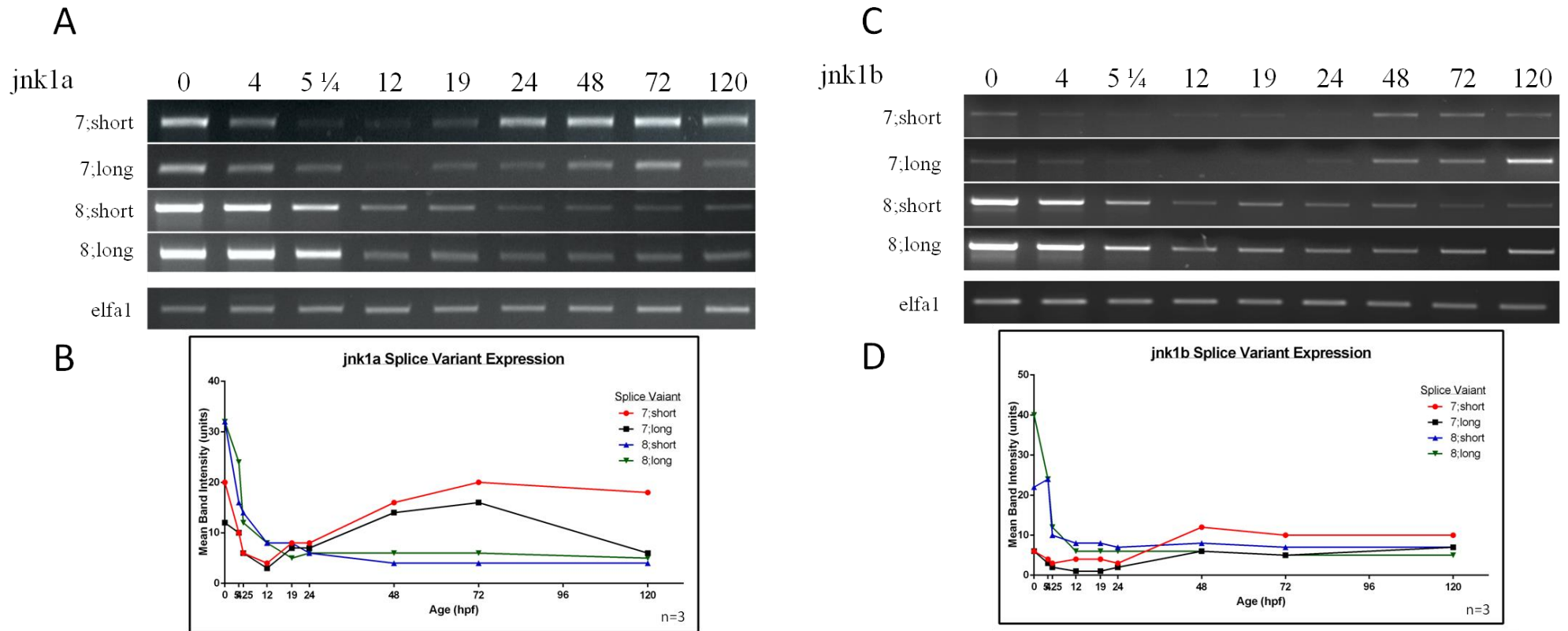


Figure 24 Expression Patterns of the jnk1 Splice-Variants During Development.

A) Representative RT-PCR agarose images of the jnk1a splice-variant expression pattern over development. B) Graph of semi-quantitative data of band intensity of variants obtained over three replicates. C) Representative RT-PCR data of jnk1b expression patterns over development. D) Semi-quantitative graph of band intensity of jnk1b variants over three replicates.

3.2.8 Differential Expression Patterns of the *jnk1* Splice Variants in Adult Tissues

To examine which tissue types the different *jnk1* splice-variants were expressed in, young adult zebrafish at 4 months of age were sacrificed and dissected to obtain the necessary tissue. Young adults were chosen for this experiment to ensure that the results represented the endogenous expression of *jnk1* in healthy tissue. Being a “stress activated” protein kinase, *JNK1* has been shown to have upregulated expression in response to disease (Migheli et al., 1997, MagiGalluzzi et al., 1997, Li et al., 1998) as well as other cellular stresses (Lo et al., 1996); therefore young, healthy adults were selected to avoid any underlying cellular stresses. Dissected tissue was immediately processed for RNA extraction and cDNA generation under standard methods.

Splice-specific *jnk1* RT-PCRs were performed to determine the expression of each of the variants in different adult tissue. A master mix suitable for 26 reactions was produced with the absence of primers and template cDNA before being split between 5 eppendorf tubes. Each tissue specific cDNA was added to a different tube and then 18µl of each mix was pipetted to a PCR tube. The five different primer pairs (*jnk1a_7;short*, *7;long*, *8;short*, *8;long*, Elfa1) were added directly to the PCR tubes and then the PCRs were run at the optimised annealing temperatures (see 2.2.4.3).

3.2.8.1 Exon 7 Containing Variants are Predominantly Restricted to the Brain

Splice-variants of *jnk1a* which contain exon 7 were primarily restricted to the brain (Figure 25A) although the testes also showed low levels of *jnk1a_7;short*. This pattern was also observed in the *jnk1b* variants. Both *jnk1b_7;short* and *jnk1b_7;long* showed very high expression within the brain, however no expression was observed in other tissue types (Figure 22).

3.2.8.2 Exon 8 Containing Variants are Expressed Fairly Ubiquitously

Exon 8 containing variants appeared to have a much broader pattern of expression than those containing exon 7. Both the short and long forms of *jnk1a* that contained exon 8 were expressed in heart, skeletal muscle, testes and the brain. Expression was highest in the testes with moderate expression levels in the other tissues (Figure 25A). The *jnk1b* variants that contain exon 8 were also expressed in the heart, skeletal muscle, testes and brain (Figure 25B), although expression was fairly equal in all of these tissues. There was also weak expression of both *jnk1b_8;short* and *jnk1b_8;long* in the liver, although band intensity was several fold weaker than in other tissues.

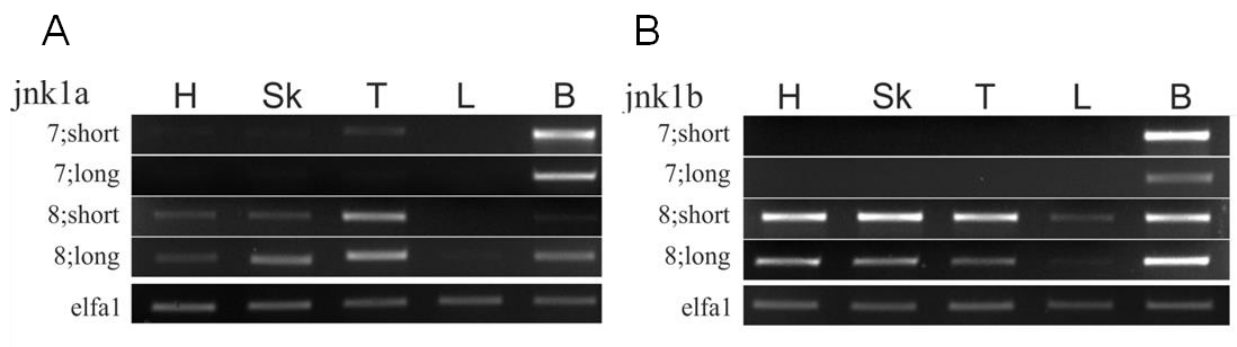


Figure 25 RT-PCR Expression of *jnk1* Splice-Variants in Adult Tissues.

A) *jnk1a* splice-variants B) *jnk1b* splice-variants. The housekeeping gene *elfa1* is used as a loading control. H heart, Sk skeletal muscle, T testes, L liver, B brain

3.2.9 Comparison of *jnk1* Expression in Zebrafish, Human and Mouse Adult Tissue

The expression levels of both zebrafish *jnk1* genes were estimated by semi-quantitative RT-PCR, which provided estimates of how strongly each *jnk1* transcript was expressed in five different tissue types. However, it is also possible to compare this zebrafish tissue-specific expression with mouse and human level expression. This analysis was carried out to answer two questions, firstly to see whether the tissue-specific expression patterns of the zebrafish *jnk1* genes matched those of other species and so strengthen the case for zebrafish as a model of human *JNK1*, and secondly to determine whether the differences observed in expression between *jnk1a* and *jnk1b*

meant that one of these genes more closely matched the expression patterns of the single vertebrate *JNK1* gene.

Gene expression data for both mouse and human tissues was taken from the European Bioinformatics Institute Expression Atlas (<https://www.ebi.ac.uk/gxa>). This freely-accessible database compiles information from microarray and RNA-seq experiments in order to detail the relative expression levels of each gene in different tissues of the adult and embryo. From this database I was able to find six studies of human adult tissue which included *JNK1* expression and six studies of mouse adult tissue including *Jnk1*. However, two of the studies in mouse had to be discounted during analysis due to too few tissue types being represented to make a reliable estimation of *Jnk1* expression levels (see section 2.1.7 on page 59). The levels of *JNK1* expression were compared between the heart, skeletal muscle, testis, liver and brain in order to determine whether the relative expression in each tissue was high, medium or low. Similarly, densitometry was performed over the four zebrafish *jnk1a* and *jnk1b* genes in order to determine their relative expression in each tissue. The results revealed that by this measure of gene expression, both zebrafish *jnk1a* and *jnk1b* genes are expressed at levels similar to the mouse and human in the tissues examined.

Species	Gene	Heart	Sk. Muscle	Testis	Liver	Brain
Zebrafish	<i>jnk1a</i>	LOW/MED	MED	MED/HIGH	LOW	MED/HIGH
Zebrafish	<i>jnk1b</i>	MED	MED	MED	LOW	MED/HIGH
Mouse	<i>Jnk1</i>	MED	MED	MED/HIGH	LOW/MED	HIGH
Human	<i>JNK1</i>	LOW	LOW	MED/HIGH	LOW/MED	HIGH

Table 10 Relative tissue-specific expression levels of zebrafish *jnk1a* and *jnk1b*, mouse *Jnk1* and human *JNK1* genes.

A comparison of the expression patterns as determined by densitometry of RT-PCR data in the zebrafish (n=3) and analysis of multiple RNA-seq studies in the mouse (n=4) and human (n=6) reveals similarities and differences between JNK1 expression in the tissues of these species.

A comparison of the tissue-specific expression patterns of the *jnk1a*, *jnk1b*, *Jnk1* and *JNK1* genes revealed that throughout these species there was similar expression patterns conserved in these tissues, although some differences were observed. The expression of these genes was low or medium in the heart, low or medium in the skeletal muscle, medium or high in the testes, low or medium in the liver and medium or high in the brain. There were no instances where low gene expression in one species contrasted with high expression in that tissue in a different species. Some conflicts in expression level did arise however, such as where *jnk1a*, *jnk1b* and *Jnk1* had medium expression in the skeletal muscle whereas human *JNK1* was lowly expressed and where low liver expression was found in *jnk1a* and *jnk1b* compared to low to medium expression in *Jnk1* and *JNK1*. These differences may reveal real changes in gene expression between species or be an artefact of the qualitative method of measurement used.

The relative expression levels of the zebrafish *jnk1a* and *jnk1b* genes differed in the heart and testis. In the heart the *jnk1a* level was low to medium whereas the *jnk1b* level was medium. In this instance the *jnk1a* level was more similar to that of human *JNK1* where low expression was displayed in the heart. In the testis *jnk1a* was medium to high whereas *jnk1b* had medium expression. In this case the *jnk1a* expression level again matched more closely with what was observed in human *JNK1* where medium to high expression was found. However, it is important to note that the *jnk1a* level did not always exactly match that found in human *JNK1* such as in the skeletal muscle where *jnk1a* was expressed at a medium level compared to low expression of human *JNK1*. In summation these data have provided an interesting comparison of *JNK1* gene expression between zebrafish, mouse and human, but require further experimental validation for more exact comparisons to be made.

3.3 DISCUSSION

In this chapter I designed primers capable of pulling out full-length *jnk1* splice-variants and discovered four novel variants that had not been predicted by the ENSEMBL pipeline. Using in silico techniques the sequences were then compared to determine whether functional domains were conserved and where in the sequences the variants differed from one another. Further analysis of protein sequences revealed that the zebrafish Jnk1 sequences are highly consistent with human and mouse orthologs, and that all orthologs have conserved the functional domains of the proteins. Primers were then designed to bind specifically to each variant and PCR conditions were optimised to ensure specificity. Finally the expression patterns of the individual *jnk1* splice variants were determined during development of the zebrafish embryo and in different adult tissues.

A large proportion of the research that deals with the *JNK* family genes do not differentiate between the *JNK* family members (*JNK1*, 2 or 3) - particularly where the methods include small molecule inhibitors that effect all forms. This means that it is impossible to differentiate between the individual roles of each *JNK* family gene, despite evidence that in several organisms the genes have non-overlapping expression patterns (Kuan et al., 1999, Yamanaka et al., 2002). However, a further level of complexity is introduced to the function of *JNK* when the different splice-variants are taken into consideration. In humans the four core variants of *JNK1*, which differ in middle exon and length, were shown to exist in 1996 (Gupta et al., 1996). I have been able to show that these four variants also exist within zebrafish *jnk1a* and *jnk1b* which had not previously been predicted. The conservation of four different variants for both paralogs is likely to represent important functional properties that each variant possesses. Despite this there are very few papers that take individual splice-variants into consideration. In this investigation I have been able to characterise the individual transcripts of zebrafish *jnk1* in detail, as well as determine their individual expression patterns.

3.3.1 Identification of Novel Splice-Variants

3.3.1.1 *The ZF jnk1 Paralogs are Highly Similar to One Another and their Orthologs*

The discovery of an additional splice acceptor in *jnk1a*, and the missing exon 7 within *jnk1b* has revealed that the two *jnk1* paralogs are more similar than was previously thought. Both zebrafish paralogs have thirteen exons, many of which are of identical length, and both contain two middle exons that are used in a mutually exclusive manner. In addition, both genes give rise to four splice-variants that have homologous variants in human *JNK1*. The implications of this discovery are significant for future research into the *jnk1* genes both in terms of function designation to each variant and when using zebrafish to model human genetics. Since the “core” four variants have been conserved between teleosts and humans it is reasonable to conclude that some selective pressure must exist to ensure that each of the transcripts are maintained. One possible reason for this conservation would be that each variant has a different functional role, however, no evidence has been published to show this in *JNK1*. However, it has been shown that middle exon usage of *JNK1* causes different binding affinity to downstream transcription factors (Gupta et al., 1996).

The fact that orthologs of the core *JNK1* variants exist in zebrafish suggests that it may be a good genetic model for understanding human *JNK1* function. Zebrafish have proved a powerful model for genetic modelling due to their rapid generation time, multiple developed forward genetic techniques, and their robustness to survive significant insult during development. However the existence of two *jnk1* paralogs in zebrafish may undermine their use as a genetic model since there is only a single human *JNK1* gene. If the zebrafish *jnk1* genes have gained function which the human ortholog does not possess then the two genes would not be directly comparable. However, if the function of *JNK1* is instead shared between the two *jnk1* paralogs, then zebrafish may prove more powerful than other models which possess only one gene. With different facets of *JNK1* function shared between two genes it would be possible to examine certain functions of the gene without perturbing all function. Further study is required to determine the validity of zebrafish as a human *JNK1* model, however, this project has begun the process.

These data have greatly increased what we know about zebrafish *jnk1*, proving the existence of several ENSEMBL splice-variant predictions, as well as discovering several unpredicted forms. The methodology used to gain these sequences also meant that upon discovery, the sequences were cloned into plasmid vectors and could be used for downstream procedures such as generation of RNA for rescue experiments. However there are certain limitations to the methodology that was used, primarily since the primers were not capable of amplifying all predicted splice-variants.

The primers that were ordered for this project were designed to bind at the start and end of the longest predicted splice-variants. A quirk of the splicing events of the *jnk1* paralogs meant that one primer set was able to pull out multiple transcripts. However, the ENSEMBL pipeline predicted the existence of three *jnk1a* and two *jnk1b* variants which these primers were not capable of amplifying. The choice to target the transcripts which had experimental evidence to support their existence was made to maximise the chance of successfully cloning full-length *jnk1* transcripts. Targeting a transcript which did not exist by this RT-PCR methodology would have had significant time and financial burdens associated with it because no amplification would occur; in this scenario it would be impossible to determine whether the absence of amplification was due to a problem with the PCR conditions, problems with the primers, the transcript not being expressed at that timepoint or tissue type, or whether the transcript simply did not exist. Multiple condition optimisations and primer redesigns would be required to say with any certainty that a transcript does not exist. An alternative method that would be able to target all predicted variants (as well as possible unpredicted ones) is rapid amplification of cDNA ends (RACE). 5' and 3' RACE have advantages over standard RT-PCR because multiple targets with significantly different sequences at their ends can be amplified with a single gene-specific primer. It would therefore be possible to determine whether the *jnk1b* transcripts -003 and -201 (Figure 12) exist which are predicted to differ only at the 3' end. The major disadvantage to this method is that full-length transcripts cannot be cloned without further steps, something that was particularly important in this project. Therefore, although it is a viable method for proving the existence of transcripts it is not as efficient at generating full-length sequences as standard RT-PCR.

3.3.2 Bioinformatical Analysis

3.3.2.1 *The jnk1 Paralogs Differ Most in Sequence Outside of the Protein Kinase Domain*

I have shown that despite arising from a common ancestor the two *jnk1* paralogs contain a surprisingly large number of basepair changes to one another (Figure 18). However, the majority of these changes are silent and percentage identity of the amino acid sequence is over 90%. The region of greatest amino acid conservation is within the protein kinase domain, suggesting that both paralogs are capable of functioning as a MAPK. Changes outside of this domain mostly cluster downstream of the 3' splicing event, and therefore reside only in the long paralogs. Since no functional domains are known to be present in this region it is not possible to predict what functional consequences that these changes might cause. Furthermore, no x-ray crystallographic data of the long variant exists, so I cannot ascertain what consequence to 3-D structure these changes will cause.

The two middle exons are used in a mutually exclusive manner and result in amino acid changes to the protein. Examination of secondary structure produced by the middle exons with Jalview software reveals that the middle exon contributes to a coil and short sheet structure (Figure 19B). Interestingly the majority of changes that occur between exon 7 and exon 8 of *jnk1* reside outside of these regions that produce secondary structure, and instead fall within a region of random coils. X-ray crystallographic data for zebrafish Jnk1 is not available, however the human JNK1 data can be found on the Protein Data Bank (www.rcsb.org/pdb). This data provides a 3-D structure of the protein that helps to illustrate how the protein folds. From the 3-D rendering of the human protein I was able to identify the region of the protein which arises from exon 7 or exon 8 (Figure 26). The helical structure that forms from the middle exon contribution runs through the centre of the JNK1 molecule, whereas the random coiled region lies at the surface of the molecule. Since the majority of amino acid differences that exist between the two zebrafish middle exons reside outside of the helix it is unlikely that these changes will affect the secondary or tertiary shape of the molecule. Instead the changes exist in the random coiled region, and are likely found at the surface of the protein, where they may interact with other molecules.

This finding supports the experimental evidence that exists in human JNK1 which shows that the isoforms containing either exon 7 or exon 8 have different binding abilities to downstream transcription factors (Gupta et al., 1996).

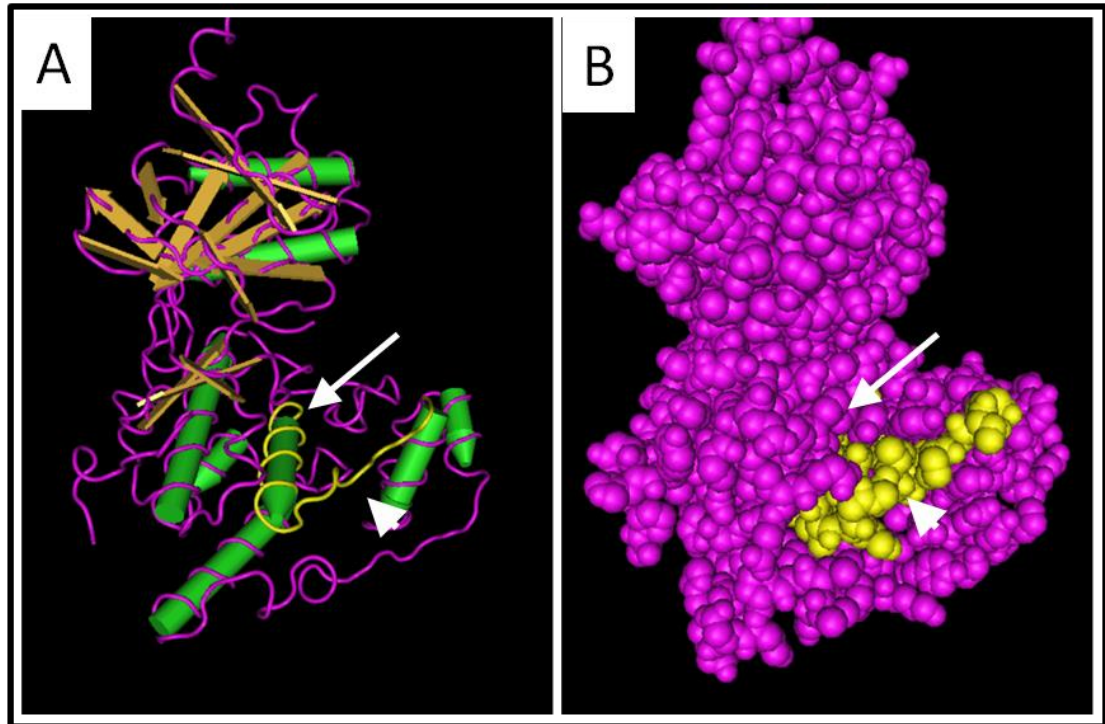


Figure 26 Structural 3-D Model of the JNK1 Protein Shows the Location of the Middle Exon Within the Structure.

A) Tube rendering of human JNK1 displaying beta-sheets (orange) and helices (green) within the protein. The amino acids that originate from the middle exon sequence are coloured yellow. The contribution of the middle exon to a helix (arrow) and random coil (arrowhead) are highlighted. B) Space fill rendering of human JNK1 showing the location within the protein of the helix (arrow) and random coil (arrowhead) that arise from the middle exon. X-ray crystallographic data obtained from www.rcsb.org/pdb ref no. 2XRW_A.

3.3.2.2 Strong Conservation to Homologous Sequences Suggest Function is Preserved

I have shown that there is a high level of conservation between the zebrafish *jnk1* paralogs and their orthologs in other vertebrates. Since the majority of work on *JNK1* has been conducted on mouse or using human cell lines, this result is important as it means that results in these species are probably also relevant to the zebrafish. Ortholog information has been invaluable in this investigation to determine predictive expression and functional properties of zebrafish *jnk1*. More importantly though this result suggests that findings within zebrafish may be translatable to human. Modelling *Jnk1* knockout in the mouse has provided underwhelming results because only very mild, behavioural changes were seen (Reinecke et al., 2013) due to compensation by *Jnk2* (Kuan et al., 1999). The mild phenotype is not recapitulated in other species though such as in *Xenopus* where convergent extension defects develop (Yamanaka et al., 2002) and *Drosophila* where gut chirality becomes randomised (Taniguchi et al., 2007). Now that zebrafish have been shown to possess splice-variants homologous to the four core variants seen in human *JNK1* they represent a good candidate for modelling *JNK1* function in the human. It will be very interesting whether deficiency of the *jnk1* paralogs in zebrafish cause mild defects (as in mouse) or severe defects (as in *Xenopus*).

3.3.3 *jnk1* Expression Analysis

Previously published expression data for the zebrafish *jnk1* genes have been contradictory and often incomplete. To address this issue I conducted splice-variant specific RT-PCRs throughout development and in adult tissues. I have shown that despite all variants being maternally inherited, there is clearly a differential expression pattern between variants incorporating different middle exons. Splice-variants incorporating exon 8 are most abundantly expressed during early development before settling to a baseline level. Exon 7 variants by contrast are weakly expressed early on, but become strongly expressed by larval stages (Figure 24).

The differential expression of individual splice-variants over development is likely to be a highly regulated process that is controlled by transcription factor binding to the *jnk1*

gene, although to date no known transcription factors have been identified that up or downregulate the expression of individual splice-variants of zebrafish *jnk1* or one of its orthologs. It would therefore be very interesting to perform analysis of transcription factor binding (e.g. chromatin immunoprecipitation) as a method of cataloguing which transcription factors bind to the *jnk1* genes which may lead on to analysis of splice-specific expression regulation; overexpression of these transcription factors within cell lines could possibly identify which transcription factors differentially affect *jnk1* splice-variant expression.

3.3.3.1 Differential Expression of Exon 8 Containing Splice-Variants Switch May Coincide with Proliferation Changes

The differential expression patterns of different *jnk1a* and *jnk1b* splice-variants during development are probably representative of what developmental processes are occurring at these time-points. Although no data for functional differences in the zebrafish variants has been published, some evidence may be available from the human *JNK1* ortholog. The 1996 paper by Gupta et al. investigated the individual splice-variants of the ten human splice-variants that arise from *JNK1*, *JNK2*, and *JNK3* (Gupta et al., 1996). In addition they examined the binding efficiency of different splice-variants to three downstream transcription factors – *ATF2*, *c-JUN* and *ELK-1* – by glutathione-agarose pull down assay.

In Gupta et al. (1996) the binding affinity of human *JNK1* splice-variants to C-JUN was found to differ depending upon which “middle-exon” was used in the transcript. These results demonstrated that the exon 8 containing variants of *JNK1* bound preferentially to C-JUN with barely any binding with exon 7 containing variants (Gupta et al., 1996). These data therefore suggest that exon 8 containing *JNK1* transcripts may be more important in regulating cell proliferation since C-JUN has been shown to be important for proliferation and progression through G1-phase (Wisdom et al., 1999, Angel and Karin, 1991). Such a function would seem to fit with the differential expression pattern that has been found for zebrafish exon 8 containing variants of *jnk1*. Exon 8 containing variants are expressed most highly during early development when proliferation rates

in the embryo are also high, however expression drops after about 12 hours down to baseline. A detailed analysis of proliferation during early development would be a logical step to determine whether these rates correlate with the expression of exon 8 containing *jnk1*. Furthermore by overexpressing these exon 8 containing variants during development we would expect to see an increase in cell proliferation. These experiments could help to elucidate a splice-variant specific role for *jnk1* during development.

3.3.3.2 Differential Expression of Exon 7 Containing Splice Variants Coincides with Brain Development

Exon 7 containing *jnk1* variants are maternally inherited and then show highest expression during late developmental time-points (24-72hpf). In adult tissue the exon 7 containing variants are found highly in the brain and very rarely in other tissues that were studied. These data suggest that exon 7 *jnk1* transcripts are important in neural tissue. This hypothesis would fit with the change that is observed during late development because exon 7 containing variants are expressed highly during late development when brain development is occurring. However, this does not explain why these variants are maternally inherited. It may therefore be that exon 7 containing variants possess other functions during these very early developmental timepoints that cannot be answered here. It would be interesting to knockdown and overexpress different splice-variants individually in order to determine what role each variant had. However, since much of the sequence is identical between different splice-variants it may be that such knockdowns would be compensated by other transcripts.

3.3.3.3 RT-PCR is Limited by being a Semi-Quantitative Measure of Gene Expression

The use of RT-PCR as a method of measuring splice-variant abundance has greatly increased what is known about the expression patterns of *jnk1* during development, and in different tissue types. However, RT-PCR is a technique that measures mRNA abundance in a semi-quantitative manner and therefore does not fully quantify

expression levels. The use of RT-PCR was decided upon because of the restrictions of where primers can be designed to pick out individual splice-variants. The four variants that have been shown to exist per paralog differ in only two place: the middle exon and the 3' splice-acceptor site. These two regions are therefore the only places that primers can be designed to which will make them specific to a single splice-variant. The two regions where primers have been designed to are ~500bp apart, a distance which is much too large to amplify with quantitative real-time PCR (qPCR). To remain efficient the amplicon of qPCR is typically 50-100bp in length, therefore this was not an option in this experiment. Furthermore, the use of *in situ* hybridisation to stain tissues that express an individual splice-variant during development was also not a viable option. The riboprobes used during *in situ* hybridisation are typically between 500 to >1000bp in length and must be significantly unique to the target mRNA so that they do not bind off target. Since the different splice-variants of a single *jnk1* paralog can differ by as little as 5bp, this method of examining expression patterns would be very unlikely to produce specific results.

When measuring the mRNA expression patterns of a particular gene, the main goal is most often to estimate the abundance of protein that that cell / embryo is producing at that timepoint; mRNA is measured as an indirect measure of protein abundance. However, it has been observed that often mRNA expression levels do not equate to total protein abundance (Tian et al., 2004, Vogel et al., 2010), so where possible it is better to measure protein levels directly. In the case of zebrafish *jnk1* there are no commercially available antibodies which can distinguish between *jnk1*, 2 or 3 at the time of writing. This lack of specific antibodies was problematic for proving morpholino knockdown later in the project, and also meant that measuring splice-variant specific protein levels was unachievable with conventional immunoblotting techniques. A possible method that could be used is 2D gel electrophoresis followed by mass spectrometry which could identify different splice-variants and estimate the abundance within the sample. However, this process is considerably more time consuming than RT-PCR and requires specialist equipment. Since protein quantification of the different *jnk1* splice variants was not the major priority of this project it was felt

that the additional information gained over RT-PCR did not justify the additional time and cost.

3.3.3.4 Evidence of Tissue-Specific Gene Expression Pattern Conservation between Zebrafish, Mouse and Human

In order to compare the tissue-specific *jnk1* expression patterns that were observed in zebrafish with the mouse and human, data from the EBI Expression Atlas were compiled (<https://www.ebi.ac.uk/gxa>). These levels of gene expression in each tissue were then compared against the zebrafish tissue levels that were found by the sum of expression of each splice-variant. The comparison revealed that expression levels in those tissues examined were well conserved between zebrafish, mouse and human, and no tissues had low expression for *JNK1* in a species where high levels were reported in another species. This result is supportive of a conserved function between the zebrafish genes (*jnk1a* and *jnk1b*) and the mammalian genes where only a single copy is present (*Jnk1* or *JNK1*). Of the differences that were observed the greatest differences were found in the heart and skeletal muscle (see Table 10). In the heart human *JNK1* was expressed at low levels compared to low/medium expression in *jnk1a*, and medium expression in *jnk1b* and mouse *Jnk1*. In the skeletal muscle low human *JNK1* levels were contrary to medium expression of *jnk1a*, *jnk1b* and *Jnk1*. These differences could represent a genuine difference in expression level between species or be an artefact of the qualitative nature of this study. I believe that further evidence is therefore necessary before a definitive difference in expression is concluded.

When comparing the tissue-specific expression of the two zebrafish *jnk1* genes to human *JNK1* it appeared that zebrafish *jnk1a* was a closer match to human expression than *jnk1b* (Table 10). In both heart and the testis where *jnk1a* and *jnk1b* expression levels were different from one another, the *jnk1a* level was closer to human *JNK1*. This result may suggest that of the two zebrafish *jnk1* genes the one which is more similar to the human gene is *jnk1a*. However, caution is necessary firstly due to the qualitative nature of the test, and also because the zebrafish *jnk1a* levels did not always closely match human *JNK1* in all tissues (e.g. in the skeletal muscle). I therefore believe that a

side-by-side experimental measure of tissue-specific expression is required before this conclusion can be reached. However, this test provides the first indication of similar tissue-specific expression patterns between zebrafish and human *JNK1* genes.

3.3.3.5 Concluding Remarks

These data have achieved the aims of this chapter by proving the existence of and characterising several *jnk1* splice-variants in the zebrafish genetic model. Furthermore the expression patterns of these variants have been shown in a semi-quantitative manner through development and in different adult tissues. In addition, preliminary evidence of conserved tissue-specific gene expression has been demonstrated between zebrafish, mouse and human. These data can now be used in the design of morpholino oligonucleotides to specifically knockdown the zebrafish *jnk1* genes, as well as attempt a rescue of the knockdown by overexpression of these splice-variants.

CHAPTER 4 - CHARACTERISATION OF THE JNK1 MORPHANT PHENOTYPE

4.1 INTRODUCTION

4.1.1 The Role of *jnk1* During Development

As has been previously stated in the introduction, the role of c-Jun N-terminal Kinase during development is poorly understood. In *Drosophila melanogaster* the loss of the single *JNK* ortholog *basket* (*bsk*) results in failure of dorsal closure as well as gut laterality defects (Taniguchi et al., 2007, Martin-Blanco et al., 1998). In *Xenopus* loss of *jnk1* has been linked with convergent extension defects, although this result was not recapitulated when zebrafish *jnk1a* and *jnk1b* were knocked down by splice modifying morpholinos (Kim and Han, 2005, Seo et al., 2010). In a mouse knockout system for *Jnk1*, only mild behavioural defects were demonstrated (Reinecke et al., 2013). The relatively mild nature of defects caused by loss of *JNK1* in the zebrafish and mouse are surprising considering how many processes that the *JNK* genes have been associated with. Furthermore, loss of the major downstream gene *Jun* causes embryonic lethality with cardiac and hepatic defects (Eferl et al., 1999, Hilberg et al., 1993). It appears therefore that the *JNK* genes have some overlapping function and are capable of compensating for loss of one another. Evidence for this comes from mouse where loss of a single *JNK* gene can be tolerated but the *JNK1*^{-/-} *JNK2*^{-/-} compound genotype is lethal due to a failure to close the neural tube and hepatic apoptosis (Kuan et al., 1999).

Due to the considerable confusion about the role of *JNK1* during development I decided to investigate *jnk1* loss in the zebrafish. As I have shown in the previous chapter the two *jnk1* paralogs are strongly expressed during development, although the splice-variant usage changes during the first five days of development. In order to affect the loss of *jnk1* I used a morpholino oligonucleotide antisense method which can be delivered to every cell of the developing embryo. I then studied the phenotypic effects of *jnk1* loss by various imaging techniques.

4.1.2 Morpholino Oligonucleotides

4.1.2.1 Morpholino Oligonucleotides Represent an Efficient and Specific Anti-Sense Reagent to Knock Down Gene Products

The ability to knock down the protein product of a gene efficiently and specifically has been sought through several iterations of anti-sense technology e.g. RNase-H dependent knockdown, siRNA, morpholinos. However, these approaches have often been problematic due to cell toxicity and off-target effects (Summerton, 2007). Morpholino oligonucleotides (MO) have surpassed earlier technologies because their morpholino backbone is resistant to RNase activity and their design as 25-mer chains ensures very high sequence specificity compared to other technologies (Summerton and Weller, 1997a).

Morpholinos act by binding to the target mRNA in the cytosol and preventing the translation of the correct protein product. In the case of translation-blocking MOs this is achieved by binding at, or up to 80bp upstream, of the AUG start site (www.gene-tools.com). Following binding of the morpholino the ribosome complex is not capable of forming on the mRNA and therefore translation of the gene is blocked. Splice modifying MOs overlap an intron-exon or exon-intron boundary of the pre- / pri-mRNA of interest. Binding of the morpholino prevents correct splicing of the molecule and results in either exon skipping or intron inclusion to the mature mRNA. Splice modifying MOs are designed to produce non-functional and / or truncated protein products following the translation of the modified mRNA (www.gene-tools.com).

Morpholino oligonucleotides have many advantages as a reverse genetic approach to study gene function, and have been a popular technology within the zebrafish community. They are readily soluble, have low toxicity and have been shown to be target-specific between 1-10 μ M concentration ranges, resulting in up to 85% in-cell protein inhibition (Summerton et al., 1997). In zebrafish they are commonly administered directly into the yolk sac before the 8-cell stage by microinjection and are shuttled into the cells by microtubule bridges (Shestopalov and Chen, 2010). Injection of MOs at this early stage ensures that each cell of the developing embryo is treated and allows for results to be generated immediately instead of having to wait 4-5 months for animals to reach sexual maturity when heterozygous mutants are created.

Furthermore, the injection of morpholinos later in development has been utilised to knockdown genes in specific tissue types (Wang et al., 2011). Since MOs are not degraded by RNases they remain at working concentrations in the embryo until they are diluted sufficiently by subsequent mitotic cell divisions, for zebrafish this is at around three days after fertilisation (Summerton et al., 1997). In zebrafish this is sufficient time for development of all the major organs and is around the time that hatching will occur (Kimmel et al., 1995). These features of MOs, as well as the ease of microinjection into the large zebrafish embryo, has made the morpholino a popular reagent for genetic studies in zebrafish development.

4.1.2.2 Limitations of Morpholino Oligonucleotides

As with all technologies, MOs have been shown to have limitations and unintended effects that must be overcome for them to provide insight into gene function. One limitation of MOs experiments is that they are a dose-dependent reagent and that there can be very large variance in the morphant phenotype over a dose range. This dosing effect, or MO penetrance, means that when new morpholinos are developed it is necessary to trial several different doses, and observe the phenotype generated by each dose, in order to gauge an effective dose. This problem is further complicated if the morpholino causes off-target effects at doses close to the effective dose (Heasman, 2002).

Despite initial reports showing that morpholinos were capable of recapitulating the phenotype of N-ethyl-N-nitrosourea generated mutants in 6/6 (Lele et al., 1999) and 5/5 (Nasevicius and Ekker, 2000) cases, the ability for MOs to phenocopy mutants has recently been brought into question. A report by Kok et al (2015) examined fourteen MOs previously implicated in causing vascular or lymphatic developmental defects and added several novel morpholinos directed at genes that were known to be involved in these processes. Of the 24 genes studied, only three of the morpholinos were reportedly able to recapitulate the phenotype generated when the authors made a mutant with one of either zinc finger nucleases, transcription activator-like effector nucleases (TALEN), or clustered regularly interspaced short palindromic repeats (CRISPR) reverse genetic techniques (Kok et al., 2015). Such poor correlation between

techniques for gene knockdown and knockout are worrying, although a recent examination of this issue has provided a possible explanation for the poor correlation between the two technologies. Rossi et al. (2015) compared the gene expression patterns of zebrafish when two genes (*egfl7* and *vegfaa*) were targeted with morpholinos or TALEN / CRISPR genome editing (Rossi et al., 2015). In those mutants that did not correlate phenotypically to the morphants it was shown that there was upregulation of related genes that the authors claimed could compensate for *egfl7* or *vegfaa* loss-of-function. Interestingly these related genes were not upregulated in the morphants or in a CRISPR mutant whose phenotype correlated with the morphant. Whether genetic compensation via the upregulation of related genes explains the discordance between observed mutant and morphant phenotypes remains to be seen, and more research is required. However, these publications highlight the need for caution when inferring the function of a gene if only one technology is used.

Off-target effects have plagued the knockdown technologies, and strictly defined they relate to any phenotype that occurs via binding of the antisense molecule to a transcript other than the target gene. Such off-target effects have been claimed to be caused by as many as 15-20% of morpholinos (Eisen and Smith, 2008) although empirical evidence to support this claim has not been demonstrated. However throughout the history of morpholinos, and the different controls that have been implemented in MO experiments, the term “off-target effects” has been used to describe phenotypic effects that a) are not replicated in the knockout genetic mutant, b) are not replicated by a second, non-overlapping morpholino or c) are not resolved by the overexpression of a MO-resistant mRNA in a so-called mRNA rescue experiment (Kok et al., 2015, Baden et al., 2007, Eisen and Smith, 2008). Considering the lack of correlation between mutants and morphants, and the difficulty of rescue experiments, I believe that it is not possible to definitively call a phenotype off-target unless the transcript being aberrantly knocked down is identified, and through targeted disruption and rescue it is shown that this is the gene responsible for causing the phenotype. Despite this difficulty in identifying actual off-target phenotypes caused by morpholinos, several groups have provided convincing evidence for non-specific MO phenotypes, or morpholino toxicity.

In two instances where MO toxicity was reported the presentation was early developmental arrest and gastrula-stage defects in sea urchin (Coffman et al., 2004), and as a narrowing of the hindbrain and midbrain ventricles in zebrafish (Wright et al., 2004). It has also been shown that MO use can cause dark clouding of the CNS and failure for the eyes to develop as well as curling of the somites from their normal chevron shape into a “U-shape” (Gerety and Wilkinson, 2011). These phenotypes have been associated with the upregulation of p53 and an increase in apoptosis within the developing CNS and trunk of the embryo. Interestingly, in morphants where clouding and increased apoptosis is observed this can be rescued via co-injection of a p53 MO (Robu et al., 2007). This technique has been suggested as a way of confirming that morphant phenotypes are created via a non-specific or toxic mechanism (Eisen and Smith, 2008), however it cannot be used as a control where gene knockdown is predicted to increase apoptosis or alter p53 expression. In zebrafish where cytochrome c oxidase is knocked down via translation and splice-blocking morpholinos there is an increase in apoptosis in the body, including the CNS, which cannot be rescued by p53 MO co-injection (Baden et al., 2007). These data highlight the need for robust controls to be designed into MO experiments to ensure that observed phenotypes are not the result of off-target or non-specific effects.

4.1.2.3 Suitable Controls and Validation of MO Experiments

Suitable controls for morpholino experiments are imperative for the correct interpretation of data and validation of results, particularly considering the recent reports of failure for MOs to recapitulate the mutant phenotype (KOK, 2015 AND ROSSI, 2015). Although the type and rigor of controls differs in morpholino experiments, each integrated control can add confidence in the generated results.

In addition to the gene-of-interest knockdown groups that are to be studied, each morpholino experiment should include an appropriate control group which can be used as a comparison. This control should be a morpholino administered in the same way, but that is not predicted to target endogenous mRNA, and therefore will cause no affect within the embryo. Control morpholinos (CMOs) take two common forms, either a standard control morpholino which is available from Gene-Tools™ and is specific to

human β -globin pre-mRNA, or a MO with identical sequence to the experimental MO except for the introduction of five evenly spaced basepair mismatches. These 5 mismatches have been reported to be sufficient to prevent MO binding to its target (ADD GENE-TOOLS WEBSITE TO REF)(Eisen and Smith, 2008). Both controls should be ineffectual in the embryo, but provide a more commensurate control than inclusion of only an uninjected group of animals.

When novel morpholino oligonucleotides are developed it is imperative to determine whether the MO is knocking down the target gene. In the case of splice-blocking morpholinos this is often simple to do with the use of reverse transcription PCR which is capable of demonstrating that the mRNA transcript length is truncated or elongated when MO is added (Eisen and Smith, 2008). However, when translation-blocking MOs are used there is no observable change to the mRNA, and it is therefore necessary to demonstrate the change of protein abundance. If an appropriate antibody is available then this may be conducted through a standard western blot, however where no suitable antibody exists then it may be necessary to create a tagged protein (Eisen and Smith, 2008). Through molecular cloning it is possible to tag a transcript with a sequence that codes for a protein tag. When mRNA coding for this fusion protein is injected into the embryo then MO binding affinity for this transcript can be measured, However, it does not provide a clear measure of affinity for the MO to the endogenous gene, since the injected mRNA may have a different abundance or accessibility to the MO than the endogenous gene product.

In several publications where morpholino toxicity has been observed in the zebrafish, some consistency in phenotype is observed. Morphants present with dark clouding in the usually transparent tissue, particularly in the brain, have small or undeveloped eyes, and rounded somites (Gerety and Wilkinson, 2011, Robu et al., 2007). These phenotypes appear to be associated with upregulation of p53 throughout the embryo, and these non-specific effects can be rescued with p53 MO co-injection (Robu et al., 2007). It is therefore recommended that p53 co-injection is conducted if these phenotypes are observed as a means of validating an off-target mechanism underlying the phenotype. However, as discussed in the previous section, this technique is not

compatible with knockdowns whose on-target effects alter p53 or apoptosis in the embryo.

A method that has been utilised to validate that morpholino oligonucleotides are acting through specific binding to the gene of interest is to recapitulate the phenotype with a second, non-overlapping morpholino. The rationale is that since MO off-target effects appear to be sequence specific (Eisen and Smith, 2008) then use of a second morpholino targeted to the same gene but with a completely different sequence would be very unlikely to also bind to the same off-target transcripts. If the second morpholino phenocopies the first then the validation of the phenotypes being caused by loss of the gene-of-interest is strengthened. Although this is a good method by which to provide evidence that the morpholino acts “on-target” it does not show it conclusively, and is likely to be challenged if the morphant phenotype does not match that of a mutant.

Until recently, the gold standard control for identifying off-target activity of MOs was to produce a mRNA rescue (Eisen and Smith, 2008). Overexpression of MO-resistant mRNA (containing silent mutations at the MO binding site) has been shown to rescue the phenotypic defects observed when morpholinos are used to knock down gene function (Wang et al., 2011, Little and Mullins, 2005), thus providing evidence that the morphant phenotype is caused by knockdown of the target gene specifically. However, this methodology can be difficult, and often results in only partial rescue of the phenotype (Wang et al., 2011). The over-expression of an artificially introduced mRNA in every cell of the developing embryo is unlikely to closely recapitulate the temporal and spatial expression of your gene of interest, and may itself cause novel developmental defects (Sumanas et al., 2001). In addition, where partial rescue is observed the phenotypes that are not rescued may still be due to off-target binding of the morpholino. Recently a new gold standard for morpholino experiments has been suggested that takes advantage of the efficacy and simplicity of CRISPR site-directed mutagenesis. The injection of a morpholino into a null mutant for the gene of interest should not result in any phenotypic difference to the null mutant (Stainier et al., 2015). Where differences are observed this must be due to an off-target effect of the MO since the null mutant will not be producing protein for your gene of interest. Such a

control could be used as a validation to show that the morpholino does not cause off-target effects at your effective dose, however, a combination of these different controls would be required to increase confidence in the experimental results.

4.1.2.4 Design of the jnk1 Morpholinos

Translation blocking morpholino oligonucleotides were designed by Gene Tools™ in order to bind to zebrafish *jnk1a* and *jnk1b* genes. Both of these MOs overlap the translation start site of their respective gene (Figure 27A) and are predicted to prevent protein translation. Since they arose from a genome duplication, the sequences of the two zebrafish paralogs are highly similar to one another; as a result the morpholino sequences are also very similar, and there is a possibility that one MO might bind to the *jnk1* paralog which it is not targeted to i.e. *jnk1a* MO to the *jnk1b* transcripts, *jnk1b* MO to the *jnk1a* transcripts. The morpholinos do contain four and three mismatched bases respectively to the opposing gene (Figure 27B), however typically it is thought that five mismatches are required to ensure that binding does not occur (Summerton and Weller, 1997a). As such there is a possibility of some cross-reactivity whereby each MO knocks down both genes to a degree.

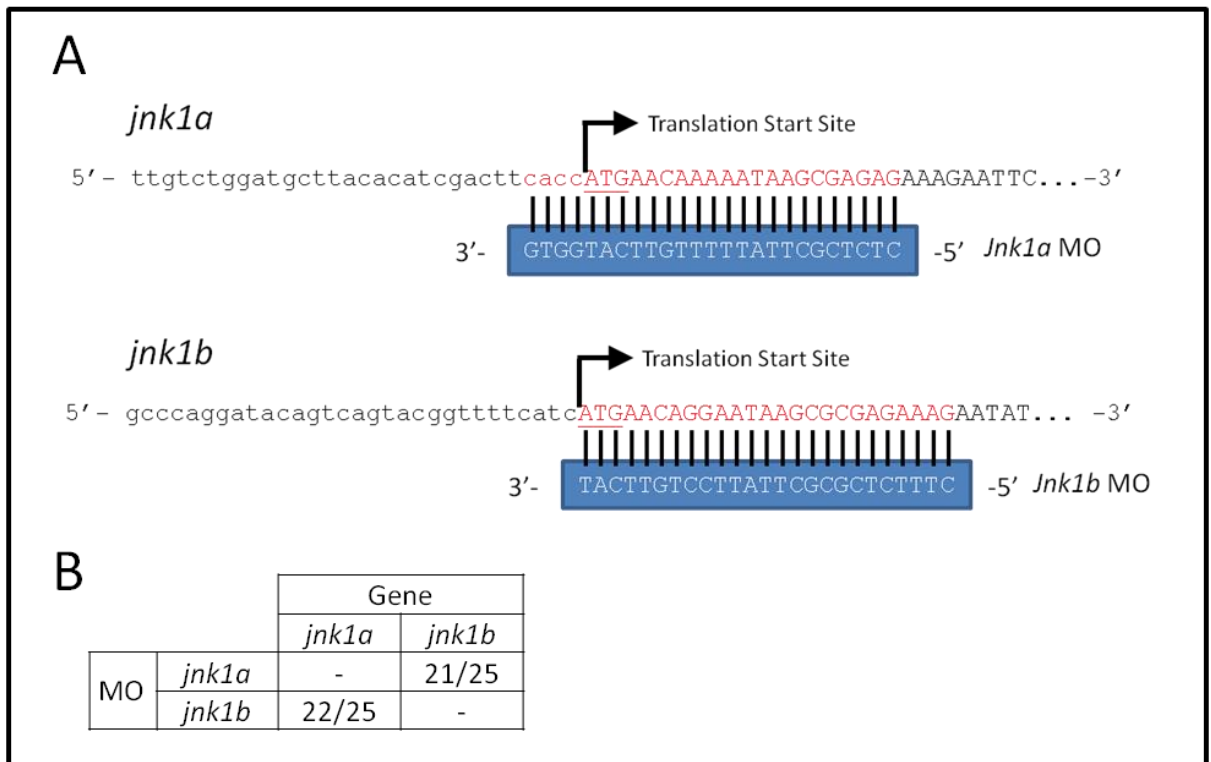


Figure 27 Morpholino Oligonucleotides were Designed to Bind to the *jnk1a* and *jnk1b* Genes.

A) Schematic representation of where the two morpholinos bind (red). Both MOs overlap the translation start site (underlined) of the gene. Coding sequence is uppercase, 5' UTR is lowercase. B) Table displaying the number of matching bases between each MO and the paralog that it is not designed to target.

4.1.3 Aims of the Chapter

The aim of this chapter was to optimise and characterise a morpholino-based knockdown of *jnk1a* and *jnk1b* during development. To achieve this aim the objectives were:

1. Test different doses of *jnk1a*, *jnk1b* and compound *jnk1a* + *jnk1b* morpholino and determine whether they are tolerated or result in lethality.
2. Determine whether developmental delay is caused by *jnk1* knockdown.
3. Examine the gross phenotype over an appropriate dose range in stage matched controls.
4. Decide upon an optimal dose of each morpholino for further characterisation.
5. Examine morphant histology at appropriate MO doses for changes at tissue / organ level.
6. Prove that phenotypic changes result from *jnk1a* and *jnk1b* knockdown.

4.1.4 RESULTS

4.1.4.1 3.2.1 *Effect of the jnk1 MOs on Survival*

Morpholino oligonucleotides act in a dose dependant manner and can result in up to an 85% reduction in the production of protein from the target gene (Summerton et al., 1997). In order to determine whether the newly designed *jnk1a* and *jnk1b* morpholinos were well tolerated or caused significant embryonic death, the survival rate of morphants was monitored over a dose range. Low survival rates during early development have been associated with morpholino toxicity in the sea squirt (Coffman et al., 2004). However, low survival rates could also indicate that *jnk1* knockdown during early development is lethal. Survival of morphants was therefore monitored until 24hpf in order to determine whether there was a significant difference between *jnk1* morphants and controls.

4.1.4.2 *Survival of the jnk1 Morphants between 7-24hpf*

Morphants were obtained by standard husbandry and injection protocols as described in section 2.3 page 86. Approximately fifty embryos per clutch were injected at each MO dose (Table 11), and replicates were achieved with different breeding pairs on separate days. As controls, 50 uninjected (fitness) and 50 morphants injected with the standard Gene-Tools control morpholino (CMO) were also collected. Embryos developed in E3 media at 28.5°C until 24hpf.

Despite an inspection of the eggs at the time of injection, the quality of a clutch of eggs can be very poor independent of their appearance. In these cases a large proportion of the uninjected embryos will fail during gastrulation and can be identified at 24hpf. At 24hpf the uninjected (fitness) controls were examined to ensure that fitness of each clutch was good. Any clutches of embryos where the fitness of the uninjected controls dropped below 80% were immediately dismissed from the experiment. This check of fitness was performed during all morpholino experiments. In clutches with good fitness of the uninjected controls the survival rate of morphants and controls was compared at 24hpf.

Individual Morpholino Dose	Compound Morpholino Dose
2ng <i>jnk1a</i>	1ng <i>jnk1a</i> ; 1ng <i>jnk1b</i>
3ng <i>jnk1a</i>	2ng <i>jnk1a</i> ; 1ng <i>jnk1b</i>
4ng <i>jnk1a</i>	1ng <i>jnk1a</i> ; 2ng <i>jnk1b</i>
2ng <i>jnk1b</i>	2ng <i>jnk1a</i> ; 2ng <i>jnk1b</i>
3ng <i>jnk1b</i>	4ng <i>jnk1a</i> ; 4ng <i>jnk1b</i>
4ng <i>jnk1b</i>	

Table 11 List of *jnk1* Morpholino Doses Trialled

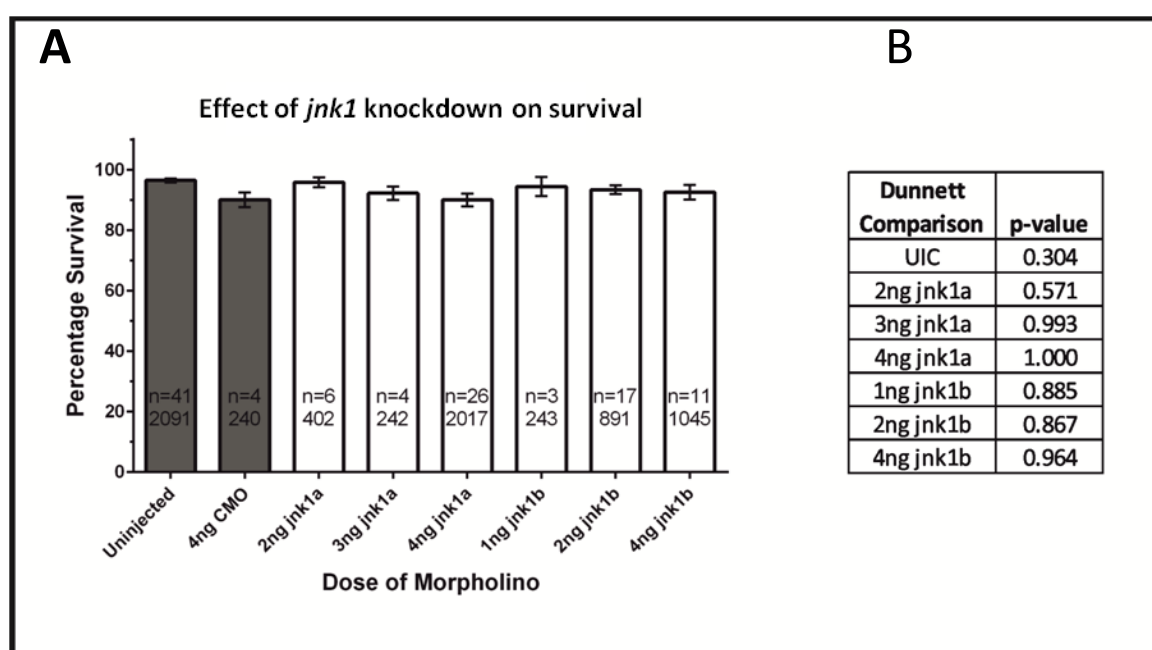


Figure 28 Percentage Survival of *jnk1a* and *jnk1b* Morphants.

A) The morphants displayed an ~90% survival rate over the dose ranges studied. B) One-way ANOVA suggested a significant difference in the fitness of these groups compared to the 4ng CMO sample ($p=0.047$), however a Dunnett post-hoc test was unable to determine which groups were significantly different. The lowest p-value (0.304) was generated when the 4ng CMO was compared to the uninjected controls.

The percentage survival of embryos treated with *jnk1a* or *jnk1b* morpholinos was not found to be different from those treated with a control morpholino (CMO). This result shows that the knockdown of *jnk1a* or *jnk1b* does not increase the number of embryos which fail during early development. Overall the average fitness of all single *jnk1* knockdown experimental groups were >90% (Figure 28A) showing that these *jnk1*

morpholinos were not causing developmental arrest. Performing a one-way ANOVA test on these data did suggest that a significant difference between groups might exist ($p=0.047$), however the power of the Dunnett post-hoc test was not sufficient to determine any groups that were significantly different (Figure 28B). The two groups with the greatest difference were the uninjected controls and the 4ng CMO morphants. If a difference in survival does exist between groups then it may therefore be due to the process of injection into the embryo, or as a result of any morpholino within the cells. This result highlights the importance of generating control morphants instead of comparing results to uninjected controls.

This test for embryo survival was also carried out over the different doses of compound *jnk1a*; *jnk1b* knockdown (Table 11). Again, each group was compared to a morpholino-injected control; in this case 8ng CMO. The outcome of this analysis was that no significant difference was observed between groups ($p=0.173$) by one-way ANOVA, even at the highest dose of 4ng *jnk1a*; 4ng *jnk1b* (Figure 29). This result again provides evidence that the *jnk1* morpholinos used here were well tolerated and that *jnk1* knockdown during development does not result in failure during embryogenesis.

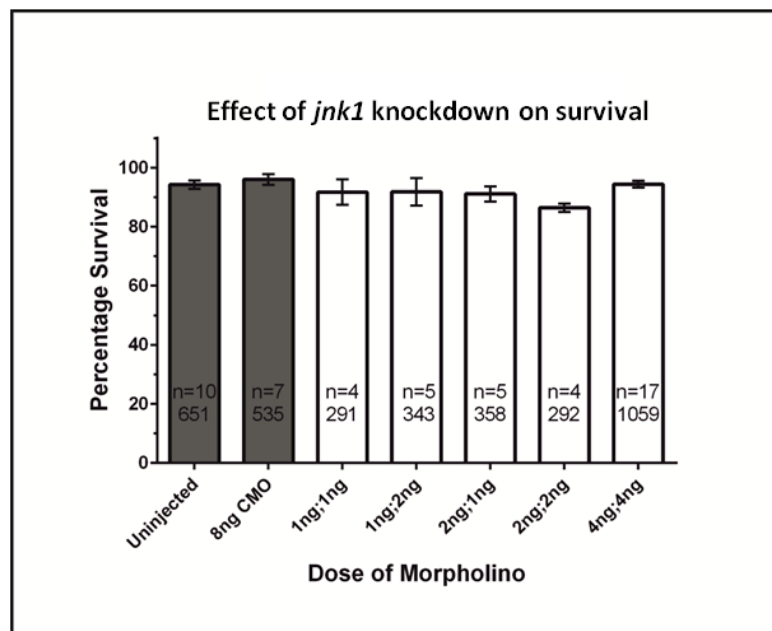


Figure 29 Percentage Survival of compound *jnk1a*; *jnk1b* Morphants. Compound *jnk1a*; *jnk1b* morpholino doses as high as 4ng *jnk1a*; 4ng *jnk1b* did not cause an increased frequency of embryo death between 7 and 24hpf. One-way ANOVA was used to compare the groups to an 8ng CMO dose ($p=0.173$).

In this section I have shown that survival of zebrafish embryos is not affected when doses up to 4ng *jnk1a*, 4ng *jnk1b* or 4ng *1a*; 4ng *1b* morpholino is used. This result indicates that knockdown of *jnk1* by morpholino does not cause early developmental failure. Furthermore this provides evidence that the morpholinos were not causing embryonic toxicity even at doses as high as 4ng *1a*; 4ng *1b* and therefore could be used to investigate *jnk1* function.

4.1.5 Developmental Delay

Once it was demonstrated that *jnk1* morpholinos were well tolerated I wanted to determine whether knockdown of *jnk1* caused any developmental delay. This analysis was very important for informing future experiments because it allowed for the analysis of phenotypes between morphants and stage-matched controls. One of the most accurate methods by which to stage development is by counting of somites during the segmentation stage (Kimmel et al., 1995). The latest timepoint at which this method can be performed is at 22hpf when there are expected to be 26 somites in normal wildtype embryos.

Morphants were generated by standard methods and allowed to develop until 22hpf in E3 media. The morpholino doses tested were the same as those examined for survival rates and both 4ng and 8ng CMO controls were collected. At 22hpf the embryos were anaesthetised in 0.1mg/ml Tricaine[®] for five minutes and then examined under a dissection light microscope. Forceps were used to manipulate the embryos within their chorion and the somite number of six embryos was counted per morpholino dose, per clutch. The somite number over at least three clutches was then plotted and a one-way ANOVA was used to compare statistically.

It was found that doses of *jnk1a* or *jnk1b* morpholino up to 4ng did not delay the developmental progress of embryos (Figure 30A). This result was also found for compound 2ng *1a*; 2ng *1b* morphants (Figure 30B) where no difference between control morphants and *jnk1* morphants were found. However, at the 4ng *1a*; 4ng *1b* dose there was a significant difference between the number of somites present at 22hpf. These morphants were delayed by around three hours compared to 8ng CMOs

since somites appear at a rate of two per hour (Kimmel et al., 1995). This result was important for future experiments since stage-matched controls are required for all comparisons. The time that 4ng 1a; 4ng 1b morphants were examined was therefore adjusted accordingly.

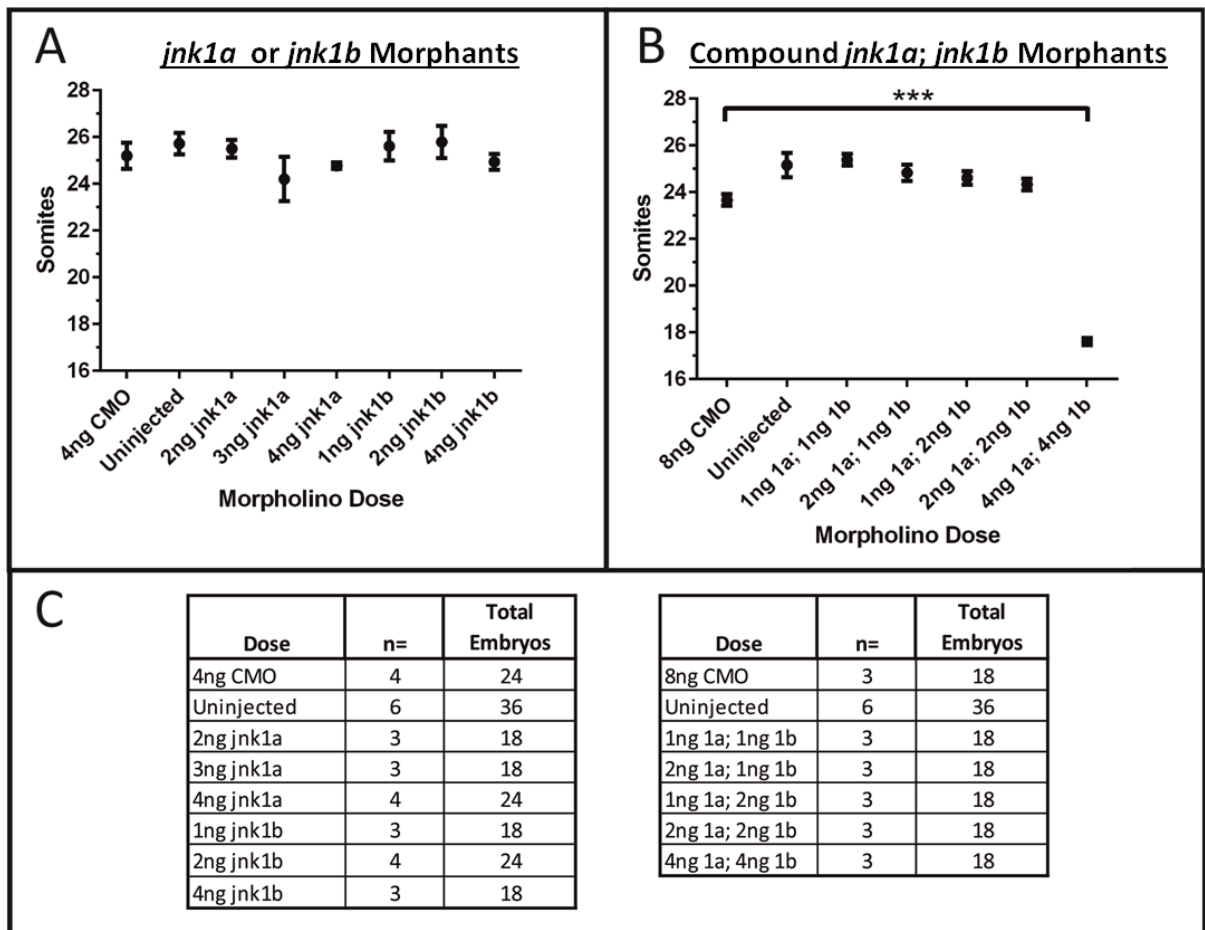


Figure 30 High Compound *jnk1a*;*jnk1b* Morpholino Doses Cause Developmental Delay. Staging of *jnk1* morphants by somites counting at 22hpf.

A) morpholino doses up to 4ng *jnk1a* or 4ng *jnk1b* did not cause developmental delay to the embryo ($p=0.554$). B) The compound 4ng *jnk1a*; 4ng *jnk1b* dose did result in developmental delay ($*** p<0.001$). C) Tables listing the number of replicates and total number of embryos examined.

4.1.6 Gross Phenotype by Light Microscopy

In order to determine whether *jnk1* knockdown caused developmental defects I next examined the gross phenotype of *jnk1* morphants at 28hpf and 48hpf. Morphants were generated by standard methods over different morpholino doses (Table 11). The gross phenotype of the morphants was assessed by light microscopy on anaesthetised embryos to reveal gross phenotypic changes that affected the body or organ development.

4.1.6.1 Characterisation of the *jnk1a* Morphant Gross Phenotype

An initial dose of 2ng *jnk1a* MO was trialled on AB strain embryos, however no observable gross phenotypic defects were apparent at 28hpf (Figure 31C) or 48hpf (Figure 32C); embryos were indistinguishable from controls. The anterior-posterior axis of 2ng *jnk1a* morphants had extended away from the yolk by 28hpf and the somites had formed a regular chevron shape. Furthermore the eyes and otic vesicles were well developed and the heartbeat was visible. The 2ng *jnk1a* morphants remained indistinguishable from morphants at 48hpf when the body length was comparable to controls and head extension around the yolk had increased. The pectoral fin buds were also visible at this time and blood circulation could be seen.

Due to the 2ng morphants being indistinguishable from controls the dose was raised to 3ng *jnk1a*. At 28hpf the 3ng *jnk1a* embryos were smaller than the controls and the tails of morphants did not appear normal (Figure 32D). The tails of morphants had successfully extended away from the yolk but they were curled or kinked at the posterior end. This defect was more pronounced at 48hpf (Figure 32D) where the tail was curled either dorsally (away from the yolk sac) or in the left-right embryonic axis. Despite this tail defect, the shape of the somites appeared normal, and normal eyes, and otic vesicle had developed. At 48hpf circulation could be observed through the caudal artery of the tail. This morphant dose provided an overall mild change in gross phenotype.

At a 4ng *jnk1a* dose there were more obvious and more frequent phenotypic changes between controls and morphants. At 28hpf the 4ng *jnk1a* embryos were smaller than

controls and the tails of the morphants were curved dorsally or kinked (Figure 31E). In addition the yolk sac was misshapen; instead of being spherical the yolk of morphants was commonly elongated along one axis. Another common defect observed was to the head between the cerebellum and the otic vesicle, a region that contains the hindbrain ventricles (hbv). This region of the head was sunken in morphants at both 28hpf and 48hpf. Despite these changes both the eyes and otic vesicle of the morphants appeared to have developed normally. The tail and yolk sac defects persisted to 48hpf and at this point blood circulation was visibly reduced from controls. Many morphants also displayed oedema around the yolk and pericardial sac which deformed the yolk sac of affected embryos (Figure 32E).

4.1.6.2 Characterisation of the *jnk1b* Morphant Gross Phenotype

The starting dose of *jnk1b* morpholino was 1ng which resulted in no observable gross defects. At 28hpf the embryo had extended away from the yolk with regular chevron-shaped somite formation and otic vesicle and eye development appeared normal (Figure 32F). At 48hpf the head was extending from the yolk (Figure 32F) and blood flow was visible in the tail.

An increase of the dose to 2ng *jnk1b* resulted in embryos developing a ventral curling of the body in the anterior-posterior axis at 28hpf (Figure 32G). In comparison to the controls where the tail had extended away from the yolk, the tail of morphants curled ventrally around the yolk. Despite this body curling, no other defects were observable; somites were chevron-shaped, eyes and otic vesicles were indistinguishable from controls, and the heartbeat could be seen. At 48hpf the curled body axis phenotype of morphants had persisted and was more pronounced due to the increase in body length (Figure 32G). This remained the only observable phenotype defect.

A higher dose of 4ng *jnk1b* morpholino was tried in order to increase the severity of the morphant phenotype. At 28hpf the morphants again displayed a curling of the anterior-posterior axis towards the yolk sac (Figure 31H), however this was again the only observable defect as somites, eyes and otic vesicles appearing normal. At 48hpf

the anterior-posterior axis remained curled around the yolk and embryos were visibly shorter than controls. Blood flow through the tail was present but reduced.

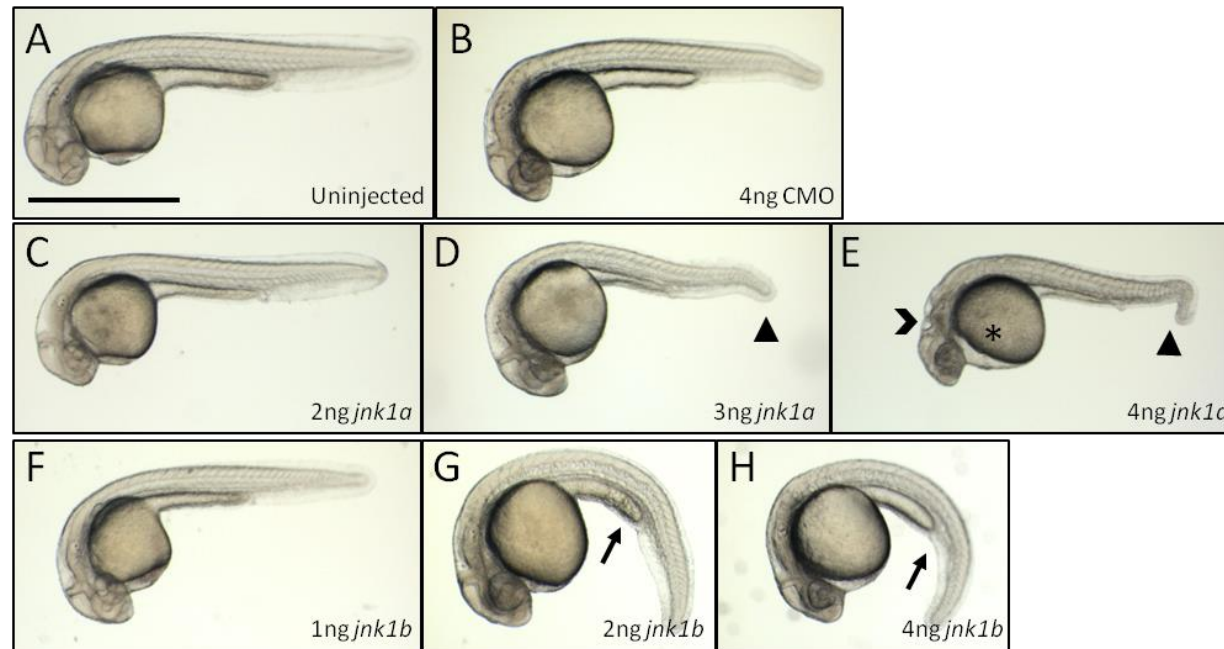


Figure 31 Gross morphology of *jnk1* morphants at 28hpf.

Injection of 4ng Control MO (B) did not cause any detectable developmental defects within the embryos as compared to uninjected controls (A). At low doses it can be seen that 2ng *jnk1a* (C) and 1ng *jnk1b* MO (F) do not show any phenotypic difference to controls. However, at higher doses the *jnk1a* morphants (D+E) displayed a curling or kinking of the tail (arrowhead). At the highest dose this was associated with misshapen yolk sac (*) and a defect of the head (chevron). At doses of 2ng and 4ng *jnk1b* the only defect observed was a ventral curling of the tail (arrow). All other structures appeared normal. Scale=1mm

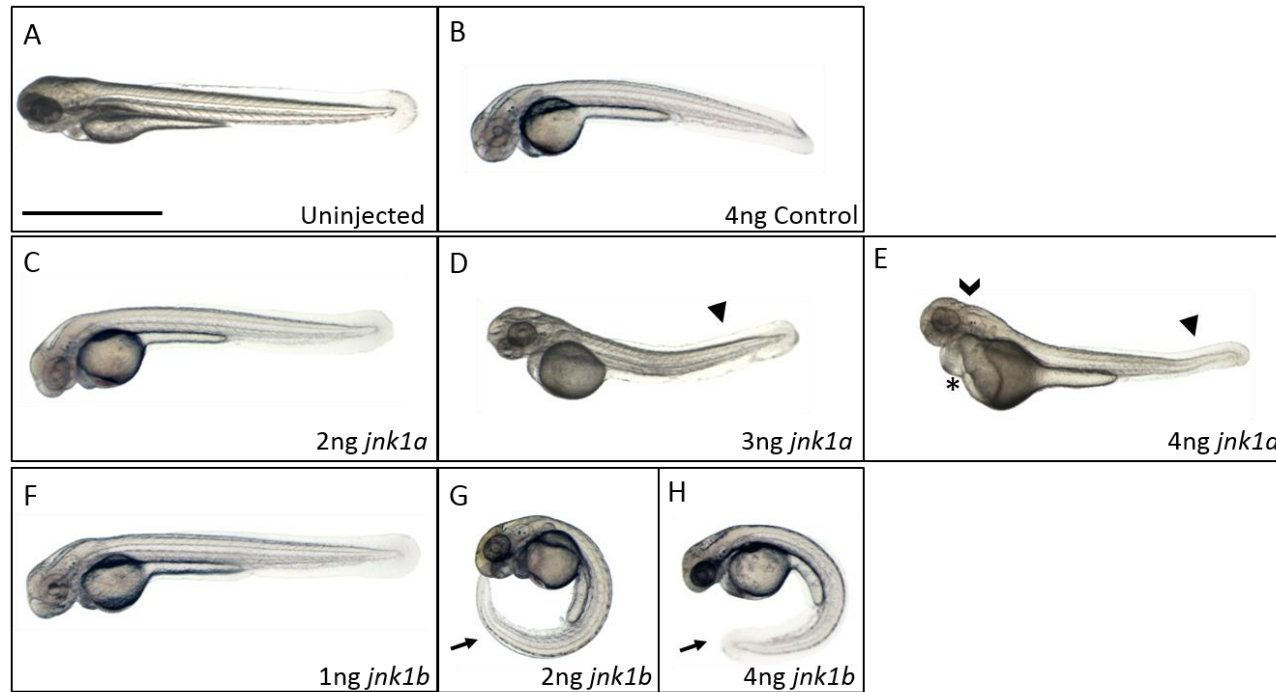


Figure 32 Gross morphology of *jnk1* morphants at 48hpf.

The low morphant doses of both *jnk1* paralogs (C+F) remain indistinguishable from control embryos (A+B) at 48hpf. At 3ng *jnk1b* (D) the only distinguishing feature was a dorsal curling or kinking of the tail (arrowhead). At the 4ng dose (E) the morphants displayed this tail phenotype as well as severe oedema (*) and a defect of the head (chevron). The higher doses of *jnk1b* (G+H) caused a ventral curving of the tail around the yolk sac (arrows) and embryos were shorter. Despite this the rest of the embryo appeared to have developed normally. Scale = 1mm.

4.1.6.3 Morpholino Toxicity at a 6ng *jnk1a* Dose

At 4ng *jnk1a* the embryos displayed some developmental defects, although by light microscopy these defects appeared quite mild. A mild phenotype could suggest that the morpholino was only partially knocking down protein production, or that loss of the gene caused only a mild phenotype. Without a high-affinity, specific antibody it is not possible to accurately quantify the knockdown efficiency of a translation modifying morpholino in vivo (Eisen and Smith, 2008). To overcome this limitation I trialed a higher dose of 6ng *jnk1a* morpholino and examined whether phenotype severity increased; an increase in severity would have been suggestive that greater protein reduction was achieved at this higher dose. At a dose of 6ng *jnk1a* the phenotype of morphants was indeed more severe, however there was evidence that this phenotype was caused by morpholino toxicity. Approximately 15-20% of morpholinos are estimated to cause toxicity (Eisen and Smith, 2008) which manifests in the zebrafish as dark clouding within the central nervous system (CNS) and rounded somites (Robu et al., 2007). Morpholino toxicity is sequence specific and is caused by upregulation of *p53* leading to high levels of apoptosis. A knockdown of *p53* by morpholino has been shown to rescue the toxic phenotype (Robu et al., 2007).

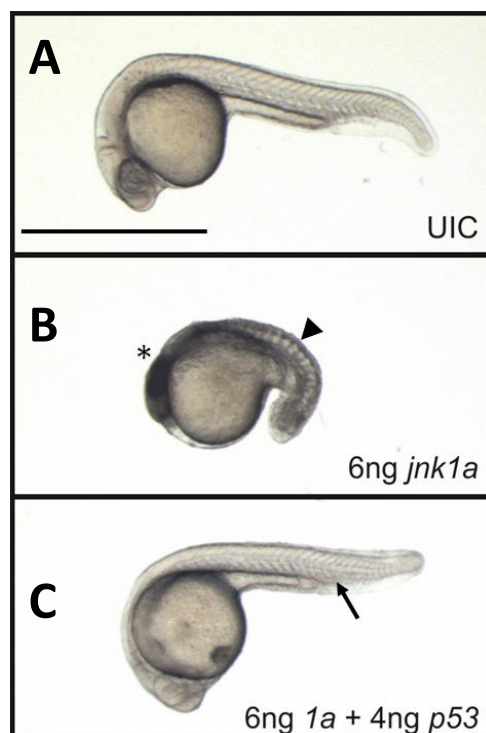


Figure 33 The Morpholino Toxicity of 6ng *jnk1a* can be rescued by 4ng *p53* MO.

A) Uninjected control at 28hpf displaying normal development. B) The 6ng *jnk1a* morphants show dark clouding of the CNS (*) as well as curling of the somites (arrowhead), both features associated with MO toxicity. In addition the embryos are much smaller than controls and fail to form the eyes. C) A combined dose of 6ng *jnk1a* + 4ng *p53* MO is capable of rescuing the morpholino toxicity. Embryos are smaller than controls but somites are chevron shaped (arrow), and no clouding of the CNS is present. Scale = 1mm.

AB embryos were injected with 6ng *jnk1a* morpholino before the 4-cell stage and allowed to develop at 28.5°C in E3 media. At 28hpf the embryos were inspected by light microscopy and were found to be displaying signs of MO toxicity. Overall the embryos were far smaller than controls with dark clouding in the head and through the tail (Figure 33B). The heads of the morphants were smaller and the eyes failed to develop. The somites of 6ng *jnk1a* morphants were small and rounded, and had failed to form the characteristic chevron-shape as is observed in controls. These phenotypes have been described previously (Gerety and Wilkinson, 2011, Robu et al., 2007), and are associated with p53 upregulation and morpholinos toxicity. In order to identify whether the observed defects were caused by upregulation of *p53*, a dual injection of 6ng *jnk1a* and 4ng *p53* morpholino were administered together. This compound *p53* and *jnk1a* knockdown was only conducted at this 6ng *jnk1a* dose because this was the only dose at which this “cloudy” CNS phenotype was observed.

This co-knockdown with *p53* partially rescued the severe phenotype observed in 6ng *jnk1a* morphants as clouding of the head and tail did not appear and the somites and eyes formed normally. Although embryo length was greater in *p53* MO rescued embryos than 6ng *jnk1a* morphants, they remained shorter than uninjected controls, and tail kinking was still present. These results are consistent with morpholino toxicity and therefore the 6ng *jnk1a* dose was excluded from later experiments. Since morpholino toxicity is observed at high doses of *jnk1a* morpholino, the highest dose used in this project was 4ng *jnk1a*.

4.1.6.4 Compound *jnk1a;jnk1b* Morphants Display Severe Phenotypic Changes

Gross phenotypic data of either *jnk1a* or *jnk1b* knockdowns revealed differences in the phenotype when either gene was targeted. Since I showed in Chapter 3 that these two genes give rise to proteins which differ in almost 10% of their amino acid sequence (Figure 18), it is unsurprising that some functional differences exist. Since higher vertebrates have only a single copy of *jnk1*, compound *jnk1a;jnk1b* paralog knockdown may better model the loss of this gene in higher species. Furthermore, the appearance of severe defects at low doses of compound *jnk1a;jnk1b* knockdown

would be suggestive of over-lapping function between the two paralogs. In order to create compound *jnk1a; jnk1b* knockdowns the two morpholinos were mixed at various doses and injected into embryos under standard conditions. Gross phenotype characterisation at each dose was then carried out at 28hpf and 48hpf.

At a dose of 1ng *jnk1a*; 1ng *jnk1b* there was a mild phenotype observed at 28hpf (Figure 34B), consisting of a curling of the tail dorsally away from the yolk. This phenotype was observed at a medium (3ng) and high (4ng) dose of *jnk1a*, but was not at 2ng *jnk1a*. This tail defect was more pronounced by 48hpf due to the increased length of the embryo (Figure 35B). However, this was the only noticeable developmental defect in the 1ng *1a*; 1ng *1b* morphants. Increasing the dose to 2ng *jnk1a*; 1ng *jnk1b* resulted in more pronounced defects that are associated with 2ng *jnk1a* alone. At 28hpf (Figure 34C) the embryos had significant dorsal curling and kinking of the tail and by 48hpf the embryos were noticeably smaller than controls (Figure 35B). In addition the yolk sac was misshapen and many embryos displayed oedema. None of these phenotypes were observed when a 2ng dose of *jnk1a* was injected alone.

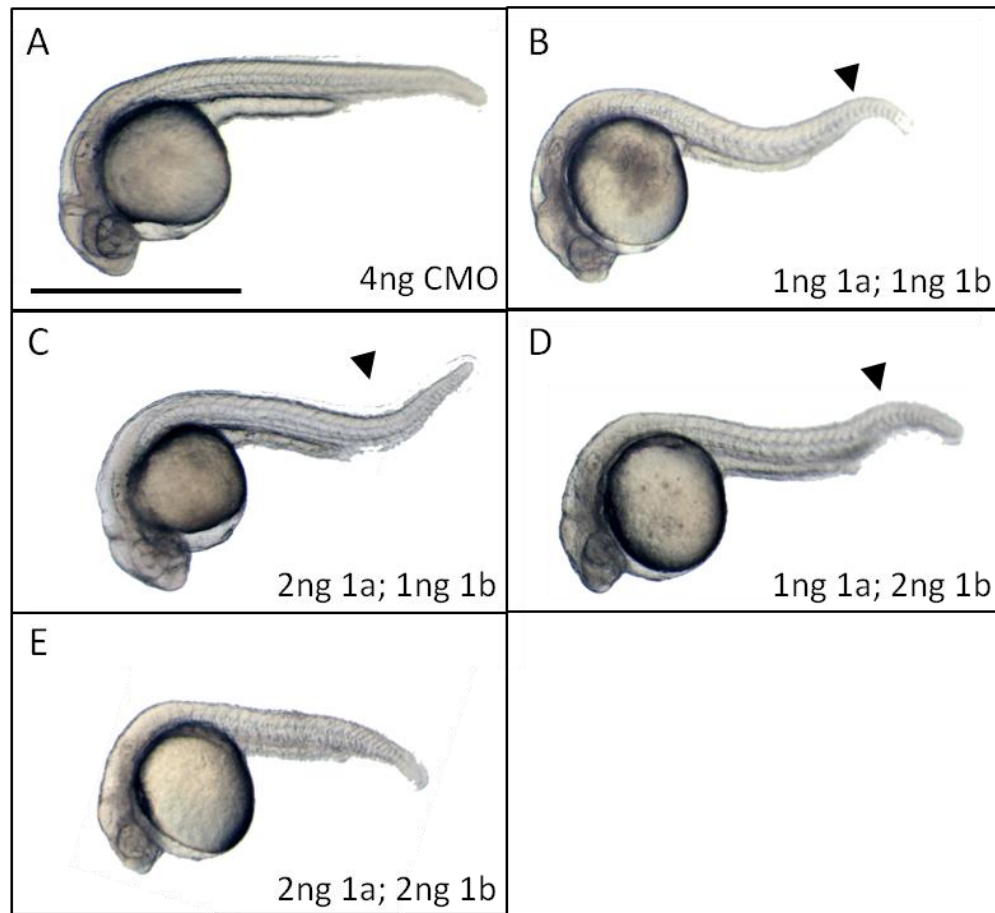


Figure 34 Low Compound *jnk1a*; *jnk1b* Morpholinos Doses Caused Developmental Defects at 28hpf.

A) Control morphant at 28hpf. B) The compound *jnk1a*; *jnk1b* morphants caused a curling of the tail (arrowhead) at 24hpf at relatively low doses. This tail defect was observed in the 1ng;1ng (B), 2ng;1ng (C) and 1ng;2ng (D) morpholino doses. A compound 4ng *jnk1a*; 4ng *jnk1b* morpholino dose (E) resulted in embryo that were much smaller than controls. Scale = 1mm.

The 1ng *jnk1a*; 2ng *jnk1b* dose interestingly did not display the severe ventral curling of the tail at 28hpf (Figure 34D) that was seen in the 2ng *jnk1b* morphants, although the tail did not project away from the yolk as straight as those of the controls. However, by 48hpf the majority of embryos did display this ventral curling tail (Figure 35D) that is observed in the 2ng and 4ng *jnk1b* morphants. A more severe phenotype was seen at the 2ng *jnk1a*; 2ng *jnk1b* dose. At 28hpf these morphants were visibly shorter than the controls and had ventral curling body defects (Figure 34E). By 48hpf these morphants remained shorter and had tails displaying both ventral curling and kinking. In addition,

the majority of morphants displayed severe oedema which deformed the yolk sac (Figure 35E). Interestingly, the brain defect that was seen in the highest doses of *jnk1a* (4ng) was not seen in the 2ng *jnk1a*; 2ng *jnk1b* dose suggesting that it is a feature of high *jnk1a* knockdown only. These defects appear to be a combination of the defects which are seen at high doses of *jnk1a* and *jnk1b*, but they are occurring at a dose half that required when a single *jnk1a* or *jnk1b* morpholino is used.

At the highest compound *jnk1a*; *jnk1b* dose tried (4ng *jnk1a*; 4ng *jnk1b*) the phenotype was the most severe out of all the morpholinos doses examined. In order to determine whether this 4ng *jnk1a*; 4ng *jnk1b* dose is more severe than an equally large dose of a *jnk1a* or *jnk1b* morpholino it would be necessary to compare with the phenotype of 8ng *jnk1a* or 8ng *jnk1b* MO. However, at 6ng *jnk1a* MO there was a toxic effect observed (see section 4.1.6.3) that resulted in upregulation of the *p53* gene, and non-specific phenotypic effects such as “clouding” of the CNS and “rounding” of the somites. It was therefore not considered to be appropriate to use such high doses of the single *jnk1a* or *jnk1b* MOs, as the results would be unreliable.

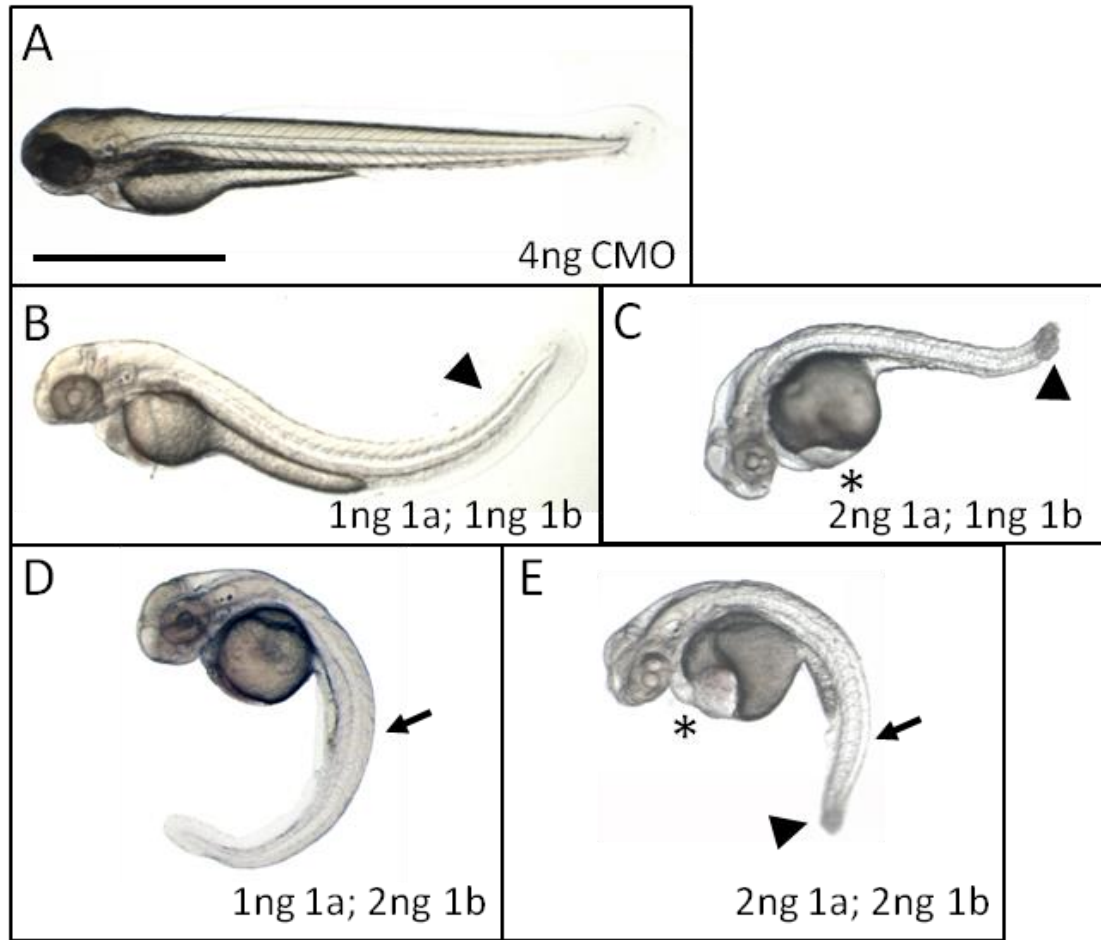


Figure 35 The Compound *jnk1a*; *jnk1b* Morphants Display Significant Body Defects and Oedema at 48hpf.

A) 4ng control morphant. B) At the 1ng 1a;1ng 1b dose the morphants displayed significant curling of the tail (arrowhead) but the length of the embryos is unaffected. C) The 2ng 1a;1ng 1b morphants are smaller than controls and have curled or kinked tails (arrowhead) and most display oedema and misshapen yolk sacs (*). D) The 1ng 1a;2ng 1b *jnk1* morphants display ventral curling of the body axis (arrow) but the rest of the embryo appears normal. E) The 2ng 1a;2ng 1b dose causes the most severe phenotype. Morphants displayed both ventral curling (arrow) and kinking (arrowhead) of the tail and displayed severe oedema and misshapen yolk (*). The embryos were also noticeably smaller than controls. Interestingly no brain defects were observed at this dose. Scale = 1mm.

Morphants of either *jnk1a* or *jnk1b* displayed paralogue-specific defects when higher doses of morpholino were administered (Figure 31 and Figure 32). Since morpholinos act in a dose dependent manner it is likely that these higher doses are required to cause sufficient reduction in protein levels to result in the morphant phenotype. As the defects observed in compound *jnk1a; jnk1b* morphants were cumulative of those observed in single *jnk1a* or *jnk1b* morphants, but remained relatively mild, a high compound 4ng *jnk1a*; 4ng *jnk1b* dose was administered. This high dose represents the highest knockdown of both paralogs that was achieved during this project, and therefore is putatively the model that most closely recapitulates a complete loss of *jnk1*.

At 4ng *jnk1a*; 4ng *jnk1b* the phenotype of the morphant embryos was very severe. Morphants at 28hpf displayed curling and kinking of the tail as well as misshapen yolk sacs (Figure 36C+D). In addition the head of the embryo was sunken posteriorly to the cerebellum, recapitulating the defect observed in 4ng *jnk1a* morphants. Importantly, despite such a large dose of morpholino being used there was no evidence of morpholino toxicity and clouding within the embryo was not observed.

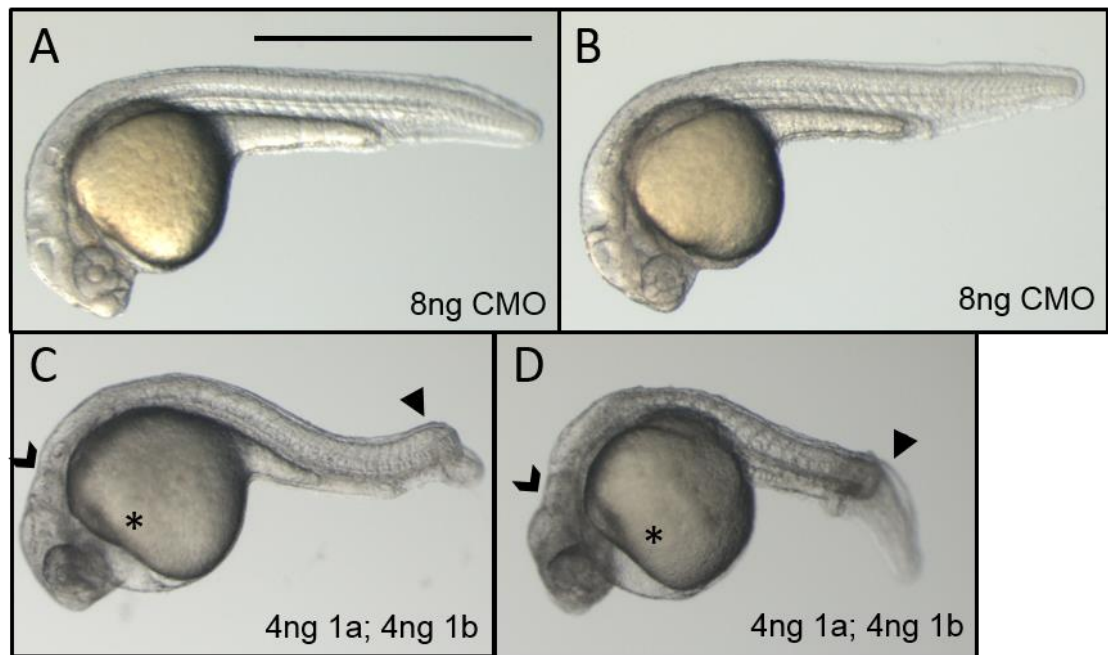


Figure 36 At 4ng *jnk1a*; 4ng *jnk1b* dose the Morphants Display Severe Developmental Defects.

A+B) 8ng control morphants developed normally at 28hpf. Despite the high morpholino dose no toxicity was caused. C+D) 4ng 1a; 4ng 1b morphants displayed significant curling and kinking of the tail (arrowhead) at 28hpf and embryos were smaller. The yolk sac of morphants was often misshapen (*) and there was a defect of the head posterior to the cerebellum (chevron).

At 48hpf the 4ng 1a; 4ng 1b morphants displayed severe defects of the body and tail (Figure 37C+D). The body axis did not project correctly from the yolk and instead curled ventrally around it. At the most caudal end of the tail were kinks and sharp turns towards the left or right (Figure 37D'). Overall the embryos appeared shorter than controls. At this 4ng 1a; 4ng 1b dose morphants also displayed very pronounced oedema around the developing heart and yolk sac which deformed the yolk. Despite this misshapen appearance the yolk sac appeared larger than in controls. In addition the morphants displayed a defect of the head in a region just posterior to the cerebellum. This defect was characterised by a sunken region of the head similar to what was observed in the 4ng *jnk1a* morphants.

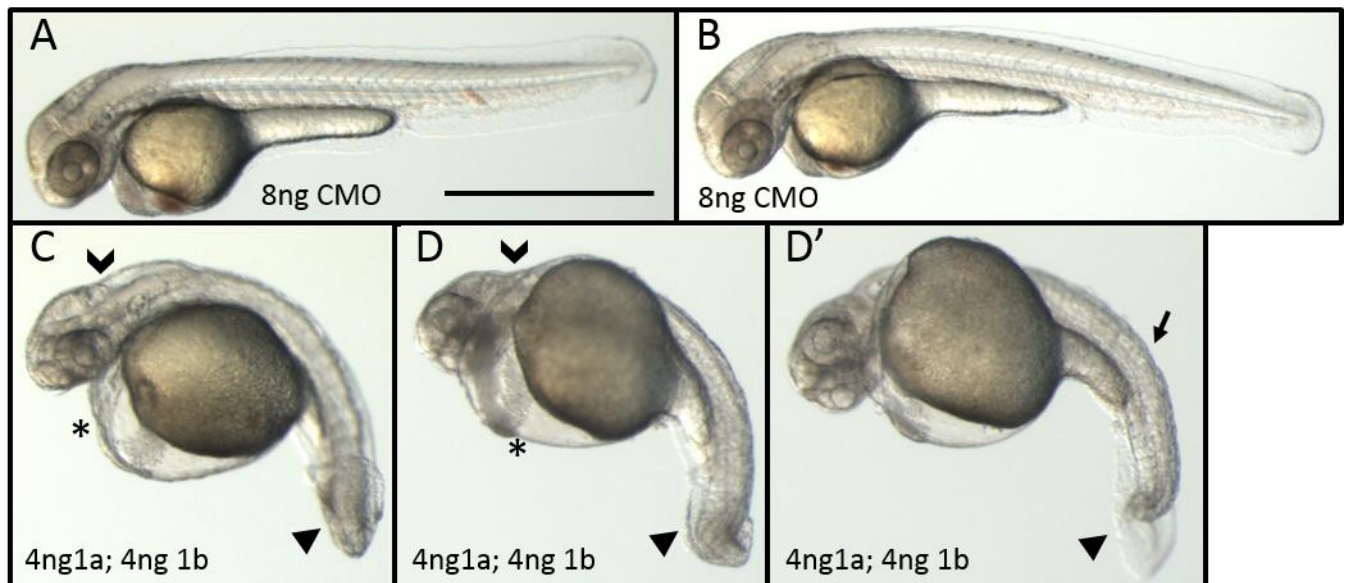


Figure 37 At 48hpf 4ng 1a; 4ng 1b Morphants Displayed Severe Tail Defects, Oedema and Brain Defects.

A+B) 8ng Control morphants displayed no developmental abnormalities at 48hpf. C+D) 4ng 1a; 4ng 1b morphants displayed severe oedema at 48hpf (*) which caused the yolk to become misshapen. In addition the head was sunken posteriorly of the cerebellum (chevron). The tails of morphants were kinked (arrowhead) which often took them out of the microscope focal plane. D') Rotation of the embryo in D shows the whole of the tail. This orientation revealed that the tail was both ventrally curled (arrow) and kinked (arrowhead) at the caudal end.

The gross phenotype examination of *jnk1* morphants revealed that knockdown of both genes individually gave rise to paralog-specific defects. These defects were observed at the higher doses of morpholino tested, where knockdown of protein was greatest. Interestingly these defects were observed at lower doses when compound *jnk1a*; *jnk1b* MOs were administered, possibly indicating that the two genes possess overlapping function. Even when both paralogs of *jnk1* were knocked down, embryonic development was permissive, although there were unusual phenotypes such as curling and kinking of the body axis, anterior-posterior axis shortening, oedema and a defect of the brain. These data showed that although *jnk1* function was required for normal zebrafish development, a loss of these paralogs could be fairly well tolerated for general form of the embryo. To determine more precisely what developmental processes were perturbed by *jnk1* knockdown it was necessary to perform more detailed examination of the morphant.

4.1.6.5 Deciding Upon Optimal jnk1 Morpholino Doses

In order to further analyse the phenotypic defects that were caused by *jnk1* knockdown it was necessary to choose suitable doses for further examination. I have shown here that the morpholinos do not cause an increase in death up to a 4ng *jnk1a*, 4ng *jnk1b* or compound 4ng *jnk1a*; 4ng *jnk1b* doses. Furthermore, no morpholino toxicity was observed at these doses. Analysis of gross morphology revealed that phenotypic defects were observed but only at higher doses. I therefore decided to proceed with doses of 4ng *jnk1a*, 4ng *jnk1b* and 4ng *1a*; 4ng *1b* for future experimentation. These doses represent the highest doses tested and therefore should result in the greatest level of protein knockdown. Furthermore these doses caused the highest frequency of those phenotypes observed. In order to determine the frequency of each phenotypic defect I counted the occurrence of these gross phenotypes in samples from these selected doses.

4.1.6.6 *Frequency of Gross Phenotype Developmental Defects*

The frequency of each developmental defect observed in *jnk1* morphants was performed at the chosen doses. Fixed morphant samples were investigated at 48hpf by dissection light microscopy and the frequency of different developmental defects was calculated from at least three replicate clutches (Table 12). In 8ng CMO morphants there was a very small incidence of cardiac oedema (6%) but that was the only discernible gross defects that could be observed. In 4ng *jnk1a* morphants the incidence of tail defects was very high with 24% having curling and over 50% a kinking in the body axis (not mutually exclusive traits). Oedema was also very commonly observed in morphants with over 40% of morphants affected and brain and eye defects were observed in 33% and 60% respectively. In 4ng *jnk1b* morphants the ventral curling of the body axis was almost ubiquitous with 97% displaying this defect. In addition there was oedema around the heart and yolk in almost two-third of embryos (Table 12). At 4ng *1a*; 4ng *1b* the morphants displayed high frequency of all the defects examined. In particular tail curling and kinking was very common and oedema was observed in 59% of morphants. Defects of the brain and eyes were observed in 28% and 37% respectively and over a quarter of embryos were considerably smaller than controls.

Dose	Defect Frequency (%)			
	8ng CMO n=6	4ng <i>jnk1a</i> n=3	4ng <i>jnk1b</i> n=5	4ng 1a; 4ng 1b n=3
Small Embryo	0/189 (0)	31/93 (33)	3/220 (1)	13/46 (28)
Tail Curl	0/189 (0)	22/93 (24)	214/220 (97)	30/46 (65)
Tail Kink	0/189 (0)	48/93 (52)	0/220 (0)	24/46 (52)
Oedema	12/189 (6)	40/93 (43)	136/220 (62)	27/46 (59)
Small Eyes	0/189 (0)	56/93 (60)	0/220 (0)	13/46 (28)
Brain Defect	0/189 (0)	31/93 (33)	0/220 (0)	17/46 (37)

Table 12 The Frequency of Gross Phenotypic Defects at the Chosen Optimal Doses.

The frequency of each developmental defect was counted from fixed samples at 48hpf. Total number of morphants displaying the defect is shown as well as the percentage frequency in brackets.

4.1.7 Histology of the *jnk1* Morphants

In order to characterise the developmental defects of the *jnk1* morphants in greater detail a sample of morphants at the optimal doses were sectioned. Morphants were collected at 48hpf or 72hpf, fixed and embedded in epoxy resin. Embryos were orientated in both a coronal and sagittal orientation to enable visualisation of morphants through two separate body axes. Slides were stained with Lee's Trichrome (an alternative to hematoxylin and eosin stain) which dyed structures with negative charge blue and positive regions pink. Brightfield images of the slides was then obtained using a compound microscope and measurements were taken from these images using the program FIJI (<http://fiji.sc/Fiji>) in order to have metrics that could be compared statistically.

4.1.7.1 Somitic Defects

At 48hpf the somites of control embryos were highly organised structures that segmented the trunk and tail at regular intervals. The somites were tall, chevron shaped subunits of parallel muscle fibres that were separated by the epithelial somitic furrows (Figure 38A arrow). In the sagittal plane the horizontal myoseptum could be distinguished (Figure 38A arrowhead), separating the somite into a ventral and dorsal hemisphere at the level of the notochord. Although the somite was already well formed at 48hpf, over the next 24 hours the somite increased in height and the somitic furrows became better defined. At 72hpf the horizontal myoseptum was also easily visible and the surrounding dermis thickness was greater (Figure 38D).

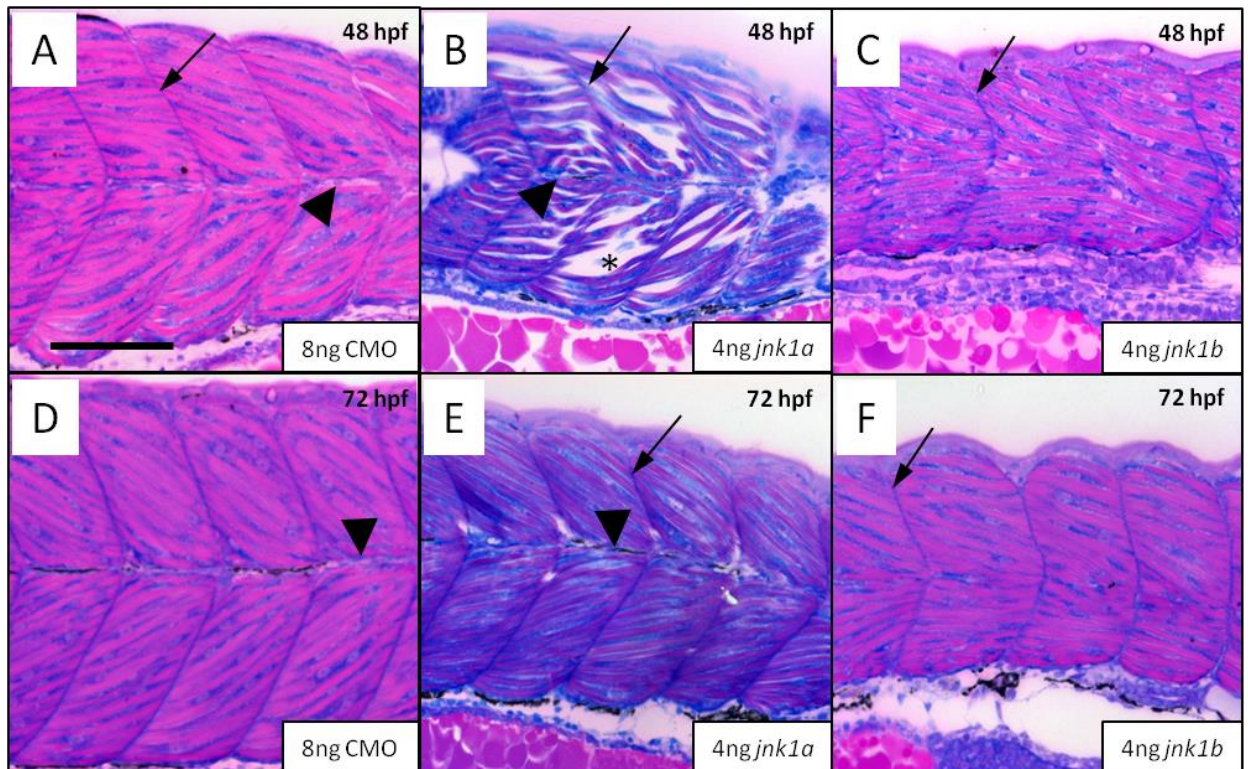


Figure 38 *jnk1a* and *jnk1b* Morphants Display Different Defects in Somite Formation.

At 48hpf the somites of control embryos (A) have formed into their characteristic chevron shape and are segmented by the semitic furrows (arrow). Within each somite the muscle fibres run parallel in an organised manner without spaces between the fibres. The somites are separated into ventral and dorsal hemispheres at the midline by the horizontal myoseptum (arrowhead). Over the next 24 hours (D) the somites increase in size and become more clearly separated by the somitic furrows and horizontal myoseptum. However the chevron shape of the somites remain. In *jnk1a* morphants (B) the preaxial mesoderm successfully segments and forms somitic furrows which separating the somites (arrowhead). In addition the horizontal myoseptum forms and runs through the middle of the somite (arrow). However, the fibres of *jnk1a* morphants have large gaps between them (*). At 72hpf (E) the gaps between fibres are still evident but less pronounced, although the height of the exon is much less than the control. *jnk1b* morphants at 48hpf (C) form somites that are rounded and shorter and wider than controls. Furthermore the horizontal myoseptum fails to form, and is still missing by 72hpf (F). At this later timepoint the somites still remain smaller and wider than controls and the shape is rounded. Scalebar = 100µm. Lee's Trichrome stained sections at 48hpf and 72hpf in sagittal cross-section show the somites at the level of the yolk sac, anterior right, posterior left.

In comparison to controls, the somites of the 4ng *jnk1a* morphants appeared quite different. The most striking feature of the *jnk1a* morphant somites was the emergence of large gaps between the muscle fibres (Figure 38B asterisks). In control embryos the muscle fibres were compacted together in parallel, with no space between adjacent fibres. However the *jnk1a* morphants displayed large gaps between parallel fibres and large gaps which no fibres occupied. Despite this deficit in muscle fibre density, other structures were conserved within the somites. The horizontal myoseptum appeared to be formed normally and the shape and size of the somite was comparable to controls at 48hpf (Figure 39). However, by 72hpf there appeared to be a difference in somite height evident between the controls and 4ng *jnk1a* morphants (Figure 38E). When compared statistically this disparity was found to be statistically different after 3 replicates and by calculating the ratio of somite length vs height this value was also found to be significantly different compared to controls (Figure 39). The gaps between muscle fibres were still apparent at this later timepoint, although they were less pronounced than at 48hpf suggesting that there may have been some improvement in the histology of the somites.

The 4ng *jnk1b* morphants also had defects in the developing somites, however the defects were vastly different to what was observed in *jnk1a* morphants. At 48hpf the preaxial mesoderm of the *jnk1b* embryos had undergone successful segmentation, and the somitic furrows were visible separating the neighbouring somites (Figure 38C arrows). However, individual somites appeared shorter and wider than the controls although at n=3 this was not found to be statistically significant by one-way ANOVA (Figure 39). Calculation of the length vs height ratio of the 4ng *jnk1b* somites was performed and variability was found to be much lower than of the somite height itself; ANOVA tests showed that this ratio was significantly different between the *jnk1b* morphants and controls. In addition, the shape of the somites was different, and instead of the characteristic chevron shape, the somites of *jnk1b* morphants were more rounded or “U-shaped”. Furthermore, the horizontal myoseptum, which forms from pioneer slow muscle cells (van Eeden et al., 1996), had failed to form completely. Observation at 72hpf showed that the *jnk1b* morphant somite height did not greatly change over the 24 hour period (Figure 39) and both height and length:height ratio

were significantly different to controls at this stage. The structural defects to the somite remained (Figure 38F) with a rounded appearance and lack a horizontal myoseptum at this stage.

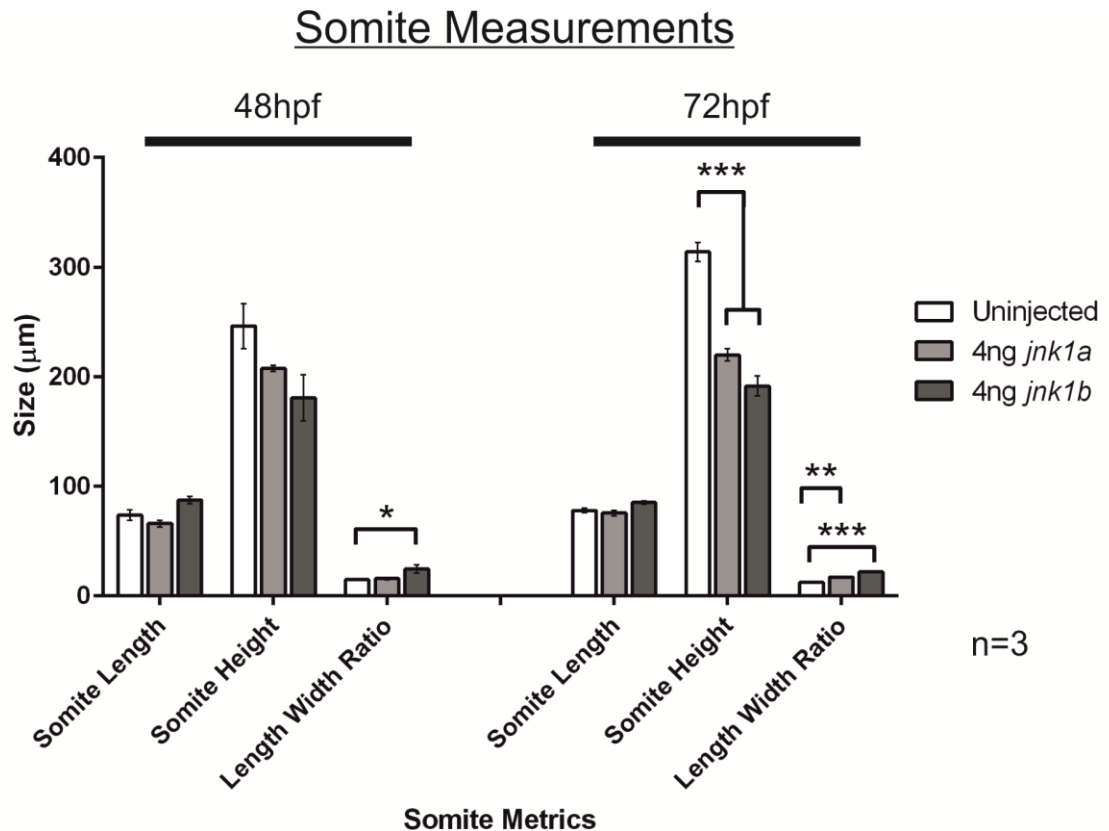


Figure 39 Somite size was affected by the knockdown of *jnk1a* and *jnk1b*.

Metrics of somite length, height and the ratio between the two was calculated from histology pictures. At 48hpf the length and height of somites were not statistically different from controls, although there appeared to be a trend of reduced somite height in *jnk1b* morphants. The ratio of length to height at 48hpf was significantly different in *jnk1b* morphants compared to controls ($p=0.039$). At 72hpf the length of the somites were not affected by knockdown of the *jnk1* paralogs, however height was significantly different in *jnk1a* and *jnk1b* morphants ($p<0.001$). The ratio of length to height was also significantly different between controls and the *jnk1a* ($p=0.001$) and *jnk1b* ($p<0.001$) morphants at 72hpf. All statistical tests performed were one-way ANOVA analysis with 2-sided Dunnett post-hoc tests where appropriate.

4.1.7.2 Eye Defects

In 8ng CMO embryos the eye was well formed by 48hpf and all of the histological layers could be identified (Figure 40A). When stained with Lee's methylene blue-basic fuchsin stain the negatively charged nuclei that reside within the ganglion layer (GL), inner nuclear layer (INL), outer nuclear layer (ONL) and the photoreceptor layer (PL) were stained a dark blue. In contrast the inner plexiform layer (IPL) and outer plexiform layer (OPL) which contain the axonal projections were stained a light pink allowing for easy identification. Over the next 24 hours the eye increased in size due predominantly to increases in the IPL and INL and these layers become more easily detectable (Figure 40D).

Histology of the *jnk1* morphant eye revealed several differences to the controls of the same stage. At 48hpf the *jnk1a* morphants had not yet developed distinguishable plexiform layers (Figure 40C), however the lens, optic nerve, and retinal pigmented epithelia were all present. By 72hpf all of the retinal cell layers could be distinguished (Figure 40D) and therefore it appears that there may have been some developmental delay at 48hpf. Despite all of the cell layers being present at 72hpf, the size of the eye appeared much smaller than the control, something that was also evident at the earlier timepoint. Measurements of eye and lens diameters at 72hpf however did not identify any statistically significant differences in eye size after three replicates, although variability was high (Figure 41A). In comparison several of the retinal layers were significantly smaller in 4ng *jnk1a* morphants compared to controls, the photoreceptor, inner nuclear and inner plexiform layers were all reduced in size (Figure 41B).

The *jnk1b* morphants also appeared to suffer from some developmental delay at 48hpf because again the plexiform layers could not be seen in the retinal sections (Figure 40E). Despite this the eye appeared to be of the same size as the control and no difference was found when these metrics were quantified. By 72hpf the *jnk1b* morphant eye was indistinguishable from the control as all of the retinal layers had developed (Figure 40F). Furthermore, the eye and lens size were comparable to the control, as were the retinal layers as no differences were found (Figure 41A+B).

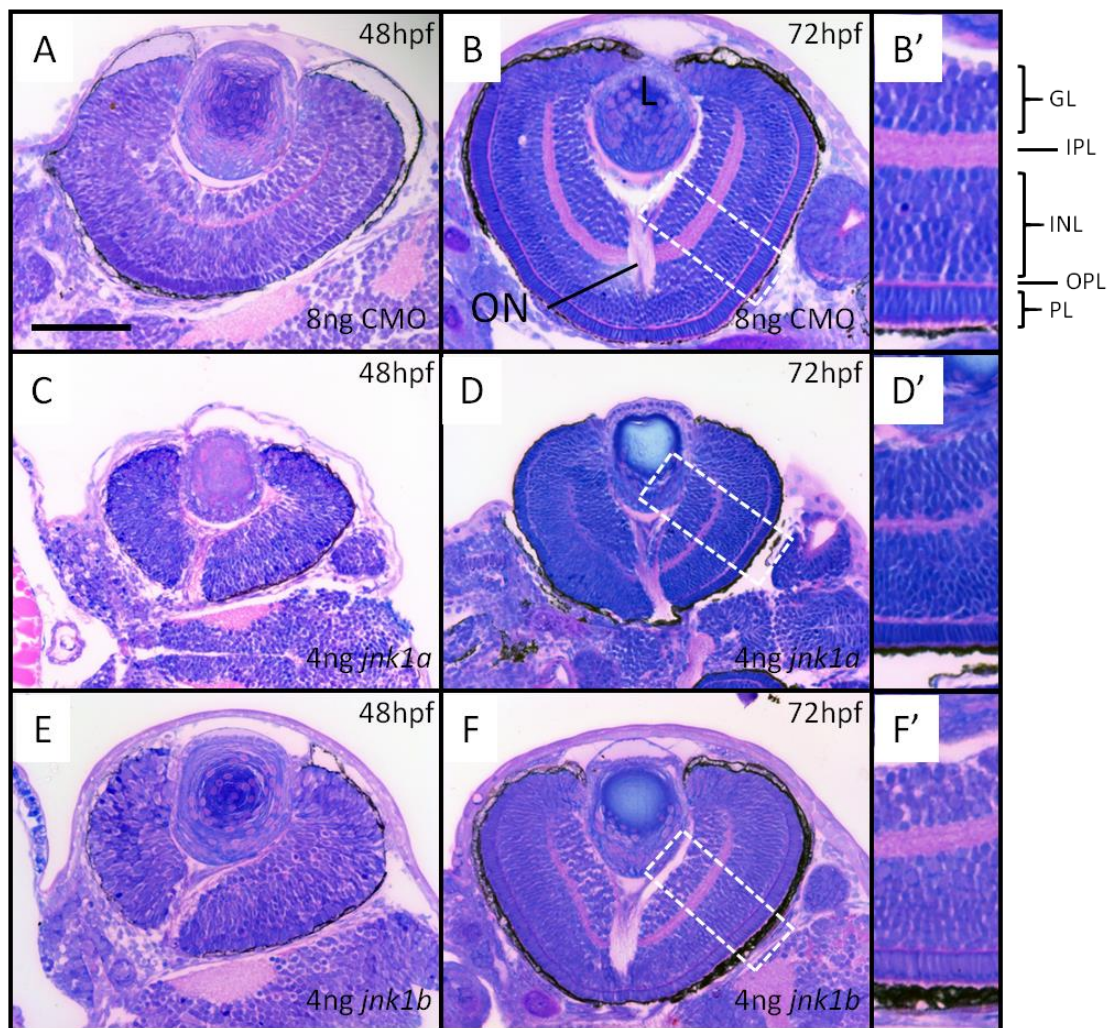


Figure 40 Histology of the Eye in *jnk1a* and *jnk1b* Morphants.

Lee's Trichrome staining of 5 μ m resin sections reveal histological organisation of the developing retina at 48hpf (A, C, E) and 72hpf (B, D, F). The third panel per row (B', D', F') is a higher magnification image of the retina at 72hpf as represented by the white dashed box. At 48hpf the eye of 8ng MM control morphant embryos (A) has developed the different cell layers of the adult retina and a rounded lens. By 72hpf (B) these layers have expanded and are more well defined. By contrast the *jnk1a* morphants (C) lack clear separation of the two discrete plexiform layers at 48hpf and eye size appears much smaller. By 72hpf (D) all cellular layers can be distinguished (D') however the eye remains much smaller than that of the controls. In comparison the *jnk1b* morphants have normal eye size at 48hpf (E), although again there are no clear plexiform layers present at 48hpf. At 72hpf (F) the eye of *jnk1b* morphants is again comparable in size to the control, and all of the layers have formed normally (F'). L – lens, GL – ganglion cell layer, IPL – inner plexiform layer, INL – inner nuclear layer, OPL – outer plexiform layer, PL – photoreceptor layer, RPL – retinal pigmented epithelium, ON – optic nerve. Scalebar = 100 μ m

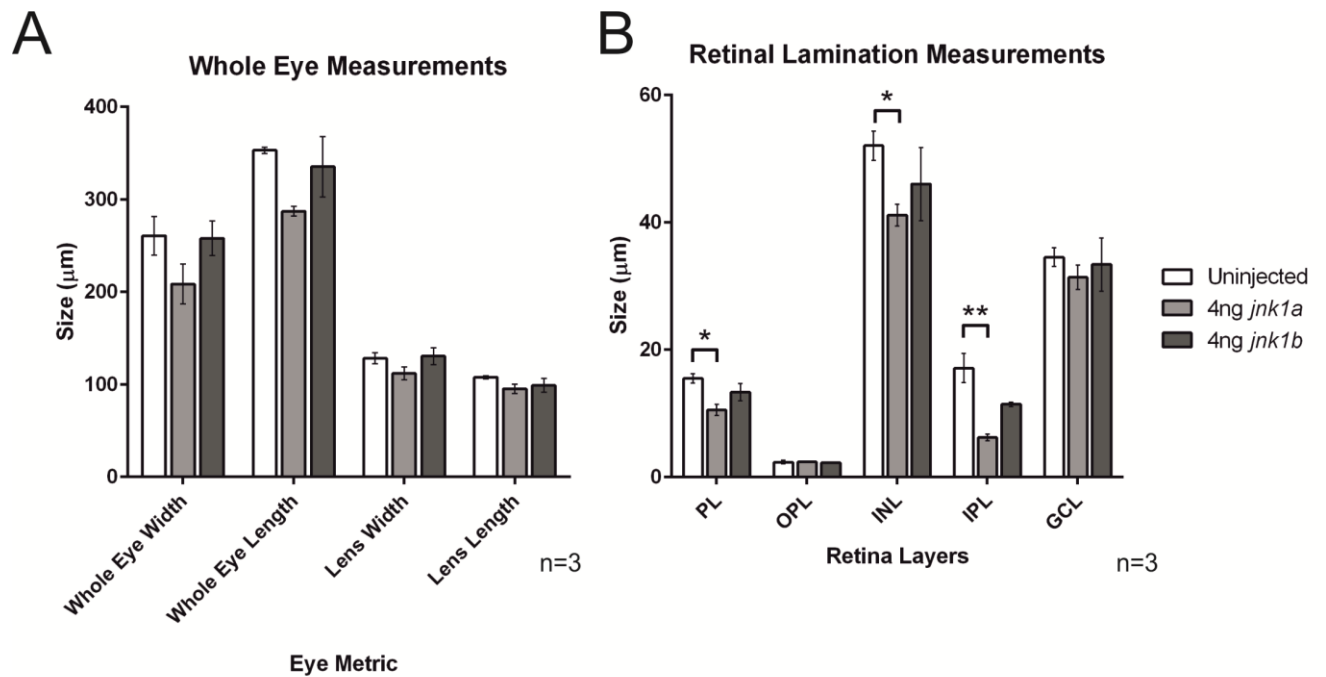


Figure 41 Retinal lamination sizes were affected by *jnk1a* knockdown.

Metrics of the eye and retina were calculated from histology pictures. A) The width and length of the morphant eyes did display a statistically significant change when *jnk1a* or *jnk1b* was knocked down although there appeared to be a trend of reduction in these two values in *jnk1a* morphants. The width and length of the lens was also not significantly affected by *jnk1a* or *jnk1b* knockdown. B) The size of some of the retinal laminations was significantly reduced by loss of *jnk1a*, although was unchanged with loss of *jnk1b*. The photoreceptor layer, inner nuclear layer, and inner plexiform layer were all significantly reduced in size in *jnk1a* morphants. PL=photoreceptor layer, OPL=outer plexiform layer, INL=inner nuclear layer, IPL=inner plexiform layer, GCL=ganglion cell layer.

4.1.7.3 Heart Defects

One of the gross developmental defects that were picked up by gross phenotyping was oedema around the heart and yolk of *jnk1a* and *jnk1b* morphants. One possible cause of oedema is poor cardiac function, therefore the histology of the heart was examined between morphants and controls. By 48hpf the heart of controls had formed the two contractile chambers which both had a distinct histology (Figure 42A). At this stage the atrium is a thin, single celled myocardial layer, whereas the ventricle is multiple cells thick (Peal et al., 2011). Both chambers are lined with endocardium and are separated at the atrioventricular canal by a valve. The ventricle is much smaller than the atrium, but both chambers have large lumens to accommodate the passage of blood. Blood enters the atrium from the sinus venosis (Figure 42A arrowhead) which is a narrowed opening separating the blood that pools in the cardinal vein from the heart itself. Over the next 24 hours the heart of the 8ng CMO embryos continued to develop and by 72hpf the ventricle had moved posteriorly to a location medial of the atrium (Figure 43A). Furthermore, the wall of the ventricle has thickened further and the valve has increased in size. The atrium by 72hpf remained one cell thick. The extracellular matrix (ECL) located between the myocardium and endocardium - known as the cardiac jelly can be seen at 72hpf in the atrium (Figure 43 asterisks).

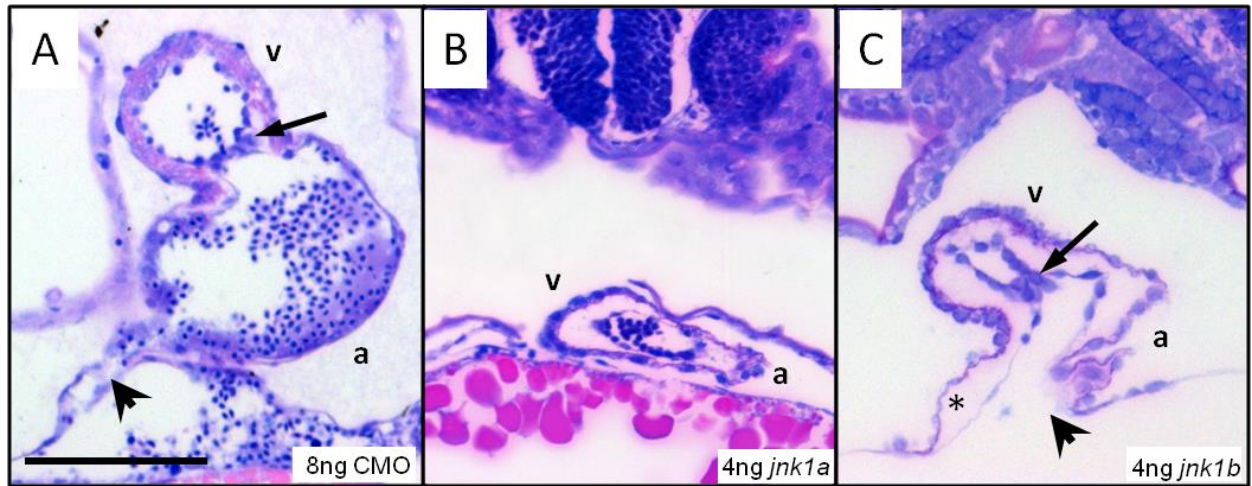


Figure 42 Heart Histology of Single Morphants at 48hpf.

By 48hpf the 8ng control MO heart (A) has a morphologically distinct ventricle (v) and atrium (a) separated by the primitive valve (arrow) which forms at the atrio-ventricular canal. Also visible is the sinus venosus (arrowhead) which forms a narrow opening for blood to enter the heart. In comparison the *jnk1a* morphant heart (B) is much smaller and more primitive than the control at 48hpf. The heart has successfully moved away from the midline but still appears like a primitive tube without formation of the valve. The ventricle and atrium can be distinguished by the myocardium since the ventricle wall contains multiple cell layers whereas the atrium is one-cell thick. Both chambers are much smaller than the control heart. The *jnk1b* morphant heart (C) is also smaller than the control but also appears to have defects. The atrioventricular valve has formed (arrow) separating the ventricle and atrium, but both chambers are smaller than in the control. The atrium looks particularly disorganised with abnormal projections of the wall at the venous pole. The sinus venosus (arrowhead) appears much more dilated in *jnk1b* morphants but despite this there are very few blood cells seen in the heart. Finally the cardiac jelly (*) which is extracellular matrix that separates the myocardium and endocardium is greatly expanded in morphants. Scalebar = 100µm.

The hearts of *jnk1a* morphants appeared as a primitive structure at 48hpf, with two chambers that were not separated and formed a tube (Figure 42B). The valve had not developed by this stage and the only way to distinguish between the two chambers was from the histology of the myocardium. The ventricle (as in controls) had multiple cells layers, and the atrium was only one cell thick. However both of the chambers were far smaller than the control and lumen size was also drastically reduced. One of the contributing factors to the small lumen size was that the cardiac jelly layer was far larger around both chambers than in controls. By 72hpf the hearts of *jnk1a* morphants

had grown in size but still appeared primitive in design. The chambers remained smaller than in the control and the valve had still failed to form correctly. Additionally the cardiac jelly layer was massively expanded (Figure 43B) in comparison to controls so that lumen size was very small.

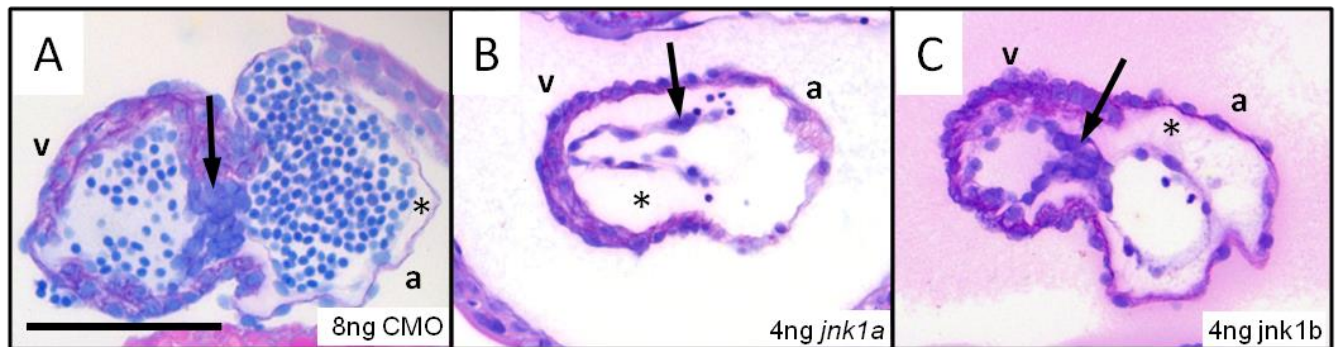


Figure 43 Heart Histology of Single Morphants at 72hpf.

At 72hpf the 8ng control heart (A) had looped round so that the atrium and ventricle were parallel to one other and both chambers had expanded to increase cardiac output. The atrium (a) at 72hpf was one-cell thick whereas the ventricle (v) was multiple cells thick, and the two chambers were separated by the atrioventricular valve (arrow). In the atrium a thin layer of cardiac jelly (*) was visible which separated the myocardium and endocardium. In *jnk1a* morphants (B) the heart was poorly formed without clear chamber separation. Despite this the ventricle did have multiple cell layers that helped to distinguish it from the atrium. At 72hpf the valve has not formed correctly although the beginnings of a primitive valve are visible (arrow), however it was much smaller than the valve of the controls and did not separate the chambers. Both the atrium and ventricle of *jnk1a* morphants are small with a small lumen constricted by an expanded cardiac jelly (*). The *jnk1b* morphant heart (C) was fairly well formed at 72hpf with both chambers clearly separated and with a mature valve separating them (arrow). However the atrium was misshapen with abnormal projections of the myocardium at the venous pole. In addition, both chambers were far smaller than the control and the lumen of both was restricted by cardiac jelly expansion (*).

The 4ng *jnk1b* morphant heart also appeared more primitive than the control heart at 48hpf. Although the two chambers had formed normally, they were small and irregular in shape. Despite this the atrioventricular valve had formed correctly to separate the two chambers (Figure 42C arrow). The morphant atrium was considerably smaller in

size and there were often projections of the myocardium at the venous pole that give the impression of folding in the chamber. Furthermore the opening to the rest of the circulatory system is far more dilated in morphants and does not show the narrow constriction of the control sinus venosus (Figure 42 arrowhead). Despite this, far fewer blood cells were found within the heart or cardinal vein of morphants, suggesting that they were not circulating normally. The size of both chambers was increased in *jnk1b* morphants by 72hpf (Figure 43), however, both remained far smaller than normal. Looping movements of the heart continued despite the overt defects with the ventricle, moving to a more medial and posterior position. The valve also increased in size and maturity similar to the control (Figure 43 arrow). Despite this the lumen of the chambers remained constricted by an expanded cardiac jelly layer found predominantly in the atrium. Overall the heart appeared to be better formed than in the *jnk1a* morphants.

4.1.8 Proof of Knockdown

4.1.8.1 Knockdown Analysis by Western Blot

From the gross phenotype and histological data I was able to show that use of *jnk1* morpholinos cause some developmental defects in the zebrafish. Since 25-mer morpholino oligonucleotides are usually highly specific for their target (Eisen and Smith, 2008) these defects are likely due to the knockdown of *jnk1a* and *jnk1b* during development. However, these morpholinos are novel and therefore require validation to ensure that they are specific for their target. In order to prove specificity of the *jnk1* translational MOs I performed western blot analysis to measure protein abundance directly.

Western blot analysis requires a sensitive and specific antibody that is capable of binding to the protein of interest. Unfortunately the only antibodies that were commercially available and cross-react with zebrafish are (human) pan-JNK antibodies which bind to human JNK1, JNK2 and JNK3 proteins. Despite this limitation in reagent availability the western blots were carried out to determine whether protein abundance levels of Jnk were reduced in morphants.

Samples for western blot were generated via standard morpholino injection protocols. Approximately 100 embryos at 48hpf were collected at doses of 4ng *jnk1a*, 4ng *jnk1b*, and uninjected controls, dechorionated and deyolked to improve the resolution on the blot (Link et al., 2006). These sample proteins were denatured and stored as described in section 2.2.13 and loaded into the acrylamide gel such that protein from five embryos ran per lane. The western blots were probed with antibodies against pan-Jnk and Gapdh to act as a loading control. This experiment was repeated in triplicate and average density changes were calculated from densitometry analysis via one-way ANOVA

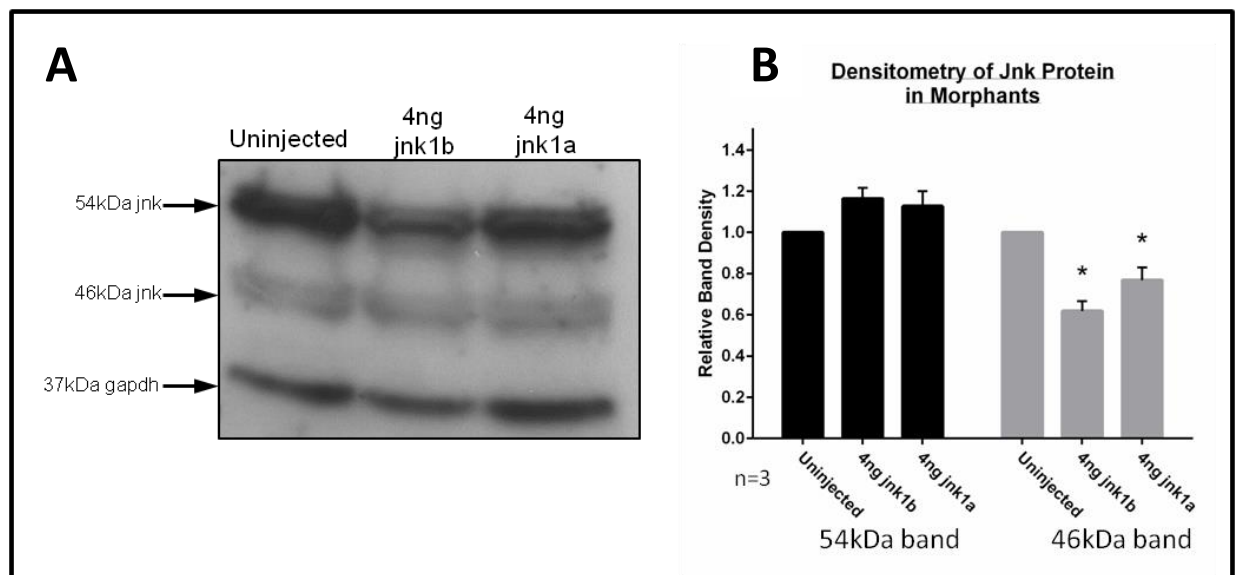


Figure 44 Pan-JNK Western Blot Revealed Partial Knockdown of Jnk protein.

Western blots were used to determine whether single morpholino doses were capable of knocking down Jnk abundance. A) Bands are picked up at 46kDa and 54kDa which represent the long and short forms of Jnk. The morphant samples were run against an uninjected control to compare protein abundance. A Gapdh control antibody was also probed for and loading of the wells was normalised against this band. B) Densitometry over three replicates revealed a trend of the 54kDa band of morphants being greater relative to controls. However this result was not found to be significant (One-Way ANOVA, $p=0.14$). The 46kDa band was found to be significantly lower in morphants that controls (One-Way ANOVA, $p=0.003$) for both paralogs. Errorbars=SEM.

The western blot results revealed that probing with a pan-Jnk antibody reveals two major bands of different sizes (Figure 44A). The 54kDa band corresponded to the long transcripts of the *jnk* genes, whereas the 46kDa band corresponded to the short transcripts (Sabapathy et al., 1999). For my analysis these two bands were treated separately by densitometry to distinguish whether changes in protein abundance was evident in either the long or short protein products. Despite the pan-Jnk antibody being used (which also picks up Jnk2 and Jnk3) it was possible to find a significant difference in protein abundance between the *jnk1* morphants and uninjected controls. However, this reduction in band density was only observed for the 46kDa transcripts of Jnk, representing the short splice-variants produced by *jnk1a*, *jnk1b*, *jnk2* or *jnk3*. For *jnk1b* morphants there was a nearly 40% reduction in the 46kDa band whereas for the *jnk1a* morphants it was reduced by approximately 20% (Figure 44B). Interestingly, the abundance of the heavier 54kDa band was not found to significantly change between the three groups. This result is unexpected because both long and short transcripts of *jnk1a* and *jnk1b* share an AUG start site, over which the respective morpholino is designed to bind. It is therefore not clear why only short transcript products would display a reduced protein abundance.

4.1.8.2 Myc-Tagged Western Blot Analysis

Western blot analysis of endogenous Jnk protein was unable to definitively answer whether the morpholinos were capable of knocking down *jnk1* translation. The results suggested that the lighter (46kDa) Jnk products did have reduced abundance, but the heavier (54kDa) products could be increasing in abundance. Since there could be no distinction made between the different Jnk family members (Jnk1,2,3) with the pan-JNK antibody this result did not show that the *jnk1* paralogs specifically were being affected by the MOs. To determine whether the morpholinos were capable of preventing Jnk1 protein translation I had two of the full-length *jnk1* transcripts myc-tagged. The addition of protein tags was carried out by Dr Lindsay Murphy.

Western blot samples were generated by microinjection where embryos were administered with morpholino or morpholino plus myc-tagged mRNA. There were three different morpholino doses used (4ng CMO, 4ng *jnk1a*, 4ng *jnk1b*) and three

mRNA doses (no RNA, 400pg *jnk1a*, 400pg *jnk1b*) which were used in combination leading to a total of nine different conditions (Table 13). Three of these doses were morpholino only and represent negative controls since no myc-tag protein was present in the embryo. There were also two positive controls where myc-*jnk1a* or myc-*jnk1b* was administered in the presence of the CMO morpholino which does not knockdown the *jnk1* genes translation. These controls were used to demonstrate the total amount of protein produced from both of the 400pg doses of RNA. These positive controls were compared to the bands in the *jnk1* morphant samples to gauge whether protein production was reduced. The final four experimental conditions used were to answer whether each of the two morpholinos was capable of knocking down RNA from the paralog that it was targeted to, and whether it cross-reacted to knock down RNA from the paralog that it was not targeted to i.e. did *jnk1a* morpholino knock down *jnk1b* translation. Each of these nine conditions were administered to embryos from the same clutch to reduce variability. Furthermore, RNA and morpholinos were added as two separate injections to ensure that the same amount of RNA was administered to the positive controls as to the experimental samples.

The MO and RNA doses were administered to AB embryos from the same clutch within half an hour of being spawned. In each case a morpholino was administered first and then the morphants were split into three equal groups: *jnk1a* mRNA, *jnk1b* mRNA, no mRNA. A total of 400pg mRNA was administered also by microinjection. In this way it was possible to work sequentially through the nine different sample groups and use the same microneedles for all doses to reduce variability in dose administered. However, due to the sheer number of injections required (30 embryos for 9 sample groups = 270) it was not possible to perform alone before the embryos had developed beyond the eight-cell stage. Therefore I performed the morpholino injections and was supported by Dr Simon Ramsbottom who performed the RNA injections. At 48hpf the embryos were collected and 20 embryos were added to 400µl of tissue extraction buffer. The tissue was homogenised by needle gradient and stored at -80°C until needed.

mRNA	Morpholino	Purpose
-	CMO	-ve control
-	<i>jnk1a</i>	<i>jnk1a</i> -ve control
-	<i>jnk1b</i>	<i>jnk1b</i> -ve control
<i>jnk1a</i>	CMO	<i>jnk1a</i> +ve control
<i>jnk1a</i>	<i>jnk1a</i>	Target specificity
<i>jnk1a</i>	<i>jnk1b</i>	Cross-reactivity
<i>jnk1b</i>	CMO	<i>jnk1b</i> +ve control
<i>jnk1b</i>	<i>jnk1a</i>	Cross-reactivity
<i>jnk1b</i>	<i>jnk1b</i>	Target specificity

Table 13 Different Doses of myc-tagged *jnk1* RNA and Morpholino used to Demonstrate Morpholino Specificity.

Table showing the nine different conditions used to prove *jnk1* morpholinos knock down *jnk1* protein production. Each of these nine conditions was produced within the same clutch of embryos. The tagged *jnk1a* RNA used was *jnk1a_8;long* and the *jnk1b* RNA was *jnk1b_8;long*. Morpholinos were all used at a dose of 4ng.

A western blot to determine whether morpholinos could knockdown myc-tagged *jnk1* splice-variants was performed by Dr. Ramsbottom. The tissue was loaded into the wells of a 10% acrylamide gel so that protein from one embryo ran per lane. Samples that had been injected with the same RNA were loaded side-by-side so that comparisons in protein abundance could be made (Figure 45). Equal loading of the gel was confirmed by use of a Gapdh loading control antibody that was used to probe the bottom half of the PVDF membrane. The top of the membrane was probed with an anti-Myc antibody.

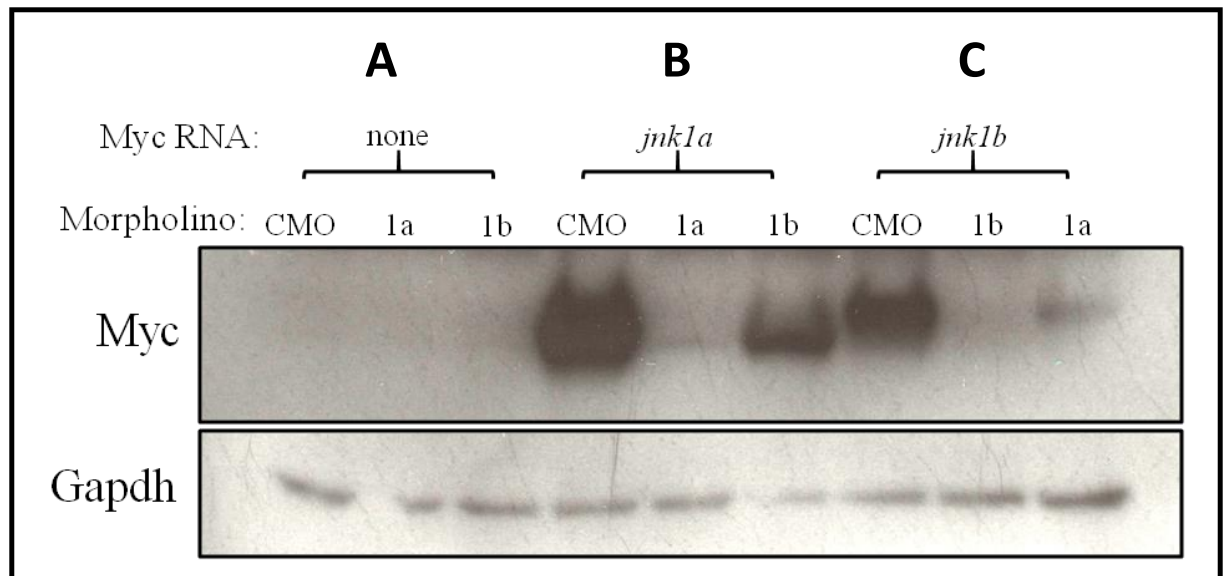


Figure 45 The *jnk1* Morpholinos Knockdown both Paralogs of *jnk1*.

Myc-tagged *jnk1a*_{8;long} or *jnk1b*_{8;long} RNA was injected into morphants to determine the knockdown ability of the MOs. A) No myc-tagged bands were found when morpholino only was injected. B) In embryos injected with *jnk1a*-myc the control MO did not knock down myc-tagged protein, however the *jnk1a* MO abolished this band completely. *jnk1b* morpholino was found to cross-react with the *jnk1a* RNA and myc-tagged protein abundance was reduced considerably. C) Myc-tagged *jnk1b* protein was abundant when injected with the control morpholino, but was completely abolished when injected with *jnk1b* MO. There was cross-reactivity observed with the *jnk1a* MO as the myc band was heavily reduced. Western blot carried out by Dr Simon Ramsbottom.

The process of overexpressing RNA in the embryo that codes for a myc-tagged *jnk1a* or *jnk1b* transcript makes it possible to gauge the specificity of our morpholinos. The RNA variants were introduced artificially and therefore do not represent endogenous proteins, however, the sequence of the injected RNA was identical to the endogenous counterpart at the morpholino binding site so should act in an identical manner to translation blocking MOs. Western blot analysis revealed that both the *jnk1a* and *jnk1b* morpholinos were capable of knocking down transcription from the gene to which they were targeted. However, it was also illustrated that there is cross-reactivity between the MOs and the RNA of the opposite paralog i.e. *jnk1a* MO is capable of knocking down *jnk1b* and vice versa. The MOs do not seem capable of knocking down the opposite paralog as strongly as they knockdown their actual target gene, so

compound *jnk1a*; *jnk1b* MOs remain the most appropriate way of knocking down both *jnk1* paralogs. Although this experiment appears to show strong cross-reactivity between the *jnk1* morpholinos and both paralogs of *jnk1*, replicates need to be performed before this can be shown conclusively.

4.2 DISCUSSION

c-Jun N-terminal Kinase is a protein which has been shown to have a role in multiple signalling pathways and mediate the action of dozens of downstream effectors (Bogoyevitch, 2006, Davis, 2000). It is therefore unsurprising that reducing protein translation of the two zebrafish *jnk1* paralogs results in defects to normal development. With the use of morpholino oligonucleotides targeted to *jnk1a* and *jnk1b* it has been possible to show that these genes are vital for correct development of the somitic muscle, heart, brain, and eyes of the zebrafish. This zebrafish morphant system may therefore prove to be a useful tool for studying *jnk1* function in a versatile model organism.

4.2.1 Morpholinos Can Successfully be used to Study *jnk1* During Development

4.2.1.1 The *jnk1* Morpholinos Successfully Knock Down their Targets

The use of morpholino oligonucleotides has proved a popular and valuable tool for developmental biologists to examine gene function in the zebrafish, particularly in the absence of a viable mutant. However, as with all genetic manipulations they require thorough validation and study before meaningful conclusions can be drawn. In this project I have established that these two morpholinos are a viable option to study *jnk1* function and have provided evidence that they successfully knock down their target genes at chosen optimal doses. In the absence of a commercially-available antibody which reacts specifically with zebrafish *jnk1* it was necessary to examine pan-Jnk protein levels in *jnk1* morphants. The pan-Jnk antibody is predicted to bind to not only Jnk1a and Jnk1b, but also the other family members Jnk2 and Jnk3. Despite this

limitation I showed that pan-Jnk levels were significantly reduced in the presence of both *jnk1a* and *jnk1b* morpholinos, but specifically it was the 46kDa band that was reduced.

The 54kDa pan-Jnk band did not display any significant change in abundance between the control and *jnk1* morphants. This is an interesting result because it could suggest that the morpholinos are capable of knocking down only the short transcripts of *jnk1* – a theory which seems unlikely considering that the short and long *jnk1* splice-variants share the same start site. An alternative theory may be that the knockdown of *jnk1* results in an upregulation of *jnk2* or *jnk3*. In fact it has been shown in *Jnk1* null mice that *Jnk2* is upregulated and vice versa (Reinecke et al., 2013). In order to cause the result observed in this western blot, the knockdown of *jnk1* would have to result in an upregulation of the long splice-variant(s) of Jnk2 and/or Jnk3 sufficient to not only mask the reduction in Jnk1 protein, but also exceed it. However, in the absence of antibodies that are specific for individual zebrafish Jnk proteins it was not possible to test this by western blot.

A further contributor to the western blot result which showed a reduction in the 46kDa Jnk band only, is that there may be more transcription of the 46kDa splice-variants at that 48hpf timepoint than the longer 54kDa variant; these two different sized proteins correspond to the short and long splice-variants respectively which were investigated by RT-PCR in the previous chapter. From the RT-PCR data it was shown that the expression pattern of the *jnk1* splice-variants was dependent upon which middle exon was integrated into the variant, and not whether it was a short or long variant (Figure 24A+C). Although absolute abundance of each variant could not be measured by this RT-PCR methodology, and nor could direct comparisons be made between abundance of each transcript since different primers were used, these data still suggest that the short form is not the only transcript expressed at 48hpf. In fact, *jnk1a_7;long* and *jnk1b_7;long* were approaching their highest expression levels at 48hpf, so this result contradicts the theory that all long transcripts were only lowly expressed at this timepoint. Since this method measures mRNA abundance and not protein abundance it is not a direct measure of the proteins that make up the 46 and 54kDa bands so this theory cannot be ruled out entirely; however without access to

specific antibodies for each variant, or use of a sophisticated proteomics approach such as 3D gel chromatography and mass spectrometry, this may be the most suitable way to predict protein levels.

Further evidence that the morpholinos are capable of knocking down their target was generated by the use of myc-tagged transcripts of *jnk1a_8;long* and *jnk1b_8;long*. When these tagged transcripts were overexpressed in zebrafish embryos the addition of the appropriate morpholino at the optimal dose was sufficient to prevent protein production. These data reveals that the morpholinos are capable of knocking down the long (54kDa producing) transcript of each paralog, something that was not revealed in the western blot. Although both of these experiments reveal that the morpholinos are capable of knocking down their target, they do not prove their specificity to *jnk1* alone. The gold standard method to show that phenotypic changes are causal of a particular gene knockdown is to rescue the phenotype with overexpression of a morpholino-resistant RNA. This experiment would therefore be the next logical step to validate the *jnk1* morpholinos, although may require some trial and error to determine which of the different splice-variant(s) are necessary for phenotypic rescue. Although I did attempt this mRNA rescue once, the positive and negative controls did not match with what was expected so this data had to be dismissed. Time constraints unfortunately meant that repeats were not possible, although this experiment would be a priority for future work on this project.

Morpholinos have previously been used to knockdown *jnk1* in a study of convergent extension movements (Seo et al., 2010) however no developmental defects were reported. The binding sites of these MOs were in exon 3 and exon 4 of *jnk1a* and *jnk1b* respectively (See appendices Figure 63). One explanation for this absence of defects is that the timepoints looked at were during early development (11 and 16hpf) which may be before developmental defects can be seen; certainly it is before elongation of the body axis would have made curling of the tail apparent, and it is also before heart tube formation and appearance of the different retinal layers. Another explanation is that in the Seo et al. study (2010), splice-variant MOs were used. Splice-variant morpholinos bind to pre-mRNA molecules and cause the skipping of exons or inclusion of introns into the translated protein product (www.gene-tools.com). These

morpholinos are incapable of knocking down maternally inherited mRNAs which are already in a mature state. As was shown in chapter 2, there is considerable inheritance of *jnk1* mRNA from the mother which persists until at least the start of gastrulation (5.25hpf) and may therefore be important during early stages of development. In this project translation blocking MOs were used, ensuring that both maternally inherited and zygotic *jnk1* was knocked down. I would therefore expect to see more severe defects using these morpholinos if *jnk1* is needed early in development.

4.2.1.2 The *jnk1* Morpholinos Cross-React

The myc-tagged western blot enabled the identification of cross-reactivity between each morpholino and the two *jnk1* paralogs. This cross-reactivity means that phenotypic data generated for single *jnk1a* or *jnk1b* knockdowns may not represent a true knockdown of only one gene and both paralogs are affected. It is therefore interesting to note that the phenotypes of *jnk1a* and *jnk1b* morphants were very distinctive with very little cross-over (the developmental defects caused by the *jnk1a* morpholino were not the same as those caused by the *jnk1b* morpholino). This difference in phenotype is suggestive that although both paralogs are being knocked down to a degree, the morpholino is favouring one gene over the other. Design of new morpholinos which target each gene specifically to determine whether they provide a phenocopy of what we observed would be a way to confirm that paralog-specific phenotypes are caused by our morpholinos.

Although the cross-reactivity of the morpholinos may be viewed as a limitation, it is inconsequential when compound *jnk1a; jnk1b* knockdown is desired. Since the two *jnk1* paralogs are specific to the teleost radiation then compound *jnk1a; jnk1b* morphants would provide a more suitable method for investigating the function of *jnk1* in human development. Although it still remains to be determined how similar the function of zebrafish *jnk1* is to its human ortholog, this morphant system could be utilised to determine what function *jnk1* plays in vertebrate development. Trying to rescue a zebrafish morphant phenotype with overexpression of human mRNA has been utilised in several papers to determine whether function is conserved between

species (Anichtchik et al., 2008, Al-Hamed et al., 2014), and could illuminate what shared function is conserved in the *jnk* gene.

4.2.1.3 High Doses of jnk1 Morpholino are Tolerated Without Causing Toxicity.

Toxicity is predicted to arise in between 15-20% of morpholinos and cause developmental arrest or CNS apoptosis (Eisen and Smith, 2008). None of these features were found to occur in doses up to 4ng *jnk1a* or 4ng *jnk1b*. Some toxicity was observed at the 6ng *jnk1a* dose, which rules out this dose from being used in future experiments. However, a compound 4ng *jnk1a*; 4ng *jnk1b* dose could be used without any signs of toxicity. Overall this evidence suggests that the *jnk1* morpholinos used here represent a robust and reliable tool to investigate the involvement of *jnk1* during zebrafish development.

4.2.2 The *jnk1a* and *jnk1b* Genes Play a Role in Development

The literature concerning JNK1 function in development is limited and contradictory; in mouse *JNK1* mutants were found to have only minor neurological changes (Kuan et al., 1999, Reinecke et al., 2013) whereas in *xenopus* there were convergent extension defects reported (Kim and Han, 2005, Yamanaka et al., 2002). In this project I have been able to show that *jnk1* does have a role to play in the development of the zebrafish, particularly in formation of several organs. Despite the cross-reactivity of the morpholinos there is also evidence of paralog-specific function of the two *jnk1* genes.

4.2.2.1 jnk1a is Vital for Development of the Heart, Brain and Tail

Knockdown of *jnk1a* revealed that this gene is vital for normal zebrafish development. Morphants at the 4ng *jnk1a* dose display dorsal curling or kinking of the tail instead of elongating normally from the yolk. Histology of the somites showed that the structure was also abnormal, and although the somites successfully segment from the preaxial mesoderm there are large gaps between muscle fibres; whether this abnormal histology is causal of the tail defect remains to be seen. *jnk1a* is also important in the

development of the brain and eyes. Loss of *jnk1a* during development results in the eyes being smaller, due primarily to the reduction in size of the two synaptic layers of the retina: the inner and outer plexiform layers. These layers are responsible for early processing of vision (Masland, 2001) so testing the vision of *jnk1a* morphants may reveal differences to controls. It is interesting to note that small eye size and underdevelopment of the retina has been reported previously in pan-jnk inhibition with the SP600125 drug (Xiao et al., 2013, Valesio et al., 2013), which suggests that this defect is a specific effect of loss of *jnk1a*. However, it is also important to note that small eyes, or failure of eye development, has been associated with morpholino off-target effects via the increase of apoptosis in the central nervous system (Robu et al., 2007). Although no CNS clouding was observed in these *jnk1a* morphants it would be beneficial to prove that the eye phenotype is rescued by mRNA co-injection before this can be confirmed as a specific effect of *jnk1a* knockdown.

In addition, it was found that a loss of *jnk1a* resulted in a defect of the brain posterior of the cerebellum. This region is where the hindbrain ventricle develops, and may be suggestive of a failure for the ventricle to inflate. Knockdown of *jnk1a* also resulted in severe oedema around the heart around 72hpf. Further analysis revealed that the morphant heart was primitive in construction and failed to have developed a valve. The hearts appeared smaller and had expansion of the cardiac jelly. It would be interesting to determine whether fewer cells were present in these hearts to contribute to their smaller size since the JNK genes have been linked with the processes of proliferation, apoptosis and differentiation (BossyWetzel et al., 1997, Mingo-Sion et al., 2004, Gururajan et al., 2005, Wei et al., 2014).

Although these developmental defects were reproducible there remains much work to be done in order to fully characterise the *jnk1a* morphant phenotype and investigate the mechanisms by which *jnk1a* is acting during development. Firstly, much of the histology characterisation requires further replication in order to become convincing and in order to quantify the differences in metrics associated with morphant tissue vs controls e.g. somite length, retinal layer size. Only with further replicates will it be possible to determine how much smaller the somites are or what the average reduction in heart lumen size is in *jnk1a* morphants. Once phenotype is fully

characterised to a high standard it would also be interesting to investigate the mechanism by which the *jnk1a* knockdown is causing these phenotypes. Analysis of proliferation and apoptosis rates for example would help to identify why certain layers of the retina are smaller, and lineage tracing of the cardiomyocytes could be used to determine whether cells are successfully differentiating and migrating to the heart tube. Determining the mechanism by which these defects are occurring would help to determine the role of this gene during development but is unfortunately something that I did not have the time to explore in this thesis.

4.2.2.2 jnk1b is Vital for Development of the Tail and Heart

Loss of *jnk1b* by MO knockdown caused the embryos to be shorter than controls with a very pronounced curling of the body axis ventrally towards the yolk, a feature that was accompanied by loss of the horizontal myoseptum from the somitic muscle. Interestingly horizontal myoseptum formation has been shown to fail in mutants with convergent extension defects via altered sonic hedgehog signalling (Yin and Solnica-Krezel, 2007). Whether deficient convergent extension is a feature of *jnk1b* morphants remains to be shown conclusively, as previous work has failed to show that *jnk1* functions in this process (Seo et al., 2010). However, other mutations in the PCP pathway have been shown to affect convergent extension (Jessen et al., 2002, Veeman et al., 2003, Wang et al., 2006a). Further work should address whether slow muscle is successfully differentiating in *jnk1b* morphants as this may provide a mechanism by which the horizontal myoseptum is failing to form.

The development of the heart also appears to be affected by *jnk1b* knockdown. In contrast to the histology of the *jnk1a* morphant heart, knockdown of *jnk1b* does not cause a failure for the atrioventricular valve to form which separates the two cardiac chambers. However, the chambers of the heart do appear to be smaller, particularly the lumen which may be hampered by the expansion of the cardiac jelly. Again, further investigation is required to determine whether number of cells is reduced in the *jnk1b* morphant heart and determination of whether apoptosis and proliferation rates are affected could help to determine a mechanism for the smaller size of the cardiac chambers. These heart results seem to fit with what has been observed in pan-jnk

inhibited morphants treated with SP600125 where curled tail and pericardial oedema were observed (Xiao et al., 2013, Valesio et al., 2013).

4.2.2.3 *The Zebrafish jnk1 Morphant Results in Context of PCP*

As has been discussed at some length, the *JNK* genes are known to be active in the planar cell polarity pathway where they lie downstream of the core protein complex. This signalling pathway is known to be critically important for several developmental processes, with disruption of several different genes resulting in similar developmental defects (see section 1.2.2 page 17). It is therefore necessary to put the results of this study into the context of the PCP family and determine whether the developmental defects observed in *jnk1* morphants resemble or contrast those seen in other loss-of-PCP studies.

Convergence and extension movements during gastrulation are important for extending the embryonic axis while reducing the medio-lateral axis and are critical for normal body patterning. Many instances have been shown where loss of normal PCP signalling results in the reduction of CE cell migration (Heisenberg et al., 2000, Seo et al., 2010, Kilian et al., 2003, Veeman et al., 2003, Jessen et al., 2002, Carreira-Barbosa et al., 2009) in the zebrafish and *Xenopus* vertebrate models, suggesting that these organisms are particularly susceptible to CE defects. It is therefore interesting to find that 4ng *jnk1b* and 4ng *jnk1a*; 4ng *jnk1b* morphants display a shortening of body length at 48hpf compared to controls. Although this body-length shortening could be the result of a CE-like defect I was not able to investigate this further. In order to determine whether *jnk1a* is required for convergent and extension (something which has been suggested in *Xenopus* (Yamanaka et al., 2002) it would be necessary to examine the migration of cells during the two phases of convergent and extension.

Interestingly this same shortening is not observed in *jnk1b* morphants, possibly suggesting a divergence in function between the two genes. However, the *jnk1b* morphants do display a failure to form the horizontal myoseptum during somatic development. Published work shows that there is a link between normal zebrafish CE movement and the patterning of the horizontal myoseptum progenitors via SHH

signalling (Yin and Solnica-Krezel, 2007, van Eeden et al., 1996). Since *jnk1b* morphants do not display shortening it is therefore possible that a mechanism other than CE is the cause of this somatic defect, or that the length reduction is too mild in *jnk1b* morphants to be detected by the methods used. Indeed it would be very interesting to determine whether the pioneer slow muscle cells are correctly patterned within *jnk1b* morphants as a possible mechanism for this defect.

Another common phenotype that has been associated with PCP disruption is a failure for the neural tube to close in mouse and *Xenopus* genetic models (Goto and Keller, 2002, Wallingford and Harland, 2002). A failure for the neural tube to close during primary neurulation has also been shown in *Jnk1* and *Jnk2* null mice due to a reduction in the controlled apoptosis of the hindbrain neural tube resulting in exencephaly (Kuan et al., 1999). Similar phenotypes have not been observed in zebrafish PCP mutants, perhaps due to the different mechanism by which the neural tube is formed (Kimmel et al., 1995), therefore it is not surprising that no neural tube defects are detectable in the *jnk1* morphants. However, there was a defect of the brain observed in the 4ng *jnk1a* and 4ng *jnk1a*; 4ng *jnk1b* morphants which presented as a depression of the hindbrain (Figure 32 page 150). It is not clear from these results whether this defect is a result of neural tube development, or through a different process, however it will be interesting to examine this phenotype in greater detail.

In the *Drosophila* wing as well as ciliated mammalian tissues and Kupffer's vesicle in the zebrafish, loss of PCP can result in loss of polarization in ciliated cells. Randomisation of tissue polarity can significantly reduce tissue function and also result in aberrant left-right patterning in certain models. During the gross phenotype characterisation of the *jnk1* morphants, it appeared that left-right formation of the visceral organs may well be affected. I therefore decided to investigate this feature more closely (see chapter 5 page 191).

4.2.2.4 Similarities of the *jnk1* Retinal Phenotype to Ciliopathy-Associated Gene Knockdowns

One of the most striking changes to be seen between the control and *jnk1a* histology data was that of the loss of retinal lamination. In addition both 4ng *jnk1a* and 4ng *jnk1a*; 4ng *jnk1b* morphants display a smaller eye size (microphthalmia) phenotype when gross phenotype is observed by light microscopy. Considering the association between PCP pathway genes and cilia (for review see (Karner et al., 2006a)) it is therefore interesting to note the similarities that are observed between the eye phenotypes of the *jnk1* morphants and those with disruption of cilia function.

Many ciliopathies have been shown to have associated retinal phenotypes such as Usher Syndrome, macular degeneration, Joubert Syndrome, primary ciliary dyskinesia, and Bardet-Biedl syndrome (for review see (Adams et al., 2007)). This association is not surprising considering that the photoreceptor cells arise from primitive primary cilia (Wheway et al., 2014). The zebrafish has become a popular model for the retinal ciliopathies because of their well studied genetics and highly developed retina by only three days of age. This has led to several human cilia-associated orthologs being mutated or knocked down in zebrafish to determine the role of these genes in eye development and retinal patterning (Wheway et al., 2014).

Shu et al. knocked down the retinitis pigmentosa 2 homolog *rp2* with morpholino oligonucleotides and found that retinal lamination failed to form the ganglion cell layer, inner nuclear layer and outer nuclear layer of the retina by 72hpf. In addition these morphants displayed a smaller global eye size than controls (microphthalmia) and smaller lens size. This phenotype was then successfully rescued by injection of human *RP2* mRNA which was resistant to the MOs (Shu et al., 2011). A similar result was found to occur with loss of the ciliary gene *ahi1* which is associated with Joubert syndrome in humans. Knockdown of this gene in zebrafish showed that again the lamination of the retina failed to differentiate and microphthalmia was apparent as well as a loss of cilia developing in the left-right organiser Kupffer's Vesicle (Simms et al., 2009). This consistency of microphthalmia and loss of lamination has also been observed in the *topors* and *bbs5* morphants (Al-Hamed et al., 2014, Chakarova et al., 2011) suggesting a strong association between ciliogenesis and eye development

within the zebrafish. In the *topors* morphant this lamination loss was coincident with increased levels of apoptosis, although causation was not established.

In *jnk1a* morphants there is indeed a small-eye phenotype with no laminations being developed by 48hpf. However, by 72hpf there are retinal laminations present in *jnk1a* morphants although some of these layers are significantly smaller than controls. The photoreceptor, inner nuclear and inner plexiform layers are smaller in 4ng *jnk1a* morphants than controls, in comparison to the ganglion, inner and outer nuclear layers defects and photoreceptor absence observed when *rp2* morphants. These phenotypes do therefore appear similar although not identical as *jnk1a* morphants have reduced size of the IPL. However, in *ahi1* and *bbs5* morphants there was a loss of both the inner and outer plexiform layers demonstrating that these layers may also be affected in zebrafish-modelled ciliopathies. Furthermore, in those journal articles mentioned there was an absence of the laminations whereas in 4ng *jnk1a* morphants there was only a reduction in the lamination size. This could be suggestive of a reduced MO penetrance of the *jnk1a* MO and require a larger dose to achieve a full loss of lamination, or it could arise because *jnk1a* is not as crucial for retinal development as those other cilia genes studied. Further work is required to determine which of these possibilities is correct, and whether the mechanisms by which these ocular defects arise is shared. However, since JNK activity is linked to increased cellular apoptosis (Fuchs et al., 1998, Kuan et al., 1999) it does not seem likely that this is the mechanism for reduced lamination size in the *jnk1a* morphants. Despite these inconsistencies with ciliopathy related genes, these data are suggestive of a function of *jnk1a* in cilia development, and further investigation is warranted.

4.2.2.5 Concluding Remarks

Overall these results have successfully demonstrated that morpholinos are a viable way to examine developmental function of the *jnk1* paralogs, although it does appear that some cross-reactivity occurs. Further replicates of this myc-tagged western blot are required to confirm this cross-reactivity and to quantify the degree to which cross reactivity occurs. Despite this cross-reactivity the two *jnk1* morpholinos cause different

phenotypes when administered which has begun to address the paralog-specific roles of the two zebrafish genes.

Broadly *jnk1a* appears to function in development of the brain and eye - where retinal laminations appear to be reduced in size. However, further work is required to quantify the retinal reduction and determine the mechanisms by which this defect arises. Heart development is also severely disrupted by *jnk1a* knockdown and the organ appears as a very primitive structure even at 72hpf, without a visible valve and with a much smaller lumen. It would be interesting to determine whether reduction in function of these morphant hearts contributes to the cardiac oedema that was observed at the 4ng *jnk1a* MO dose.

The *jnk1b* morphants displayed far more severe curling of the body axis compared to the *jnk1a* morphants, as well as a failure for the somitic horizontal myoseptum to form. To further investigate this defect it would be interesting to perform wholemount immunohistochemistry for slow muscle markers to determine whether these cells were differentiating correctly adjacent to the notochord. If failure to form the horizontal myoseptum was confirmed then it could help to explain the more rounded appearance of the somites, as this is one of the features which has been shown to occur when the horizontal myoseptum fails to develop (van Eeden et al., 1996).

CHAPTER 5 - LEFT-RIGHT PATTERNING DEFECTS OF THE JNK1 MORPHANTS

5.1 INTRODUCTION

5.1.1 Breaking Symmetry of the Visceral Organs

Despite the external appearance of left-right symmetry in the zebrafish, internally many organs are positioned on one side of the body, or are themselves asymmetrical e.g. the heart, liver, pancreas, gut, pineal gland (Ahmad et al., 2004, Field et al., 2003, Liang et al., 2000). Establishment of this asymmetry is critical for development, and just like in other species, incorrect left-right patterning can lead to disruptions in development or function. One of the signalling pathways shown to be critical for left-right patterning of the zebrafish visceral organs is the planar cell polarity (PCP) pathway. It has been shown that when members of this pathway are disrupted in zebrafish it results in left-right patterning defects (Song et al., 2010, Walentek et al., 2013, Wang et al., 2011). Interestingly it has also been shown that *rock2b*, one of the two kinases downstream of the core PCP proteins, is vital for left-right patterning, and knockdown of this gene by morpholino oligonucleotides (MO) causes disruption of left-right patterning of the visceral organs (Wang et al., 2011). As the other kinase downstream of the PCP core proteins, the *jnk* family are prime candidates for regulating left-right asymmetry during development. I therefore decided to determine whether *jnk1* knockdown during zebrafish development resulted in left-right situs defects of the visceral organs.

5.1.1.1 Jogging and Looping Movements of the Heart

The mature zebrafish heart is asymmetrical in both position of the organ in the body as well as its structure. However, the organ originally develops as a primitive tube that is superficially symmetrical across the left-right axis. This primitive linear heart tube develops at the embryonic midline by 24hpf and beats in a peristaltic manner (Glickman and Yelon, 2002). Although there are no observable boundaries between the two chambers at this stage, the anterior region is patterned to become the ventricle, with the posterior region becoming the atrium. Over the next 24 hours two key morphogenetic movements occur that break symmetry and align the chambers to their mature positions. These two movements of the heart are known as jogging and looping. Cardiac jogging is the first break of symmetry conducted by the linear heart tube, but there is minimal evidence that this

occurs in mammals (Biben and Harvey, 1997). The gene ontology (GO) consortium defines cardiac jogging as the leftward displacement of the heart with respect to the anterior-posterior axis (<http://www.ebi.ac.uk/QuickGO/GTerm?id=GO:0003146>). This process occurs in wildtype zebrafish embryos between 24 and 30hpf and results in the heart projecting diagonally away from the midline (Figure 46 A) such that the venous pole is most lateral (Chin et al., 2000) before moving back towards the midline. Over the next 10 hours the heart undergoes a second movement known as looping (Chin et al., 2000), a process that is also observed in mammalian heart development. Looping of the zebrafish heart, which has only two chambers, is a much more simplified process than mammalian cardiac looping; the primitive ventricle of the linear heart tube moves rightwards (medially) and posteriorly in relation to the primitive atrium. The rightward looping that is observed in a majority (>95%) of wildtype embryos is known as D-looping (Chin et al., 2000) and is completed by about 36hpf (Stainier et al., 1993). The final location of the ventricle is to the right side, and adjacent to the leftward-lying atrium. During the looping process the two chambers become delineated and a constriction between the two chambers reveals the location of the primitive atrio-ventricular valve (Peal et al., 2011).

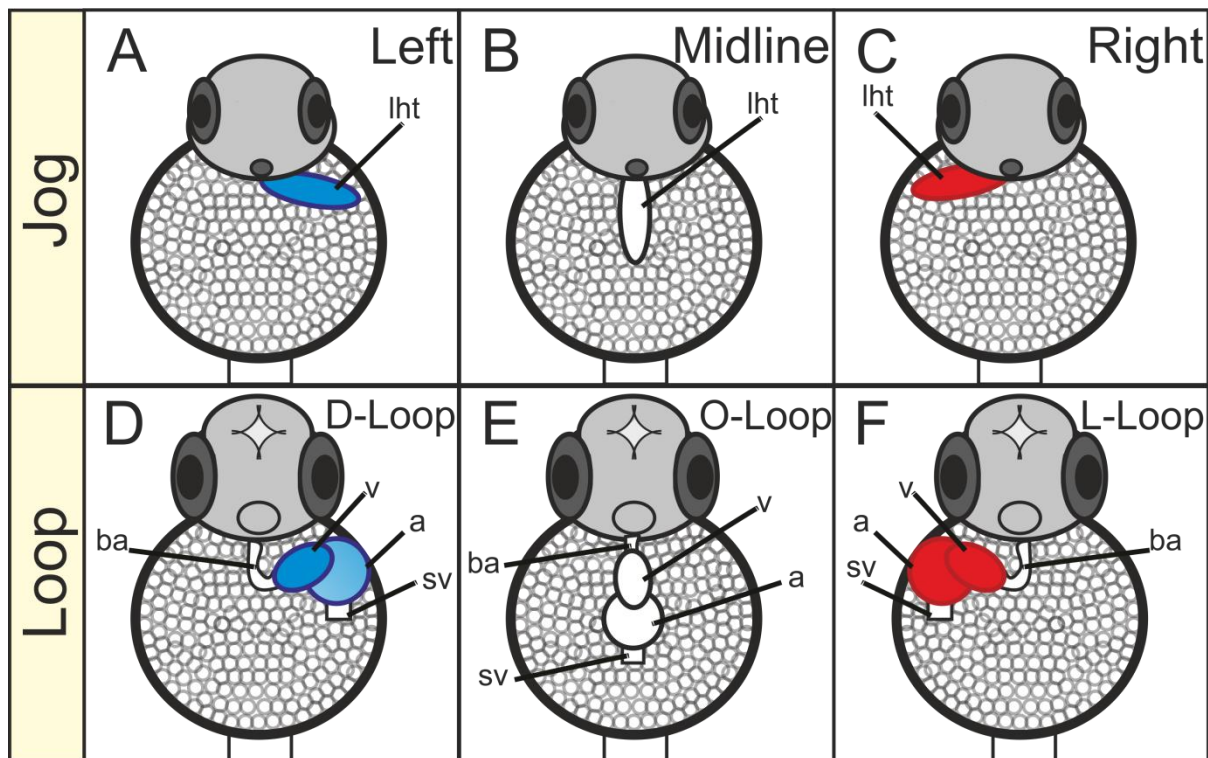


Figure 46 Schematic Representation of Jogging and Looping Movements of the Zebrafish Heart Tube.

Observations of heart tube development in zebrafish can be made through the translucent yolk. From this ventral orientation the right of the image is the embryo's left. The linear heart tube (lht) forms by 24hpf on the embryonic midline and over the next few hours it breaks asymmetry in a movement known as jogging (A-C). Normal jogging (A) involves moving over to the left side of the embryo, although in a small proportion of untreated wildtypes the heart tube may remain on the midline (B) or jog to the right (C). Over the next 10 hours the ventricle (v) moves rightwards and medially in relation to the atrium (a) in a process known as looping. This rightward ventricular looping known as a D-loop heart (D) establishes the positioning of the mature heart chambers. However, the heart may fail to loop (E) producing an O-loop, or display reversed looping (F) resulting in an L-loop heart, both of which are seen rarely in wildtypes. lht=linear heart tube, v=ventricle, a=atrium, ba=bulbous arteriosus, sv=sinus venosus.

5.1.1.2 *Uncoupling of Heart Movement*

The maturation of the asymmetrical zebrafish heart is different from that of mammals in that there are two processes which break symmetry: jogging and looping. The “normal” progression which >95% untreated wildtype embryos follow is an initial leftward jogging of the organ, before rightward heart looping occurs (Chen et al., 1997). However, a small proportion of untreated wildtype embryos undergo a complete reversal of normal heart movements (*situs inversus*) or a failure to break symmetry at all. In zebrafish with mutations / knockdowns that affect left-right signalling the proportion of embryos which undergo normal heart movements are significantly reduced. In these cases the proportion of embryos with R-looped, O-looped and L-looped hearts approaches 33% which represent a total randomisation of heart laterality (Wang et al., 2011, Ahmad et al., 2004, Chin et al., 2000). However, in the majority of those mutants studied, once the initial jogging direction is completed the looping movement is also determined i.e. a leftward jog is followed by a rightward D-loop, or a rightward jog is followed by a leftward L-loop. In these instances the jogging status of the embryo was predictive of which way the heart would loop over the next 10 hours, and the two processes were thought to be coupled to one another. Where the heart fails to jog during early development the looping direction appeared to be randomised (Chen et al., 1997). These data lead to the theory that jogging and looping of the zebrafish heart were controlled by the same genetic mechanisms.

Interestingly it has been shown that there is a subset of mutations where cardiac jogging status is not predictive of looping, effectively displaying an uncoupling of zebrafish heart movements (Chin et al., 2000). Most of the genes identified that cause uncoupling are associated with development of the physical midline barrier or notochord, such as *noto* (floating head), *dharma* (bozozok) and *ta* (no tail) (Chin et al., 2000). However, it has also been observed that knockdown of *spaw* (zebrafish *nodal*) results in uncoupling of jog / loop progression (Ahmad et al., 2004). Despite the major role of *nodal* being to pattern “left-ness” in the lateral plate mesoderm, in mouse it has also been suggested to play a part in formation of the molecular midline barrier; *Nodal* induces expression of its antagonist *Lefty1* in the embryonic midline (Yamamoto et al., 2003). Whether heart uncoupling defects are therefore restricted to incorrect midline barrier development remains to be seen. Unfortunately, most research into

zebrafish heart laterality investigates the heart laterality at a single timepoint only. This methodology means that it is not possible to determine whether uncoupling of heart movement is a common occurrence, or a feature specific to a particular genetic pathway.

5.1.2 Aims of the Chapter

The aim of this chapter is to determine whether *jnk1a* or *jnk1b* is involved in left-right patterning of the visceral organs, and if so what laterality defects are observable in morphants. This aim was investigated by completion of several objectives:

1. Determination of whether heart laterality defects arise in *jnk1a*, *jnk1b* or compound *jnk1a; jnk1b* morphants.
2. Investigation of whether any laterality defects also result in an uncoupling of cardiac jogging and looping movements during development.
3. Examination of whether the *jnk1* morphants possess laterality defects of the gut.
4. Comparison of heart and gut position to see whether heart and gut laterality is coupled, or whether there is heterotaxy in *jnk1* morphants.

5.2 RESULTS

5.2.1 Left-Right Patterning Defects of the *jnk1* Morphant Heart

5.2.1.1 Zebrafish *jnk1* Knockdown Causes L-R Heart Defects in a Dose Dependent Manner

Determination of heart laterality was initially assessed as heart looping status at 48hpf (see section 2.3.11 page 91) by light and fluorescent microscopy. Around 50 embryos per clutch of the *Tg(myl7:EGFP)* line (which express eGFP in cardiomyocytes) were injected with morpholino and at 24hpf the embryos were switched to a pigment inhibiting media (E3 / PTU). Heart laterality of the anaesthetised embryos was assessed at 48hpf and heart looping status was scored by light microscopy as D-loop, O-loop or L-loop. At this time, example pictures were also taken by fluorescent microscopy, taking advantage of the eGFP that is expressed in cardiomyocytes of the *Tg(myl7:EGFP)* line (**Figure 47**). These pictures revealed that both control and morphant hearts alike display “normal” D-looping, as well as “abnormal” O-looping and L-looping.

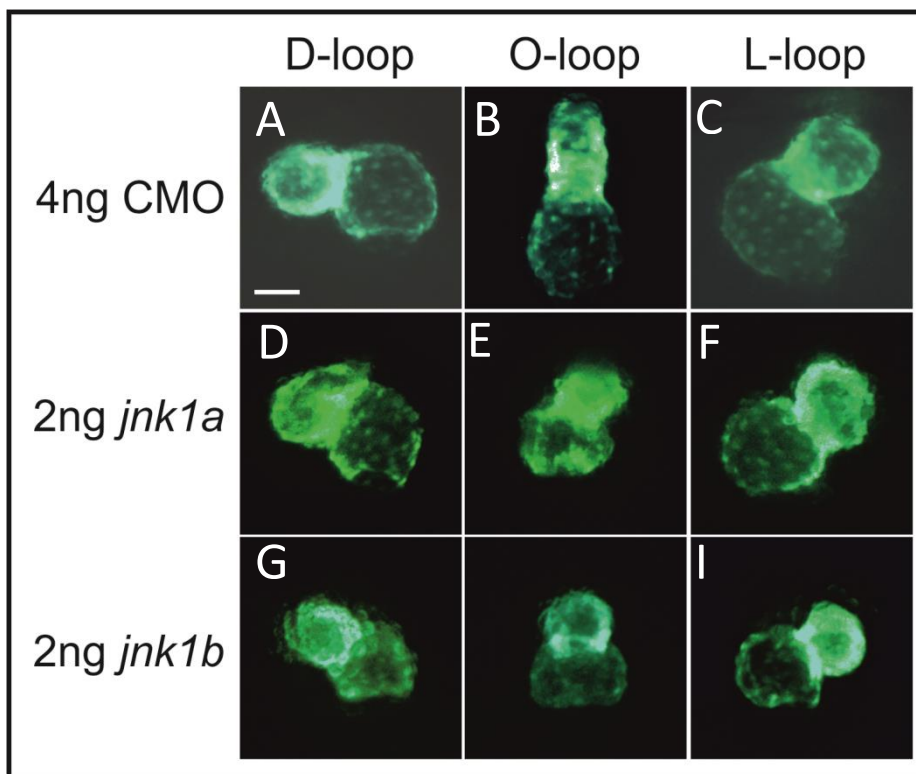


Figure 47 Heart Laterality Defects are Observable in Controls and Morphants at 48hpf.

A-C) 4ng control morpholino, D-F) 2ng *jnk1a* morpholino, G-I) 2ng *jnk1b* morpholino. Visualisation of the heart by fluorescent microscopy reveals that looping laterality defects occur in controls and *jnk1* morphants. Normal heart movement results in a D-loop (A, D, G) where the ventricle moves to the right of the atrium, however there may also be a failure to loop (B, E, H) where the heart remains on the midline, or a reversal of looping status (C, F, I) known as an L-Loop. As shown here, all three of these phenotypes occur in controls and *jnk1* knockdowns.

All images using the *Tg(myl7:EGFP)* line at 48hpf. Embryos positioned ventral-side-up so that left of image equates to right side of the embryo and right of image is left side of embryo. Scalebar=50µm.

The heart looping of both controls and morphants was scored for at least three different clutches per dose. From this laterality frequency data we are able to see that control morphants (4ng CMO) have 94% in the D-loop group with ~2% O-loop and ~4% L-loop. In comparison the uninjected controls displayed a higher incidence of D-loops with 98% of embryos developed a D-loop, ~1% O-loop, and ~1% L-loop. This deviation was found not to be significant by one-way ANOVA (Figure 49), revealing that injection of MO by itself does not significantly raise heart laterality defects.

In *jnk1a* morphants the frequency of D-loop hearts decreased in a dose-dependent manner between 2ng, 3ng and 4ng MO (Figure 48A). However, of those morphants that failed to form a D-loop heart there was no bias observed between the other two groups; at the 3ng *jnk1a* dose the frequency of L-looped hearts was greater whereas at 4ng *jnk1a* the frequency of O-looped hearts was greater (Figure 48B). From these data it was possible to determine that at the 4ng *jnk1a* dose the frequency of morphants that formed a “normal” D-loop heart was significantly reduced ($p < 0.05$) compared to morphant controls (Figure 49).

In *jnk1b* morphants there was also a dose-dependent reduction of L-loop hearts over the 1ng, 2ng and 4ng doses, however the *jnk1b* morpholino caused a lower frequency of D-looped hearts than the *jnk1a* MO at the same dose (Figure 48A). Furthermore, where morphants fail to develop D-loop hearts there appears to be a preference for the formation of an L-loop at higher doses i.e. at the 2ng and 4ng *jnk1b* doses there were greater than 3x as many L-loop hearts as O-looped (Figure 48B). Performing a one-way ANOVA revealed that there is significant divergence from the “normal” D-loop heart at both 2ng ($p < 0.001$) and 4ng ($p < 0.000$) *jnk1b* (Figure 49).

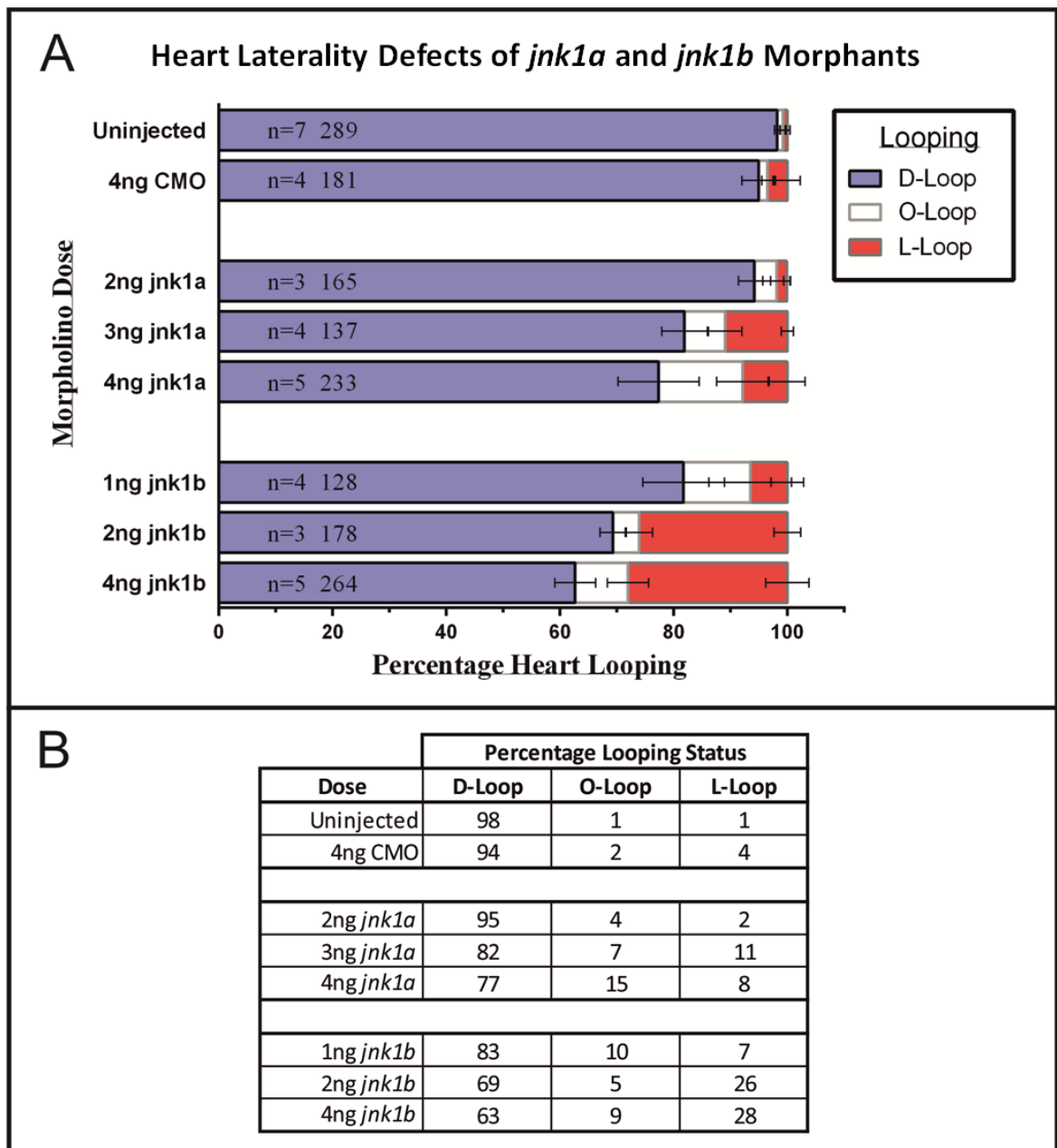


Figure 48 *jnk1* Knockdown Results in an Increased Prevalence of Heart O-loop and L-loop Formation in a Dose Dependent Manner.

A) Stacked column graph shows the prevalence of heart looping phenotypes in controls and morphants of both *jnk1a* and *jnk1b*. Although O- and L-looping are both observed in controls the frequency is low. In *jnk1a* morphants these two “abnormal” looping statuses become more frequent as dose of morpholino increases. This heart defect prevalence is greater still in *jnk1b* morphants at the same dose, and appears to cause L-looping preferentially over O-looping. Graph represents mean frequency of each phenotype per dose. The number of replicates and total number of individuals per dose is shown at the left side of each column. Error bars = SEM. B) Table displaying the mean percentage distribution of each looping phenotype per dose. Figures are equal to those represented in the graph.

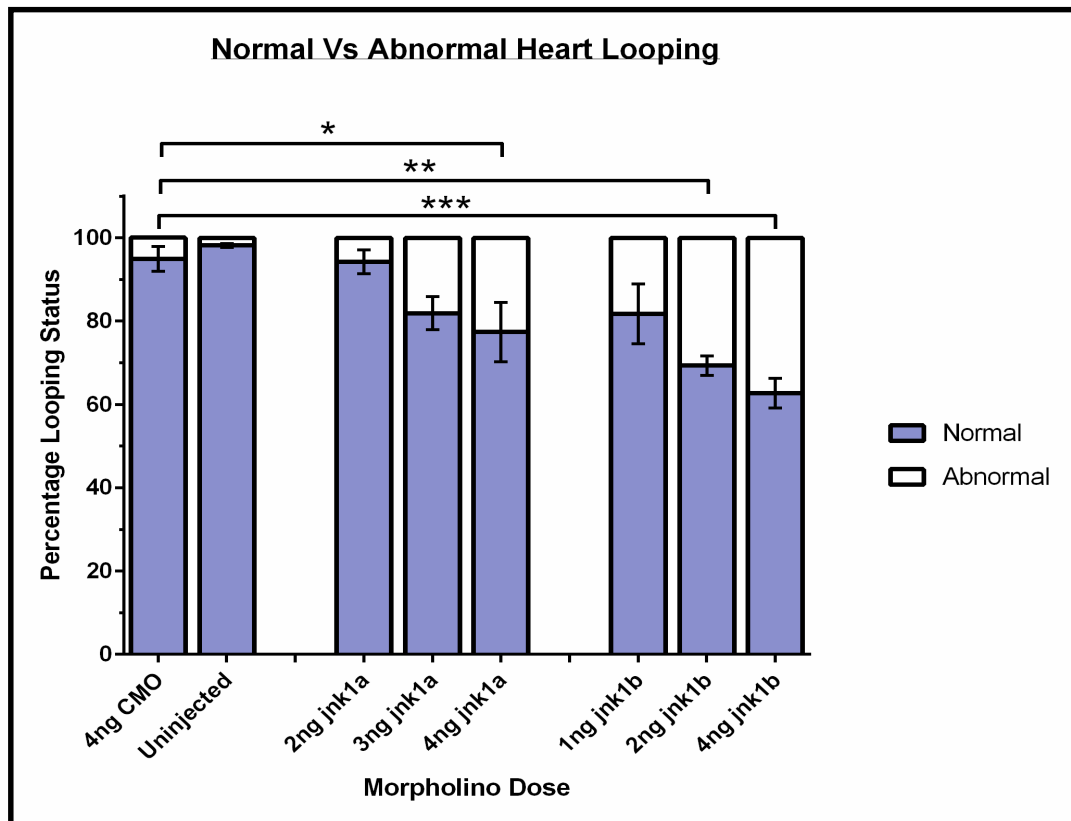


Figure 49 *jnk1* Knockdown Results in Significant Loss of Normal Heart Laterality.

Reorganisation of the heart laterality data into two groups allowed for statistical analysis to be performed. One-way ANOVA revealed that heart laterality was significantly disrupted in 4ng *jnk1a*, 2ng *jnk1b*, and 4ng *jnk1b* morphants (* $p < 0.05$, ** $p < 0.01$, *** $p < 0.001$) when compared to control morphants.

5.2.1.2 *Uncoupling of the Jog-Loop Heart Progression*

The asymmetrical movements of the developing zebrafish heart normally follow one another such that leftward jogging results in a D-loop heart and rightward jogging results in an L-Loop. However, it has been shown that these two movements can be uncoupled from one another by disrupting certain genes (Chin et al., 2000). In order to determine whether jog and loop progression was uncoupled in *jnk1* morphants I followed the hearts of *jnk1* morphants through both of these processes.

Approximately 50 morphants were generated per dose of *jnk1* morpholino and again switched to pigment-reducing media at 24hpf. These morphants were assessed for heart jogging status at 28hpf by dissection microscopy and scored as either left, midline, or right jog status. An angle of at least 5° between the anterior-posterior axis and linear heart tube was required for the scoring of a left or right jogged heart (as per Chin et al. 2000). Looping status was assessed as before at 48hpf to score the embryos as D-loop, O-loop, or L-loop. Heart jogging was found to be completed at 28hpf in all morphants (Figure 50A) except for the 4ng *jnk1a* morphants which displayed a delay in heart formation. At 28hpf the heart had not elongated into a mature heart tube, and instead appeared as a roughly spherical mass of beating cells on the midline (Figure 50B). The morphants that displayed delay in heart maturation were screened for jogging at two-hour intervals and were found to have jogged by 32hpf – displaying a four hour delay compared to controls. This delay was not observed at the time of looping assessment (48hpf), although heart looping is complete in wildtype zebrafish by around 40hpf (Chin et al., 2000).

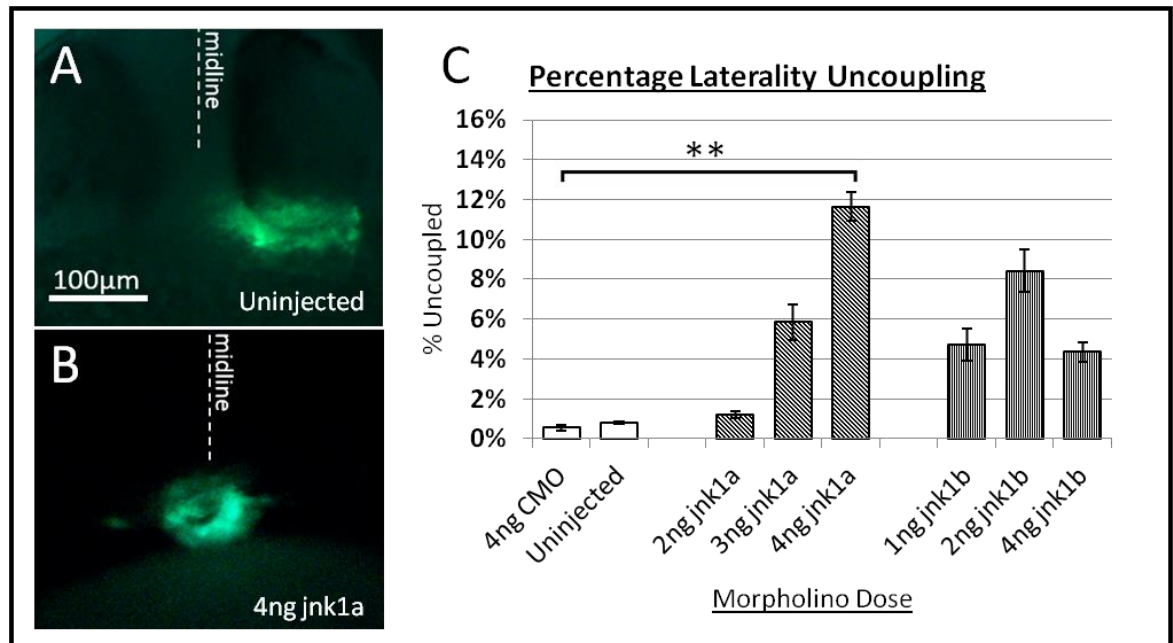


Figure 50 The 4ng *jnk1a* Morphants Displayed Heart Formation Delay and Uncoupling of Jog / Loop Movements.

A+B) Fluorescent heart pictures at 28hpf in the Tg(*myl7:EGFP*) line revealed that normal heart jogging to the left of the embryo was achieved in uninjected embryos (A) by this timepoint. However, the 4ng *jnk1a* morphants (B) displayed a delay in formation of the heart tube and at 28hpf the cardiomyocytes sat as a rounded mass on the midline (dotted line runs through the middle of the head). C) Plotting the number of *jnk1* morphants that do not follow the normal jog / loop heart progression revealed that the 4ng *jnk1a* morphants displayed a statistically significant uncoupling of the two processes (** $p < 0.01$) compared to the 4ng control morphants (4ng CMO). Graph represents the mean percentage prevalence of heart uncoupling. Error bars = SEM.

The laterality data at both timepoints (jog and loop) was analysed to determine whether uncoupling of heart movement occurred at any dose of *jnk1* knockdown. In both control morphants as well as uninjected controls there was a very small incidence of uncoupling observed (Figure 50); this feature has been previously reported in the literature (Chin et al., 2000). In the case of *jnk1a* knockdown there was a dose-dependent increase of heart uncoupling so that at the 4ng *jnk1a* dose there were almost 12% of morphants displaying uncoupling (Figure 50). At this high 4ng *jnk1a* dose, it was found that there was a significant increase in heart uncoupling compared to 4ng control morphants. The incidence of heart uncoupling was also raised over different *jnk1b* doses but not significantly. The incidence of uncoupling over the *jnk1b*

doses peaked at 2ng and was lower at 4ng *jnk1b*. However, for all of these *jnk1b* doses the absolute number of unlooped phenotypes was very low compared to the sample that was taken (6, 15 and 9 embryos respectively); therefore large numbers of embryos are necessary to accurately gauge the prevalence.

5.2.1.3 The Hearts of Compound *jnk1a; jnk1b* Morphants Display an Inability to Loop

Individual knockdown of *jnk1a* and *jnk1b* revealed that these genes are important for correct cardiac jogging and looping, and disruption leads to an increased frequency of abnormal heart laterality. Despite evidence that the morpholinos cross-react (see 4.1.8.2), individual morphants displayed distinct gross phenotypes that were unique to *jnk1a* or *jnk1b* knockdown (sections 4.1.6 and 4.1.7); compound *jnk1a; jnk1b* morphants displayed the combined phenotypes. These data suggested that injection of a single *jnk1a* or *jnk1b* morpholino was not sufficient to completely abolish pan *jnk1* signalling. To investigate the effect on heart laterality of knocking down both *jnk1* paralogs I performed dual *jnk1a* and *jnk1b* MO injections together and examined the cardiac jog / loop movements during development.

Approximately 50 compound *jnk1a; jnk1b* morphants (various doses) and 8ng control morphants were generated per clutch and allowed to develop until 24hpf. At 24hpf the media was changed to include PTU to inhibit pigment development and jogging was scored at 28hpf. The 4ng *jnk1a*; 4ng *jnk1b* dose displayed developmental delay of approximately 4 hours (Figure 30) and were therefore assessed at 32hpf (see Figure 30). Cardiac looping was scored at 48hpf for all doses except the 4ng;4ng dose which was performed at 52hpf. From these data the frequency of jog/loop uncoupling was calculated for each of the different populations.

Compound *jnk1a; jnk1b* morphants displayed heart laterality defects in a dose-dependent manner; as the MO dose was increased, the frequency of D-loop hearts was reduced. For the 1ng *jnk1a*; 1ng *jnk1b* morphants the frequency of D-Looped hearts was about 80% but by the 4ng *jnk1a*; 4ng *jnk1b* dose only 30% of morphants displayed D-looping (Figure 51A). These results resemble the knockdowns of *jnk1a* or *jnk1b* where dose-dependency is also observed. Where morphants failed to form a D-

loop, the frequency of O and L-looped hearts was increased. Interestingly at both 1ng *jnk1a*; 1ng *jnk1b* and 2ng *jnk1a*; 2ng *jnk1b* doses the percentage of morphants with an O-loop or L-loop was roughly equal, with only a few percent difference between them (Figure 51B). However, at the high dose of 4ng; 4ng the frequency of hearts which failed to undergo cardiac looping was several-fold higher than the other two groups. This large jump in O-looped heart frequency in 4ng; 4ng morphants may represent a dosage threshold whereby there is a bias towards a failure of the heart to loop.

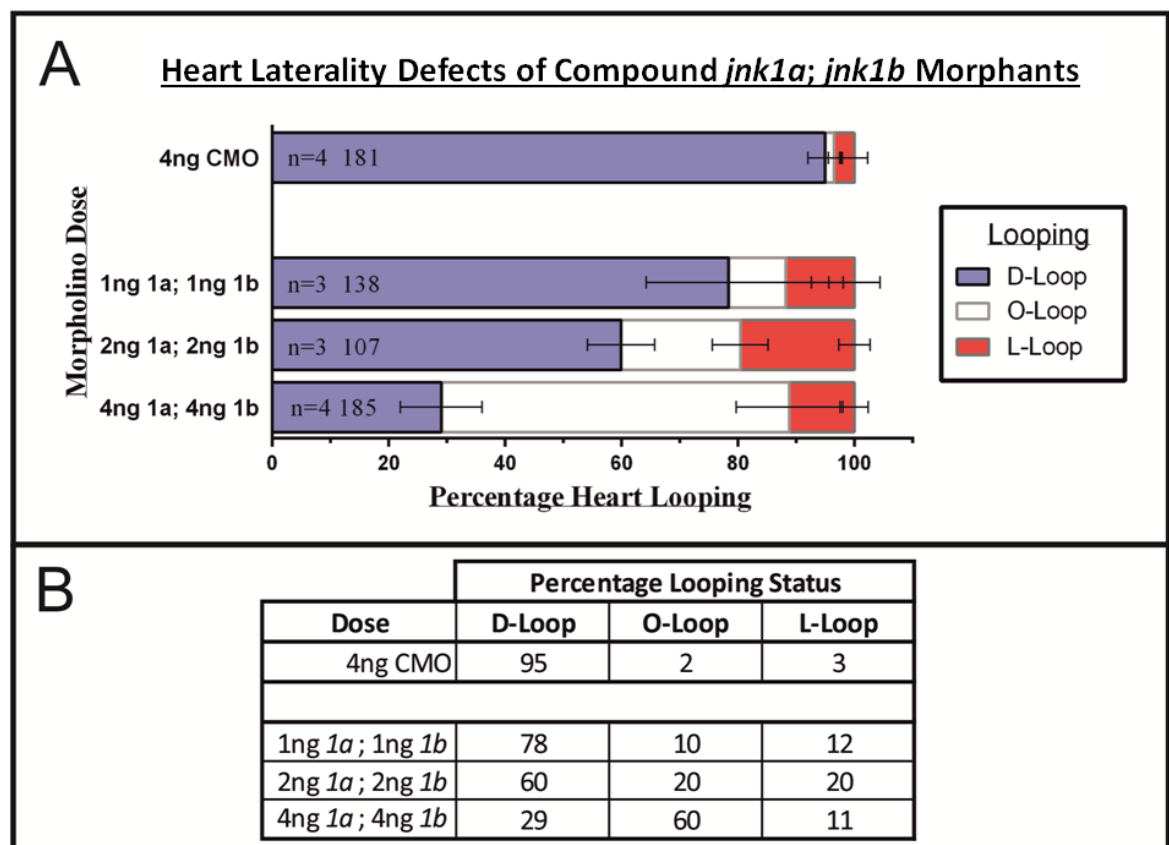


Figure 51 Compound *jnk1a*; *jnk1b* Morphants Display High Levels of Heart Laterality Defects and a Preference for O-Loop at the High Dose.

A) The frequency of heart L-looping decreases in a dose-dependent manner as compound *jnk1a*; *jnk1b* morpholino doses increased. The hearts of morphants instead displayed an increased prevalence of forming O-loop or L-loop hearts. At the 4ng *1a*; 4ng *1b* dose the most prevalent phenotype is an O-loop heart. Graph plots the mean percentage incidence of each heart looping phenotype at 48hpf. Error bars = SEM. B) Table listing the percentage frequency of each looping phenotype per group, as shown in the graph.

In order to determine whether compound *jnk1a*; *jnk1b* knockdown caused a statistically significant divergence from normal heart laterality these data were

categorised as “normal” (D-loop) or “Abnormal” (O-loop + L-loop) laterality. The normality frequency was then compared between the control morphant group and compound *jnk1a*; *jnk1b* MO groups by one-way ANOVA and a Dunnett post-hoc test revealed which groups were different. Statistical significance was found at both the 2ng *jnk1a*; 2ng *jnk1b* ($p < 0.05$) and 4ng *jnk1a*; 4ng *jnk1b* ($p < 0.01$) doses (Figure 52).

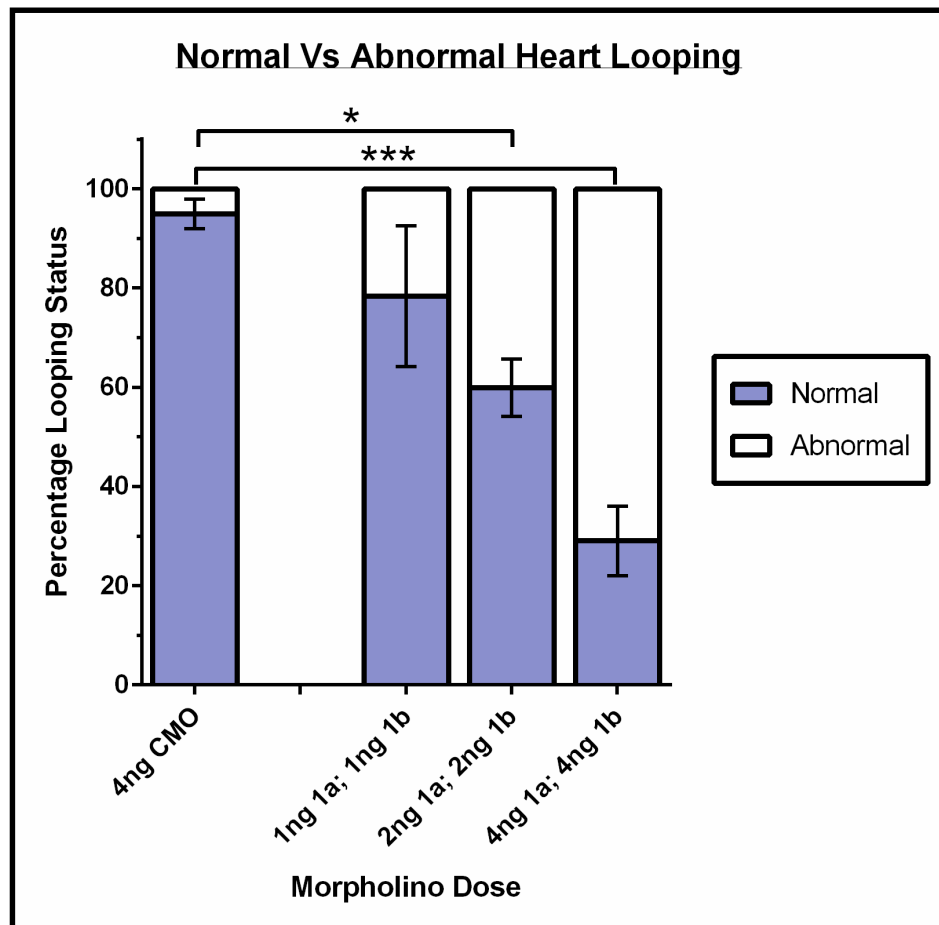


Figure 52 Normal Heart Looping Laterality is Greatly Disrupted by Knockdown of both *jnk1* Paralogs.

Plot showing the mean percentage of compound *jnk1a*; *jnk1b* morphants that display a normal cardiac looping phenotype. This analysis reveals that normal heart looping laterality was significantly disrupted in 2ng *jnk1a*; 2ng *jnk1b* ($p = 0.026$) and 4ng *jnk1a*; 4ng *jnk1b* morphants ($p = 0.000$) as assessed by one-way ANOVA and Dunnett post-hoc test. Error bars = SEM.

Once normal looping laterality was shown to be disrupted in several compound *jnk1a*; *jnk1b* MO doses I assessed whether the heart movements of jogging and looping were

uncoupled in these groups. Uncoupling was calculated by analysing the progression between jog and looping data to determine whether jog position was predictive of loop direction. Since midline jogging is not predictive of heart looping, this group was discounted from the analysis. It was found that uncoupling of the heart movements increased in a dose-dependent manner as the amount of morpholino was raised. However, only at the 4ng 1a; 4ng 1b dose was this uncoupling statistically significant when compared to 8ng control morphants. At this high 4ng *jnk1a*; 4ng *jnk1b* dose, uncoupling of the jog and looping position approaches 30% of the total morphant population (Figure 53).

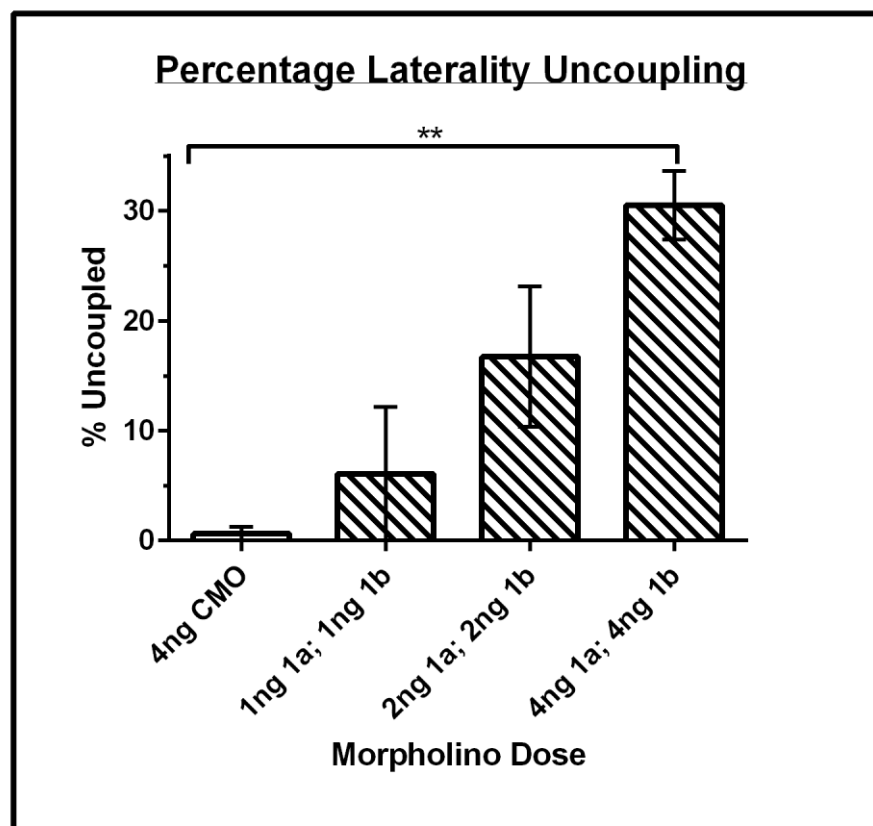


Figure 53 Compound *jnk1a*; *jnk1b* Knockdown Results in Heart Movement Uncoupling in a Dose-dependent Manner.

Plot of mean percentage compound *jnk1a*; *jnk1b* morphants that display an uncoupling of heart jogging and looping. The frequency of heart uncoupling was found to increase in a dose-dependent manner but was only statistically significant at the 4ng 1a; 4ng 1b dose as compared to controls. One-way ANOVA followed by Dunnett post-hoc test performed. (** $p < 0.001$) errorbars = SEM.

5.2.2 Patterning Defects of the Gut

5.2.2.1 Normal Liver Laterality is Disrupted in *jnk1* Morphants

In addition to the heart, several other organs in the zebrafish show left-right asymmetry in position and structure. One organ that develops asymmetric laterality is the liver which sits on the left side of wildtype embryos. In order to determine whether the laterality defects of *jnk1* morphants was restricted to the heart, or whether it also affecting other visceral organs, I performed two-probe, wholemount in situ hybridisation. The two probes used were *myl7* (*cm1c2*) which is expressed within cardiomyocytes, and *foxa3* which is expressed in the developing liver, pancreas and gut. From these data I was able to examine the location of the liver in zebrafish embryos as well as investigate whether positioning of the heart and gut were correlated; discordant organ laterality is known as heterotaxy.

The in situ hybridisations were performed on 8ng CMOs, 4ng *jnk1a*, 4ng *jnk1b* and 4ng *1a*; 4ng *1b* morphants at 48hpf. Approximately thirty-five embryos were generated per clutch and grown in PTU containing media after 24hpf to reduce pigment generation. At 48hpf the embryos were collected, dechorionated with pronase, and fixed in 4% PFA. Wholemount in situ hybridisation was performed using a protocol modified from Thisse et al. (Thisse and Thisse, 2008) using antisense probes against the developing gut (*foxa3*) and heart (*myl7*) within the same embryos.

From the in situ hybridisation data I was able to observe liver position within the morphants. The liver is predominantly positioned on the left side of wildtype zebrafish (Figure 54B), however, from my results I also found embryos without any observable liver formation (Figure 54C), with bilateral symmetry of the liver (Figure 54D), and right sided (reversed) positioning (Figure 54E). These phenotypes are rare in untreated embryos but have been described previously in the literature, such as when there is a disruption of left-right patterning (Wang et al., 2011).

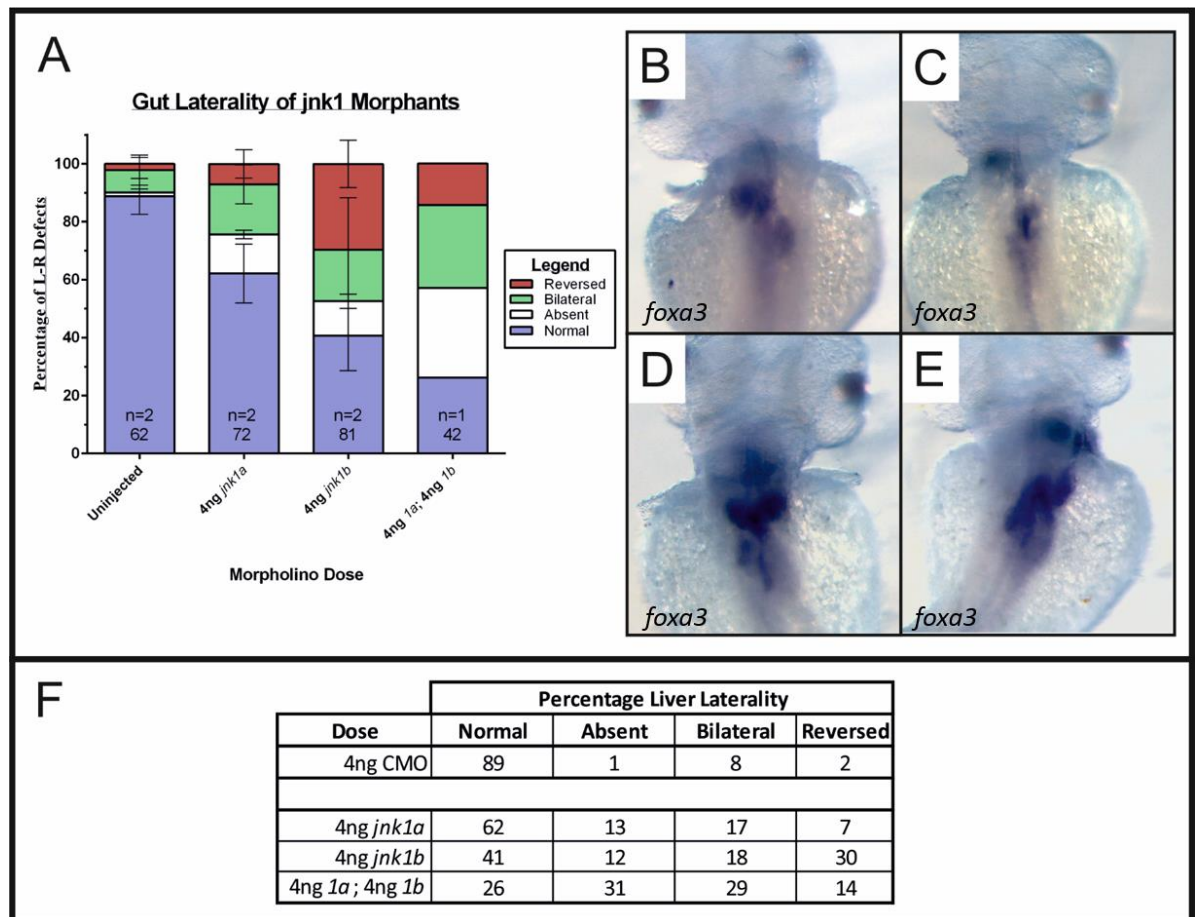


Figure 54 *jnk1* Morphants May Display Laterality Defects of the Developing Liver.

Preliminary data suggests that knockdown of *jnk1a*, *jnk1b*, or compound *jnk1a*; *jnk1b* genes causes laterality defects of the liver. Quantification of liver placement at 48hpf via in situ hybridisation analysis (*foxa3* probe) (A) appears to show that normal liver positioning is disrupted when *jnk1* morpholinos are used. These laterality defects are greatest with the 4ng *jnk1a*; 4ng *jnk1b* injections. In situ hybridisation images show examples of normal liver laterality (B), a failure to develop (C), bilateral symmetry of the liver (D) or reversal of liver asymmetry (E). The percentage frequency of each phenotype at different doses is displayed in (F). Images are taken from a ventral perspective so left of image is left of embryo.

To quantify the laterality disturbance of the liver I counted the prevalence of each phenotype at the desired MO doses. Preliminary findings (n=1 or 2) from this dataset seem to suggest that in uninjected controls 90% of embryos have the liver on the left side of the body. However, 10% of CMO treated embryos show defects of correct liver positioning (Figure 54A). The most prevalent defect that was observed in the control group was a bilateral symmetry of the liver. In comparison, each of the *jnk1* morpholino doses used resulted in a lower frequency of normal, leftward liver position compared to controls. In the 4ng *jnk1a* group only 60% of embryos had the liver on the left side of the body and instead there were high incidences of absent or bilaterally (Figure 54F) symmetrical liver formation (13% and 17% respectively). Very few 4ng *jnk1a* morphants displayed reversed asymmetry of the liver (7%). The same cannot be said for the 4ng *jnk1b* morphants; at this dose only around 40% of morphants display normal liver laterality (Figure 54A) - considerably fewer than the 60% that achieve normal heart laterality at this dose (Figure 48A). The 4ng *jnk1b* morphants also displayed large frequencies of absent or bilateral liver laterality (12% and 18% respectively), although these groups were not as highly populated as the reversed liver asymmetry; right-sided development of the liver was found in almost 30% of *jnk1b* morphants examined (Figure 54B). Finally the laterality of the liver in the 4ng *jnk1a*; 4ng *jnk1b* morphants seemed to be most greatly disturbed with only 26% of morphants forming the liver on the left of the body (Figure 54A). Although reversal of the liver was highly represented (14%), both an absence of the liver (31%) and bilateral (29%) liver development had a two-fold higher incidence (Figure 54B). Unfortunately this data could not be repeated with sufficient replications to perform statistical tests, and instead must be considered as preliminary data. However, these initial results appear to suggest that global organ laterality is disturbed in *jnk1* morphants.

The in situ hybridisation analysis performed made use of two non-overlapping probes which separately mark the liver and heart position. From this data I was therefore able to determine whether the position of the visceral organs correlated, or whether the morphants displayed visceral organ heterotaxy. In the case of the laterality defect situs inversus totalis the visceral organs all develop asymmetrically, but are mirrored (reversed) from their normal arrangement. In comparison, heterotaxy (situs ambiguous) is characterised by randomised and discordant organ laterality. I therefore examined the in situ results to determine whether the heart position and liver position correlated, or whether these two organs were independent of one another.

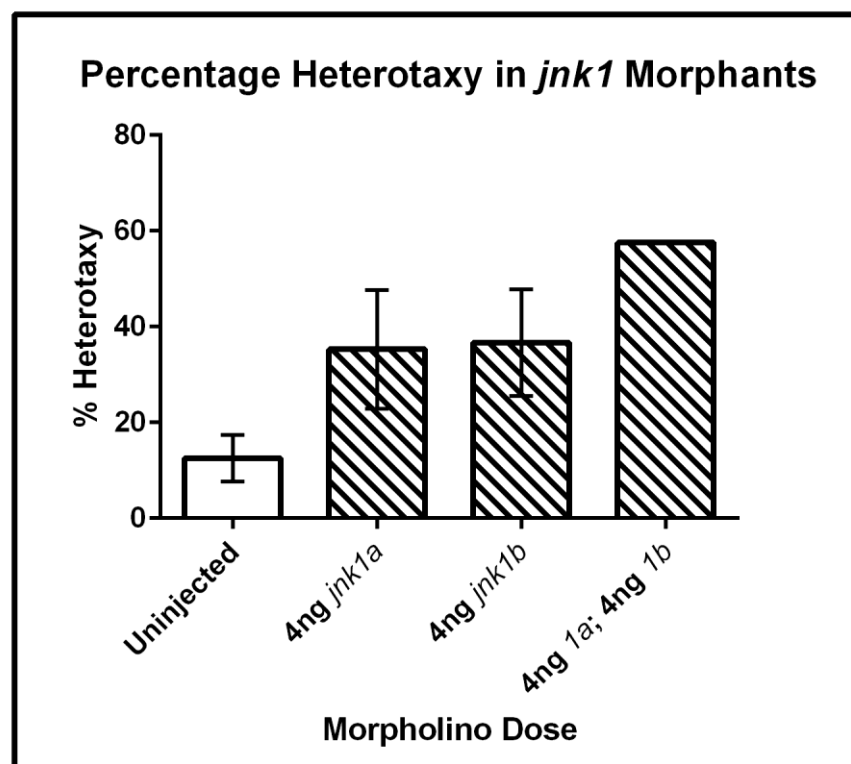


Figure 55 *jnk1* Morphants Display Heterotaxy of the Visceral Organs.

Preliminary data showing percentage heterotaxy in *jnk1* knockdowns. This data shows a trend of *jnk1* knockdown increasing the amount of organ heterotaxy in developing zebrafish. Mean percentage of heart and liver discordance plotted. Error bar = SEM.

Although these results are preliminary and few replicates are available, they suggest that knockdown of *jnk1* may cause visceral organ heterotaxy. Surprisingly in 8ng control morphants I found that organ placement does not correlate in over 10% of morphants. However, this figure is far greater in *jnk1a* and *jnk1b* morphants; at both of these doses the incidence of heterotaxy is around 35% although variability was high (Figure 55). In 4ng *jnk1a*; 4ng *jnk1b* morphants the incidence of heterotaxy was almost 60% in the one clutch that was investigated. As explained the number of replicates that were performed does not allow for any conclusions to be drawn, however there does seem to be a degree of organ discordance in these morphants.

5.3 Discussion

c-Jun N-terminal kinase 1 is a MAP kinase and member of the planar cell polarity pathway. In this latter role it sits downstream of the core PCP genes and is activated in response to non-canonical Wnts (Yamanaka et al., 2002). Since the PCP pathway has been comprehensively linked to patterning of the left-right axis during embryogenesis (Song et al., 2010, Wang et al., 2011, Walentek et al., 2013) I decided to investigate whether *jnk1* knockdown disrupts normal L-R patterning.

The laterality results show that the two *jnk1* paralogs do play a role in left-right patterning of the zebrafish visceral organs. At the highest dose (4ng) both *jnk1a* and *jnk1b* morphants displayed a significant divergence from formation of the normal cardiac D-loop; however the degree to which laterality defects were observed, and the mechanism by which they occurred appeared to be distinct between the two genes. Knockdown of *jnk1a* caused a lower overall occurrence of heart laterality defects but with a significant number of hearts that displayed jog / loop uncoupling. Conversely *jnk1b* morphants displayed a higher level of laterality defects without heart movement uncoupling. Preliminary investigation of liver laterality shows a similar trend whereby *jnk1b* knockdown causes greater frequency of laterality defects, but more replicates are required before this can be confirmed.

The *jnk1a* and *jnk1b* findings suggest that the two paralogs may possess different (possibly overlapping) function in patterning of the embryonic left-right axis because

despite some cross reactivity of the MOs they do produce different phenotypes. Functional differences between paralogs have been reported in the teleost literature previously, such as in the *JAK* family of kinases in zebrafish (Oates et al., 1999) and the *Wnt8a* paralogs of medaka (Mwafi et al., 2014). These *jnk1* paralog results therefore strengthen the theory that paralogs which survive a genome duplication event have developed novel functions or shared ancestral function (Force et al., 1999). Further investigation of what function each *jnk1* paralog has acquired is therefore necessary.

5.3.1 The Left-Right Patterning defects of the *jnk1a* Morphant May be due to Midline Barrier Defects.

At the 4ng dose of *jnk1a* morpholino there was a significant divergence of heart laterality away from normality (Figure 49) as well as jog / loop uncoupling (Figure 50). These data suggest that *jnk1a* is indeed involved in patterning of the left-right axis, however they may also reveal a role in formation of the midline barrier. All of the previous genes found to cause heart uncoupling have been shown to affect midline barrier formation or *southpaw* (zebrafish *NODAL*) signalling directly - although the literature is by no means exhaustive (Ahmad et al., 2004, Chin et al., 2000). Were *jnk1a* to participate in midline barrier regulation we could expect morphants to display changes within markers of the physical midline barrier such as *ta* (no tail) or *noto* (floating head) (Chin et al., 2000) or possibly the gene expression of molecular midline barrier members such as *lefty1* or *lefty2*. A breakdown of the midline barrier results in free diffusion of left-sided signalling molecules through the lateral plate mesoderm, resulting in aberrant spatial and temporal left-sided signalling (Lenhart et al., 2011). Preliminary results from our lab suggest that *lefty1* expression is dampened in *jnk1a* morphants which supports the theory that *jnk1a* has a role in midline barrier formation. If confirmed, this would supply mechanistic evidence for how *jnk1a* knockdown results in heart uncoupling defects – by altering the midline barrier.

5.3.2 The *jnk1b* Gene has a Greater Role in L-R Patterning of the Visceral Organs

Cardiac laterality defects were consistently observed in *jnk1b* morphants at a higher frequency than *jnk1a* morphants of the same dose (Figure 48B). This higher prevalence of laterality defects also appeared to occur in liver formation, although more replicates are required to prove this. These data suggest that *jnk1b* may be the major paralog required for patterning of the left-right axis in the lateral plate mesoderm.

The prevalence of heart defects observed when *jnk1b* was knocked down at a dose of 4ng (~40%) was comparable to what was found when the other downstream PCP kinase was targeted; the frequency of defects observed when *rock2b* was knocked down at a dose of 4.4ng was between 35-40% based on two different MOs (Wang et al., 2011). *jnk1b* therefore appears to have an equal role in left-right patterning as the other kinase in the PCP pathway. Disruption of either kinase in this pathway has a significant effect on positioning of the visceral organs suggesting that both are vital. Knockdown of both kinases together to determine whether any genetic redundancy exists between these two kinases may be an interesting experiment for the future.

An interesting feature that has been discovered in my heart laterality analysis is that when *jnk1b* is knocked down there appears to be a bias toward reversal of heart looping laterality. At both a 2ng and 4ng dose the prevalence of reversed heart looping (L-loop) is >2.5 times greater than a failure to loop (O-loop). A possible explanation for this is that loss of *jnk1b* results in an increase of aberrant *southpaw* expression on the right side of the embryo. In the *inversin* mouse mutant there is consistent right-sided expression of *Nodal*, and mutants develop situs inversus totalis (Yokoyama et al., 1993). Although the *jnk1b* morphants do not appear to have the same 100% penetrance of reversed organ laterality that is observed in *inversin* mutants, there may be a bias towards reversal. Investigation of *southpaw* expression in morphants is therefore an important future experiment which would determine whether *jnk1b* acts through the same mechanism as *inversin*.

5.3.3 Compound *jnk1a; jnk1b* Knockdown Effects the Ability of the Heart to Loop

Knockdown of both *jnk1* paralogs together results in a severe loss of normal organ laterality which appears to be the summation of what is observed at individual doses. Compound *jnk1a; jnk1b* morphants display approximately double the laterality defects of the morphants with either *jnk1a* or *jnk1b* knocked down, and both organ laterality and organ uncoupling defects are observed. This observation further supports the idea that each paralog may possess a different function, although a doubling of organ laterality defects highlights their overlapping functions.

At the highest compound *jnk1a; jnk1b* dose that was administered (4ng *jnk1a*; 4ng *jnk1b*) only ~30% of hearts form a D-loop, a percentage which corresponds with complete randomisation of which way the heart moves given that there are three possible choices: D-loop, O-loop, L-loop. However, as shown in Figure 51 many more morphants at this dose fail to loop than achieve it. The prevalence of O-loops is suggestive that knockdown of both *jnk1* paralogs may result in an inability of the heart tube to loop. It is not clear why *jnk1* knockdown might bias O-loop formation, although it could be due to a loss of left-sided signalling, an inability to respond to these signals, or even due to mechanical forces that arise from the pericardial oedema that develops in compound *jnk1a; jnk1b* morphants. In the latter case the mechanical forces that the heart is subjected to cause it to form a very distinct “strung-out” phenotype, where the heart develops in a very long and thin tube as it is stretched (Ghosh et al., 2009). Although this phenotype is not observed in fluorescent microscopy or sectioning of compound *jnk1a; jnk1b* morphant hearts, it cannot be thoroughly ruled out in this study. Determination of the mechanism by which these hearts fail to loop could be an interesting experiment which could shed light on the exact signalling role of *jnk1* in the left-right patterning pathway.

Uncoupling of heart movement was also significantly effected in the 4ng *jnk1a*; 4ng *jnk1b* morphants which may be judged as evidence that the midline barrier is failing to form correctly. However, due to the way that heart uncoupling is scored, proposed by Chin et al., caution should be taken when making any conclusion. As described above, there may be some mechanism which is preventing the hearts of compound *jnk1a*;

jnk1b morphants from looping. Uncoupling of the heart is considered to be where the jogging position of the heart (left or right) is not predictive of the looping direction that follows (Chin et al., 2000), therefore a left jog followed by O-loop is scored as uncoupled. Were some secondary defect such as oedema causing the heart to fail in looping, then uncoupling of heart movement may be falsely scored. This possible explanation highlights a limitation of uncoupling scoring; uncoupling of the heart may be overestimated if mechanical forces prevent looping from occurring.

5.3.4 Evidence for left-right patterning and ciliogenesis defects in *jnk1* morphants

As discussed above, both heart and gut scoring revealed left-right situs defects of the visceral organs in *jnk1* morphants. These situs defects were suggestive of aberrant left-right patterning of the lateral plate mesoderm from which the visceral organs originate. To determine whether there was indeed aberrant LPM left-right patterning Dr. Simon Ramsbottom conducted *in situ* hybridisation experiments to visualise the expression of *spaw* (zf *NODAL*), *lefty1* and *lefty2* at the 18 somite stage. These preliminary results seem to confirm the hypothesis that left-right patterning of the lateral plate mesoderm is indeed disrupted in *jnk1* morphants.

In controls embryos at the 18 somite stage *spaw* is highly expressed throughout the length of the body in the left lateral plate mesoderm (Long et al., 2003b), *lefty1* is expressed just left of the notochord and medially of *spaw*, and *lefty2* is expressed in the distal left lateral plate mesoderm, partially overlapping *spaw* expressing regions, where it experiences upregulation by *spaw* (Bisgrove et al., 1999). However, both 4ng *jnk1a* morphants and 4ng *jnk1b* morphants were shown to have aberrant expression of these three genes which could help to explain the observed organ situs defects.

In 4ng *jnk1a* morphants expression of *southpaw* was left-sided (normal) in <50% of embryos, whereas around 15% had right-sided (reversed) and >30% had absent or substantially reduced *spaw* expression domains that did not extend into the embryonic trunk. *Lefty2* expression was found to be <80% left-sided in 4ng *jnk1a* morphants with <20% displaying midline and almost 5% having bilateral expression profiles. The molecular midline-barrier component gene *lefty1* was also found to display an

aberrant expression domain with <60% having normal medial expression in the tail and trunk and ~40% having faint or reduced expression regions and ~8% having very short expression restricted to the tail alone. This disruption of normal left-right patterning gene expression could prove to be the mechanism for organ situs defects within the *jnk1a* morphants.

In 4ng *jnk1b* morphants normal left-sided expression of *spaw* was only observed in about 15% of morphants whereas ~20% had right-sided, ~55% displayed absent *spaw* and ~10% had *spaw* expression restricted to the posterior tail. Despite this severe divergence from normality >50% embryos expressed *lefty2* on the left side of the embryo in 4ng *jnk1b* morphants. Of those that diverged from normal *lefty2* expression profiles there were ~20% with midline and ~20% right *lefty2* expression. Finally, for *lefty1* expression the 4ng *jnk1b* morphants had only ~40% with normal midline expression whereas ~60% were far weaker or had reduced expression regions. Interestingly the most severe phenotype – very short and weak expression restricted to the tail – was not observed in 4ng *jnk1b* morphants.

These preliminary results performed by Dr. Ramsbottom support and strengthen what I found during my PhD, that knockdown of *jnk1* during development disrupts normal left-right patterning of the embryo. In particular the observation that normal nodal expression is as low as ~50% in 4ng *jnk1a* and ~15% in 4ng *jnk1b* morphants is broadly consistent with the significantly reduced rates of normal heart and gut situs observed during phenotyping (Figure 49 and Figure 54). In addition, these *nodal in situ* results support my hypothesis that *jnk1b* is more important in establishing left-right asymmetry within the visceral organs since loss of this gene shows a greater impact upon nodal signalling than the *jnk1a* MO at the same dose. Furthermore, the patterns of *lefty2* expression also support this greater role of the *jnk1b* gene since 4ng *jnk1a* morphants have <80% normal expression compared to the ~50% of *jnk1b* morphants. Although further investigation is required, this correlation between left-right situs defects and aberrant left-right patterning genes could be causative. Finally the observation that the most severe *lefty1* expression defects are seen only in *jnk1a* morphants appear to correlate with the small but significant percentage of heart uncoupling that is observed at the 4ng *jnk1a* dose (Figure 50). Again, further work is

required to confirm this link, particularly in light of experiments showing that *spaw* knockdown can also cause cardiac uncoupling (Ahmad et al., 2004) and the high frequency of *jnk1* morphants that displayed a reduced *spaw* expression range.

To further probe the possibility of whether left-right patterning was disrupted in *jnk1* morphants, Dr. Ramsbottom conducted some immunofluorescent examination of cilia within Kupffer's vesicle of morphants. These preliminary results showed that for both 4ng *jnk1a* and 4ng *jnk1b* morphants the size of Kupffer's vesicle and the length of the cilia within the vesicle were shorter. Similar phenotypes have been demonstrated in zebrafish embryos with left-right patterning defects and a causative link has been shown to exist between Kupffer's vesicle defects and aberrant left-right patterning gene expression (Song et al., 2010, Walentek et al., 2013, Wang et al., 2011), however further work is required to demonstrate a causative link in the *jnk1* morphants.

5.3.5 Concluding Remarks

These data have been able to show that *jnk1* is indeed involved in left-right patterning of the embryo, as are many other members of the PCP pathway. The two zebrafish paralogs are implicated in patterning laterality of the visceral organs the heart and liver, although loss of each individually does not result in the same phenotype. These data provide further evidence for a distinct functional difference between the two zebrafish *jnk1* paralogs in embryonic development, specifically organogenesis. Further work is required to fully elucidate the exact roles and mechanisms by which the *jnk1* genes act, although this study provides a solid foundation upon which any future work can be based.

CHAPTER 6 - GENERAL DISCUSSION

6.1 SUMMARY

The aim of this thesis was to increase what was known about zebrafish *jnk1* genetics, develop a robust model system for the study of *jnk1* function during development, and explore the phenotypic consequences of *jnk1* knockdown during embryogenesis. The role of *JNK1* during development is a contested and poorly understood topic due in part to the lack of a suitable model system. Much of the early research favoured small molecule inhibitors of *JNK* which did not differentiate between different *JNK* family members. Furthermore the knockout of mouse *Jnk1* resulted in no observable morphological changes, although behaviour was affected as determined by exposure to different maze tests (Reinecke et al., 2013). This mild phenotype is likely due to genetic redundancy between *Jnk1* and *Jnk2* function since compound *Jnk1/Jnk2* null mutants die displaying neural tube closure defects (Kuan et al., 1999); this compensatory function between isoforms was not observed in *Xenopus* however. Morpholino knockdown of *Xenopus jnk1* (as well as *mkk7*, an activator of all *jnk* isoforms) resulted in short and wide embryos reminiscent of a convergent extension defect. These inconsistencies between models therefore confound the understanding of *JNK1* function during development because they imply vastly different importance of *JNK1* during development in each case. Zebrafish, which are a favourable model for the study of vertebrate embryogenesis, may therefore provide an amenable model to better understand the function of this gene during development.

The objectives of this project were met by a combination of *in silico* bioinformatics and general developmental biology techniques. Use of the ENSEMBL and NCBI databases provided a starting point from which to study the two *jnk1* paralogs and allowed for primers to be designed for full-length transcript PCR. Once precise sequences had been determined for the AB zebrafish strain *jnk1* genes, it was possible to generate accurate morpholinos and primers for further studies. Morpholino oligonucleotides provided a “forward genetic method” by which *jnk1* function could be studied. During the project the morphant dose was refined and phenotype was characterised, which revealed several organs and tissues that required *jnk1* function for normal development.

6.2 DISCUSSION

6.2.1 Summary of Findings

Through the amplification of full-length transcripts I was able to demonstrate that at least four splice-variants are generated by each of the two *jnk1* paralogs (*jnk1a* and *jnk1b*). These variants differ in their inclusion of either exon 7 or exon 8, and in the exon 13 splice-acceptor site used, determining the ORF length. Via semi-quantitative RT-PCR it was shown that although these transcripts have different expression patterns, the pattern generally depends upon “middle exon” usage; exon 7 containing variants were absent at early segmentation stages (12hpf) and restricted to the adult brain, whereas exon 8 containing variants were most abundant very early in development (0-5.25hpf) and were expressed in most tissues examined. This data is suggestive of different roles for the *jnk1* splice-variants dependent upon which exon is included.

Morpholino oligonucleotide knockdown of each paralog enabled a global overview of *jnk1* function during development. Interestingly the phenotype of *jnk1a* or *jnk1b* morphants was paralog-specific, demonstrating that the two genes have at least some non-overlapping functions. Knockdown of *jnk1a* resulted in defects of the somitic muscle and smaller eye size, as well as severe underdevelopment of the heart and pericardial oedema. Furthermore the cardiac jog-loop progression was uncoupled in these morphants suggestive of midline barrier disruption. In *jnk1b* morphants the embryonic axis was severely curled ventrally and the somitic horizontal myoseptum failed to develop. The structural heart defects of *jnk1b* morphants were milder, although reversal of cardiac looping was more prevalent in these morphants. Compound *jnk1a; jnk1b* morphants displayed a combination of defects seen in *jnk1a* or *jnk1b* morphants, and demonstrated the most severe phenotypic effects. Of particular note was the high frequency of morphants that failed to undergo cardiac looping and remained as O-looped hearts. These data demonstrate how critical the role of *jnk1* is in orchestrating the process of heart looping.

6.2.2 Validity of Studying *jnk1* Function in the Zebrafish

6.2.2.1 Sequence Conservation to Human JNK1

In order to provide meaningful insight into the function of human *JNK1* it is necessary to demonstrate that some aspects of *jnk1* function are conserved in zebrafish. In this thesis I have shown that the two zebrafish *jnk1* proteins each share >85% sequence identity to that of the human form, with still greater conservation in the protein kinase domain. A comparable level of sequence identity has also been reported previously (87%) at the DNA level when *jnk1b* was aligned to human *JNK1* (Krens et al., 2006b). However, the zebrafish *jnk1a* gene is a more recent discovery so this has not been previously compared. In addition to sequence identity, it is interesting to find that the splicing events of zebrafish *jnk1* genes are conserved with those of human *JNK1*. Human *JNK1* has been shown to give rise to four different splice-variants which differ in their exon usage (exon 7 or 8) and amino acid length (384 or 427 amino acids). These variants have homologous zebrafish variants that arise from both *jnk1a* and *jnk1b*, strengthening the idea of functional conservation (Figure 56).

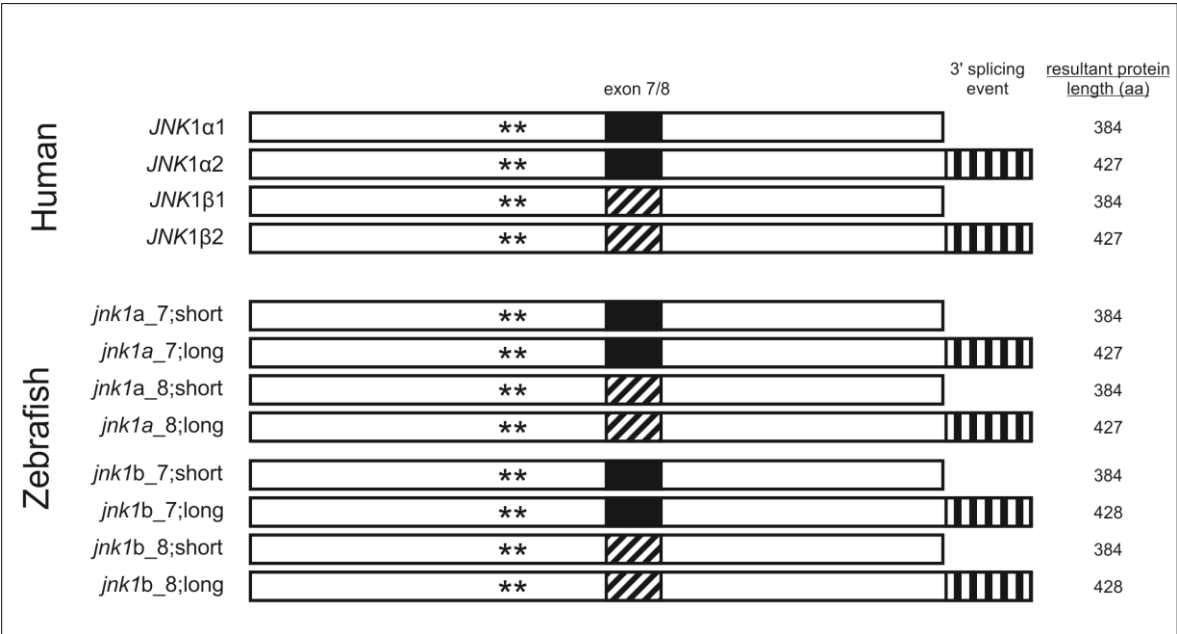


Figure 56 The zebrafish *jnk1* splice-variants are homologous to human *JNK1*. Schematic representation of the human *JNK1* and zebrafish *jnk1a* and *jnk1b* splice-variants in the style of (Barr and Bogoyevitch, 2001). Both human *JNK1* and the two zebrafish paralogs give rise to at least four different splice-variants which differ in the inclusion of either exon 7 or 8, and the length of the transcript (dependent upon the choice of 3' splice acceptor site). The similarities in transcript length and structure between human and zebrafish are suggestive that these eight zebrafish splice-variants are homologous. Black and diagonally striped boxes representative of exon 7 or exon 8 integration. Horizontal striped box represents longer open reading frame created by use of the alternative 3' splice acceptor site. Asterisks represent the thr/tyr phosphorylation site.

Despite the observed conservation, it remains an inconsistency that zebrafish possess two *jnk1* copies whereas there is only a single human ortholog. Preservation of both zebrafish copies indicates that some selective pressure is experienced to retain both paralogs, either by creation of a new function (neofunctionalization) or distribution of the ancestral gene functions amongst the two paralogs (subfunctionalization) (Force et al., 1999). Were the zebrafish *jnk1* genes to have evolved novel functions since the divergence of the two species then their validity to model human *JNK1* might be limited.

The accepted model of duplicate gene conservation (duplication-degeneration-complementation) proposes that the sharing of a gene's functions (subfunctionalization) accounts for a significant amount of duplicate genes which have been retained; primarily this is suggested because the incidence of random mutations which cause novel functions is much smaller than the deleterious mutations which result in subfunctionalization (Lynch and Force, 2000). Evidence of this theory is observed in the zebrafish *pax6* (Kleinjan et al., 2008), *hoxb5* (Bruce et al., 2001) and *fabp1* (Sharma et al., 2006) paralogs, each of which possess partial function of their ortholog. However, for each of these duplications the two transcripts were shown to have differential expression patterns (which when combined mirror the expression patterns in mouse), meaning that both forms are necessary for function in all the tissues of the body (i.e. *pax6b* is the only variant expressed in the pancreas). This difference in expression pattern might also be observed in the *jnk1* genes, although my experiments did not find any evidence of this at the timepoints and tissues examined. Instead I found that there was different expression patterns between different splice-variants, although these patterns were largely similar for both *jnk1* paralogs. It still remains to be shown whether each of the *jnk1* paralogs has partial function of the human *JNK1* gene, however, were this to be shown then it would further validate the use of a zebrafish *jnk1* model.

6.2.2.2 Off-target Effects of Morpholinos

The use of morpholinos targeted to *jnk1a* and *jnk1b* produces phenotypes that are reproducible and which do not resemble features which have previously been found to be due to morpholino toxicity – namely gastrula arrest and clouding of the central nervous system due to increased apoptosis (Coffman et al., 2004, Robu et al., 2007). However, further tests are required in order to confirm that off-target effects are not caused by the two morpholinos. Generally co-injection with p53 MO is advised in order to abrogate any increased p53 activity that MOs can provoke; if the morphant phenotype is not rescued by knockdown of p53 then this is further evidence that the phenotype is a specific effect. Furthermore a phenotypic rescue with MO-resistant mRNA further demonstrates that the morphant phenotype is due to knockdown of your target, and not some off-target gene. Both of these experiments would be suitable for future work in order to increase confidence in the specific effect of the *jnk1* morpholinos.

In both *jnk1a* and *jnk1b* morphants we see cardiac oedema, and curling/kinking of the body axis which are phenotypes that are very commonly observed in morpholino experiments. The zebrafish gene *lingo1b* (Leucine-rich repeat and immunoglobulin-like domain-containing nogo receptor-interacting protein 1) is necessary for axonal growth and *in situ* hybridisation reveals that it is expressed only in the central nervous system during development. Despite this restricted expression, *lingo1b* morphants display a curled tail phenotype and cardiac oedema at 96hpf (Yin and Hu, 2014), suggestive that these two features may be non-specific morpholino phenotypes. Interestingly both features were reported to be alleviated by mRNA rescue, although this could be explained by a binding of the MO to the exogenous mRNA; the injected mRNA was not modified to protect it from the binding of the MO. This experiment highlights the need for caution when interpreting morpholino experiments, especially for commonly seen traits such as tail curling, because there have been several phenotypes attributed to off-target or non-specific effects of morpholinos (Robu et al., 2007, Coffman et al., 2004, Eisen and Smith, 2008).

Despite the *jnk1* morphants displaying phenotypes commonly observed in other morpholino experiments this does not prove that they are off-target effects. Both *jnk1a* and *jnk1b* knockdown resulted in cardiac oedema which is not surprising

considering the severity of the heart phenotypes. The histology of the *jnk1a* morphant heart at 48hpf and 72hpf resembled the immature linear tube observed between 24-28hpf in normal development. Furthermore the absence of a recognisable atrioventricular valve and the small lumen size (exacerbated by expansion of the cardiac jelly) suggest that cardiac function would be severely compromised in these embryos. In sections of *jnk1b* morphants, although cardiac looping did occur the heart chamber and lumen size appeared smaller than controls and function may therefore be reduced. Were this to be the case then this could explain the oedema phenotype.

It has been shown comprehensively that several unrelated chemicals (2,3,7,8-tetrachlorodibenzo-p-dioxin, retinoic acid carbaryl and valproic acid) and a MO for the *tbx5* gene all result in a strikingly similar pericardial oedema and a heart failure-like phenotype in zebrafish embryos between 72-120hpf (Chen, 2013); the authors conclude that each of the heart development insults had initially different mechanisms, but resulted in the same phenotype later in development, including reduced cardiomyocyte proliferation, lower organ contractility and a common transcriptional response. Whether this represents a common end-point for all insults that perturb early heart formation remains to be seen, although it could potentially explain the *jnk1* morphant oedema. An alternative mechanism whereby renal failure results in the oedema could also explain this fluid accumulation therefore further investigation is necessary (Rider et al., 2012).

6.2.2.3 Similarity and Conflicts with other *jnk1* Research

Further evidence that the phenotypes reported in this thesis are due to *jnk1* knockdown and not non-specific effects come from the literature. As discussed earlier, the role of the zebrafish *jnk* genes has been studied before using shRNAs (small hairpin RNAs) and the JNK inhibitor SP600125 (Xiao et al., 2013). When *jnk1b* was knocked down with shRNA this resulted in embryonic lethality of around 90%. Those embryos that survived the treatment displayed developmental delay, body axis bending and yolk deformities (Xiao et al., 2013). Certainly the body axis defects are consistent with my own results and also developmental delay was found when both *jnk1a* and *jnk1b* was knocked down at the 4ng *jnk1a*; 4ng *jnk1b* dose. However, the fact that a majority of embryos failed before 24hpf contradicts what I have shown because morpholino

jnk1 knockdown did not significantly affect embryonic survival. It is possible that this embryonic death is therefore an artefact of the methodology or dosage (300ng) used in the Xiao et al. paper (2013). The authors went on to utilise the drug SP600125 to inhibit pan-*jnk* function, and these experiments also show some similarity to what I have found.

Xiao et al. (2013) reported that embryos dosed with SP600125 before the hatching period (48-72hpf) commonly had pericardial oedema, body length reductions and undifferentiated gonads in comparison to controls. Furthermore, histology of this group revealed that the retina was underdeveloped and had not formed laminations (Xiao et al., 2013); comparatively dosing after hatching caused almost 100% mortality at high (1.4µM) doses and a reduced body length and cranial bone deficiencies of the embryos at a lower dose (0.8µM). Several of these phenotypes had previously been reported in Valesio et al. (2011) where SP600125 was administered from 0-30hpf, 18-24hpf or 22-28hpf at 1.25µM and 5µM. The most severe phenotypes were observed when SP600125 was administered for the first 30 hours of development, however in each treatment group there was oedema and failure of the swim bladder to inflate. However, at the 5µM dose between 0-30hpf it was also shown that embryos had reduced body length, bent tail and trunk, jaw and retina defects, multiple or ectopic lens formation, and disorganisation of brain structures.

Previous work within our lab also supports these results when the SP600125 drug is used. Dosing embryos during gastrulation (5.25-10hpf) or segmentation (10-22hpf) resulted in an increased prevalence of tail curling/kinking, shortened body length, small eye development, and cardiac oedema. In addition it was found that about 25% of embryos had abnormal heart looping situs, reduced cardiomyocyte numbers and approximately 10% had otic vesicle defects (Unpublished data – Papoutsis, 2011 PhD Thesis).

These previous findings strengthen the validity of the *jnk1* morpholino system since there is a consistency of several defects between these different methodologies (i.e. body length reduction, bent/kinked tail, retinal defects, cardiac oedema and heart situs defects). It is also unsurprising that not all of the defects were observed in the morphants because the morpholinos target only *jnk1a* or *jnk1b*, whereas all *jnk*

proteins are inhibited by the SP600125 drug (Bennett et al., 2001). Furthermore, although the frequency of situs defects, oedema, and small eye development are greater in *jnk1* morphants than those treated with a jnk inhibitor, this inconsistency probably reflects the methodologies that were used. The drug must be used at low doses (Valesio et al., 2013, Xiao et al., 2013) and over restricted timepoints to avoid embryonic lethality (Papoutsis, 2011 PhD Thesis). Conversely the *jnk1* morpholinos are specific to *jnk1* and are effective between the one-cell stage and 72hpf (Summerton et al., 1997). These morphants therefore represent only *jnk1* loss of function, but over the duration of the experiment.

Although the *jnk1* morphant phenotype in this thesis recapitulates some of the phenotypes observed in pan-jnk inhibited zebrafish, there are inconsistencies with other studies that have been published. In Seo et al. (2010) they used splice-modifying morpholinos to knock-down *jnk1a+jnk1b* or *jnk2* to determine whether convergence extension was affected (Seo et al., 2010). Convergent extension-like defects were not observed in the compound *jnk1a; jnk1b* knockdowns in this paper and no phenotypic defects or developmental delay was reported. Since no data was shown beyond 16hpf for *jnk1* morphants it may be that observable defects only occur at later timepoints (certainly for eye and heart defects). However, it seems unusual that developmental delay would not be present at 16hpf whereas my data shows delay in compound *jnk1a; jnk1b* morphants at 22hpf. One possible explanation for this difference is that the morpholinos used initiate knockdown at different timepoints. Splice-modifying morpholinos like those used in Seo et al. (2010) target immature RNA molecules (i.e. pre-mRNA) before splicing occurs in order to knock down functional protein production, and therefore do not affect the maternally inherited mRNAs in the zygote. Knockdown of the target therefore begins when zygotic transcription commences, shortly after 3hpf (Aanes et al., 2011). Translation-blocking MOs like those used in this thesis are capable of knocking down maternal and zygotic protein production, therefore ensuring knockdown from the 1-cell stage.

In the *Jnk1* null mouse the mice develop normally and are fertile, only displaying behavioural changes when run through maze tests (Kuan et al., 1999, Reinecke et al., 2013). The mildness of the phenotype has been hypothesised to be due to genetic redundancy with *Jnk2* since loss of both isoforms is lethal (Kuan et al., 1999, Sabapathy

et al., 1999). However, this redundancy was not observed in the zebrafish *jnk1* morphant, a conflict which could be advantageous (allowing for functional investigation of *jnk1*) or a limitation of studying *jnk1* function in zebrafish (if for example human *JNK1* is also compensated for by *JNK2*). Although this project cannot rule out some genetic redundancy between the zebrafish *jnk* genes, the degree to which they are able to compensate for loss of *jnk1* is not the same in the zebrafish as in the mouse; I have shown clear morphological defects when *jnk1* is knocked down by morpholino so the *jnk2* and *jnk3* genes cannot completely compensate in zebrafish. Since no reports of mutations to human *JNK1* have been reported, it is unclear whether *JNK1* loss can be compensated for, or is lethal in humans. However, the absence of the zebrafish genes to completely compensate for the loss of *jnk1* allows for us to examine the role of *jnk1* in a way that would not be possible in the mouse. In zebrafish we can knockdown *jnk1* and observe which developmental processes are perturbed during normal embryogenesis. A similar experiment in the mouse would produce results that are masked by the compensatory function of the *jnk2* gene.

6.2.3 Evidence of *jnk1* Action through the PCP Pathway

JNK can function in the MAPK and PCP signalling pathways, both of which have been found to be crucial for normal development e.g. heart development (Phillips et al., 2007, Yu et al., 2007, Moeller et al., 2006, Keren-Politansky et al., 2009, Kelly et al., 2014), kidney development (Balbi et al., 2009, Omori et al., 2000, Saburi et al., 2008, Simons et al., 2005), convergent and extension cell movement (Wang et al., 2006a, Veeman et al., 2003, Jessen et al., 2002, Yamanaka et al., 2002, Nie and Chang, 2007, Nutt et al., 2001, Keren et al., 2005). In this thesis I have not tried to tease apart which of these signalling pathways *jnk1* is acting through during development, or which pathway gives rise to the individual developmental defects that are observed. However there appears to be circumstantial evidence that the PCP pathway (at least) is perturbed in *jnk1* morphants which gives rise to the left-right patterning defects.

The planar cell polarity pathway has been extensively linked to establishment of the left-right axis during embryogenesis (Zhang and Levin, 2009, Mochizuki et al., 1998, Marques et al., 2004, May-Simera et al., 2010, Oishi et al., 2006, Walentek et al.,

2013). The major line of thought is that PCP signalling is required for uniform alignment of epidermal cells in the node which project cilia into the vesicle and contribute to nodal flow (Borovina et al., 2010, Oteiza et al., 2010, Wang et al., 2011, Song et al., 2010). Critically the MAPK pathway has not been observed to contribute to the left-right patterning of the embryo at the time of writing.

Knockdown of both *jnk1a* and *jnk1b* has been found to result in left-right patterning defects of the heart, although this defect is more frequent with *jnk1b* knockdown. Initial in situ hybridisation results also suggest that normal liver situs is disrupted by *jnk1* loss, putatively revealing a systemic aberration in left-right patterning; however due to the number of repeats that were achieved this cannot be confirmed in this study. These data suggest that *jnk1* may function through the PCP pathway to regulate left-right patterning as has been observed in the Rho kinase2b morphant (Wang et al., 2011). Rho kinase lies downstream of the core PCP proteins at the same level in the signalling pathway as JNK and has been shown to be crucial for Kupffer's vesicle (the node) cell alignment, and establishment of nodal flow in the zebrafish. In order to confirm this hypothesis it would be necessary to examine Kupffer's vesicle in *jnk1* morphants to determine whether cilia positioning or nodal flow was indeed affected. This would provide strong evidence that *jnk1* does function through the PCP pathway to mediate left-right patterning.

6.2.4 Evidence of a Role in Left-Right Patterning and Ciliogenesis

Previous research on the role of *JNK1* in vertebrate development had not linked the gene to left-right patterning of the embryo or ciliogenesis, however in part this may have been due to the very mild phenotype that was observed when *Jnk1* was knocked out in the mouse and the embryonic lethality caused by *Jnk1* + *Jnk2* loss (Kuan et al., 1999). In *Drosophila melanogaster* where only a single *JNK* orthologue exists it was shown that loss or upregulation of *JNK* resulted in laterality defects of the developing gut (Martin-Blanco et al., 1998). I believe that my own work has further strengthened the link between the *JNK* genes, and in zebrafish *jnk1* specifically, and left-right patterning during embryogenesis.

Knockdown of *jnk1a* and *jnk1b* in the zebrafish revealed that the heart (and possibly the gut) developed laterality defects consistent with embryonic left-right patterning defects. Furthermore, uncoupling of the jog-loop heart movements was observed in *jnk1a* knockdowns which have previously been identified when members of the molecular midline barrier or *southpaw* (zebrafish *NODAL*) has been disrupted; both of these contribute to left-right patterning in the zebrafish (Yamamoto et al., 2003, Ahmad et al., 2004, Chin et al., 2000). Although I was not able to investigate the effect of *jnk1* knockdown on embryonic left-right patterning, Dr. Simon Ramsbottom did perform some preliminary experiments which supports a role of *jnk1* in this process. In these preliminary experiments it was shown that the main signalling molecule of left-sidedness – *NODAL* – was aberrantly expressed in some, and displayed reduced expression region in other *jnk1* morphants. Furthermore the *NODAL* antagonists *lefty1* and *lefty2* showed a similar aberrant expression or reduced expression pattern. These data are suggestive that *jnk1* function does indeed play some role in left-right patterning of the embryo.

To further examine the underlying mechanism of left-right patterning defects in *jnk1* morphants Dr. Ramsbottom investigated Kupffer's Vesicle size and cilia length in *jnk1a* and *jnk1b* morphants. Both node size and cilia length were reduced in this analysis suggesting that *jnk1* may also have a role in KV development and ciliogenesis. Although anecdotal, my own results also support a role for *jnk1* in ciliogenesis. The 4ng *jnk1a* morphants were shown to have retinal lamination defects that were strikingly similar to those of genes known to be involved in ciliogenesis (Shu et al., 2011, Simms et al., 2012, Al-Hamed et al., 2014). Considering the development of photoreceptors from primary cilia these retinal defects are common in mutants for ciliogenesis-related genes (Wheway et al., 2014).

In conclusion I believe that my own research in addition to the preliminary work carried out by Dr. Ramsbottom in the Chaudhry lab has uncovered a role for *jnk1* in left-right patterning of the zebrafish embryo. I hypothesise that this role is directly or indirectly mediated by a contribution to development of Kupffer's Vesicle and the KV cilia. The retinal phenotypes in *jnk1a* morphants suggest that cilia outside of KV may require *jnk1* for normal function. I believe that further investigation into these roles for

jnk1 are necessary but may not be possible in the mouse where genetic redundancy has been found between the *Jnk* genes (Kuan et al., 1999).

6.3 Future Work

This project has succeeded in establishing a *jnk1* morphant in the zebrafish, however there is far more that needs to be done in order to determine the full role of *jnk1* during development. Firstly, although four splice-variants were discovered for each *jnk1* gene, there are additional predicted transcripts from the ENSEMBL pipeline which I have not investigated. Use of additional primers to target these predicted transcripts specifically, or 5' and 3' RACE (Rapid amplification of cDNA ends), could be used in order to look for additional transcripts. Furthermore, temporal and tissue-specific expression of these splice-variants was examined in a semi-quantitative manner by RT-PCR, however, this methodology does not provide accurate expression levels, and because different primers were used there cannot be any accurate comparison between levels of different variants. A more accurate measure of expression patterns would be qRT-PCR (quantitative RT-PCR), although this technique requires amplicons of around 100bp, whereas the eight variants described here differ only in sequences that are ~500bp apart. Instead it may be possible to use a proteomics approach such as 3D gel electrophoresis followed by consecutive mass spectrometry (MS/MS) to quantify total amounts of protein from each variant. In addition to being a more quantitative approach than the RT-PCR methodology used here, it would measure protein levels directly, since mRNA and protein abundances don't always strongly correlate (Gygi et al., 1999).

In addition, only a rather small number of developmental timepoints and tissues were examined as a way of gaining a broad overview of expression patterns through development and tissue-types. For future analysis it would be more useful to answer specific questions using this technique, particularly looking at both spatial and temporal expression during development. Since the different variants are identical to one another for runs of hundreds of basepairs it is unlikely that *in situ* hybridisation probes would be capable of differentiating between them. It is possible though that

microdissection of different tissues would make it possible to examine expression in different tissues during development. For example the Tg(*myl7:EGFP*) zebrafish line which has green fluorescent protein expression is under the control of the myosin light chain 7 promoter enables these cells to be identified from stages of the linear heart tube. The use of several such reporter lines could allow for embryonic tissue expression to be analysed in greater detail than it was here.

Although much of this thesis was dedicated to exploring the phenotype of *jnk1* morphants, several of the experiments require further work in order to confirm the results; the *in situ* hybridisation experiments appear to suggest that left-right patterning is disrupted throughout the whole embryo, and not simply within the heart. However, too few replicates were performed in order to show this conclusively. In addition to repeats it may also be possible to examine other asymmetrical organs such as the pancreas, gall bladder, gut and habenula (part of the pineal gland) which have all been shown to be asymmetrical in the zebrafish (Concha et al., 2000, Long et al., 2003b, Essner et al., 2005a). These data which could be obtained through further *in situ* hybridisations would demonstrate whether the organ situs defects were indeed global or were restricted to certain organs.

In situ hybridisation could be further utilised to explore the mechanism by which the *jnk1* morphant organs are developing with incorrect situs. Analysis of *southpaw* (*nodal*) and *pitx2* expression have been shown to be required on the embryonic left for normal organ situs (Ahmad et al., 2004, Campione et al., 1999), so this may be affected in the *jnk1* morphants as it has been shown to be in morphants that display organ situs defects (Wang et al., 2011, Bisgrove et al., 2005, Francescatto et al., 2010). If these determinants of left-sidedness were shown to be aberrantly expressed then greater analysis of structure of the node, nodal cilia and the nodal flow would be beneficial to determine whether loss of *jnk1* was affecting the polarisation of nodal cells or preventing proper nodal flow. As *jnk1a* morphants also cause a disparity between cardiac jog and loop directions there may also be improper molecular midline barrier formation, as has been observed in other genetic models that have uncoupled cardiac movements (Chin et al., 2000). The use of *in situ* hybridisation for the molecular midline barrier gene *lefty1* could highlight whether the molecular midline barrier was

successfully formed in *jnk1a* morphants, a possible mechanism for the left-right patterning defects and the uncoupling of the heart.

The use of morpholinos for targeted knockdown has been hampered by the frequency (15-20%) of off-target effects (Eisen and Smith, 2008) and therefore it is necessary to further qualify this method of knockdown before further investigation. Previously the gold-standard model for proof of knockdown was to perform a rescue experiment whereby a MO resistant mRNA for the gene of interest was overexpressed in order to rescue the morphant phenotype. However, as this exogenous mRNA is overexpressed in the embryo and expression may not bear any resemblance to the temporal and spatial restrictions of endogenous gene expression, rescue experiments are often problematic and show only partial rescue (Wang et al., 2011, Bauer et al., 2001, Hernandez-Lagunas et al., 2005).

An alternative method of morpholino validation is to demonstrate that the MO recapitulates the phenotype of a mutant. The introduction of CRISPR (clustered regularly interspaced short palindromic repeats) technology has significantly increased the ease and efficiency of directed mutagenesis generation in zebrafish (Cong et al., 2013, Hwang et al., 2013b) and would be a sensible next step for investigating *jnk1* function. Generation of *jnk1a* and *jnk1b* mutant zebrafish would allow for further validation of, or could supercede the morphant methodology. The mutant would result in 100% loss of the target genes as opposed to the partial (~85%) knockdown that is caused by MO injection, and no cross-reactivity between paralogs would be caused. Furthermore, a mutant would not experience the dosing effects that are observed by morphant generation, reducing the variability of the observed phenotypes. These two systems could also complement each other with mutants modelling systemic *jnk1* loss and morpholinos being used at later developmental stages to knockdown function specifically in the dorsal forerunner cells that give rise to Kupffer's vesicle (Wang et al., 2011). Generation of a *jnk1* mutant would certainly aid in the investigation of *jnk1* during development.

Both *jnk1a* and *jnk1b* morpholino injections resulted in left-right patterning defects of the embryo, which is a feature that requires further investigation. If the defect is systemic, as preliminary liver *in situ* data was suggesting, then there may be

perturbation in the *NODAL* (*southpaw*) cascade that has been shown to propagate left-sided signalling through the lateral plate mesoderm (Brennan et al., 2002, Lowe et al., 1996, Ahmad et al., 2004). This mechanism would correlate with several other PCP members which have been shown to cause left-right patterning defects, including *rock2b* (Wang et al., 2011, Borovina et al., 2010, Song et al., 2010, Walentek et al., 2013). In situ hybridisation of *southpaw* expression, as well as genes whose protein products make up the midline barrier (e.g. *lefty 1*, *lefty 2*, *bmp*) could determine whether these core left-right patterning members are affected. Further testing of this hypothesis could be performed by examination of cell alignment and nodal flow within Kupffer's vesicle. Finally knockdown of *jnk1* specifically into Kupffer's vesicle cells could help to determine which developmental defects are caused by systemic loss of *jnk1* and which result specifically from loss of left-right patterning signals.

Oedema around the pericardial sac and yolk are observed in both *jnk1a* and *jnk1b* morphants. The cause of this oedema could be due to poor circulation of the heart, or reduced pronephric duct function. Normal kidney development has been shown to require proper PCP pathway signalling (Mochizuki et al., 1998, Saburi et al., 2008, Simons et al., 2005), and loss of normal signalling can result in pronephric cysts. In order to determine whether *jnk1* loss affects the kidney it may be possible to observe cysts by light microscopy. Insulin clearance methods also provide accurate measures of renal function, and take into account both renal and cardiac impact (Rider et al., 2012).

6.4 Concluding Remarks

This project has increased our knowledge of the zebrafish *jnk1* genes, and established zebrafish as an appropriate model for the study of *JNK1* during development. The lack of any identified human cases of congenital inherited or de novo mutations in the *JNK* genes may suggest that such mutations are not amenable to life as proposed by Sabapathy et al. (Sabapathy, 2012), or that sufficient genetic redundancy exists, as is seen in mouse, to prevent any overt developmental defects (Kuan et al., 1999). However, zebrafish have proven to be a useful model for examining *jnk1* function during development because developmental defects do arise when gene function is

knocked down, and there is conservation of splice-variants common between the zebrafish and human gene. From these results I propose that *jnk1* is critical for establishment of the left-right axis during zebrafish embryogenesis and that loss of *jnk1* function can result in improper situs development of the heart and liver. The mechanism by which these defects arise is not fully elucidated, however preliminary evidence suggests that a reduction in Kupffer's Vesicle size and/or ciliogenesis could be altered in *jnk1* knockdowns which could result in L-R patterning defects. Histology analysis later in development may also support a role for *jnk1* in ciliogenesis within the retina, whereas heart and somite defects at these later timepoints also suggests that *jnk1* function is required for normal development of these tissues. The exact role of *jnk1* in the development of these organs is yet to be discovered, however this project has identified the importance of *jnk1* in organ development.

Importantly the analyses presented here represent only the beginning of elucidating the function of *JNK1* during development, and much more research is needed to discover the exact role of this gene. Due to the complexity of the *JNK* genes and all the numerous processes that they have been implicated in regulating, there must exist very sophisticated regulatory networks that ensure these genes mediate the correct response in temporal and tissue-specific scenarios. I believe that one method of achieving this may be through the use of different splice-variants which have different affinities to downstream effectors. In future research I propose that it will not be appropriate to talk about "JNK function" and instead the individual genes and indeed specific splice-variants will need to be analysed as separate entities. In this work the zebrafish model may play a role, due to its high conservation of different splice-variants. Until then there is far more to be learnt about the role of *jnk1* in the developing heart, eye, somitic muscle, Kupffer's vesicle, and left-right signalling pathway. This thesis will hopefully provide a foundation for future work in the field.

CHAPTER 7 - APPENDICES

A >jnk1a-002_CodingSequence

```

Fwd      5' AGAGAGGGATCCATGAACAAAAATAAGCGAGAG 3'
          |||
1  -----ATGAACAAAAATAAGCGAGAGAAAGAATTCTACAGTGTAGATGTGGGG
49  GATTCGACATTACAGTGTGAAGCGCTATCAGAATCTAAGACCCATTGGCTCGGGTGCT
109 CAGGGAATAGTCTGCTCAGCGTATGACAACAACCTTGAGCGAAACGTGGCTATAAAGAAA
169 CTCAGCCGGCCTTTTCAAAATCAAACATCATGCCAAACGTGCGTACAGAGAGCTGGTGCTC
229 ATGAAATGTGTCAACCATAAAAAATATAATAGGCCTCTTAAATGTTTTTACACCGCAAAA
289 ACATTAGAAGAATTCCAAGATGTTTACCTAGTAATGGAGCTGATGGATGCGAACCTCTGC
349 CAAGTCATTCAGATGGAGCTGGACCACGAGCGGCTGTCTATCTGCTGTACCAGATGCTG
409 TGTGGAATAAAACACCTCCACGCGCGGGGATCATCCACAGGGACCTGAAACCCAGTAAC
469 ATCGTGGTAAAGTCAGACTGTACCCTGAAGATCCTGGATTTTCGGTCTGGCGCGGACAGCA
529 GCTACAGGTCTGCTGATGACACCATATGTGGTGACCCGTTACTACAGAGCCCCTGAAGTC
589 ATCCTGGGAATGGGATATCAAGCCAATGTGGACATTTGGTCTGTGGGCTGCATTTTGGCA
649 GAAATGGTCCGTCACAAAATCCTTTTTTCTGGGAGGGACTATATTGATCAGTGGAATAAA
709 GTAATAGAGCAGCTGGGAACGCCAACTCAGGAGTTCCTGTTGAAACTCAACCAGTCTGTG
769 CGGACCTATGTGGAGAACAGGCCCCGGTACACTGGATATAGCTTTGAGAAGCTGTTTCCT
829 GATGTCCTGTTCCCTGCTGATTGAGAACACAGCAAATAAAAGCGAGTCAGGCGCGGGAC
889 CTGCTGTCTAAAATGCTGGTGATTGATGCATCAAAACGAATCTCGGTGGATGAGGCTTTG
949 CAGCACCCCTACATTAACGTGTGGTACGACCCGGCTGAAGTGGAAGCGCCTTCTCCTCTG
1009 ATCACAGACAAACAGCTCGATGAGAGGGAACACACAGTGGAAGAGTGGAAGAAGTATGATC
1069 TATAAAGAAGTGCTGGATTGGGAAGAACGGATGAAGAACGGTGTTATTCGAGGTCAGCCC
1129 TCCCCCTAGGTGCAGCAGTGATCAACGGCTCACCCAGCCCTCATCCTCATCTCCATC
1189 AACGACGTGTCTCCATGTCCACAGAGCCCACCGTGCCCTCAGACACAGACAGCAGCTTA
1249 GAGGCCTCGGCGGGACCCCTGAGCTGCTGCAGATGA-----
          |||
3' GACTCGACGACGTCTACTGAGCTCGATGAT 5' Rev

```

B >jnk1b-002_CodingSequence

```

Fwd      5' AGAGAGGGATCCATGAACAGGAATAAGCGCGAG 3'
          |||
1  -----ATGAACAGGAATAAGCGCGAGAAAGAATATTACAGCATAGATGTAGGA
49  GATTCAACGTTACCGTTTTGAAGCGCTATCAGAATTTAAGACCAATCGGGTCCGGAGCA
109 CAAGGCATCGTCTGCTCAGCGTATGACCACGTCTCGATCGAAATGTGGCAATTAAGAAA
169 CTCAGCCGACCTTTTCAAAACCAAACATCATGCCAAACGGGCCTACAGAGAAGTGGTCTG
229 ATGAAATGCGTCAACCACAAAAATATAATTGGCTTACTAAACGTGTTACACCACAGAAG
289 ACACTTGAAGAGTTCAGGATGTTTATCTGGTGATGGAGCTGATGGATGCAAACCTGTGT
349 CAGGTGATTGATGGAGCTGGACCACGAGAGGCTGTCTACCTGCTCTATCAGATGCTC
409 TGCGGCATTAACACCTGCACGCTGCTGGCATCATACACAGGGATCTGAAACCCAGTAAT
469 ATAGTAGTGAAATCGGACTGCACGCTGAAGATCCTGGATTTTCGGTCTGGCCCGAACGGCT
529 GCAACCGGCCTCCTCATGACTCCTTATGCTGTGACACGCTATTATCGGGCCCCAGAGGTC
589 ATCCTGGGCATGGGTATCAAGCTAACGTTGATGTCTGGTCTATTGGCTGCATCATGGCT
649 GAAATGGTCAGAGGTAGTGTGTTGTTTCTGGCACAGACCATATTGACCAGTGGAATAAA
709 GTGATCGAGCAGCTGGGCACGCCGTCACAGGAGTTCATGATGAAGCTGAATCAGTCTGTG
769 AGGACGTATGTGGAGAACCGGCTCGGTATGCGGGATACAGCTTTGAGAAGCTCTTCCCA
829 GACGTGCTCTTCCCCGCAGACTCGGACCACAACAACTCAAGGCGAGTCAGGCACGAGAC
889 TTGTTATCCAAAATGCTGGTAATAGATGCATCCAAGCGGATCTCTGTAGACGAGGCGCTT
949 CAGCACCCCTACATCAACGTTTGGTACGACCCATCAGAAGTGAGGCGCCGCCACAGCG
1009 ATCACGGATAAACAGCTCGATGAGAGAGAACACTCAGTGGAAGAGTGGAAGAGCTCATA
1069 TACAAGGAAGTGCTGGAATGGGAGGAGCGAACAAAAATGGAGTGATCAGAGGACAGCCG
1129 GCCTCGCTAGGTGCAGCAGTGAGCAGTGACTCCCATGAGCCCTCGACGTGCTCCTCCTCC
1189 ATAAACGATGTGTCTCATGTCCACCGAGGTCACGCTGACCTCAGACACCGACAGCAGT
1249 CAGGAGACGTCCAACGGAGCGCTGCACTGCTGCAGATGA
          |||
3' CGCGACGTGACGACGTCTACTAGATCTGAGAGA 5' Rev

```

Figure 57 The Binding Sites of the Full-Length jnk1 Primers.

The complete CDS of the ENSEMBL predicted jnk1a-002 (A) and jnk1b-002 (B) variants displaying the primer binding sites of the full-length primers (Black). Each primer contains additional bases at the 5' end consisting of a restriction site and some non-sense sequence to allow for the production of sticky ends for directional sub-cloning.

CES

```

jnk1a_7;short      1  ATGAACAAAAATAAGCGAGAGAAAAGAATTCTACAGTGTAGATGTGGGGGATTTCGACATTC
jnk1a_7;long       1  ATGAACAAAAATAAGCGAGAGAAAAGAATTCTACAGTGTAGATGTGGGGGATTTCGACATTC
jnk1a_8;short      1  ATGAACAAAAATAAGCGAGAGAAAAGAATTCTACAGTGTAGATGTGGGGGATTTCGACATTC
jnk1a_8;long       1  ATGAACAAAAATAAGCGAGAGAAAAGAATTCTACAGTGTAGATGTGGGGGATTTCGACATTC

-----Exon 2-----
jnk1a_7;short      61  ACAGTGTGGAAGCGCTATCAGAATCTAAGACCCATTGGCTCGGGTGCTCAGGGAATAGTC
jnk1a_7;long       61  ACAGTGTGGAAGCGCTATCAGAATCTAAGACCCATTGGCTCGGGTGCTCAGGGAATAGTC
jnk1a_8;short      61  ACAGTGTGGAAGCGCTATCAGAATCTAAGACCCATTGGCTCGGGTGCTCAGGGAATAGTC
jnk1a_8;long       61  ACAGTGTGGAAGCGCTATCAGAATCTAAGACCCATTGGCTCGGGTGCTCAGGGAATAGTC

-><-----
jnk1a_7;short      121 TGCTCAGCGTATGACAACAACCTCGAGCGAAACGTGGCTATAAAGAAACTCAGCCGGCCT
jnk1a_7;long       121 TGCTCAGCGTATGACAACAACCTCGAGCGAAACGTGGCTATAAAGAAACTCAGCCGGCCT
jnk1a_8;short      121 TGCTCAGCGTATGACAACAACCTCGAGCGAAACGTGGCTATAAAGAAACTCAGCCGGCCT
jnk1a_8;long       121 TGCTCAGCGTATGACAACAACCTCGAGCGAAACGTGGCTATAAAGAAACTCAGCCGGCCT

-----Exon 3-----
jnk1a_7;short      181 TTTCAAAATCAAACCTCATGCCAAACGTGCGTACAGAGAGCTGGTGCTCATGAAATGTGTC
jnk1a_7;long       181 TTTCAAAATCAAACCTCATGCCAAACGTGCGTACAGAGAGCTGGTGCTCATGAAATGTGTC
jnk1a_8;short      181 TTTCAAAATCAAACCTCATGCCAAACGTGCGTACAGAGAGCTGGTGCTCATGAAATGTGTC
jnk1a_8;long       181 TTTCAAAATCAAACCTCATGCCAAACGTGCGTACAGAGAGCTGGTGCTCATGAAATGTGTC

-----><-----Exon 4-----
jnk1a_7;short      241 AACCATAAAAAATATAATAGGCCTCTTAAATGTTTTTACACCGCAAAAAACATTAGAAGAA
jnk1a_7;long       241 AACCATAAAAAATATAATAGGCCTCTTAAATGTTTTTACACCGCAAAAAACATTAGAAGAA
jnk1a_8;short      241 AACCATAAAAAATATAATAGGCCTCTTAAATGTTTTTACACCGCAAAAAACATTAGAAGAA
jnk1a_8;long       241 AACCATAAAAAATATAATAGGCCTCTTAAATGTTTTTACACCGCAAAAAACATTAGAAGAA

-----><-----
jnk1a_7;short      301 TTCCAAGATGTTTACCTAGTAATGGAGCTGATGGATGCGAACCTCTGCCAAGTCATTTCAG
jnk1a_7;long       301 TTCCAAGATGTTTACCTAGTAATGGAGCTGATGGATGCGAACCTCTGCCAAGTCATTTCAG
jnk1a_8;short      301 TTCCAAGATGTTTACCTAGTAATGGAGCTGATGGATGCGAACCTCTGCCAAGTCATTTCAG
jnk1a_8;long       301 TTCCAAGATGTTTACCTAGTAATGGAGCTGATGGATGCGAACCTCTGCCAAGTCATTTCAG

-----Exon 5-----
jnk1a_7;short      361 ATGGAGCTGGACCACGAGCGGCTGTCCTATCTGCTGTACCAGATGCTGTGTGGAATAAAA
jnk1a_7;long       361 ATGGAGCTGGACCACGAGCGGCTGTCCTATCTGCTGTACCAGATGCTGTGTGGAATAAAA
jnk1a_8;short      361 ATGGAGCTGGACCACGAGCGGCTGTCCTATCTGCTGTACCAGATGCTGTGTGGAATAAAA
jnk1a_8;long       361 ATGGAGCTGGACCACGAGCGGCTGTCCTATCTGCTGTACCAGATGCTGTGTGGAATAAAA

-----><-----
jnk1a_7;short      421 CACCTCCACGCGCGGGGATCATCCACAGGGACCTGAAACCCAGTAACATCGTGGTAAAG
jnk1a_7;long       421 CACCTCCACGCGCGGGGATCATCCACAGGGACCTGAAACCCAGTAACATCGTGGTAAAG
jnk1a_8;short      421 CACCTCCACGCGCGGGGATCATCCACAGGGACCTGAAACCCAGTAACATCGTGGTAAAG
jnk1a_8;long       421 CACCTCCACGCGCGGGGATCATCCACAGGGACCTGAAACCCAGTAACATCGTGGTAAAG

-----Exon 6-----
jnk1a_7;short      481 TCAGACTGTACCCTGAAGATCCTGGATTTTCGGTCTGGCGCGGACAGCAGCTACAGGTCTG
jnk1a_7;long       481 TCAGACTGTACCCTGAAGATCCTGGATTTTCGGTCTGGCGCGGACAGCAGCTACAGGTCTG
jnk1a_8;short      481 TCAGACTGTACCCTGAAGATCCTGGATTTTCGGTCTGGCGCGGACAGCAGCTACAGGTCTG
jnk1a_8;long       481 TCAGACTGTACCCTGAAGATCCTGGATTTTCGGTCTGGCGCGGACAGCAGCTACAGGTCTG

```

```

-----
jnk1a_7;short 541 CTGATGACACCATATGTGGTGACCCGTTACTACAGAGCCCCTGAAGTCATCCTGGGAATG
jnk1a_7;long 541 CTGATGACACCATATGTGGTGACCCGTTACTACAGAGCCCCTGAAGTCATCCTGGGAATG
jnk1a_8;short 541 CTGATGACACCATATGTGGTGACCCGTTACTACAGAGCCCCTGAAGTCATCCTGGGAATG
jnk1a_8;long 541 CTGATGACACCATATGTGGTGACCCGTTACTACAGAGCCCCTGAAGTCATCCTGGGAATG

-----><-----Exon 7/8-----
jnk1a_7;short 601 GGATATCAAGCCAATGTGGACATTTGGTCTGTGGGCTGCATTTTGGCAGAAATGGTCCGT
jnk1a_7;long 601 GGATATCAAGCCAATGTGGACATTTGGTCTGTGGGCTGCATTTTGGCAGAAATGGTCCGT
jnk1a_8;short 601 GGATATCAAGCCAATGTGGATGTGTGGTCTGTGGGCTGTATCATGGCTGAAATGGTCAGA
jnk1a_8;long 601 GGATATCAAGCCAATGTGGATGTGTGGTCTGTGGGCTGTATCATGGCTGAAATGGTCAGA

-----><-----
jnk1a_7;short 661 CACAAAATCCTTTTTCCTGGGAGGGACTATATTGATCAGTGAATAAAGTAATAGAGCAG
jnk1a_7;long 661 CACAAAATCCTTTTTCCTGGGAGGGACTATATTGATCAGTGAATAAAGTAATAGAGCAG
jnk1a_8;short 661 GGTAGTGTATTATTTCCGGGTTTCAGATCATATTGATCAGTGAATAAAGTAATAGAGCAG
jnk1a_8;long 661 GGTAGTGTATTATTTCCGGGTTTCAGATCATATTGATCAGTGAATAAAGTAATAGAGCAG

-----
jnk1a_7;short 721 CTGGGAACGCCAACTCAGGAGTTCCTGTTGAAACTCAACCAGTCTGTGCGGACCTATGTG
jnk1a_7;long 721 CTGGGAACGCCAACTCAGGAGTTCCTGTTGAAACTCAACCAGTCTGTGCGGACCTATGTG
jnk1a_8;short 721 CTGGGAACGCCAACTCAGGAGTTCCTGTTGAAACTCAACCAGTCTGTGCGGACCTATGTG
jnk1a_8;long 721 CTGGGAACGCCAACTCAGGAGTTCCTGTTGAAACTCAACCAGTCTGTGCGGACCTATGTG

-----Exon 9-----
jnk1a_7;short 781 GAGAACAGGCCCCGGTACACTGGATATAGCTTTGAGAAGCTGTTTCCTGATGTCCTGTTC
jnk1a_7;long 781 GAGAACAGGCCCCGGTACACTGGATATAGCTTTGAGAAGCTGTTTCCTGATGTCCTGTTC
jnk1a_8;short 781 GAGAACAGGCCCCGGTACACTGGATATAGCTTTGAGAAGCTGTTTCCTGATGTCCTGTTC
jnk1a_8;long 781 GAGAACAGGCCCCGGTACACTGGATATAGCTTTGAGAAGCTGTTTCCTGATGTCCTGTTC

-----><-----
jnk1a_7;short 841 CCTGCTGATTTCAGAACACAGCAAACATAAAGCGAGTCAGGCGCGGGACCTGCTGTCTAAA
jnk1a_7;long 841 CCTGCTGATTTCAGAACACAGCAAACATAAAGCGAGTCAGGCGCGGGACCTGCTGTCTAAA
jnk1a_8;short 841 CCTGCTGATTTCAGAACACAGCAAACATAAAGCGAGTCAGGCGCGGGACCTGCTGTCTAAA
jnk1a_8;long 841 CCTGCTGATTTCAGAACACAGCAAACATAAAGCGAGTCAGGCGCGGGACCTGCTGTCTAAA

-----Exon 10-----
jnk1a_7;short 901 ATGCTGGTGATTGATGCATCAAAACGAATCTCGGTGGATGAGGCTTTGCAGCACCCCTAC
jnk1a_7;long 901 ATGCTGGTGATTGATGCATCAAAACGAATCTCGGTGGATGAGGCTTTGCAGCACCCCTAC
jnk1a_8;short 901 ATGCTGGTGATTGATGCATCAAAACGAATCTCGGTGGATGAGGCTTTGCAGCACCCCTAC
jnk1a_8;long 901 ATGCTGGTGATTGATGCATCAAAACGAATCTCGGTGGATGAGGCTTTGCAGCACCCCTAC

-----><-----
jnk1a_7;short 961 ATTAACGTGTGGTACGACCCGGCTGAAGTGGAAGCGCCTTCTCCTCTGATCACAGACAAA
jnk1a_7;long 961 ATTAACGTGTGGTACGACCCGGCTGAAGTGGAAGCGCCTTCTCCTCTGATCACAGACAAA
jnk1a_8;short 961 ATTAACGTGTGGTACGACCCGGCTGAAGTGGAAGCGCCTTCTCCTCTGATCACAGACAAA
jnk1a_8;long 961 ATTAACGTGTGGTACGACCCGGCTGAAGTGGAAGCGCCTTCTCCTCTGATCACAGACAAA

-----Exon 11-----><-----
jnk1a_7;short 1021 CAGCTCGATGAGAGGGAACACACAGTGGAAGAGTGGAAGAAGTCTATATAAGAAGTG
jnk1a_7;long 1021 CAGCTCGATGAGAGGGAACACACAGTGGAAGAGTGGAAGAAGTCTATATAAGAAGTG
jnk1a_8;short 1021 CAGCTCGATGAGAGGGAACACACAGTGGAAGAGTGGAAGAAGTCTATATAAGAAGTG
jnk1a_8;long 1021 CAGCTCGATGAGAGGGAACACACAGTGGAAGAGTGGAAGAAGTCTATATAAGAAGTG

```

```

-----Exon 12-----><-
jnk1a_7;short      1081 CTGGATTGGGAAGAACGGATGAAGAACGGTGTTATTTCGAGGTCAGCCCTCCCCCCTAGCA
jnk1a_7;long       1081 CTGGATTGGGAAGAACGGATGAAGAACGGTGTTATTTCGAGGTCAGCCCTCCCCCCTAG--
jnk1a_8;short      1081 CTGGATTGGGAAGAACGGATGAAGAACGGTGTTATTTCGAGGTCAGCCCTCCCCCCTAGCA
jnk1a_8;long       1081 CTGGATTGGGAAGAACGGATGAAGAACGGTGTTATTTCGAGGTCAGCCCTCCCCCCTAG--

-----*-----
jnk1a_7;short      1141 CAGGTGCAGCAGTGAtcaacggctcccccagccctcatcctcatcctccatcaacgacg
jnk1a_7;long       1137 ---GTGCAGCAGTGATCAACGGCTCACCCCAGCCCTCATCCTCATCCTCCATCAACGACG
jnk1a_8;short      1141 CAGGTGCAGCAGTGAtcaacggctcccccagccctcatcctcatcctccatcaacgacg
jnk1a_8;long       1137 ---GTGCAGCAGTGATCAACGGCTCACCCCAGCCCTCATCCTCATCCTCCATCAACGACG

-----Exon 13-----
jnk1a_7;short      1201 tgtcctccatgtccacagagcccaccgtggcctcagacacagacagcagcttagaggcct
jnk1a_7;long       1196 TGTCCTCCATGTCCACAGAGCCCACCGTGGCCTCAGACACAGACAGCAGCTTAGAGGCCT
jnk1a_8;short      1201 tgtcctccatgtccacagagcccaccgtggcctcagacacagacagcagcttagaggcct
jnk1a_8;long       1196 TGTCCTCCATGTCCACAGAGCCCACCGTGGCCTCAGACACAGACAGCAGCTTAGAGGCCT

----->
jnk1a_7;short      1261 cggcgggacccctgagctgctgcagatga
jnk1a_7;long       1256 CGGCGGGACCCCTGAGCTGCTGCAGATGA
jnk1a_8;short      1261 cggcgggacccctgagctgctgcagatga
jnk1a_8;long       1256 CGGCGGGACCCCTGAGCTGCTGCAGATGA

```

Figure 58 Alignment of the Four jnk1a Variants Identified in this Study.

The four different splice-variants of jnk1a identified by sequencing of the sub-cloned products aligned to each other. Conserved bases are highlighted in black, above the sequence is annotation showing exon contribution. There are two regions where the four variants differ from one another: the middle exon usage (red) and the exon 13 splicing acceptor (*). The region of jnk1a_7;short and jnk1a_8;short that forms part of the 3' UTR is shown in lower case.

<-----	
jnk1b_7;short	1 ATGAACAGGAATAAGCGCGAGAAAGAATATTACAGCATAGATGTAGGAGATTTCGACGTTT
jnk1b_7;long	1 ATGAACAGGAATAAGCGCGAGAAAGAATATTACAGCATAGATGTAGGAGATTTCGACGTTT
jnk1b_8;short	1 ATGAACAGGAATAAGCGCGAGAAAGAATATTACAGCATAGATGTAGGAGATTTCGACGTTT
jnk1b_8;long	1 ATGAACAGGAATAAGCGCGAGAAAGAATATTACAGCATAGATGTAGGAGATTTCGACGTTT
-----Exon 2-----	
jnk1b_7;short	61 ACCGTTTTGAAGCGCTATCAGAATTTAAGACCAATCGGGTCCGGAGCACAAGGCATCGTC
jnk1b_7;long	61 ACCGTTTTGAAGCGCTATCAGAATTTAAGACCAATCGGGTCCGGAGCACAAGGCATCGTC
jnk1b_8;short	61 ACCGTTTTGAAGCGCTATCAGAATTTAAGACCAATCGGGTCCGGAGCACAAGGCATCGTC
jnk1b_8;long	61 ACCGTTTTGAAGCGCTATCAGAATTTAAGACCAATCGGGTCCGGAGCACAAGGCATCGTC
-><-----	
jnk1b_7;short	121 TGCTCAGCGTATGACCACGTCCTCGATCGAAATGTGGCGATTAAGAACTCAGCCGACCC
jnk1b_7;long	121 TGCTCAGCGTATGACCACGTCCTCGATCGAAATGTGGCGATTAAGAACTCAGCCGACCC
jnk1b_8;short	121 TGCTCAGCGTATGACCACGTCCTCGATCGAAATGTGGCGATTAAGAACTCAGCCGACCC
jnk1b_8;long	121 TGCTCAGCGTATGACCACGTCCTCGATCGAAATGTGGCGATTAAGAACTCAGCCGACCC
-----Exon 3-----	
jnk1b_7;short	181 TTTCAAAACCAAACTCATGCCAAACGGGCCTACAGAGAACTGGTCCTGATGAAATGCGTC
jnk1b_7;long	181 TTTCAAAACCAAACTCATGCCAAACGGGCCTACAGAGAACTGGTCCTGATGAAATGCGTC
jnk1b_8;short	181 TTTCAAAACCAAACTCATGCCAAACGGGCCTACAGAGAACTGGTCCTGATGAAATGCGTC
jnk1b_8;long	181 TTTCAAAACCAAACTCATGCCAAACGGGCCTACAGAGAACTGGTCCTGATGAAATGCGTC
-----><-----Exon 4-----	
jnk1b_7;short	241 AACCACAAAAATATAATTGGCTTACTAAACGTGTTACACCACAGAAGACCCTTGAAGAG
jnk1b_7;long	241 AACCACAAAAATATAATTGGCTTACTAAACGTGTTACACCACAGAAGACCCTTGAAGAG
jnk1b_8;short	241 AACCACAAAAATATAATTGGCTTACTAAACGTGTTACACCACAGAAGACCCTTGAAGAG
jnk1b_8;long	241 AACCACAAAAATATAATTGGCTTACTAAACGTGTTACACCACAGAAGACCCTTGAAGAG
-----><-----	
jnk1b_7;short	301 TTCCAGGATGTTTATCTGGTGATGGAGCTGATGGATGCAAACCTGTGTCAGGTGATTTCAG
jnk1b_7;long	301 TTCCAGGATGTTTATCTGGTGATGGAGCTGATGGATGCAAACCTGTGTCAGGTGATTTCAG
jnk1b_8;short	301 TTCCAGGATGTTTATCTGGTGATGGAGCTGATGGATGCAAACCTGTGTCAGGTGATTTCAG
jnk1b_8;long	301 TTCCAGGATGTTTATCTGGTGATGGAGCTGATGGATGCAAACCTGTGTCAGGTGATTTCAG
-----Exon 5-----	
jnk1b_7;short	361 ATGGAGCTGGACCACGAGAGGCTGTCTACCTGCTCTATCAGATGCTCTGCGGCATTAAA
jnk1b_7;long	361 ATGGAGCTGGACCACGAGAGGCTGTCTACCTGCTCTATCAGATGCTCTGCGGCATTAAA
jnk1b_8;short	361 ATGGAGCTGGACCACGAGAGGCTGTCTACCTGCTCTATCAGATGCTCTGCGGCATTAAA
jnk1b_8;long	361 ATGGAGCTGGACCACGAGAGGCTGTCTACCTGCTCTATCAGATGCTCTGCGGCATTAAA
-----><-----	
jnk1b_7;short	421 CACCTGCACGCTGCTGGCATCATACACAGGGACCTGAAACCCAGTAATATAGTAGTGAAA
jnk1b_7;long	421 CACCTGCACGCTGCTGGCATCATACACAGGGACCTGAAACCCAGTAATATAGTAGTGAAA
jnk1b_8;short	421 CACCTGCACGCTGCTGGCATCATACACAGGGACCTGAAACCCAGTAATATAGTAGTGAAA
jnk1b_8;long	421 CACCTGCACGCTGCTGGCATCATACACAGGGACCTGAAACCCAGTAATATAGTAGTGAAA
-----Exon 6-----	
jnk1b_7;short	481 TCGGACTGCACGCTGAAGATCCTGGATTTTCGGTCTGGCCAGAACGGCTGCAACCGGCCTC
jnk1b_7;long	481 TCGGACTGCACGCTGAAGATCCTGGATTTTCGGTCTGGCCAGAACGGCTGCAACCGGCCTC
jnk1b_8;short	481 TCGGACTGCACGCTGAAGATCCTGGATTTTCGGTCTGGCCAGAACGGCTGCAACCGGCCTC
jnk1b_8;long	481 TCGGACTGCACGCTGAAGATCCTGGATTTTCGGTCTGGCCAGAACGGCTGCAACCGGCCTC

jnk1b_7;short	541	CTCATGACTCCTTATGTAGTGACACGCTATTATCGGGCCCCAGAGGTCATCCTGGGCATG
jnk1b_7;long	541	CTCATGACTCCTTATGTAGTGACACGCTATTATCGGGCCCCAGAGGTCATCCTGGGCATG
jnk1b_8;short	541	CTCATGACTCCTTATGTAGTGACACGCTATTATCGGGCCCCAGAGGTCATCCTGGGCATG
jnk1b_8;long	541	CTCATGACTCCTTATGTAGTGACACGCTATTATCGGGCCCCAGAGGTCATCCTGGGCATG
-----><-----Exon 7/8-----		
jnk1b_7;short	601	GGTTATCAAGCTAACGTGGATATTTGGGCTGTTGGCTGCATTATGGCAGAGATGGTGCGG
jnk1b_7;long	601	GGTTATCAAGCTAACGTGGATATTTGGGCTGTTGGCTGCATTATGGCAGAGATGGTGCGG
jnk1b_8;short	601	GGTTATCAAGCTAACGTTGATGTCTGGTCTATTGGCTGCATCATGGCTGAAATGGTCAGA
jnk1b_8;long	601	GGTTATCAAGCTAACGTTGATGTCTGGTCTATTGGCTGCATCATGGCTGAAATGGTCAGA
-----><-----		
jnk1b_7;short	661	CACAAAATCCTTTTTCACAGGAGGGAATATATTGACCAAGTGAATAAAGTGATCGAGCAG
jnk1b_7;long	661	CACAAAATCCTTTTTCACAGGAGGGAATATATTGACCAAGTGAATAAAGTGATCGAGCAG
jnk1b_8;short	661	GGTAGTGTGTTGTTTCTGGCACAGACCATATTGACCAAGTGAATAAAGTGATCGAGCAG
jnk1b_8;long	661	GGTAGTGTGTTGTTTCTGGCACAGACCATATTGACCAAGTGAATAAAGTGATCGAGCAG
-----><-----		
jnk1b_7;short	721	CTCGGCACGCCGTACAGGAGTTTCATGATGAAGCTGAATCAGTCTGTGAGGACGTATGTG
jnk1b_7;long	721	CTCGGCACGCCGTACAGGAGTTTCATGATGAAGCTGAATCAGTCTGTGAGGACGTATGTG
jnk1b_8;short	721	CTCGGCACGCCGTACAGGAGTTTCATGATGAAGCTGAATCAGTCTGTGAGGACGTATGTG
jnk1b_8;long	721	CTCGGCACGCCGTACAGGAGTTTCATGATGAAGCTGAATCAGTCTGTGAGGACGTATGTG
-----Exon 9-----		
jnk1b_7;short	781	GAGAACCGGCCTCGGTATGCGGGATACAGCTTTGAGAAGCTCTTCCCAGACGTGCTCTTC
jnk1b_7;long	781	GAGAACCGGCCTCGGTATGCGGGATACAGCTTTGAGAAGCTCTTCCCAGACGTGCTCTTC
jnk1b_8;short	781	GAGAACCGGCCTCGGTATGCGGGATACAGCTTTGAGAAGCTCTTCCCAGACGTGCTCTTC
jnk1b_8;long	781	GAGAACCGGCCTCGGTATGCGGGATACAGCTTTGAGAAGCTCTTCCCAGACGTGCTCTTC
-----><-----		
jnk1b_7;short	841	CCCGCAGACTCGGACCACAACAACTCAAGGCGAGTCAGGCACGAGACTTGTTATCCAAA
jnk1b_7;long	841	CCCGCAGACTCGGACCACAACAACTCAAGGCGAGTCAGGCACGAGACTTGTTATCCAAA
jnk1b_8;short	841	CCCGCAGACTCGGACCACAACAACTCAAGGCGAGTCAGGCACGAGACTTGTTATCCAAA
jnk1b_8;long	841	CCCGCAGACTCGGACCACAACAACTCAAGGCGAGTCAGGCACGAGACTTGTTATCCAAA
-----Exon 10-----		
jnk1b_7;short	901	ATGCTGGTAATAGATGCGTCCAAGCGGATCTCTGTAGACGAGGCGCTTCAGCACCCCTAC
jnk1b_7;long	901	ATGCTGGTAATAGATGCGTCCAAGCGGATCTCTGTAGACGAGGCGCTTCAGCACCCCTAC
jnk1b_8;short	901	ATGCTGGTAATAGATGCGTCCAAGCGGATCTCTGTAGACGAGGCGCTTCAGCACCCCTAC
jnk1b_8;long	901	ATGCTGGTAATAGATGCGTCCAAGCGGATCTCTGTAGACGAGGCGCTTCAGCACCCCTAC
-----><-----		
jnk1b_7;short	961	ATCAACGTTTGGTACGACCCGTCAGAAGTGGAGGCGCCACCACCAGCGATCACGGATAAA
jnk1b_7;long	961	ATCAACGTTTGGTACGACCCGTCAGAAGTGGAGGCGCCACCACCAGCGATCACGGATAAA
jnk1b_8;short	961	ATCAACGTTTGGTACGACCCGTCAGAAGTGGAGGCGCCACCACCAGCGATCACGGATAAA
jnk1b_8;long	961	ATCAACGTTTGGTACGACCCGTCAGAAGTGGAGGCGCCACCACCAGCGATCACGGATAAA
-----Exon 11-----><-----		
jnk1b_7;short	1021	CAGCTCGATGAGAGAGAACACTCAGTGGAAGAGTGGAAGAGCTCATATATAAGGAAGTG
jnk1b_7;long	1021	CAGCTCGATGAGAGAGAACACTCAGTGGAAGAGTGGAAGAGCTCATATATAAGGAAGTG
jnk1b_8;short	1021	CAGCTCGATGAGAGAGAACACTCAGTGGAAGAGTGGAAGAGCTCATATATAAGGAAGTG
jnk1b_8;long	1021	CAGCTCGATGAGAGAGAACACTCAGTGGAAGAGTGGAAGAGCTCATATATAAGGAAGTG

-----Exon 12-----><--		
jnk1b_7;short	1081	CTGGAATGGGAGGAGCGAACAAAAAATGGAGTGATCAGAGGACAGCCGGCCTCGCTAGCA
jnk1b_7;long	1081	CTGGAATGGGAGGAGCGAACAAAAAATGGAGTGATCAGAGGACAGCCGGCCTCGCTAG--
jnk1b_8;short	1081	CTGGAATGGGAGGAGCGAACAAAAAATGGAGTGATCAGAGGACAGCCGGCCTCGCTAGCA
jnk1b_8;long	1081	CTGGAATGGGAGGAGCGAACAAAAAATGGAGTGATCAGAGGACAGCCGGCCTCGCTAG--
-----*		
jnk1b_7;short	1141	CAGGTGCAGCAGTGAGcagtgactcccatgagccctcgacgtcgtcctcctccataaacg
jnk1b_7;long	1138	---GTGCAGCAGTGAGCAGTGACTCCCATGAGCCCTCGACGTCGTCCTCCTCCATAAACG
jnk1b_8;short	1141	CAGGTGCAGCAGTGAGcagtgactcccatgagccctcgacgtcgtcctcctccataaacg
jnk1b_8;long	1138	---GTGCAGCAGTGAGCAGTGACTCCCATGAGCCCTCGACGTCGTCCTCCTCCATAAACG
-----Exon 13-----		
jnk1b_7;short	1201	atgtgtcgtccatgtccaccgaggtcacgctgacctcagacaccgacagcagtcaggaga
jnk1b_7;long	1196	ATGTGTCTGTCATGTCCACCGAGGTCACGCTGACCTCAGACACCGACAGCAGTCAGGAGA
jnk1b_8;short	1201	atgtgtcgtccatgtccaccgaggtcacgctgacctcagacaccgacagcagtcaggaga
jnk1b_8;long	1196	ATGTGTCTGTCATGTCCACCGAGGTCACGCTGACCTCAGACACCGACAGCAGTCAGGAGA
----->		
jnk1b_7;short	1261	cgtccaacggagcgctgcactgctgcagatga
jnk1b_7;long	1256	CGTCCAACGGAGCGCTGCACTGCTGCAGATGA
jnk1b_8;short	1261	cgtccaacggagcgctgcactgctgcagatga
jnk1b_8;long	1256	CGTCCAACGGAGCGCTGCACTGCTGCAGATGA

Figure 59 Alignment of the Four jnk1b Variants Identified in this Study.

The four different splice-variants of jnk1b identified by sequencing of the sub-cloned products aligned to each other. Conserved bases are highlighted in black and above the sequence is annotation showing exon contribution. There are two regions where the four variants differ from one another: the middle exon usage (red) and the exon 13 splicing acceptor (*). The region of jnk1a_7;short and jnk1a_8;short that forms part of the 3' UTR is in lower case.

jnk1a	1	ATGAACAAAATAAGCGAGAGAAAGAATTCTACAGTGTAGATGTGGGGATTTCGACATTC
jnk1b	1	ATGAACAGGAATAAGCGCGAGAAAGAATATTACAGCATAGATGTAGGAGATTTCGACGTTT
jnk1a	61	ACAGTGTTTGAAGCGCTATCAGAATCTAAGACCCATTGGCTCGGGTGCTCAGGGAATAGTC
jnk1b	61	ACCGTTTTGAAGCGCTATCAGAATTTAAGACCAATCGGGTCCGGAGCACAGGCATCGTC
jnk1a	121	TGCTCAGCGTATGACAACAAACCTCGAGCGAAACGTGGCTATAAAGAACTCAGCCGGCCT
jnk1b	121	TGCTCAGCGTATGACCACGTCCTCGATCGAAATGTGGCGATTAAAGAACTCAGCCGACCC
jnk1a	181	TTTCAAAATCAAACCTCATGCCAAACGTGGCTACAGAGAGCTGGTGCTCATGAAATGTGTC
jnk1b	181	TTTCAAAACCAAACCTCATGCCAAACGGCCTACAGAGAACTGGTCTCATGAAATGCGTC
jnk1a	241	AACCATAAAAATATAATAAGGCTCTTAAATGTTTTTACACCGCAAAAAACATTAGAAGAA
jnk1b	241	AACCACAAAAAATATAATTGGCTTACTTAAACGTGTTACACCCACAGAAAGACCCTTGAAGAG
jnk1a	301	TTCCAAGATGTTTACCTAGTAATGGAGCTGATGGATGCGAACCTCTGCCAGTCAATTCAG
jnk1b	301	TTCCAGGATGTTTATCTGGTGATGGAGCTGATGGATGCAAACTCTGTCAGGTGATTTCAG
jnk1a	361	ATGGAGCTGGACCACGAGCGGGCTGTCTTATCTGCTGTACCCAGATGCTCTCTGGAAATAAA
jnk1b	361	ATGGAGCTGGACCACGAGAGGGCTGTCTTACTCTGCTCTATCCAGATGCTCTCGGGCATTA
jnk1a	421	CACCTCCACGCGGGCGGGGATCATCCACAGGGACCTGAAACCCAGTAACATCGTGGTAAAG
jnk1b	421	CACCTGCACGCTGCTGGCATCATACACAGGGACCTGAAACCCAGTAATATAGTAGTGAAA
jnk1a	481	TCAGACTGTACCTGAAGATCCTGGATTTCCGGTCTGGCGGGACAGCAGCTACAGGTCTG
jnk1b	481	TCGGACTGCACGCTGAAGATCCTGGATTTCCGGTCTGGCCAGAACGGCTGCCAACGGGCTC
jnk1a	541	CTGATGACACCATATGTGGTGACCGTTACTACAGAGCCCTGAAGTCATCCTGGGAATG
jnk1b	541	CTCATGACTCCTTATGTAGTGACACGCTATTATCGGGCCCCAGAGGTCATCCTGGGCATG
jnk1a	601	GGATATCAAGCCAATGTGGACATTTGGTCTGTGGGCTGCATTTGGGCAGAAATGGTCCGT
jnk1b	601	GGTTATCAAGCTAACGTGGATATTTGGGCTGTGGGCTGCATTTGGGCAGACATGGTCCGG
jnk1a	661	CACAAAATCCTTTTTCTTGGGAGGGACTTTGATGTCTGGTCTCTCGGCTGTATCATGGCT
jnk1b	661	CACAAAATCCTTTTTTCCAGGGAGGGACTTTGATGTCTGGTCTATTGGCTGCATCATGGCT
jnk1a	721	GAAATGGTCAGAGGTAGTGTATTATTTCCGGGTTTCCAGATCATATTGATCAGTGGAATAAA
jnk1b	721	GAAATGGTCAGAGGTAGTGTGTTGTTTCTTGGCACAGACCATATTGACCAGTGGAATAAA
jnk1a	781	GTAATAGAGCAGCTGGGAACGCCAACTCAGGAGTTCTGTGTGAAACTCAACCAGTCTGTG
jnk1b	781	GTGATCGAGCAGCTCGGCACGCCGCTCACAGGAGTTCTATGATGAAGCTGAATCAGTCTGTG
jnk1a	841	CGGACCTATGTGGAGAACAGGCCCGGTACACTGGATATAGCTTTGAGAAGCTGTTTCCT
jnk1b	841	AGGACGTATGTGGAGAACCAGGCCTCGGTATGCGGGATACAGCTTTGAGAAGCTCTTCCCA
jnk1a	901	GATGTCTCTGTTCCCTGCTGATTCAGAACACAGCAAACTAAAAAGCGAGTCAGGCGCGGGAC
jnk1b	901	GACGTGCTCTTCCCTCGCAGACTCGGACCAACAACAACTCAAGGCGAGTCAGGACAGAGAC
jnk1a	961	CTGCTGTCTAAAATGCTGGTGATTGATGCATCAAAACGAATCTCGGTGATGAGGCTTTG
jnk1b	961	TTGTTATCCAAAATGCTGGTAATAGATGCGTCCAAGCGGATCTCTGTAGACGAGGCGCTT
jnk1a	1021	CAGCACCCCTACATTAAACGTGTGGTACGACCCGGCTGAAGTGGAAGCGCCTTCTCTCTG
jnk1b	1021	CAGCACCCCTACATCAACGTTTGGTACGACCCGTGAGAAGTGGAAGCGCCACCAACAGCG
jnk1a	1081	ATCACAGACAAACAGCTCGATGAGAGGGAACACACAGTGGAAGAGTGGAAGAACTGATC
jnk1b	1081	ATCACGGATAAACAGCTCGATGAGAGAGAACACTCAGTGGAAGAGTGGAAGAGCTCATA

```

jnk1a 1141 TATAAAGAAGTGCTGGATTGGGAAGAACGGATGAAGAACGGTGTATTCGAGGTCAGCCC
jnk1b 1141 TATAAGGAAGTGCTGGAATGGGAGGAGCGAACAATAATGGAGTCATCAGAGGACAGCCG

jnk1a 1201 TCCCTCTAGGTGCAGCAGTGATCAACGGCTCACCCAGCCCTCATC---CTCATCCTCC
jnk1b 1201 GCCTCGCTAGGTGCAGCAGTGAGCAGTGAAGTCCCATGAGCCCTCGACGTCTCTCTCTCC

jnk1a 1258 ATCAACGACGTGTCTTCCATGTCCACAGAGCCACCGTGGCCTCAGACACAGACAGCAGC
jnk1b 1261 ATAAACGATGTGTCTTCCATGTCCACAGAGGTACAGGTGACCTCAGACACAGACAGCAGT

jnk1a 1318 TTAGAGGCTCTGGCGGGACCCCTGAGCTGCTGCAGATGA
jnk1b 1321 CAGGAGACGTCCAACGGAGCGCTGCACTGCTGCAGATGA

```

Figure 60 DNA Alignment of All Thirteen Exons of jnk1a and jnk1b.

This DNA alignment corresponds to Figure 18 and represents the raw data that was used to produce this figure. This alignment involves the sequence that was produced from my own sequencing experiments. The CDS of all 13 jnk1a and jnk1b exons was aligned to determine where there were regions of relative sequence conservation within the sequence.

```

jnk1a 1 MNKNKREKEFYSDVGDSTFTVLKRYQNLRLPIGSGAQGIVCSAYDNNLEERNVAIKKLSRP
jnk1b 1 MNRNKREKEYSIDVGDSTFTVLKRYQNLRLPIGSGAQGIVCSAYDHVLDNRNVAIKKLSRP

jnk1a 61 FQNQTHAKRAYRELVLMKCVNHKNIIGLLNVFTPQKTLEEFQDVYLVMEMLMDANLCQVIO
jnk1b 61 FQNQTHAKRAYRELVLMKCVNHKNIIGLLNVFTPQKTLEEFQDVYLVMEMLMDANLCQVIO

jnk1a 121 MELDHERLSYLLYQMLCGIKHLHAAGIIHRDLKPSNIVVKS DCTLKILDFGLARTAATGL
jnk1b 121 MELDHERLSYLLYQMLCGIKHLHAAGIIHRDLKPSNIVVKS DCTLKILDFGLARTAATGL

jnk1a 181 LMTPYVVTRYRAPEVILMGYQANVDIWSVGCILAEMVRHKILFPGRDL DVWSVGCIMA
jnk1b 181 LMTPYVVTRYRAPEVILMGYQANVDIWA VGCIMAEMVRHKILFPGRDF DVWSVGCIMA

jnk1a 241 EMVRGSVLFPGSDHIDQWNKVIEQLGTPTQEFLLKLNQSVRTYVENRPRYT GYSFEKLFP
jnk1b 241 EMVRGSVLFPGTDHIDQWNKVIEQLGTPTQEFMMKLNQSVRTYVENRPRYAGYSFEKLFP

jnk1a 301 DVLFPADSEHSHKLKASQARDLLSKMLVIDASKRISVDEALQHPYINVWYDPAEVEAPSPPL
jnk1b 301 DVLFPADSDHSHKLKASQARDLLSKMLVIDASKRISVDEALQHPYINVWYDPAEVEAPPPA

jnk1a 361 ITDKQLDEREHTVEEWKELIYKEVLDWEERMKNGVIRGQPSPLGAAVINGSPOPS-SSSS
jnk1b 361 ITDKQLDEREHSVEEWKELIYKEVLEWEERTKNGVIRGQPASLGAAVSSDSHEPSTSSSS

jnk1a 420 INDVSSMSTEPTVASD TDSSLEASAGPILSCCR*
jnk1b 421 INDVSSMSTEVTLTSD TDSSQETSNCAIHCCR*

```

Figure 61 Protein Alignment of All Thirteen Exons of jnk1a and jnk1b.

This protein alignment corresponds to Figure 18 and represents the raw data that was used to produce this figure. This alignment is of the protein sequence produced by the CDS of all 13 exons of jnk1a and jnk1b. The protein sequence was generating by translating the DNA sequencing data that was produced from my own sequencing experiments. This alignment was produced to determine whether the sequences had large stretches of sequence conservation.

A

```

>jnk1a MO seq
5' - CTCTCGCTTATTTTTGTTTCATGGTG - 3'
3' - GTGGTACTTGTTTTTATTCGCTCTC - 5'

>jnk1a exon 2
1   gtttgaacagtcctgtctgttgatgcttacacatcga

      3' - GTGGTACTTGTTTTTATTCGCTCTC - 5'
          |||||
41   cttcaccATGAACAAAAATAAGCGAGAGAAAGAATTCTACAGTGTAGATGTGGGGGATTC

101  GACATTACAGTGTGGAAGCGCTATCAGAATCTAAGACCCATTGGCTCGGGTGCTCAGGG

161  AATAGTCTG

```

B

```

>jnk1b MO seq
5' - CTTTCTCGCGCTTATTCCTGTTTCAT - 3'
3' - TACTTGTCTTATTCGCGCTCTTTC - 5'

>jnk1b exon 2
1   atttttgaaggtgaagctcttcttgatgccaggata

      3' - TACTTGTCTTATTCGCGCTCTTTC - 5'
          |||||
41   cagtcagtcacggttttcatcATGAACAGGAATAAGCGCGAGAAAGAATATTACA

101  GCATAGATGTAGGAGATTTCGACGTTACCGTTTTGAAGCGCTATCAGAATTTAA

```

Figure 62 The binding sites of the *jnk1* morpholinos.

Both *jnk1* morpholinos hybridize in a 3' to 5' direction with the target sequence in exon 2 of A) the *jnk1a* or B) *jnk1b* genes. The nucleotide sequences in black are those of exon 2 *jnk1a* and *jnk1b* respectively. The sequences in red represent the morpholino sequences. Verticle lines represent the binding sites of the morpholinos to their target.

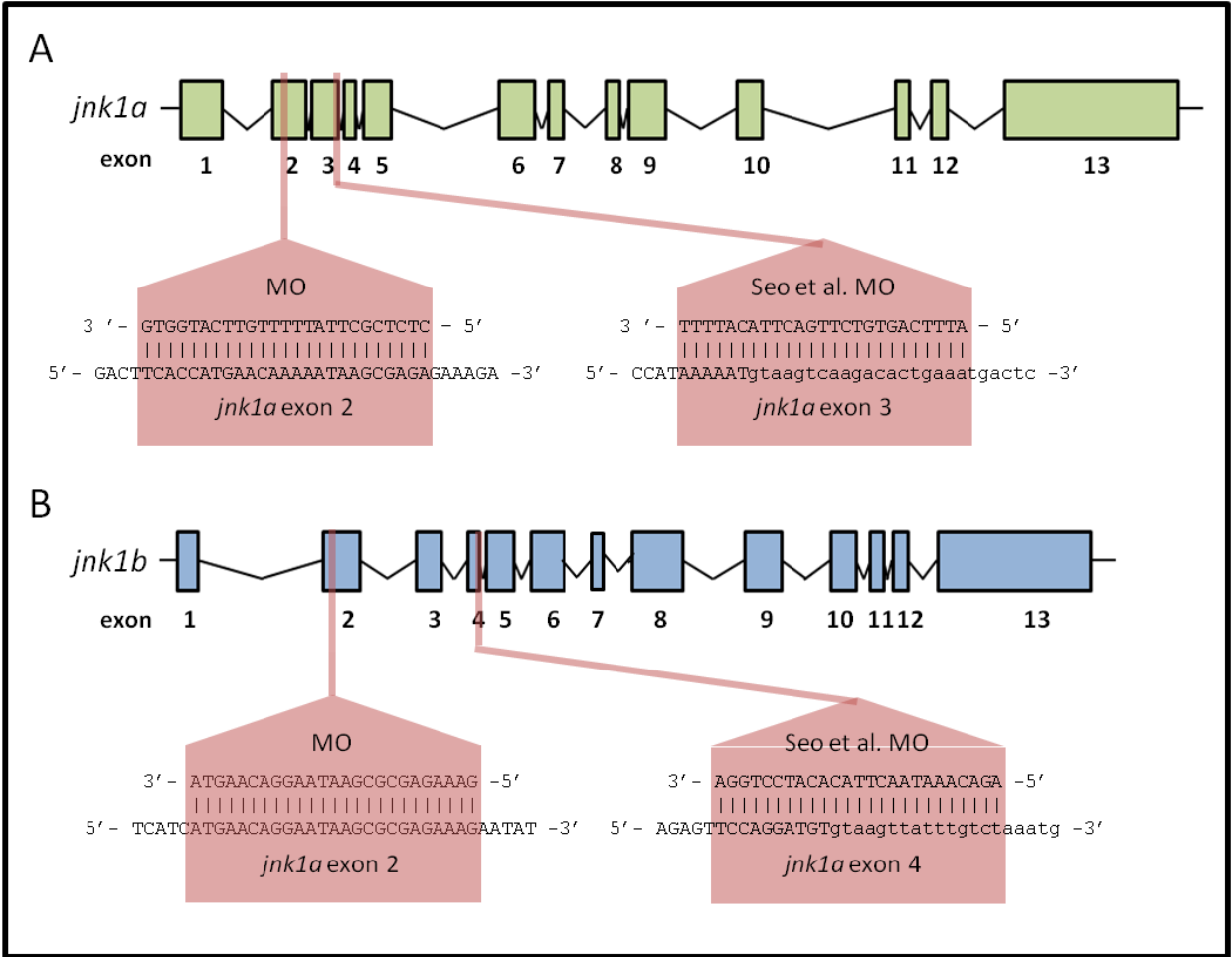


Figure 63 The binding sites of our translation blocking and the Seo et al. splice-variant morpholinos.

Schematic representation of the *jnk1a* (A) and *jnk1b* (B) genes where boxes represent exons and black lines represent intronic sequence. The pink annotation shows the approximate location of the binding sites of the morpholino oligonucleotides used by our lab and those published in the paper by Seo et al. (Seo et al., 2010). Text boxes show the MO sequence (in 3' to 5' order) as well as 35bp of the *jnk1a* or *jnk1b* genes where the MO binds. In the *jnk1* gene sequence uppercase represents exonic sequence whereas lowercase represents intronic sequence.

7.1.1 Abbreviations

ANOVA	analysis of variance
AP	anteroposterior
ASK	MAPKK kinase 5
ATP	adenosine triphosphate
BMP	bone morphogenetic protein
BP	basepair
BSK	basket / drosophila JNK
cDNA	complementary DNA
CDS	coding sequence
CE	convergent extension
CHD	congenital heart defects
CMO	control morpholino
CNS	central nervous system
CRISPR	clustered regularly interspaces short palindromic repeats
dATP	deoxyadenosine triphosphate
DEPC	diethylpyrocarbonate
DGO	diego
DHARMA	bozozok
DNA	deoxyribonucleic acid
dNTPs	deoxyribonucleotide triphosphate
DS	daschsous
DSH	dishevelled
DTT	dithiothreitol
EDTA	ethylenediaminetetraacetic acid
ELFA1	elongation factor 1-alpha
EMBL	european molecular biology laboratory
ERK	extracellular signal-related kinase
E-YSL	external yolk syncytical layer
FJ	four-jointed
FMI	flamingo
FT	fat
FZ	frizzled
GAPDH	glyceraldehyde-3-phosphate dehydrogenase
GDF1	growth/differentiation factor 1
GFP	green fluorescent protein
GL	ganglion layer
GTP	guanosine triphosphate
HBV	hindbrain ventricle
HPF	hours post fertilisation
INL	inner nuclear layer
IPL	inner plexiform layer
I-YSL	internal yolk syncytical layer
JNK	c-jun n-terminal kinase
kDA	kilo daltons

LPM	lateral plate mesoderm
L-R	left-right
LRD	left-right dynein
MAP	mitogen activated protein
MAP3K	MAPKK kinase
MAP4K	MAPKKK kinase
MAPK	mitogen activated protein kinase
MAPKAPK	MAPK activated protein kinase
MAPKK	MAPK kinase
MAPKKK	MAPKK kinase
MEK	MAPK kinase
MeOH	methanol
MGT	mid-blastula transition
MKK	MAPK kinase
ML	mediolateral
MO	morpholino oligonucleotide
NCBI	national centre for biotechnology information
NOTO	floating head
OPL	outer plexiform layer
ORF	open reading frame
PCP	planar cell polarity
PCR	polymerase chain reaction
PK	prickle
PL	photoreceptor layer
PTU	1-phenyl 2-thiourea
PVDF	polyvinylidene fluoride
qPCR	quantitative real time PCR
RACE	rapid amplification of cDNA ends
RNA	ribonucleic acid
ROCK	rho kinase
RPM	revolutions per minute
RT-PCR	reverse transcription PCR
SEM	standard error of the mean
SER	serine
SPAW	southpaw / zebrafish nodal
STAN	starry night
STBM	strabismus
TA	no tail
TAE	tris-acetate EDTA buffer
TAK	MAPKK kinase 7
TBS	tris buffered saline
TBS-T	TBS tween 20
TGF β	transforming growth factor beta
THR	threonine
TYR	tyrosine
UTR	untranslated region

UV	ultraviolet
VANG	van gogh
WNT	Wingless-related MMTV integration site
YSL	yolk syncytical layer

CHAPTER 8 - REFERENCES

- AANES, H., WINATA, C. L., LIN, C. H., CHEN, J. Q. P., SRINIVASAN, K. G., LEE, S. G. P., LIM, A. Y. M., HAJAN, H. S., COLLAS, P., BOURQUE, G., GONG, Z. Y., KORZH, V., ALESTROM, P. & MATHAVAN, S. 2011. Zebrafish mRNA sequencing deciphers novelties in transcriptome dynamics during maternal to zygotic transition. *Genome Research*, 21, 1328-1338.
- ADAMS, D. S., ROBINSON, K. R., FUKUMOTO, T., YUAN, S. P., ALBERTSON, R. C., YELICK, P., KUO, L., MCSWEENEY, M. & LEVIN, M. 2006. Early, H⁺-V-ATPase-dependent proton flux is necessary for consistent left-right patterning of non-mammalian vertebrates. *Development*, 133, 1657-1671.
- ADAMS, N. A., AWADEIN, A. & TOMA, H. S. 2007. The retinal ciliopathies. *Ophthalmic Genetics*, 28, 113-125.
- AFZELIUS, B. A. 1976. A human syndrome caused by immotile cilia. *Science*, 193, 317-9.
- AHMAD, N., LONG, S. & REBAGLIATI, M. 2004. A southpaw joins the roster: The role of the zebrafish nodal-related gene southpaw in cardiac LR asymmetry. *Trends in Cardiovascular Medicine*, 14, 43-49.
- AL-HAMED, M. H., VAN LENNEP, C., HYNES, A. M., CHRYSTAL, P., ELEY, L., AL-FADHLY, F., EL SAYED, R., SIMMS, R. J., MEYER, B. & SAYER, J. A. 2014. Functional modelling of a novel mutation in BBS5. *Cilia*, 3, 3.
- AMBROSINO, C. & NEBRED, A. R. 2001. Cell cycle regulation by p38 MAP kinases. *Biol Cell*, 93, 47-51.
- ANGEL, P. & KARIN, M. 1991. The role of Jun, Fos and the AP-1 complex in cell-proliferation and transformation. *Biochim Biophys Acta*, 1072, 129-57.
- ANICHTCHIK, O., DIEKMANN, H., FLEMING, A., ROACH, A., GOLDSMITH, P. & RUBINSZTEIN, D. C. 2008. Loss of PINK1 function affects development and results in neurodegeneration in zebrafish. *Journal of Neuroscience*, 28, 8199-8207.
- AW, S., KOSTER, J. C., PEARSON, W., NICHOLS, C. G., SHI, N. Q., CARNEIRO, K. & LEVIN, M. 2010. The ATP-sensitive K⁺-channel (K-ATP) controls early left-right patterning in *Xenopus* and chick embryos. *Developmental Biology*, 346, 39-53.
- AXELROD, J. D. 2009. Progress and challenges in understanding planar cell polarity signaling. *Seminars in Cell & Developmental Biology*, 20, 964-971.
- BACUS, S. S., GUDKOV, A. V., LOWE, M., LYASS, L., YUNG, Y., KOMAROV, A. P., KEYOMARSI, K., YARDEN, Y. & SEGER, R. 2001. Taxol-induced apoptosis depends on MAP kinase pathways (ERK and p38) and is independent of p53. *Oncogene*, 20, 147-55.
- BADEN, K. N., MURRAY, J., CAPALDI, R. A. & GUILLEMIN, K. 2007. Early developmental pathology due to cytochrome c oxidase deficiency is revealed by a new zebrafish model. *Journal of Biological Chemistry*, 282, 34839-34849.
- BALBI, A. P., FRANCESCATO, H. D., MARIN, E. C., COSTA, R. S. & COIMBRA, T. M. 2009. Roles of mitogen-activated protein kinases and angiotensin II in renal development. *Braz J Med Biol Res*, 42, 38-43.
- BAMFORTH, S. D., BRAGANCA, J., FARTHING, C. R., SCHNEIDER, J. E., BROADBENT, C., MICHELL, A. C., CLARKE, K., NEUBAUER, S., NORRIS, D., BROWN, N. A., ANDERSON, R. H. & BHATTACHARYA, S. 2004. Cited2 controls left-right patterning and heart development through a Nodal-Pitx2c pathway. *Nat Genet*, 36, 1189-96.
- BARR, R. K. & BOGOYEVITCH, M. A. 2001. The c-Jun N-terminal protein kinase family of mitogen-activated protein kinases (JNK MAPKs). *Int J Biochem Cell Biol*, 33, 1047-63.

- BARRESI, M. J., STICKNEY, H. L. & DEVOTO, S. H. 2000. The zebrafish slow-muscle-omitted gene product is required for Hedgehog signal transduction and the development of slow muscle identity. *Development*, 127, 2189-99.
- BARTRAM, U., FISCHER, G. & KRAMER, H. H. 2008. Congenitally interrupted inferior vena cava without other features of the heterotaxy syndrome: report of five cases and characterization of a rare entity. *Pediatr Dev Pathol*, 11, 266-73.
- BARTRAM, U., WIRBELAUER, J. & SPEER, C. P. 2005. Heterotaxy syndrome -- asplenia and polysplenia as indicators of visceral malposition and complex congenital heart disease. *Biol Neonate*, 88, 278-90.
- BAUER, H., LELE, Z., RAUCH, G. J., GEISLER, R. & HAMMERSCHMIDT, M. 2001. The type I serine/threonine kinase receptor Alk8/Lost-a-fin is required for Bmp2b/7 signal transduction during dorsoventral patterning of the zebrafish embryo. *Development*, 128, 849-58.
- BEARDMORE, V. A., HINTON, H. J., EFTYCHI, C., APOSTOLAKI, M., ARMAKA, M., DARRAGH, J., MCILRATH, J., CARR, J. M., ARMIT, L. J., CLACHER, C., MALONE, L., KOLLIAS, G. & ARTHUR, J. S. 2005. Generation and characterization of p38beta (MAPK11) gene-targeted mice. *Mol Cell Biol*, 25, 10454-64.
- BEIS, D., BARTMAN, T., JIN, S. W., SCOTT, I. C., D'AMICO, L. A., OBER, E. A., VERKADE, H., FRANTSVE, J., FIELD, H. A., WEHMAN, A., BAIER, H., TALLAFUSS, A., BALLY-CUIF, L., CHEN, J. N., STAINIER, D. Y. & JUNGBLUT, B. 2005. Genetic and cellular analyses of zebrafish atrioventricular cushion and valve development. *Development*, 132, 4193-204.
- BENNETT, B. L., SASAKI, D. T., MURRAY, B. W., O'LEARY, E. C., SAKATA, S. T., XU, W., LEISTEN, J. C., MOTIWALA, A., PIERCE, S., SATOH, Y., BHAGWAT, S. S., MANNING, A. M. & ANDERSON, D. W. 2001. SP600125, an anthrapyrazolone inhibitor of Jun N-terminal kinase. *Proc Natl Acad Sci U S A*, 98, 13681-6.
- BIBEN, C. & HARVEY, R. P. 1997. Homeodomain factor Nkx2-5 controls left/right asymmetric expression of bHLH gene eHand during murine heart development. *Genes Dev*, 11, 1357-69.
- BISGROVE, B. W., ESSNER, J. J. & YOST, H. J. 1999. Regulation of midline development by antagonism of lefty and nodal signaling. *Development*, 126, 3253-62.
- BISGROVE, B. W., SNARR, B. S., EMRAZIAN, A. & YOST, H. J. 2005. Polaris and Polycystin-2 in dorsal forerunner cells and Kupffer's vesicle are required for specification of the zebrafish left-right axis. *Dev Biol*, 287, 274-88.
- BJORKBLOM, B., OSTMAN, N., HONGISTO, V., KOMAROVSKI, V., FILEN, J. J., NYMAN, T. A., KALLUNKI, T., COURTNEY, M. J. & COFFEY, E. T. 2005. Constitutively active cytoplasmic c-Jun N-terminal kinase 1 is a dominant regulator of dendritic architecture: Role of microtubule-associated protein 2 as an effector. *Journal of Neuroscience*, 25, 6350-6361.
- BLAGDEN, C. S., CURRIE, P. D., INGHAM, P. W. & HUGHES, S. M. 1997. Notochord induction of zebrafish slow muscle mediated by Sonic hedgehog. *Genes & Development*, 11, 2163-2175.
- BLUM, M., FEISTEL, K., THUMBERGER, T. & SCHWEICKERT, A. 2014. The evolution and conservation of left-right patterning mechanisms. *Development*, 141, 1603-1613.
- BOGOYEVITCH, M. A. 2006. The isoform-specific functions of the c-Jun N-terminal kinases (JNKs): differences revealed by gene targeting. *Bioessays*, 28, 923-934.

- BOGOYEVITCH, M. A. & KOBE, B. 2006a. Uses for JNK: the many and varied substrates of the c-Jun N-terminal kinases. *Microbiol Mol Biol Rev*, 70, 1061-95.
- BOGOYEVITCH, M. A. & KOBE, B. 2006b. Uses for JNK: the many and varied substrates of the c-Jun N-terminal kinases. *Microbiology and Molecular Biology Reviews*, 70, 1061-+.
- BOROVINA, A., SUPERINA, S., VOSKAS, D. & CIRUNA, B. 2010. Vangl2 directs the posterior tilting and asymmetric localization of motile primary cilia. *Nature Cell Biology*, 12, 407-U242.
- BOSSYWETZEL, E., BAKIRI, L. & YANIV, M. 1997. Induction of apoptosis by the transcription factor c-Jun. *Embo Journal*, 16, 1695-1709.
- BRENNAN, J., NORRIS, D. P. & ROBERTSON, E. J. 2002. Nodal activity in the node governs left-right asymmetry. *Genes & Development*, 16, 2339-2344.
- BRITTLE, A. L., REPISO, A., CASAL, J., LAWRENCE, P. A. & STRUTT, D. 2010. Four-jointed modulates growth and planar polarity by reducing the affinity of dachsous for fat. *Curr Biol*, 20, 803-10.
- BROWN, N. A. & WOLPERT, L. 1990. The Development of Handedness in Left Right Asymmetry. *Development*, 109, 1-9.
- BRUCE, A. E. E., OATES, A. C., PRINCE, V. E. & HO, R. K. 2001. Additional hox clusters in the zebrafish: divergent expression patterns belie equivalent activities of duplicate hoxB5 genes. *Evolution & Development*, 3, 127-144.
- CAMPIONE, M., ROS, M. A., ICARDO, J. M., PIEDRA, E., CHRISTOFFELS, V. M., SCHWEICKERT, A., BLUM, M., FRANCO, D. & MOORMAN, A. F. M. 2001. Pitx2 expression defines a left cardiac lineage of cells: Evidence for atrial and ventricular molecular isomerism in the iv/iv mice. *Developmental Biology*, 231, 252-264.
- CAMPIONE, M., STEINBEISSER, H., SCHWEICKERT, A., DEISSLER, K., VAN BEBBER, F., LOWE, L. A., NOWOTSCHIN, S., VIEBAHN, C., HAFFTER, P., KUEHN, M. R. & BLUM, M. 1999. The homeobox gene Pitx2: mediator of asymmetric left-right signaling in vertebrate heart and gut looping. *Development*, 126, 1225-1234.
- CARREIRA-BARBOSA, F., KAJITA, M., MOREL, V., WADA, H., OKAMOTO, H., ARIAS, A. M., FUJITA, Y., WILSON, S. W. & TADA, M. 2009. Flamingo regulates epiboly and convergence/extension movements through cell cohesive and signalling functions during zebrafish gastrulation (vol 136, pg 383, 2009). *Development*, 136, 877-877.
- CASAL, J., LAWRENCE, P. A. & STRUHL, G. 2006. Two separate molecular systems, Dachsous/Fat and Starry night/Frizzled, act independently to confer planar cell polarity. *Development*, 133, 4561-72.
- CHAKAROVA, C. F., KHANNA, H., SHAH, A. Z., PATIL, S. B., SEDMAK, T., MURGA-ZAMALLOA, C. A., PAPAIOANNOU, M. G., NAGEL-WOLFRUM, K., LOPEZ, I., MUNRO, P., CHEETHAM, M., KOENENKOOP, R. K., RIOS, R. M., MATTER, K., WOLFRUM, U., SWAROOP, A. & BHATTACHARYA, S. S. 2011. TOPORS, implicated in retinal degeneration, is a cilia-centrosomal protein. *Human Molecular Genetics*, 20, 975-987.
- CHEN, E. & EKKER, S. C. 2004. Zebrafish as a genomics research model. *Curr Pharm Biotechnol*, 5, 409-13.
- CHEN, J. 2013. Impaired cardiovascular function caused by different stressors elicits a common pathological and transcriptional response in zebrafish embryos. *Zebrafish*, 10, 389-400.
- CHEN, J. N. & FISHMAN, M. C. 1996. Zebrafish tinman homolog demarcates the heart field and initiates myocardial differentiation. *Development*, 122, 3809-3816.

- CHEN, J. N., VANEEDEN, F. J. M., WARREN, K. S., CHIN, A., NUSSLEINVOLHARD, C., HAFFTER, P. & FISHMAN, M. C. 1997. Left-right pattern of cardiac BMP4 may drive asymmetry of the heart in zebrafish. *Development*, 124, 4373-4382.
- CHENG, A. M., THISSE, B., THISSE, C. & WRIGHT, C. V. 2000. The lefty-related factor Xatv acts as a feedback inhibitor of nodal signaling in mesoderm induction and L-R axis development in xenopus. *Development*, 127, 1049-61.
- CHENG, S. K., OLALE, F., BRIVANLOU, A. H. & SCHIER, A. F. 2004. Lefty blocks a subset of TGFbeta signals by antagonizing EGF-CFC coreceptors. *PLoS Biol*, 2, E30.
- CHI, N. C., SHAW, R. M., DE VAL, S., KANG, G., JAN, L. Y., BLACK, B. L. & STAINIER, D. Y. 2008. Foxn4 directly regulates tbx2b expression and atrioventricular canal formation. *Genes Dev*, 22, 734-9.
- CHIN, A. J., TSANG, M. & WEINBERG, E. S. 2000. Heart and gut chiralities are controlled independently from initial heart position in the developing zebrafish. *Developmental Biology*, 227, 403-421.
- CHOI, S. C. & HAN, J. K. 2002. Xenopus Cdc42 regulates convergent extension movements during gastrulation through Wnt/Ca2+ signaling pathway. *Developmental Biology*, 244, 342-357.
- CHONG, S. W., KORZH, V. & JIANG, Y. J. 2009. Myogenesis and molecules - insights from zebrafish *Danio rerio*. *J Fish Biol*, 74, 1693-755.
- CIANI, L., PATEL, A., ALLEN, N. D. & FFRENCH-CONSTANT, C. 2003. Mice lacking the giant protocadherin mFAT1 exhibit renal slit junction abnormalities and a partially penetrant cyclopia and anophthalmia phenotype. *Mol Cell Biol*, 23, 3575-82.
- COFFMAN, J. A., DICKEY-SIMS, C., HAUG, J. S., MCCARTHY, J. J. & ROBERTSON, A. J. 2004. Evaluation of developmental phenotypes produced by morpholino antisense targeting of a sea urchin Runx gene. *BMC Biol*, 2, 6.
- COLLIGNON, J., VARLET, I. & ROBERTSON, E. J. 1996. Relationship between asymmetric nodal expression and the direction of embryonic turning. *Nature*, 381, 155-8.
- CONCHA, M. L., BURDINE, R. D., RUSSELL, C., SCHIER, A. F. & WILSON, S. W. 2000. A nodal signaling pathway regulates the laterality of neuroanatomical asymmetries in the zebrafish forebrain. *Neuron*, 28, 399-409.
- CONG, L., RAN, F. A., COX, D., LIN, S., BARRETTO, R., HABIB, N., HSU, P. D., WU, X., JIANG, W., MARRAFFINI, L. A. & ZHANG, F. 2013. Multiplex genome engineering using CRISPR/Cas systems. *Science*, 339, 819-23.
- CONSTANT, S. L., DONG, C., YANG, D. D., WYSK, M., DAVIS, R. J. & FLAVELL, R. A. 2000. JNK1 is required for T cell-mediated immunity against *Leishmania major* infection. *J Immunol*, 165, 2671-6.
- CREAN, J. K., FINLAY, D., MURPHY, M., MOSS, C., GODSON, C., MARTIN, F. & BRADY, H. R. 2002. The role of p42/44 MAPK and protein kinase B in connective tissue growth factor induced extracellular matrix protein production, cell migration, and actin cytoskeletal rearrangement in human mesangial cells. *J Biol Chem*, 277, 44187-94.
- CURTIN, J. A., QUINT, E., TSIPOURI, V., ARKELL, R. M., CATTANACH, B., COPP, A. J., HENDERSON, D. J., SPURR, N., STANIER, P., FISHER, E. M., NOLAN, P. M., STEEL, K. P., BROWN, S. D., GRAY, I. C. & MURDOCH, J. N. 2003. Mutation of *Celsr1* disrupts planar polarity of inner ear hair cells and causes severe neural tube defects in the mouse. *Curr Biol*, 13, 1129-33.
- DANOS, M. C. & YOST, H. J. 1996. Role of notochord in specification of cardiac left-right orientation in zebrafish and *Xenopus*. *Dev Biol*, 177, 96-103.

- DAS, M., JIANG, F., SLUSS, H. K., ZHANG, C., SHOKAT, K. M., FLAVELL, R. A. & DAVIS, R. J. 2007. Suppression of p53-dependent senescence by the JNK signal transduction pathway. *Proc Natl Acad Sci U S A*, 104, 15759-64.
- DASHTI, S. R., EFIMOVA, T. & ECKERT, R. L. 2001. MEK7-dependent activation of p38 MAP kinase in keratinocytes. *J Biol Chem*, 276, 8059-63.
- DAVIES, A., FORMSTONE, C., MASON, I. & LEWIS, J. 2005. Planar polarity of hair cells in the chick inner ear is correlated with polarized distribution of c-flamingo-1 protein. *Dev Dyn*, 233, 998-1005.
- DAVIS, R. J. 2000. Signal transduction by the JNK group of MAP kinases. *Cell*, 103, 239-252.
- DE PATER, E., CLIJSTERS, L., MARQUES, S. R., LIN, Y. F., GARAVITO-AGUILAR, Z. V., YELON, D. & BAKKERS, J. 2009. Distinct phases of cardiomyocyte differentiation regulate growth of the zebrafish heart. *Development*, 136, 1633-1641.
- DERIJARD, B., HIBI, M., WU, I. H., BARRETT, T., SU, B., DENG, T. L., KARIN, M. & DAVIS, R. J. 1994. Jnk1 - a Protein-Kinase Stimulated by Uv-Light and Ha-Ras That Binds and Phosphorylates the C-Jun Activation Domain. *Cell*, 76, 1025-1037.
- DERIJARD, B., RAINGEAUD, J., BARRETT, T., WU, I. H., HAN, J., ULEVITCH, R. J. & DAVIS, R. J. 1995. Independent human MAP-kinase signal transduction pathways defined by MEK and MKK isoforms. *Science*, 267, 682-5.
- DJIANE, A., RIOU, J. F., UMBHAUER, M., BOUCAUT, J. C. & SHI, D. L. 2000. Role of frizzled 7 in the regulation of convergent extension movements during gastrulation in *Xenopus laevis*. *Development*, 127, 3091-3100.
- EASTER, S. S., JR. & NICOLA, G. N. 1996. The development of vision in the zebrafish (*Danio rerio*). *Dev Biol*, 180, 646-63.
- EFERL, R., SIBILIA, M., HILBERG, F., FUCHSBICHLER, A., KUFFERATH, I., GUERTL, B., ZENZ, R., WAGNER, E. F. & ZATLOUKAL, K. 1999. Functions of c-jun in liver and heart development. *Journal of Cell Biology*, 145, 1049-1061.
- EISEN, J. S. & SMITH, J. C. 2008. Controlling morpholino experiments: don't stop making antisense. *Development*, 135, 1735-1743.
- ENNOS, A. R. 2006. *Statistical and data handling skills in biology*, New York, Pearson.
- ESSNER, J. J., AMACK, J. D., NYHOLM, M. K., HARRIS, E. B. & YOST, H. J. 2005a. Kupffer's vesicle is a ciliated organ of asymmetry in the zebrafish embryo that initiates left-right development of the brain, heart and gut. *Development*, 132, 1247-60.
- ESSNER, J. J., AMACK, J. D., NYHOLM, M. K., HARRIS, E. B. & YOST, J. 2005b. Kupffer's vesicle is a ciliated organ of asymmetry in the zebrafish embryo that initiates left-right development of the brain, heart and gut. *Development*, 132, 1247-1260.
- FADOOL, J. M. & DOWLING, J. E. 2008. Zebrafish: a model system for the study of eye genetics. *Prog Retin Eye Res*, 27, 89-110.
- FANTO, M., WEBER, U., STRUTT, D. I. & MLODZIK, M. 2000. Nuclear signaling by Rac and Rho GTPases is required in the establishment of epithelial planar polarity in the *Drosophila* eye. *Curr Biol*, 10, 979-88.
- FERENCZ, C. 1964. Visceral Heterotaxy with Malformed Heart. Similar Findings in a Child and a Puppy. *Anatomical Record*, 149, 299-307.
- FERNANDES, K. A., HARDER, J. M., FORNAROLA, L. B., FREEMAN, R. S., CLARK, A. F., PANG, I. H., JOHN, S. W. M. & LIBBY, R. T. 2012. JNK2 and JNK3 are major regulators of axonal injury-induced retinal ganglion cell death. *Neurobiology of Disease*, 46, 393-401.
- FIELD, H. A., OBER, E. A., ROESER, T. & STAINIER, D. Y. R. 2003. Formation of the digestive system in zebrafish. I. Liver morphogenesis. *Developmental Biology*, 253, 279-290.

- FLEMING, Y., ARMSTRONG, C. G., MORRICE, N., PATERSON, A., GOEDERT, M. & COHEN, P. 2000. Synergistic activation of stress-activated protein kinase 1/c-Jun N-terminal kinase (SAPK1/JNK) isoforms by mitogen-activated protein kinase kinase 4 (MKK4) and MKK7. *Biochemical Journal*, 352, 145-154.
- FLICEK, P., AMODE, M. R., BARRELL, D., BEAL, K., BILLIS, K., BRENT, S., CARVALHO-SILVA, D., CLAPHAM, P., COATES, G., FITZGERALD, S., GIL, L., GIRON, C. G., GORDON, L., HOURLIER, T., HUNT, S., JOHNSON, N., JUETTEMANN, T., KAHARI, A. K., KEENAN, S., KULESHA, E., MARTIN, F. J., MAUREL, T., MCLAREN, W. M., MURPHY, D. N., NAG, R., OVERDUIN, B., PIGNATELLI, M., PRITCHARD, B., PRITCHARD, E., RIAT, H. S., RUFFIER, M., SHEPPARD, D., TAYLOR, K., THORMANN, A., TREVANION, S. J., VULLO, A., WILDER, S. P., WILSON, M., ZADISSA, A., AKEN, B. L., BIRNEY, E., CUNNINGHAM, F., HARROW, J., HERRERO, J., HUBBARD, T. J. P., KINSELLA, R., MUFFATO, M., PARKER, A., SPUDICH, G., YATES, A., ZERBINO, D. R. & SEARLE, S. M. J. 2014. Ensembl 2014. *Nucleic Acids Research*, 42, D749-D755.
- FORCE, A., LYNCH, M., PICKETT, F. B., AMORES, A., YAN, Y. L. & POSTLETHWAIT, J. 1999. Preservation of duplicate genes by complementary, degenerative mutations. *Genetics*, 151, 1531-1545.
- FRANCESCOTTO, L., ROTHSCCHILD, S. C., MYERS, A. L. & TOMBES, R. M. 2010. The activation of membrane targeted CaMK-II in the zebrafish Kupffer's vesicle is required for left-right asymmetry. *Development*, 137, 2753-62.
- FRANCIS, R. J., CHRISTOPHER, A., DEVINE, W. A., OSTROWSKI, L. & LO, C. 2012. Congenital heart disease and the specification of left-right asymmetry. *Am J Physiol Heart Circ Physiol*, 302, H2102-11.
- FRANCO, D., CHRISTOFFELS, V. M. & CAMPIONE, M. 2014. Homeobox transcription factor Pitx2: The rise of an asymmetry gene in cardiogenesis and arrhythmogenesis. *Trends Cardiovasc Med*, 24, 23-31.
- FUCHS, S. Y., ADLER, V., PINCUS, M. R. & RONAI, Z. 1998. MEKK1/JNK signaling stabilizes and activates p53. *Proc Natl Acad Sci U S A*, 95, 10541-6.
- FUKUMOTO, T., KEMA, I. P. & LEVIN, M. 2005. Serotonin signaling is a very early step in patterning of the left-right axis in chick and frog embryos. *Current Biology*, 15, 794-803.
- GAO, C. & CHEN, Y. G. 2010. Dishevelled: The hub of Wnt signaling. *Cellular Signalling*, 22, 717-727.
- GARRIOCK, R. J., D'AGOSTINO, S. L., PILCHER, K. C. & KRIEG, P. A. 2005. Wnt11-R, a protein closely related to mammalian Wnt11, is required for heart morphogenesis in *Xenopus*. *Developmental Biology*, 279, 179-192.
- GERETY, S. S. & WILKINSON, D. G. 2011. Morpholino artifacts provide pitfalls and reveal a novel role for pro-apoptotic genes in hindbrain boundary development. *Developmental Biology*, 350, 279-289.
- GHOSH, T. K., SONG, F. F., PACKHAM, E. A., BUXTON, S., ROBINSON, T. E., RONKSLEY, J., SELF, T., BONSER, A. J. & BROOK, J. D. 2009. Physical Interaction between TBX5 and MEF2C Is Required for Early Heart Development. *Molecular and Cellular Biology*, 29, 2205-2218.
- GLICKMAN, N. S. & YELON, D. 2002. Cardiac development in zebrafish: coordination of form and function. *Seminars in Cell & Developmental Biology*, 13, 507-513.

- GOETZE, S., XI, X. P., KAWANO, Y., KAWANO, H., FLECK, E., HSUEH, W. A. & LAW, R. E. 1999. TNF-alpha-induced migration of vascular smooth muscle cells is MAPK dependent. *Hypertension*, 33, 183-9.
- GONG, Y., MO, C. H. & FRASER, S. E. 2004. Planar cell polarity signalling controls cell division orientation during zebrafish gastrulation. *Nature*, 430, 689-693.
- GOTO, T. & KELLER, R. 2002. The planar cell polarity gene Strabismus regulates convergence and extension and neural fold closure in Xenopus. *Developmental Biology*, 247, 165-181.
- GUBB, D. & GARCIABELLIDO, A. 1982. A Genetic-Analysis of the Determination of Cuticular Polarity during Development in Drosophila-Melanogaster. *Journal of Embryology and Experimental Morphology*, 68, 37-57.
- GUPTA, S., BARRETT, T., WHITMARSH, A. J., CAVANAGH, J., SLUSS, H. K., DERIJARD, B. & DAVIS, R. J. 1996. Selective interaction of JNK protein kinase isoforms with transcription factors. *Embo Journal*, 15, 2760-2770.
- GUPTA, T. & MULLINS, M. C. 2010. Dissection of organs from the adult zebrafish. *J Vis Exp*.
- GURURAJAN, M., CHUI, R., KARUPPANNAN, A. K., KE, J., JENNINGS, C. D. & BONDADA, S. 2005. c-Jun N-terminal kinase (JNK) is required for survival and proliferation of B-lymphoma cells. *Blood*, 106, 1382-91.
- GYGI, S. P., ROCHON, Y., FRANZA, B. R. & AEBERSOLD, R. 1999. Correlation between protein and mRNA abundance in yeast. *Mol Cell Biol*, 19, 1720-30.
- HABAS, R., DAWID, I. B. & HE, X. 2003. Coactivation of Rac and Rho by Wnt/Frizzled signaling is required for vertebrate gastrulation. *Genes Dev*, 17, 295-309.
- HALPERN, M. E., HO, R. K., WALKER, C. & KIMMEL, C. B. 1993. Induction of muscle pioneers and floor plate is distinguished by the zebrafish no tail mutation. *Cell*, 75, 99-111.
- HAMBLET, N. S., LIJAM, N., RUIZ-LOZANO, P., WANG, J. B., YANG, Y. S., LUO, Z. G., MEI, L., CHIEN, K. R., SUSSMAN, D. J. & WYNshaw-BORIS, A. 2002. Dishevelled 2 is essential for cardiac outflow tract development, somite segmentation and neural tube closure. *Development*, 129, 5827-5838.
- HASHIMOTO, H., REBAGLIATI, M., AHMAD, N., MURAOKA, O., KUROKAWA, T., HIBI, M. & SUZUKI, T. 2004. The Cerberus/Dan-family protein Charon is a negative regulator of Nodal signaling during left-right patterning in zebrafish. *Development*, 131, 1741-53.
- HASHMI, A., ABU-SULAIMAN, R., MCCRINDLE, B. W., SMALLHORN, J. F., WILLIAMS, W. G. & FREEDOM, R. M. 1998. Management and outcomes of right atrial isomerism: A 26-year experience. *Journal of the American College of Cardiology*, 31, 1120-1126.
- HE, H. P., LI, H. L., LIN, A. N. & GOTTLIEB, R. A. 1999. Activation of the JNK pathway is important for cardiomyocyte death in response to simulated ischemia. *Cell Death and Differentiation*, 6, 987-991.
- HEASMAN, J. 2002. Morpholino oligos: Making sense of antisense? *Developmental Biology*, 243, 209-214.
- HEISENBERG, C. P., TADA, M., RAUCH, G. J., SAUDE, L., CONCHA, M. L., GEISLER, R., STEMPLE, D. L., SMITH, J. C. & WILSON, S. W. 2000. Silberblick/Wnt11 mediates convergent extension movements during zebrafish gastrulation. *Nature*, 405, 76-81.
- HENDERSON, D. J. & CHAUDHRY, B. 2011. Getting to the heart of planar cell polarity signaling. *Birth Defects Res A Clin Mol Teratol*, 91, 460-7.
- HENDERSON, D. J., CONWAY, S. J., GREENE, N. D. E., GERRELLI, D., MURDOCH, J. N., ANDERSON, R. H. & COPP, A. J. 2001. Cardiovascular defects associated with

- abnormalities in midline development in the Loop-tail mouse mutant. *Circulation Research*, 89, 6-12.
- HERNANDEZ-LAGUNAS, L., CHOI, I. F., KAJI, T., SIMPSON, P., HERSHEY, C., ZHOU, Y., ZON, L., MERCOLA, M. & ARTINGER, K. B. 2005. Zebrafish narrowminded disrupts the transcription factor *prdm1* and is required for neural crest and sensory neuron specification. *Dev Biol*, 278, 347-57.
- HIBI, M., LIN, A. N., SMEAL, T., MINDEN, A. & KARIN, M. 1993. Identification of an Oncoprotein-Responsive and Uv-Responsive Protein-Kinase That Binds and Potentiates the C-Jun Activation Domain. *Genes & Development*, 7, 2135-2148.
- HILBERG, F., AGUZZI, A., HOWELLS, N. & WAGNER, E. F. 1993. C-Jun Is Essential for Normal Mouse Development and Hepatogenesis. *Nature*, 365, 179-181.
- HILL, A. J., TERAOKA, H., HEIDEMAN, W. & PETERSON, R. E. 2005. Zebrafish as a model vertebrate for investigating chemical toxicity. *Toxicol Sci*, 86, 6-19.
- HIROKAWA, N., TANAKA, Y., OKADA, Y. & TAKEDA, S. 2006. Nodal flow and the generation of left-right asymmetry. *Cell*, 125, 33-45.
- HOFFMAN, J. I. & KAPLAN, S. 2002. The incidence of congenital heart disease. *J Am Coll Cardiol*, 39, 1890-900.
- HOLLEY, S. A. & TAKEDA, H. 2002. Catching a wave: the oscillator and wavefront that create the zebrafish somite. *Semin Cell Dev Biol*, 13, 481-8.
- HOWE, K., CLARK, M. D., TORROJA, C. F., TORRANCE, J., BERTHELOT, C., MUFFATO, M., COLLINS, J. E., HUMPHRAY, S., MCLAREN, K., MATTHEWS, L., MCLAREN, S., SEALY, I., CACCAMO, M., CHURCHER, C., SCOTT, C., BARRETT, J. C., KOCH, R., RAUCH, G. J., WHITE, S., CHOW, W., KILIAN, B., QUINTAIS, L. T., GUERRA-ASSUNCAO, J. A., ZHOU, Y., GU, Y., YEN, J., VOGEL, J. H., EYRE, T., REDMOND, S., BANERJEE, R., CHI, J. X., FU, B. Y., LANGLEY, E., MAGUIRE, S. F., LAIRD, G. K., LLOYD, D., KENYON, E., DONALDSON, S., SEHRA, H., ALMEIDA-KING, J., LOVELAND, J., TREVANION, S., JONES, M., QUAIL, M., WILLEY, D., HUNT, A., BURTON, J., SIMS, S., MCLAY, K., PLUMB, B., DAVIS, J., CLEE, C., OLIVER, K., CLARK, R., RIDDLE, C., ELIOTT, D., THREADGOLD, G., HARDEN, G., WARE, D., MORTIMER, B., KERRY, G., HEATH, P., PHILLIMORE, B., TRACEY, A., CORBY, N., DUNN, M., JOHNSON, C., WOOD, J., CLARK, S., PELAN, S., GRIFFITHS, G., SMITH, M., GLITHERO, R., HOWDEN, P., BARKER, N., STEVENS, C., HARLEY, J., HOLT, K., PANAGIOTIDIS, G., LOVELL, J., BEASLEY, H., HENDERSON, C., GORDON, D., AUGER, K., WRIGHT, D., COLLINS, J., RAISEN, C., DYER, L., LEUNG, K., ROBERTSON, L., AMBRIDGE, K., LEONGAMORNLEET, D., MCGUIRE, S., GILDERTHORP, R., GRIFFITHS, C., MANTHRAVADI, D., NICHOL, S., BARKER, G., WHITEHEAD, S., KAY, M., et al. 2013. The zebrafish reference genome sequence and its relationship to the human genome. *Nature*, 496, 498-503.
- HRUSCHA, A., KRAWITZ, P., RECHENBERG, A., HEINRICH, V., HECHT, J., HAASS, C. & SCHMID, B. 2013. Efficient CRISPR/Cas9 genome editing with low off-target effects in zebrafish. *Development*, 140, 4982-7.
- HUANG, C., RAJFUR, Z., BORCHERS, C., SCHALLER, M. D. & JACOBSON, K. 2003a. JNK phosphorylates paxillin and regulates cell migration. *Nature*, 424, 219-223.
- HUANG, C. J., TU, C. T., HSIAO, C. D., HSIEH, F. J. & TSAI, H. J. 2003b. Germ-line transmission of a myocardium-specific GFP transgene reveals critical regulatory elements in the cardiac myosin light chain 2 promoter of zebrafish. *Dev Dyn*, 228, 30-40.
- HUANG, G., SHI, L. Z. & CHI, H. 2009. Regulation of JNK and p38 MAPK in the immune system: signal integration, propagation and termination. *Cytokine*, 48, 161-9.

- HUYNH, H., NGUYEN, T. T., CHOW, K. H., TAN, P. H., SOO, K. C. & TRAN, E. 2003. Over-expression of the mitogen-activated protein kinase (MAPK) kinase (MEK)-MAPK in hepatocellular carcinoma: its role in tumor progression and apoptosis. *BMC Gastroenterol*, 3, 19.
- HWANG, W. Y., FU, Y., REYON, D., MAEDER, M. L., KAINI, P., SANDER, J. D., JOUNG, J. K., PETERSON, R. T. & YEH, J. R. 2013a. Heritable and precise zebrafish genome editing using a CRISPR-Cas system. *PLoS One*, 8, e68708.
- HWANG, W. Y., FU, Y., REYON, D., MAEDER, M. L., TSAI, S. Q., SANDER, J. D., PETERSON, R. T., YEH, J. R. & JOUNG, J. K. 2013b. Efficient genome editing in zebrafish using a CRISPR-Cas system. *Nat Biotechnol*, 31, 227-9.
- ICARDO, J. M. & SANCHEZ DE VEGA, M. J. 1991. Spectrum of heart malformations in mice with situs solitus, situs inversus, and associated visceral heterotaxy. *Circulation*, 84, 2547-58.
- JESSEN, J. R., TOPCZEWSKI, J., BINGHAM, S., SEPICH, D. S., MARLOW, F., CHANDRASEKHAR, A. & SOLNICA-KREZEL, L. 2002. Zebrafish trilobite identifies new roles for Strabismus in gastrulation and neuronal movements. *Nature Cell Biology*, 4, 610-615.
- JONO, H., XU, H., KAI, H., LIM, D. J., KIM, Y. S., FENG, X. H. & LI, J. D. 2003. Transforming growth factor-beta-Smad signaling pathway negatively regulates nontypeable Haemophilus influenzae-induced MUC5AC mucin transcription via mitogen-activated protein kinase (MAPK) phosphatase-1-dependent inhibition of p38 MAPK. *J Biol Chem*, 278, 27811-9.
- KARKERA, J. D., LEE, J. S., ROESSLER, E., BANERJEE-BASU, S., OUSPENSKAIA, M. V., MEZ, J., GOLDMUNTZ, E., BOWERS, P., TOWBIN, J., BELMONT, J. W., BAXEVANIS, A. D., SCHIER, A. F. & MUENKE, M. 2007. Loss-of-function mutations in growth differentiation factor-1 (GDF1) are associated with congenital heart defects in humans. *Am J Hum Genet*, 81, 987-94.
- KARLSSON, J., VON HOFSTEN, J. & OLSSON, P. E. 2001. Generating transparent zebrafish: A refined method to improve detection of gene expression during embryonic development. *Marine Biotechnology*, 3, 522-527.
- KARLSSON, M., MANDL, M. & KEYSE, S. M. 2006. Spatio-temporal regulation of mitogen-activated protein kinase (MAPK) signalling by protein phosphatases. *Biochem Soc Trans*, 34, 842-5.
- KARNER, C., WHARTON, K. A. & CARROLL, T. J. 2006a. Planar cell polarity and vertebrate organogenesis. *Seminars in Cell & Developmental Biology*, 17, 194-203.
- KARNER, C., WHARTON, K. A., JR. & CARROLL, T. J. 2006b. Planar cell polarity and vertebrate organogenesis. *Semin Cell Dev Biol*, 17, 194-203.
- KAULITZ, R., ZIEMER, G. & HOFBECK, M. 2004. Atrial isomerism and visceral heterotaxy. *Herz*, 29, 686-694.
- KAWAKAMI, Y., RAYA, A., RAYA, R. M., RODRIGUEZ-ESTEBAN, C. & IZPISUA BELMONTE, J. C. 2005. Retinoic acid signalling links left-right asymmetric patterning and bilaterally symmetric somitogenesis in the zebrafish embryo. *Nature*, 435, 165-71.
- KEIGHTLEY, M. C., CROWHURST, M. O., LAYTON, J. E., BEILHARZ, T., MARKMILLER, S., VARMA, S., HOGAN, B. M., DE JONG-CURTAIN, T. A., HEATH, J. K., LIESCHKE, G. J. A., SEO, J., ASAOKA, Y., NAGAI, Y., HIRAYAMA, J., YAMASAKI, T., NAMAIE, M., OHATA, S., SHIMIZU, N., NEGISHI, T., KITAGAWA, D., KONDOH, H., FURUTANI-SEIKI, M., PENNINGER, J. M., KATADA, T. & NISHINA, H. 2013, 2010. *Danio rerio* mitogen-

- activated protein kinase 8a (mapk8a), mRNA* [Online]. Available: http://www.ncbi.nlm.nih.gov/nuccore/NM_001110389.1.
- KELLY, M. L., ASTSATUROV, A., RHODES, J. & CHERNOFF, J. 2014. A Pak1/Erk Signaling Module Acts through Gata6 to Regulate Cardiovascular Development in Zebrafish. *Dev Cell*, 29, 350-359.
- KEREN-POLITANSKY, A., KEREN, A. & BENGAL, E. 2009. Neural ectoderm-secreted FGF initiates the expression of Nkx2.5 in cardiac progenitors via a p38 MAPK/CREB pathway. *Developmental Biology*, 335, 374-384.
- KEREN, A., BENGAL, E. & FRANK, D. 2005. p38 MAP kinase regulates the expression of XMyf5 and affects distinct myogenic programs during *Xenopus* development. *Developmental Biology*, 288, 73-86.
- KESHET, Y. & SEGER, R. 2010. The MAP kinase signaling cascades: a system of hundreds of components regulates a diverse array of physiological functions. *Methods Mol Biol*, 661, 3-38.
- KILIAN, B., MANSUKOSKI, H., BARBOSA, F. C., ULRICH, F., TADA, M. & HEISENBERG, C. P. 2003. The role of Ppt/Wnt5 in regulating cell shape and movement during zebrafish gastrulation. *Mech Dev*, 120, 467-76.
- KIM, G. H. & HAN, J. K. 2005. JNK and ROKalpha function in the noncanonical Wnt/RhoA signaling pathway to regulate *Xenopus* convergent extension movements. *Dev Dyn*, 232, 958-68.
- KIM, S. K., SHINDO, A., PARK, T. J., OH, E. C., GHOSH, S., GRAY, R. S., LEWIS, R. A., JOHNSON, C. A., ATTIE-BITTACH, T., KATSANIS, N. & WALLINGFORD, J. B. 2010. Planar cell polarity acts through septins to control collective cell movement and ciliogenesis. *Science*, 329, 1337-40.
- KIMMEL, C. B., BALLARD, W. W., KIMMEL, S. R., ULLMANN, B. & SCHILLING, T. F. 1995. Stages of Embryonic-Development of the Zebrafish. *Developmental Dynamics*, 203, 253-310.
- KIMURA, R. S., SCHUKNECHT, H. F. & SANDO, I. 1964. Fine Morphology of the Sensory Cells in the Organ of Corti of Man. *Acta Otolaryngol*, 58, 390-408.
- KITAMURA, K., MIURA, H., MIYAGAWA-TOMITA, S., YANAZAWA, M., KATOH-FUKUI, Y., SUZUKI, R., OHUCHI, H., SUEHIRO, A., MOTEGI, Y., NAKAHARA, Y., KONDO, S. & YOKOYAMA, M. 1999. Mouse Pitx2 deficiency leads to anomalies of the ventral body wall, heart, extra- and periocular mesoderm and right pulmonary isomerism. *Development*, 126, 5749-5758.
- KLAUSNER, R. D., ROUAULT, T. A. & HARFORD, J. B. 1993. Regulating the fate of mRNA: the control of cellular iron metabolism. *Cell*, 72, 19-28.
- KLEINJAN, D. A., BANCEWICZ, R. M., GAUTIER, P., DAHM, R., SCHONTHALER, H. B., DAMANTE, G., SEAWRIGHT, A., HEVER, A. M., YEYATI, P. L., VAN HEYNINGEN, V. & COUTINHO, P. 2008. Subfunctionalization of duplicated zebrafish pax6 genes by cis-regulatory divergence. *PLoS Genet*, 4.
- KO, S. K., CHEN, X., YOON, J. & SHIN, I. 2011. Zebrafish as a good vertebrate model for molecular imaging using fluorescent probes. *Chem Soc Rev*, 40, 2120-30.
- KOK, F. O., SHIN, M., NI, C.-W., GUPTA, A., GROSSE, A. S., VAN IMPEL, A., KIRCHMAIER, B. C., PETERSON-MADURO, J., KOURKOULIS, G., MALE, I., DESANTIS, D. F., SHEPPARD-TINDELL, S., EBARASI, L., BETSHOLTZ, C., SCHULTE-MERKER, S., WOLFE, S. A. & LAWSON, N. D. 2015. Reverse Genetic Screening Reveals Poor Correlation between

- Morpholino-Induced and Mutant Phenotypes in Zebrafish. *Developmental Cell*, 32, 97-108.
- KRAMER-ZUCKER, A. G., OLALE, F., HAYCRAFT, C. J., YODER, B. K., SCHIER, A. F. & DRUMMOND, I. A. 2005. Cilia-driven fluid flow in the zebrafish pronephros, brain and Kupffer's vesicle is required for normal organogenesis. *Development*, 132, 1907-21.
- KRENS, S. F., SPAINK, H. P. & SNAAR-JAGALSKA, B. E. 2006a. Functions of the MAPK family in vertebrate-development. *FEBS Lett*, 580, 4984-90.
- KRENS, S. F. G., HE, S. N., SPAINK, H. P. & SNAAR-JAGALSKA, B. E. 2006b. Characterization and expression patterns of the MAPK family in zebrafish. *Gene Expression Patterns*, 6, 1019-1026.
- KUAN, C. Y., YANG, D. D., ROY, D. R. S., DAVIS, R. J., RAKIC, P. & FLAVELL, R. A. 1999. The Jnk1 and Jnk2 protein kinases are required for regional specific apoptosis during early brain development. *Neuron*, 22, 667-676.
- KWOK, S., KELLOGG, D. E., MCKINNEY, N., SPASIC, D., GODA, L., LEVENSON, C. & SNINSKY, J. J. 1990. Effects of Primer Template Mismatches on the Polymerase Chain-Reaction - Human-Immunodeficiency-Virus Type-1 Model Studies. *Nucleic Acids Research*, 18, 999-1005.
- LAZIC, S. & SCOTT, I. 2011. Mef2cb regulates late myocardial cell addition from a second heart field-like population of progenitors in zebrafish. *Developmental Biology*, 356, 172-172.
- LEI, Y., ZHANG, T., LI, H., WU, B., JIN, L. & WANG, H. 2010. VANGL2 Mutations in Human Cranial Neural-Tube Defects. *New England Journal of Medicine*, 362, 2232-2235.
- LEIGH, M. D., A; NOONE, P 2015. Genetics, diagnosis and future treatment strategies for primary ciliary dyskinesia. *Expert Opinion on Orphan Drugs*, 3, 31-44.
- LELE, Z., HARTSON, S. D., MARTIN, C. C., WHITESELL, L., MATTS, R. L. & KRONE, P. H. 1999. Disruption of zebrafish somite development by pharmacologic inhibition of Hsp90. *Dev Biol*, 210, 56-70.
- LENHART, K. F., LIN, S. Y., TITUS, T. A., POSTLETHWAIT, J. H. & BURDINE, R. D. 2011. Two additional midline barriers function with midline lefty1 expression to maintain asymmetric Nodal signaling during left-right axis specification in zebrafish. *Development*, 138, 4405-4410.
- LEVIN, M., THORLIN, T., ROBINSON, K. R., NOGI, T. & MERCOLA, M. 2002. Asymmetries in H⁺/K⁺-ATPase and cell membrane potentials comprise a very early step in left-right patterning. *Cell*, 111, 77-89.
- LI, W. G., ZAHEER, A., COPPEY, L. & OSKARSSON, H. J. 1998. Activation of JNK in the remote myocardium after large myocardial infarction in rats. *Biochemical and Biophysical Research Communications*, 246, 816-820.
- LI, Z., JOSEPH, N. M. & EASTER, S. S., JR. 2000. The morphogenesis of the zebrafish eye, including a fate map of the optic vesicle. *Dev Dyn*, 218, 175-88.
- LIANG, J. O., ETHERIDGE, A., HANTSOO, L., RUBINSTEIN, A. L., NOWAK, S. J., BELMONTE, J. C. I. & HALPERN, M. E. 2000. Asymmetric Nodal signaling in the zebrafish diencephalon positions the pineal organ. *Development*, 127, 5101-5112.
- LIESCHKE, G. J. 2001. Zebrafish--an emerging genetic model for the study of cytokines and hematopoiesis in the era of functional genomics. *Int J Hematol*, 73, 23-31.

- LIN, A. E., TICHIO, B. S., HOUDE, K., WESTGATE, M. N. & HOLMES, L. B. 2000. Heterotaxy: Associated conditions and hospital-based prevalence in newborns. *Genetics in Medicine*, 2, 157-172.
- LIN, C. R., KIOUSSI, C., O'CONNELL, S., BRIATA, P., SZETO, D., LIU, F., IZPISUA-BELMONTE, J. C. & ROSENFELD, M. G. 1999. Pitx2 regulates lung asymmetry, cardiac positioning and pituitary and tooth morphogenesis. *Nature*, 401, 279-82.
- LINASK, K. K., YU, X., CHEN, Y. & HAN, M. D. 2002. Directionality of heart looping: effects of Pitx2c misexpression on flectin asymmetry and midline structures. *Dev Biol*, 246, 407-17.
- LINK, V., SHEVCHENKO, A. & HEISENBERG, C. P. 2006. Proteomics of early zebrafish embryos. *Bmc Developmental Biology*, 6.
- LITTLE, C. D. & RONGISH, B. J. 1995. The extracellular matrix during heart development. *Experientia*, 51, 873-82.
- LITTLE, S. C. & MULLINS, M. C. 2005. Twisted gastrulation promotes BMP signaling in zebrafish DV axial patterning. *Developmental Biology*, 283, 620-620.
- LO, Y. Y. C., WONG, J. M. S. & CRUZ, T. F. 1996. Reactive oxygen species mediate cytokine activation of c-jun NH2-terminal kinases. *Journal of Biological Chemistry*, 271, 15703-15707.
- LOGAN, M., PAGAN-WESTPHAL, S. M., SMITH, D. M., PAGANESSI, L. & TABIN, C. J. 1998. The transcription factor Pitx2 mediates situs-specific morphogenesis in response to left-right asymmetric signals. *Cell*, 94, 307-317.
- LONG, S., AHMAD, N. & REBAGLIATI, M. 2003a. Roles of the zebrafish nodal-related gene southpaw in visceral and brain left-right asymmetry. *Developmental Biology*, 259, 554-555.
- LONG, S., AHMAD, N. & REBAGLIATI, M. 2003b. The zebrafish nodal-related gene southpaw is required for visceral and diencephalic left-right asymmetry. *Development*, 130, 2303-2316.
- LOPES, S. S., LOURENCO, R., PACHECO, L., MORENO, N., KREILING, J. & SAUDE, L. 2010. Notch signalling regulates left-right asymmetry through ciliary length control. *Development*, 137, 3625-3632.
- LOWE, L. A., SUPP, D. M., SAMPATH, K., YOKOYAMA, T., WRIGHT, C. V. E., POTTER, S. S., OVERBEEK, P. & KUEHN, M. R. 1996. Conserved left-right asymmetry of nodal expression and alterations in murine situs inversus. *Nature*, 381, 158-161.
- LOZANO-VELASCO, E., CHINCHILLA, A., MARTINEZ-FERNANDEZ, S., HERNANDEZ-TORRES, F., NAVARRO, F., LYONS, G. E., FRANCO, D. & ARANEGA, A. E. 2011. Pitx2c modulates cardiac-specific transcription factors networks in differentiating cardiomyocytes from murine embryonic stem cells. *Cells Tissues Organs*, 194, 349-62.
- LU, M. F., PRESSMAN, C., DYER, R., JOHNSON, R. L. & MARTIN, J. F. 1999. Function of Rieger syndrome gene in left-right asymmetry and craniofacial development. *Nature*, 401, 276-278.
- LYNCH, M. & FORCE, A. 2000. The probability of duplicate gene preservation by subfunctionalization. *Genetics*, 154, 459-473.
- MAGIGALLUZZI, C., MISHRA, R., FIORENTINO, M., MONTIRONI, R., YAO, H., CAPODIECI, P., WISHNOW, K., KAPLAN, I., STORK, P. J. S. & LODA, M. 1997. Mitogen-activated protein kinase phosphatase 1 is overexpressed in prostate cancers and is inversely related to apoptosis. *Laboratory Investigation*, 76, 37-51.

- MALI, P., YANG, L., ESVELT, K. M., AACH, J., GUELL, M., DICARLO, J. E., NORVILLE, J. E. & CHURCH, G. M. 2013. RNA-guided human genome engineering via Cas9. *Science*, 339, 823-6.
- MAO, Y., MULVANEY, J., ZAKARIA, S., YU, T., MORGAN, K. M., ALLEN, S., BASSON, M. A., FRANCIS-WEST, P. & IRVINE, K. D. 2011. Characterization of a Dchs1 mutant mouse reveals requirements for Dchs1-Fat4 signaling during mammalian development. *Development*, 138, 947-57.
- MARQUES, S., BORGES, A. C., SILVA, A. C., FREITAS, S., CORDENONSI, M. & BELO, J. A. 2004. The activity of the Nodal antagonist Cerl-2 in the mouse node is required for correct L/R body axis. *Genes Dev*, 18, 2342-7.
- MARTIN-BLANCO, E., GAMPEL, A., RING, J., VIRDEE, K., KIROV, N., TOLKOVSKY, A. M. & MARTINEZ-ARIAS, A. 1998. puckered encodes a phosphatase that mediates a feedback loop regulating JNK activity during dorsal closure in *Drosophila*. *Genes & Development*, 12, 557-570.
- MASLAND, R. H. 2001. The fundamental plan of the retina. *Nature Neuroscience*, 4, 877-886.
- MATAKATSU, H. & BLAIR, S. S. 2004. Interactions between Fat and Dachous and the regulation of planar cell polarity in the *Drosophila* wing. *Development*, 131, 3785-94.
- MATSUI, T. & BESSHO, Y. 2012. Left-right asymmetry in zebrafish. *Cell Mol Life Sci*, 69, 3069-77.
- MATSUI, T., RAYA, A., KAWAKAMI, Y., CALLOL-MASSOT, C., CAPDEVILA, J., RODRIGUEZ-ESTEBAN, C. & BELMONTE, J. C. I. 2005. Noncanonical Wnt signaling regulates midline convergence of organ primordia during zebrafish development. *Genes & Development*, 19, 164-175.
- MAY-SIMERA, H. L., KAI, M., HERNANDEZ, V., OSBORN, D. P. S., TADA, M. & BEALES, P. L. 2010. Bbs8, together with the planar cell polarity protein Vangl2, is required to establish left-right asymmetry in zebrafish. *Developmental Biology*, 345, 215-225.
- MCCURLEY, A. T. & CALLARD, G. V. 2008. Characterization of housekeeping genes in zebrafish: male-female differences and effects of tissue type, developmental stage and chemical treatment. *Bmc Molecular Biology*, 9.
- MCGRATH, J., SOMLO, S., MAKOVA, S., TIAN, X. & BRUECKNER, M. 2003. Two populations of node monocilia initiate left-right asymmetry in the mouse. *Cell*, 114, 61-73.
- MCLEAN, D. L. & FETCHO, J. R. 2008. Using imaging and genetics in zebrafish to study developing spinal circuits in vivo. *Dev Neurobiol*, 68, 817-34.
- MENO, C., GRITSMAN, K., OHISHI, S., OHFUJI, Y., HECKSCHER, E., MOCHIDA, K., SHIMONO, A., KONDOH, H., TALBOT, W. S., ROBERTSON, E. J., SCHIER, A. F. & HAMADA, H. 1999. Mouse lefty2 and zebrafish antivin are feedback inhibitors of nodal signaling during vertebrate gastrulation. *Molecular Cell*, 4, 287-298.
- MENO, C., SHIMONO, A., SAIJOH, Y., YASHIRO, K., MOCHIDA, K., OHISHI, S., NOJI, S., KONDOH, H. & HAMADA, H. 1998. lefty-1 is required for left-right determination as a regulator of lefty-2 and nodal. *Cell*, 94, 287-297.
- MERKLIN, R. J. & VARANO, N. R. 1963. Situs inversus and cardiac defects. A study of 111 cases of reversed asymmetry. *J Thorac Cardiovasc Surg*, 45, 334-42.
- MIGHELI, A., PIVA, R., ATZORI, C., TROOST, D. & SCHIFFER, D. 1997. c-Jun, JNK/SAPK kinases and transcription factor NF-kappa B are selectively activated in astrocytes, but not motor neurons, in amyotrophic lateral sclerosis. *Journal of Neuropathology and Experimental Neurology*, 56, 1314-1322.

- MINGO-SION, A. M., MARIETTA, P. M., KOLLER, E., WOLF, D. M. & VAN DEN BERG, C. L. 2004. Inhibition of JNK reduces G2/M transit independent of p53, leading to endoreduplication, decreased proliferation, and apoptosis in breast cancer cells. *Oncogene*, 23, 596-604.
- MIURA, G. I. & YELON, D. 2011. A guide to analysis of cardiac phenotypes in the zebrafish embryo. *Methods Cell Biol*, 101, 161-80.
- MOCHIZUKI, T., SAIJOH, Y., TSUCHIYA, K., SHIRAYOSHI, Y., TAKAI, S., TAYA, C., YONEKAWA, H., YAMADA, K., NIHEI, H., NAKATSUJI, N., OVERBEEK, P. A., HAMADA, H. & YOKOYAMA, T. 1998. Cloning of inv, a gene that controls left/right asymmetry and kidney development. *Nature*, 395, 177-81.
- MOELLER, H., JENNY, A., SCHAEFFER, H. I., SCHWARZ-ROMOND, T., MLODZIK, M., HAMMERSCHMIDT, M. & BIRCHMEIER, W. 2006. Diversin regulates heart formation and gastrulation movements in development. *Proceedings of the National Academy of Sciences of the United States of America*, 103, 15900-15905.
- MONTCOUQUIOL, M., RACHEL, R. A., LANFORD, P. J., COPELAND, N. G., JENKINS, N. A. & KELLEY, M. W. 2003. Identification of Vangl2 and Scrb1 as planar polarity genes in mammals. *Nature*, 423, 173-7.
- MOROKUMA, J., BLACKISTON, D. & LEVIN, M. 2008. KCNQ1 and KCNE1 K⁺ channel components are involved in early left-right patterning in *Xenopus laevis* embryos. *Cellular Physiology and Biochemistry*, 21, 357-372.
- MORRIS, A. C. & FADOOL, J. M. 2005. Studying rod photoreceptor development in zebrafish. *Physiol Behav*, 86, 306-13.
- MULLER, P., ROGERS, K. W., JORDAN, B. M., LEE, J. S., ROBSON, D., RAMANATHAN, S. & SCHIER, A. F. 2012. Differential diffusivity of Nodal and Lefty underlies a reaction-diffusion patterning system. *Science*, 336, 721-4.
- MWAFI, N., BERETTA, C. A., PAOLINI, A. & CARL, M. 2014. Divergent Wnt8a Gene Expression in Teleosts. *Plos One*, 9.
- NASEVICIUS, A. & EKKER, S. C. 2000. Effective targeted gene 'knockdown' in zebrafish. *Nature Genetics*, 26, 216-220.
- NAULI, S. M., ALENGHAT, F. J., LUO, Y., WILLIAMS, E., VASSILEV, P., LIL, X. G., ELIA, A. E. H., LU, W. N., BROWN, E. M., QUINN, S. J., INGBER, D. E. & ZHOU, J. 2003. Polycystins 1 and 2 mediate mechanosensation in the primary cilium of kidney cells. *Nature Genetics*, 33, 129-137.
- NGUYEN, A. N. & SHIOZAKI, K. 1999. Heat-shock-induced activation of stress MAP kinase is regulated by threonine- and tyrosine-specific phosphatases. *Genes Dev*, 13, 1653-63.
- NIE, S. & CHANG, C. 2007. PI3K and erk MAPK mediate ErbB signaling in *Xenopus* gastrulation. *Mechanisms of Development*, 124, 657-667.
- NONAKA, S., SHIRATORI, H., SAIJOH, Y. & HAMADA, H. 2002. Determination of left-right patterning of the mouse embryo by artificial nodal flow. *Nature*, 418, 96-99.
- NONAKA, S., TANAKA, Y., OKADA, Y., TAKEDA, S., HARADA, A., KANAI, Y., KIDO, M. & HIROKAWA, N. 1998. Randomization of left-right asymmetry due to loss of nodal cilia generating leftward flow of extraembryonic fluid in mice lacking KIF3B motor protein. *Cell*, 95, 829-837.
- NÜSSLEIN-VOLHARD, C. & DAHM, R. 2002. *Zebrafish : a practical approach*, Oxford, Oxford University Press.

- NUTT, S. L., DINGWELL, K. S., HOLT, C. E. & AMAYA, E. 2001. *Xenopus* Sprouty2 inhibits FGF-mediated gastrulation movements but does not affect mesoderm induction and patterning. *Genes & Development*, 15, 1152-1166.
- OATES, A. C., BROWNLIE, A., PRATT, S. J., IRVINE, D. V., LIAO, E. C., PAW, B. H., DORIAN, K. J., JOHNSON, S. L., POSTLETHWAIT, J. H., ZON, L. I. & WILKS, A. F. 1999. Gene duplication of zebrafish JAK2 homologs is accompanied by divergent embryonic expression patterns: Only jak2a is expressed during erythropoiesis. *Blood*, 94, 2622-2636.
- OBARA, T., MANGOS, S., LIU, Y., ZHAO, J., WIESSNER, S., KRAMER-ZUCKER, A. G., OLALE, F., SCHIER, A. F. & DRUMMOND, I. A. 2006. Polycystin-2 immunolocalization and function in zebrafish. *J Am Soc Nephrol*, 17, 2706-18.
- ODENTHAL, J. & NUSSLEIN-VOLHARD, C. 1998. fork head domain genes in zebrafish. *Dev Genes Evol*, 208, 245-58.
- OISHI, I., KAWAKAMI, Y., RAYA, A., CALLOL-MASSOT, C. & BELMONTE, J. C. I. 2006. Regulation of primary cilia formation and left-right patterning in zebrafish by a noncanonical Wnt signaling mediator, duboraya. *Nature Genetics*, 38, 1316-1322.
- OISHI, I., SUZUKI, H., ONISHI, N., TAKADA, R., KANI, S., OHKAWARA, B., KOSHIDA, I., SUZUKI, K., YAMADA, G., SCHWABE, G. C., MUNDLOS, S., SHIBUYA, H., TAKADA, S. & MINAMI, Y. 2003. The receptor tyrosine kinase Ror2 is involved in non-canonical Wnt5a/JNK signalling pathway. *Genes Cells*, 8, 645-54.
- OKADA, Y., NONAKA, S., TANAKA, Y., SAIJOH, Y., HAMADA, H. & HIROKAWA, N. 1999. Abnormal nodal flow precedes situs inversus in iv and inv mice. *Mol Cell*, 4, 459-68.
- OMORI, S., HIDA, M., ISHIKURA, K., KURAMOCHI, S. & AWAZU, M. 2000. Expression of mitogen-activated protein kinase family in rat renal development. *Kidney Int*, 58, 27-37.
- OSADA, S. I., SAIJOH, Y., FRISCH, A., YEO, C. Y., ADACHI, H., WATANABE, M., WHITMAN, M., HAMADA, H. & WRIGHT, C. V. 2000. Activin/nodal responsiveness and asymmetric expression of a *Xenopus* nodal-related gene converge on a FAST-regulated module in intron 1. *Development*, 127, 2503-14.
- OTEIZA, P., KOEPPEN, M., CONCHA, M. L. & HEISENBERG, C. P. 2008. Origin and shaping of the laterality organ in zebrafish. *Development*, 135, 2807-2813.
- OTEIZA, P., KOPPEN, M., KRIEG, M., PULGAR, E., FARIAS, C., MELO, C., PREIBISCH, S., MULLER, D., TADA, M., HARTEL, S., HEISENBERG, C. P. & CONCHA, M. L. 2010. Planar cell polarity signalling regulates cell adhesion properties in progenitors of the zebrafish laterality organ. *Development*, 137, 3459-3468.
- PAGES, G., GUERIN, S., GRALL, D., BONINO, F., SMITH, A., ANJUERE, F., AUBERGER, P. & POUYSSEGUR, J. 1999. Defective thymocyte maturation in p44 MAP kinase (Erk 1) knockout mice. *Science*, 286, 1374-7.
- PAPAKRIVOPOULOU, E., DEAN, C. H., COPP, A. J. & LONG, D. A. 2014. Planar cell polarity and the kidney. *Nephrology Dialysis Transplantation*, 29, 1320-1326.
- PARK, H. J., KIM, H. J., LEE, J. H., LEE, J. Y., CHO, B. K., KANG, J. S., KANG, H., YANG, Y. & CHO, D. H. 2005. Corticotropin-releasing hormone (CRH) downregulates interleukin-18 expression in human HaCaT keratinocytes by activation of p38 mitogen-activated protein kinase (MAPK) pathway. *J Invest Dermatol*, 124, 751-5.
- PARNG, C., SENG, W. L., SEMINO, C. & MCGRATH, P. 2002. Zebrafish: a preclinical model for drug screening. *Assay Drug Dev Technol*, 1, 41-8.

- PEAL, D. S., LYNCH, S. N. & MILAN, D. J. 2011. Patterning and Development of the Atrioventricular Canal in Zebrafish. *Journal of Cardiovascular Translational Research*, 4, 720-726.
- PELSTER, B. & BURGGREN, W. W. 1996. Disruption of hemoglobin oxygen transport does not impact oxygen-dependent physiological processes in developing embryos of zebra fish (*Danio rerio*). *Circ Res*, 79, 358-62.
- PENNEKAMP, P., KARCHER, C., FISCHER, A., SCHWEICKERT, A., SKRYABIN, B., HORST, J., BLUM, M. & DWORNICZAK, B. 2002. The ion channel polycystin-2 is required for left-right axis determination in mice. *Current Biology*, 12, 938-943.
- PHILLIPS, R., SVENSSON, M. & KAYE, P. 2007. A role for IRF-7 in regulating the intracellular fate of *Leishmania donovani*. *American Journal of Tropical Medicine and Hygiene*, 77, 307-307.
- POURQUIE, O. 2003. The segmentation clock: converting embryonic time into spatial pattern. *Science*, 301, 328-30.
- PULVERER, B. J., KYRIAKIS, J. M., AVRUCH, J., NIKOLAKAKI, E. & WOODGETT, J. R. 1991. Phosphorylation of C-Jun Mediated by Map Kinases. *Nature*, 353, 670-674.
- QIAN, D., JONES, C., RZADZINSKA, A., MARK, S., ZHANG, X., STEEL, K. P., DAI, X. & CHEN, P. 2007. Wnt5a functions in planar cell polarity regulation in mice. *Dev Biol*, 306, 121-33.
- RAMAN, M., CHEN, W. & COBB, M. H. 2007. Differential regulation and properties of MAPKs. *Oncogene*, 26, 3100-12.
- RAMSDELL, A. F. 2005. Left-right asymmetry and congenital cardiac defects: Getting to the heart of the matter in vertebrate left-right axis determination. *Developmental Biology*, 288, 1-20.
- RANKIN, C. T., BUNTON, T., LAWLER, A. M. & LEE, S. J. 2000. Regulation of left-right patterning in mice by growth/differentiation factor-1. *Nat Genet*, 24, 262-5.
- REINECKE, K., HERDEGEN, T., EMINEL, S., ALDENHOFF, J. B. & SCHIFFELHOLZ, T. 2013. Knockout of c-Jun N-terminal kinases 1, 2 or 3 isoforms induces behavioural changes. *Behavioural Brain Research*, 245, 88-95.
- RIDA, P. C., LE MINH, N. & JIANG, Y. J. 2004. A Notch feeling of somite segmentation and beyond. *Dev Biol*, 265, 2-22.
- RIDER, S. A., TUCKER, C. S., DEL-POZO, J., ROSE, K. N., MACRAE, C. A., BAILEY, M. A. & MULLINS, J. J. 2012. Techniques for the in vivo assessment of cardio-renal function in zebrafish (*Danio rerio*) larvae. *J Physiol*, 590, 1803-9.
- RIESGOESCOVAR, J. R., JENNI, M., FRITZ, A. & HAFEN, E. 1996. The *Drosophila* Jun-N-terminal kinase is required for cell morphogenesis but not for DJun-dependent cell fate specification in the eye. *Genes & Development*, 10, 2759-2768.
- ROBU, M. E., LARSON, J. D., NASEVICIUS, A., BEIRAGHI, S., BRENNER, C., FARBER, S. A. & EKKER, S. C. 2007. p53 activation by knockdown technologies. *PLoS Genet*, 3, 787-801.
- ROSSI, A., KONTARAKIS, Z., GERRI, C., NOLTE, H., HOELPER, S., KRUEGER, M. & STAINIER, D. Y. R. 2015. Genetic compensation induced by deleterious mutations but not gene knockdowns. *Nature*, 524, 230-+.
- SABAPATHY, K. 2012. Role of the JNK pathway in human diseases. *Prog Mol Biol Transl Sci*, 106, 145-69.

- SABAPATHY, K., JOCHUM, W., HOCHEDLINGER, K., CHANG, L. F., KARIN, M. & WAGNER, E. F. 1999. Defective neural tube morphogenesis and altered apoptosis in the absence of both JNK1 and JNK2. *Mechanisms of Development*, 89, 115-124.
- SABIO, G., ARTHUR, J. S., KUMA, Y., PEGGIE, M., CARR, J., MURRAY-TAIT, V., CENTENO, F., GOEDERT, M., MORRICE, N. A. & CUENDA, A. 2005. p38gamma regulates the localisation of SAP97 in the cytoskeleton by modulating its interaction with GKAP. *EMBO J*, 24, 1134-45.
- SABURI, S., HESTER, I., FISCHER, E., PONTOGLIO, M., EREMINA, V., GESSLER, M., QUAGGIN, S. E., HARRISON, R., MOUNT, R. & MCNEILL, H. 2008. Loss of Fat4 disrupts PCP signaling and oriented cell division and leads to cystic kidney disease. *Nat Genet*, 40, 1010-5.
- SADLER, T. W. 1998. Mechanisms OF neural tube closure and defects. *Mental Retardation and Developmental Disabilities Research Reviews*, 4, 247-253.
- SAIJOH, Y., ADACHI, H., SAKUMA, R., YEO, C. Y., YASHIRO, K., WATANABE, M., HASHIGUCHI, H., MOCHIDA, K., OHISHI, S., KAWABATA, M., MIYAZONO, K., WHITMAN, M. & HAMADA, H. 2000. Left-right asymmetric expression of lefty2 and nodal is induced by a signaling pathway that includes the transcription factor FAST2. *Molecular Cell*, 5, 35-47.
- SAIJOH, Y., VIOTTI, M. & HADJANTONAKIS, A. K. 2014. Follow your gut: relaying information from the site of left-right symmetry breaking in the mouse. *Genesis*, 52, 503-14.
- SCAAL, M. & WIEGREFFE, C. 2006. Somite compartments in anamniotes. *Anat Embryol (Berl)*, 211 Suppl 1, 9-19.
- SCHULTE-MERKER, S., VAN EEDEN, F. J., HALPERN, M. E., KIMMEL, C. B. & NUSSLEIN-VOLHARD, C. 1994. no tail (ntl) is the zebrafish homologue of the mouse T (Brachyury) gene. *Development*, 120, 1009-15.
- SCHWABE, R. F., BRADHAM, C. A., UEHARA, T., HATANO, E., BENNETT, B. L., SCHOONHOVEN, R. & BRENNER, D. A. 2003. c-Jun-N-terminal kinase drives cyclin D1 expression and proliferation during liver regeneration. *Hepatology*, 37, 824-32.
- SCHWEICKERT, A., WEBER, T., BEYER, T., VICK, P., BOGUSCH, S., FEISTEL, K. & BLUM, M. 2007. Cilia-driven leftward flow determines laterality in Xenopus. *Curr Biol*, 17, 60-6.
- SEO, J., ASAOKA, Y., NAGAI, Y., HIRAYAMA, J., YAMASAKI, T., NAMAIE, M., OHATA, S., SHIMIZU, N., NEGISHI, T., KITAGAWA, D., KONDOH, H., FURUTANI-SEIKI, M., PENNINGER, J. M., KATADA, T. & NISHINA, H. 2010. Negative Regulation of wnt11 Expression by Jnk Signaling During Zebrafish Gastrulation. *Journal of Cellular Biochemistry*, 110, 1022-1037.
- SHARMA, M. K., LIU, R. Z., THISSE, C., THISSE, B., DENOVAN-WRIGHT, E. M. & WRIGHT, J. M. 2006. Hierarchical subfunctionalization of fabp1a, fabp1b and fabp10 tissue-specific expression may account for retention of these duplicated genes in the zebrafish (Danio rerio) genome. *Febs Journal*, 273, 3216-3229.
- SHESTOPALOV, I. A. & CHEN, J. K. 2010. Oligonucleotide-Based Tools for Studying Zebrafish Development. *Zebrafish*, 7, 31-40.
- SHIRATORI, H. & HAMADA, H. 2006. The left-right axis in the mouse: from origin to morphology. *Development*, 133, 2095-104.
- SHIRATORI, H. & HAMADA, H. 2014. TGFbeta signaling in establishing left-right asymmetry. *Semin Cell Dev Biol*, 32, 80-4.
- SHU, X. H., ZENG, Z. Q., GAUTIER, P., LENNON, A., GAKOVIC, M., CHEETHAM, M. E., PATTON, E. E. & WRIGHT, A. F. 2011. Knockdown of the Zebrafish Ortholog of the Retinitis

- Pigmentosa 2 (RP2) Gene Results in Retinal Degeneration. *Investigative Ophthalmology & Visual Science*, 52, 2960-2966.
- SIMMS, R. J., ELEY, L., CHAUDHRY, B. & SAYER, J. A. 2009. Ahi1 Knockdown in Zebrafish Models the Ciliopathy Joubert Syndrome. *Pediatric Nephrology*, 24, 1804-1804.
- SIMMS, R. J., HYNES, A. M., ELEY, L., INGLIS, D., CHAUDHRY, B., DAWE, H. R. & SAYER, J. A. 2012. Modelling a ciliopathy: Ahi1 knockdown in model systems reveals an essential role in brain, retinal, and renal development. *Cellular and Molecular Life Sciences*, 69, 993-1009.
- SIMON, M. A., XU, A., ISHIKAWA, H. O. & IRVINE, K. D. 2010. Modulation of fat:dachsous binding by the cadherin domain kinase four-jointed. *Curr Biol*, 20, 811-7.
- SIMONS, M., GLOY, J., GANNER, A., BULLERKOTTE, A., BASHKUROV, M., KRONIG, C., SCHERMER, B., BENZING, T., CABELLO, O. A., JENNY, A., MLODZIK, M., POLOK, B., DRIEVER, W., OBARA, T. & WALZ, G. 2005. Inversin, the gene product mutated in nephronophthisis type II, functions as a molecular switch between Wnt signaling pathways. *Nat Genet*, 37, 537-43.
- SIMONS, M. & MLODZIK, M. 2008. Planar cell polarity signaling: from fly development to human disease. *Annu Rev Genet*, 42, 517-40.
- SONG, H., HU, J. X., CHEN, W., ELLIOTT, G., ANDRE, P., GAO, B. & YANG, Y. Z. 2010. Planar cell polarity breaks bilateral symmetry by controlling ciliary positioning. *Nature*, 466, 378-U130.
- STAINIER, D. Y. R., KONTARAKIS, Z. & ROSSI, A. 2015. Making Sense of Anti-Sense Data. *Developmental Cell*, 32, 7-8.
- STAINIER, D. Y. R., LEE, R. K. & FISHMAN, M. C. 1993. Cardiovascular Development in the Zebrafish .1. Myocardial Fate Map and Heart Tube Formation. *Development*, 119, 31-40.
- STICKNEY, H. L., BARRESI, M. J. & DEVOTO, S. H. 2000. Somite development in zebrafish. *Dev Dyn*, 219, 287-303.
- STREISINGER, G., WALKER, C., DOWER, N., KNAUBER, D. & SINGER, F. 1981. Production of clones of homozygous diploid zebra fish (*Brachydanio rerio*). *Nature*, 291, 293-6.
- STRUTT, D. I., WEBER, U. & MLODZIK, M. 1997. The role of RhoA in tissue polarity and Frizzled signalling. *Nature*, 387, 292-5.
- STRUTT, H., MUNDY, J., HOFSTRA, K. & STRUTT, D. 2004. Cleavage and secretion is not required for Four-jointed function in *Drosophila* patterning. *Development*, 131, 881-90.
- STRUTT, H. & STRUTT, D. 2009. Asymmetric localisation of planar polarity proteins: Mechanisms and consequences. *Semin Cell Dev Biol*, 20, 957-63.
- SULIK, K., DEHART, D. B., INAGAKI, T., CARSON, J. L., VRABLIC, T., GESTELAND, K. & SCHOENWOLF, G. C. 1994. Morphogenesis of the Murine Node and Notochordal Plate. *Developmental Dynamics*, 201, 260-278.
- SUMANAS, S., KIM, H. J., HERMANSON, S. & EKKER, S. C. 2001. Zebrafish frizzled-2 morphant displays defects in body axis elongation. *Genesis*, 30, 114-8.
- SUMMERTON, J., STEIN, D., HUANG, S. B., MATTHEWS, P., WELLER, D. & PARTRIDGE, M. 1997. Morpholino and phosphorothioate antisense oligomers compared in cell-free and in-cell systems. *Antisense & Nucleic Acid Drug Development*, 7, 63-70.
- SUMMERTON, J. & WELLER, D. 1997a. Morpholino antisense oligomers: design, preparation, and properties. *Antisense Nucleic Acid Drug Dev*, 7, 187-95.

- SUMMERTON, J. & WELLER, D. 1997b. Morpholino antisense oligomers: Design, preparation, and properties. *Antisense & Nucleic Acid Drug Development*, 7, 187-195.
- SUMMERTON, J. E. 2007. Morpholino, siRNA, and S-DNA compared: Impact of structure and mechanism of action on off-target effects and sequence specificity. *Current Topics in Medicinal Chemistry*, 7, 651-660.
- SUNG, Y. H., KIM, J. M., KIM, H. T., LEE, J., JEON, J., JIN, Y., CHOI, J. H., BAN, Y. H., HA, S. J., KIM, C. H., LEE, H. W. & KIM, J. S. 2014. Highly efficient gene knockout in mice and zebrafish with RNA-guided endonucleases. *Genome Res*, 24, 125-31.
- SUTHERLAND, M. J. & WARE, S. M. 2009. Disorders of Left-Right Asymmetry: Heterotaxy and Situs Inversus. *American Journal of Medical Genetics Part C-Seminars in Medical Genetics*, 151C, 307-317.
- TABIN, C. J. & VOGAN, K. J. 2003. A two-cilia model for vertebrate left-right axis specification. *Genes Dev*, 17, 1-6.
- TADA, M. & HEISENBERG, C. P. 2012. Convergent extension: using collective cell migration and cell intercalation to shape embryos. *Development*, 139, 3897-3904.
- TADA, M. & SMITH, J. C. 2000. Xwnt11 is a target of Xenopus Brachyury: regulation of gastrulation movements via Dishevelled, but not through the canonical Wnt pathway. *Development*, 127, 2227-2238.
- TANAKA, C., SAKUMA, R., NAKAMURA, T., HAMADA, H. & SAIJOH, Y. 2007. Long-range action of Nodal requires interaction with GDF1. *Genes & Development*, 21, 3272-3282.
- TANAKA, Y., OKADA, Y. & HIROKAWA, N. 2005. FGF-induced vesicular release of Sonic hedgehog and retinoic acid in leftward nodal flow is critical for left-right determination. *Nature*, 435, 172-7.
- TANIGUCHI, K., HOZUMI, S., MAEDA, R., OOIKE, M., SASAMURA, T., AIGAKI, T. & MATSUNO, K. 2007. D-JNK signaling in visceral muscle cells controls the laterality of the Drosophila gut. *Developmental Biology*, 311, 251-263.
- TAYLOR, C. A., ZHENG, Q., LIU, Z. & THOMPSON, J. E. 2013. Role of p38 and JNK MAPK signaling pathways and tumor suppressor p53 on induction of apoptosis in response to Ad-eIF5A1 in A549 lung cancer cells. *Mol Cancer*, 12, 35.
- TAYLOR, J., ABRAMOVA, N., CHARLTON, J. & ADLER, P. N. 1998. Van Gogh: a new Drosophila tissue polarity gene. *Genetics*, 150, 199-210.
- TAYLOR, J. S. & RAES, J. 2004. Duplication and divergence: The evolution of new genes and old ideas. *Annual Review of Genetics*, 38, 615-643.
- TAYLOR, J. S., VAN DE PEER, Y., BRAASCH, I. & MEYER, A. 2001. Comparative genomics provides evidence for an ancient genome duplication event in fish. *Philosophical Transactions of the Royal Society of London Series B-Biological Sciences*, 356, 1661-1679.
- THEISEN, H., PURCELL, J., BENNETT, M., KANSAGARA, D., SYED, A. & MARSH, J. L. 1994. Dishevelled is required during wingless signaling to establish both cell polarity and cell identity. *Development*, 120, 347-60.
- THISSE, C. & THISSE, B. 2008. High-resolution in situ hybridization to whole-mount zebrafish embryos. *Nat Protoc*, 3, 59-69.
- THORNTON, T. M. & RINCON, M. 2009. Non-classical p38 map kinase functions: cell cycle checkpoints and survival. *Int J Biol Sci*, 5, 44-51.
- TIAN, Q., STEPANIANTS, S. B., MAO, M., WENG, L., FEETHAM, M. C., DOYLE, M. J., YI, E. C., DAI, H. Y., THORSSON, V., ENG, J., GOODLETT, D., BERGER, J. P., GUNTER, B., LINSELEY, P. S., STOUGHTON, R. B., AEBERSOLD, R., COLLINS, S. J., HANLON, W. A. &

- HOOD, L. E. 2004. Integrated genomic and proteomic analyses of gene expression in mammalian cells. *Molecular & Cellular Proteomics*, 3, 960-969.
- TOYOIZUMI, R., OGASAWARA, T., TAKEUCHI, S. & MOGI, K. 2005. Xenopus nodal related-1 is indispensable only for left-right axis determination. *Int J Dev Biol*, 49, 923-38.
- VALESIO, E. G., ZHANG, H. & ZHANG, C. 2013. Exposure to the JNK inhibitor SP600125 (anthrapyrazolone) during early zebrafish development results in morphological defects. *J Appl Toxicol*, 33, 32-40.
- VAN DER VELDEN, A. W. & THOMAS, A. A. 1999. The role of the 5' untranslated region of an mRNA in translation regulation during development. *Int J Biochem Cell Biol*, 31, 87-106.
- VAN EEDEN, F. J., GRANATO, M., SCHACH, U., BRAND, M., FURUTANI-SEIKI, M., HAFETER, P., HAMMERSCHMIDT, M., HEISENBERG, C. P., JIANG, Y. J., KANE, D. A., KELSH, R. N., MULLINS, M. C., ODENTHAL, J., WARGA, R. M., ALLENDE, M. L., WEINBERG, E. S. & NUSSLEIN-VOLHARD, C. 1996. Mutations affecting somite formation and patterning in the zebrafish, *Danio rerio*. *Development*, 123, 153-64.
- VANDENBERG, L. N. & LEVIN, M. 2010. Far From Solved: A Perspective on What We Know About Early Mechanisms of Left-Right Asymmetry. *Developmental Dynamics*, 239, 3131-3146.
- VANDENBERG, L. N., MORRIE, R. D., SEEBOHM, G., LEMIRE, J. M. & LEVIN, M. 2013. Rab GTPases are required for early orientation of the left-right axis in *Xenopus*. *Mechanisms of Development*, 130, 254-271.
- VARLET, I., COLLIGNON, J. & ROBERTSON, E. J. 1997. nodal expression in the primitive endoderm is required for specification of the anterior axis during mouse gastrulation. *Development*, 124, 1033-1044.
- VEEMAN, M. T., SLUSARSKI, D. C., KAYKAS, A., LOUIE, S. H. & MOON, R. T. 2003. Zebrafish prickle, a modulator of noncanonical Wnt/Fz signaling, regulates gastrulation movements. *Current Biology*, 13, 680-685.
- VINSON, C. R. & ADLER, P. N. 1987. Directional non-cell autonomy and the transmission of polarity information by the frizzled gene of *Drosophila*. *Nature*, 329, 549-51.
- VOGEL, A. M. & WEINSTEIN, B. M. 2000. Studying vascular development in the zebrafish. *Trends Cardiovasc Med*, 10, 352-60.
- VOGEL, C., ABREU, R. D., KO, D. J., LE, S. Y., SHAPIRO, B. A., BURNS, S. C., SANDHU, D., BOUTZ, D. R., MARCOTTE, E. M. & PENALVA, L. O. 2010. Sequence signatures and mRNA concentration can explain two-thirds of protein abundance variation in a human cell line. *Molecular Systems Biology*, 6.
- WAGNER, E. F. & NEBRED, A. R. 2009. Signal integration by JNK and p38 MAPK pathways in cancer development. *Nat Rev Cancer*, 9, 537-49.
- WALENTEK, P., SCHNEIDER, I., SCHWEICKERT, A. & BLUM, M. 2013. Wnt11b Is Involved in Cilia-Mediated Symmetry Breakage during *Xenopus* Left-Right Development. *Plos One*, 8.
- WALL, N. A., CRAIG, E. J., LABOSKY, P. A. & KESSLER, D. S. 2000. Mesendoderm induction and reversal of left-right pattern by mouse *Gdf1*, a *Vg1*-related gene. *Dev Biol*, 227, 495-509.
- WALLINGFORD, J. B. & HARLAND, R. M. 2002. Neural tube closure requires Dishevelled-dependent convergent extension of the midline. *Development*, 129, 5815-5825.
- WALSH, E. C. & STAINIER, D. Y. 2001. UDP-glucose dehydrogenase required for cardiac valve formation in zebrafish. *Science*, 293, 1670-3.

- WANG, G. L., CADWALLADER, A. B., JANG, D. S., TSANG, M., YOST, H. J. & AMACK, J. D. 2011. The Rho kinase Rock2b establishes anteroposterior asymmetry of the ciliated Kupffer's vesicle in zebrafish. *Development*, 138, 45-54.
- WANG, J. B., HAMBLET, N. S., MARK, S., DICKINSON, M. E., BRINKMAN, B. C., SEGIL, N., FRASER, S. E., CHEN, P., WALLINGFORD, J. B. & WYNshaw-BORIS, A. 2006a. Dishevelled genes mediate a conserved mammalian PCP pathway to regulate convergent extension during neurulation. *Development*, 133, 1767-1778.
- WANG, Y., GUO, N. & NATHANS, J. 2006b. The role of Frizzled3 and Frizzled6 in neural tube closure and in the planar polarity of inner-ear sensory hair cells. *J Neurosci*, 26, 2147-56.
- WATERHOUSE, A. M., PROCTER, J. B., MARTIN, D. M., CLAMP, M. & BARTON, G. J. 2009. Jalview Version 2--a multiple sequence alignment editor and analysis workbench. *Bioinformatics*, 25, 1189-91.
- WEI, J., WANG, W., CHOPRA, I., LI, H. F., DOUGHERTY, C. J., ADI, J., ADI, N., WANG, H. & WEBSTER, K. A. 2011. c-Jun N-terminal kinase (JNK-1) confers protection against brief but not extended ischemia during acute myocardial infarction. *Journal of Biological Chemistry*, 286, 13995-4006.
- WEI, Z. Z., YU, S. P., LEE, J. H., CHEN, D. D., TAYLOR, T. M., DEVEAU, T. C., YU, A. C. H. & WEI, L. 2014. Regulatory Role of the JNK-STAT1/3 Signaling in Neuronal Differentiation of Cultured Mouse Embryonic Stem Cells. *Cellular and Molecular Neurobiology*, 34, 881-893.
- WESTERFIELD, M. 1993. *The zebrafish book : a guide for the laboratory use of zebrafish (Brachydanio rerio)*, Eugene, OR, M. Westerfield.
- WESTERFIELD, M. 1995. *The zebrafish book : a guide for the laboratory use of zebrafish (danio rerio)*, Eugene, Or., [M. Westerfield?].
- WHEWAY, G., PARRY, D. A. & JOHNSON, C. A. 2014. The role of primary cilia in the development and disease of the retina. *Organogenesis*, 10, 69-85.
- WIDMANN, C., GIBSON, S., JARPE, M. B. & JOHNSON, G. L. 1999. Mitogen-activated protein kinase: conservation of a three-kinase module from yeast to human. *Physiol Rev*, 79, 143-80.
- WINTER, C. G., WANG, B., BALLEW, A., ROYOU, A., KARESS, R., AXELROD, J. D. & LUO, L. 2001. Drosophila Rho-associated kinase (Drok) links Frizzled-mediated planar cell polarity signaling to the actin cytoskeleton. *Cell*, 105, 81-91.
- WISDOM, R., JOHNSON, R. S. & MOORE, C. 1999. c-Jun regulates cell cycle progression and apoptosis by distinct mechanisms. *EMBO J*, 18, 188-97.
- WRIGHT, G. J., LESLIE, J. D., ARIZA-MCNAUGHTON, L. & LEWIS, J. 2004. Delta proteins and MAGI proteins: an interaction of Notch ligands with intracellular scaffolding molecules and its significance for zebrafish development. *Development*, 131, 5659-5669.
- WU, G., GE, J., HUANG, X. P., HUA, Y. M. & MU, D. Z. 2011. Planar Cell Polarity Signaling Pathway in Congenital Heart Diseases. *Journal of Biomedicine and Biotechnology*.
- WU, J. & MLODZIK, M. 2008. The frizzled extracellular domain is a ligand for Van Gogh/Stbm during nonautonomous planar cell polarity signaling. *Dev Cell*, 15, 462-9.
- XIAO, Y. M., ZHOU, Y. H., XIONG, Z., ZOU, L. J., JIANG, M. G., LUO, Z. W., WEN, S., LIU, W. B., LIU, S. J. & LI, W. C. 2013. Involvement of JNK in the Embryonic Development and Organogenesis in Zebrafish. *Marine Biotechnology*, 15, 716-725.

- XU, J., LIU, X., JIANG, Y., CHU, L., HAO, H., LIUA, Z., VERFAILLIE, C., ZWEIER, J., GUPTA, K. & LIU, Z. 2008. MAPK/ERK signalling mediates VEGF-induced bone marrow stem cell differentiation into endothelial cell. *J Cell Mol Med*, 12, 2395-406.
- YAMAMOTO, M., MINE, N., MOCHIDA, K., SAKAI, Y., SAIJOH, Y., MENO, C. & HAMADA, H. 2003. Nodal signaling induces the midline barrier by activating Nodal expression in the lateral plate. *Development*, 130, 1795-1804.
- YAMANAKA, H., MORIGUCHI, T., MASUYAMA, N., KUSAKABE, M., HANAFUSA, H., TAKADA, R., TAKADA, S. & NISHIDA, E. 2002. JNK functions in the non-canonical Wnt pathway to regulate convergent extension movements in vertebrates. *Embo Reports*, 3, 69-75.
- YANG, C. H., AXELROD, J. D. & SIMON, M. A. 2002. Regulation of Frizzled by fat-like cadherins during planar polarity signaling in the *Drosophila* compound eye. *Cell*, 108, 675-688.
- YANG, G., LIU, Y., YANG, K., LIU, R., ZHU, S., COQUINCO, A., WEN, W., KOJIC, L., JIA, W. & CYNADER, M. 2012. Isoform-specific palmitoylation of JNK regulates axonal development. *Cell Death and Differentiation*, 19, 553-561.
- YASHIRO, K., SAIJOH, Y., SAKUMA, R., TADA, M., TOMITA, N., AMANO, K., MATSUDA, Y., MONDEN, M., OKADA, S. & HAMADA, H. 2000. Distinct transcriptional regulation and phylogenetic divergence of human LEFTY genes. *Genes Cells*, 5, 343-57.
- YELON, D., HORNE, S. A. & STAINIER, D. Y. R. 1999. Restricted expression of cardiac myosin genes reveals regulated aspects of heart tube assembly in zebrafish. *Developmental Biology*, 214, 23-37.
- YIN, C. Y. & SOLNICA-KREZEL, L. 2007. Convergence and extension movements mediate the specification and fate maintenance of zebrafish slow muscle precursors. *Developmental Biology*, 304, 141-155.
- YIN, W. & HU, B. 2014. Knockdown of Lingo1b protein promotes myelination and oligodendrocyte differentiation in zebrafish. *Exp Neurol*, 251, 72-83.
- YOKOYAMA, T., COPELAND, N. G., JENKINS, N. A., MONTGOMERY, C. A., ELDER, F. F. & OVERBEEK, P. A. 1993. Reversal of left-right asymmetry: a situs inversus mutation. *Science*, 260, 679-82.
- YOSHIOKA, H., MENO, C., KOSHIBA, K., SUGIHARA, M., ITOH, H., ISHIMARU, Y., INOUE, T., OHUCHI, H., SEMINA, E. V., MURRAY, J. C., HAMADA, H. & NOJI, S. 1998. Pitx2, a bicoid-type homeobox gene, is involved in a lefty-signaling pathway in determination of left-right asymmetry. *Cell*, 94, 299-305.
- YOSIMICHI, G., NAKANISHI, T., NISHIDA, T., HATTORI, T., TAKANO-YAMAMOTO, T. & TAKIGAWA, M. 2001. CTGF/Hcs24 induces chondrocyte differentiation through a p38 mitogen-activated protein kinase (p38MAPK), and proliferation through a p44/42 MAPK/extracellular-signal regulated kinase (ERK). *Eur J Biochem*, 268, 6058-65.
- YU, A., RUAL, J. F., TAMAI, K., HARADA, Y., VIDAL, M., HE, X. & KIRCHHAUSEN, T. 2007. Association of Dishevelled with the clathrin AP-2 adaptor is required for Frizzled endocytosis and planar cell polarity signaling. *Dev Cell*, 12, 129-41.
- YU, H., SMALLWOOD, P. M., WANG, Y., VIDALTAMAYO, R., REED, R. & NATHANS, J. 2010. Frizzled 1 and frizzled 2 genes function in palate, ventricular septum and neural tube closure: general implications for tissue fusion processes. *Development*, 137, 3707-17.
- ZEIDLER, M. P., PERRIMON, N. & STRUTT, D. I. 1999. The four-jointed gene is required in the *Drosophila* eye for ommatidial polarity specification. *Current Biology*, 9, 1363-1372.

- ZHANG, T., LIU, J. C., ZHANG, J., THEKKETHOTTIYIL, E. B., MACATEE, T. L., ISMAT, F. A., WANG, F. & STOLLER, J. Z. 2013. Jun Is Required in Isl1-Expressing Progenitor Cells for Cardiovascular Development. *Plos One*, 8.
- ZHANG, Y. & LEVIN, M. 2009. Left-Right Asymmetry in the Chick Embryo Requires Core Planar Cell Polarity Protein Vangl2. *Genesis*, 47, 719-728.
- ZHAO, X. C., YEE, R. W., NORCOM, E., BURGESS, H., AVANESOV, A. S., BARRISH, J. P. & MALICKI, J. 2006. The zebrafish cornea: structure and development. *Invest Ophthalmol Vis Sci*, 47, 4341-8.
- ZHOU, Y., CASHMAN, T. J., NEVIS, K. R., OBREGON, P., CARNEY, S. A., LIU, Y., GU, A., MOSIMANN, C., SONDALLE, S., PETERSON, R. E., HEIDEMAN, W., BURNS, C. E. & BURNS, C. G. 2011. Latent TGF-beta binding protein 3 identifies a second heart field in zebrafish. *Nature*, 474, 645-8.

Acknowledgements

Firstly I would like to thank my co-supervisors Dr. Bill Chaudhry, and Prof. Deborah Henderson who was incredibly supportive, particularly during the difficult process of writing this thesis. I would also like to thank my third supervisor Prof. Ioakim Spyridopoulos, without whose infectious positivity and enthusiasm this thesis would not have been completed. I would like to give a special mention to Dr. Mike Jackson and Dr. Simon Bamforth who examined my progress throughout the PhD and provided lots of advice and guidance as I was learning how to become a competent researcher. I would also like to thank Dr. Helen Philips and Dr. Gavin Richardson for their help and advice.

I would like to thank Dr. Simon Ramsbottom who taught me most of the techniques that were required for this body of work, and who was always happy to answer questions. Without his help I would not have been able to complete this work, and I owe him a lot as both a friend and colleague. I would also like to thank Dr. David Burns, Dr. Amy Leigh-Johnson, Hannah Rigby, Natasha, Curley, Dr. Nina Genneback, Kate Bailey and Rebecca Dodds who became my lab family and helped me both in and out of the laboratory. Without the friendship of these people then the PhD would have been a very lonely place.

Finally I wish to thank my parents John and Angela, brother David, aunt Mary Bulbeck, uncle Jeremy Bulbeck, and girlfriend Dr. Laura Corbett who helped to pick me up when I felt that I could not go on. The completion of this thesis is as much a result of your support as any of the other names listed. I thank you from the bottom of my heart for everything that you have done for me.

To all of you, thank you!